



Terms and Conditions of Use of Digitised Theses from Trinity College Library Dublin

Copyright statement

All material supplied by Trinity College Library is protected by copyright (under the Copyright and Related Rights Act, 2000 as amended) and other relevant Intellectual Property Rights. By accessing and using a Digitised Thesis from Trinity College Library you acknowledge that all Intellectual Property Rights in any Works supplied are the sole and exclusive property of the copyright and/or other IPR holder. Specific copyright holders may not be explicitly identified. Use of materials from other sources within a thesis should not be construed as a claim over them.

A non-exclusive, non-transferable licence is hereby granted to those using or reproducing, in whole or in part, the material for valid purposes, providing the copyright owners are acknowledged using the normal conventions. Where specific permission to use material is required, this is identified and such permission must be sought from the copyright holder or agency cited.

Liability statement

By using a Digitised Thesis, I accept that Trinity College Dublin bears no legal responsibility for the accuracy, legality or comprehensiveness of materials contained within the thesis, and that Trinity College Dublin accepts no liability for indirect, consequential, or incidental, damages or losses arising from use of the thesis for whatever reason. Information located in a thesis may be subject to specific use constraints, details of which may not be explicitly described. It is the responsibility of potential and actual users to be aware of such constraints and to abide by them. By making use of material from a digitised thesis, you accept these copyright and disclaimer provisions. Where it is brought to the attention of Trinity College Library that there may be a breach of copyright or other restraint, it is the policy to withdraw or take down access to a thesis while the issue is being resolved.

Access Agreement

By using a Digitised Thesis from Trinity College Library you are bound by the following Terms & Conditions. Please read them carefully.

I have read and I understand the following statement: All material supplied via a Digitised Thesis from Trinity College Library is protected by copyright and other intellectual property rights, and duplication or sale of all or part of any of a thesis is not permitted, except that material may be duplicated by you for your research use or for educational purposes in electronic or print form providing the copyright owners are acknowledged using the normal conventions. You must obtain permission for any other use. Electronic or print copies may not be offered, whether for sale or otherwise to anyone. This copy has been supplied on the understanding that it is copyright material and that no quotation from the thesis may be published without proper acknowledgement.

**Adaptation of growing bone to altered mechanical
load: Morphological change, structural strength and
gene expression**

David A. Hardiman, BA. BAI.

A thesis submitted to the University of Dublin in partial fulfilment of the
requirements for the degree of

Doctor in Philosophy

Department of Mechanical Engineering
Trinity College Dublin

&

Departments of Anatomy and Biochemistry
Royal College of Surgeons in Ireland

October 2003

Prof. D.T. Croke

Prof. T.C. Lee

Prof. P.J. Prendergast

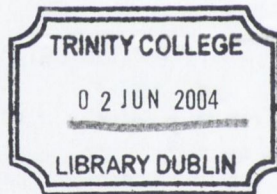
Supervisors

Prof. M.C.H van der Meulen

External examiner

Prof. B. O'Connell

Internal examiner



THORIS
~~7951~~
7490

Table of Contents

	Page
Preface	i
Acknowledgements.....	ii
Declaration	iv
Summary	v
Nomenclature.....	vi
Chapter 1 Introduction.....	1
1.1 Overview	1
1.2 Introduction to Bone.....	2
1.2.1 Bone Structure	3
1.2.2 Bone development and Growth.....	5
1.2.3 Modelling.....	7
1.2.4 Remodelling.....	8
1.2.5 Microdamage	10
1.2.6 Cell signalling and gene expression.....	11
1.3 Clinical Applications	11
1.4 Wolff's Law	12
1.5 Observational studies	13
1.6 Experimental studies	15
1.6.1 Increased loading.....	15
1.6.2 Decreased Loading	17
1.7 Aims and Objectives	19

Chapter 2 Hindlimb Suspension.....	20
2.1 Introduction.....	20
2.1.1 Calcium and other metabolic markers	21
2.1.2 Bone mass and mineralization.....	22
2.1.3 Bone formation and resorption rates.....	22
2.1.4 Biomechanical properties	23
2.1.5 Summary	23
2.1.6 Aims	23
2.2 Materials and Methods.....	24
2.2.1 Experimental Design	24
2.2.2 Conditions of altered load.....	25
2.2.3 Sample Preparation.....	25
2.2.4 Statistical Analysis.....	27
2.3 Results	27
2.4 Conclusions.....	28

Chapter 3 Gene Expression Analysis following Altered Mechanical Load	29
3.1 Introduction.....	29
3.1.1 Gene Expression	31
3.1.2 Candidate genes.....	32
3.1.2.1 <i>c-fos</i>	33
3.1.2.2 <i>Osteocalcin</i>	38
3.1.2.3 <i>Insulin-Like Growth Factor-1</i>	41
3.1.3 Translation from mRNA to protein	45
3.1.4 Research Questions	45
3.2 Molecular Biology Materials	47
3.3 Molecular Biology Methods	49
3.3.1 Tissue Harvesting	49
3.3.2 RNA Isolation.....	49
3.3.3 Polymerase Chain Reaction.....	50
3.3.3.1 <i>Optimising PCR Conditions for Candidate genes</i>	52

3.3.4	Semi-Quantitative Reverse Transcription PCR	54
3.3.4.1	<i>cDNA synthesis</i>	55
3.3.4.2	<i>Optimising Semi-Quantitative RT-PCR</i>	56
3.4	Switching Mechanism at 5' end of RNA Transcript (SMART)	58
3.4.1	Standard SMART Protocol	59
3.4.1.1	<i>Assessing the optimal cycle number</i>	61
3.4.2	Alterations to the SMART protocol	62
3.4.2.1	<i>Synthesising Primers</i>	63
3.4.2.2	<i>Balancing Steps</i>	65
3.4.2.3	<i>Balancing via a Trial 'Dot Blot'</i>	65
3.4.2.4	<i>Multi-blot Replicator Kit</i>	68
3.4.2.5	<i>Gene specific Radioactive labelling and Probing protocol</i>	69
3.4.2.6	<i>Data Analysis and Data Cleaning</i>	71
3.5	Statistical Analysis	74
3.6	Results	75
3.6.1	c-fos	75
3.6.2	Osteocalcin	79
3.6.3	Insulin-like Growth Factor I	82
3.7	Discussion	85
3.8	Conclusions	92

Chapter 4 Morphological Change and Microdamage 94

4.1	Introduction	94
4.1.1	Previous work	94
4.1.2	Fluorescent Markers	95
4.1.3	Research Questions	96
4.2	Materials and Methods	97
4.2.1	Measuring Bone Length and Weight	97
4.2.2	Tissue Infiltration and embedding	97
4.2.3	Slide preparation	102
4.2.4	Morphological Analysis (transmitted light)	102
4.2.5	Morphological Analysis (UV epi-fluorescence)	104
4.2.5.1	<i>Bone Formation Index and formation rates</i>	105
4.2.5.2	<i>Detection of Haversian systems and microcracking</i>	107

4.2.6	Statistical Analysis.....	109
4.3	Results	110
4.3.1	Body Weight Results	110
4.3.2	Humeri Results	111
4.3.2.1	<i>Humeral Gross Morphology Results.....</i>	<i>111</i>
4.3.2.2	<i>Humeri Cross Sectional Area.....</i>	<i>113</i>
4.3.2.3	<i>Humeral Shape.....</i>	<i>115</i>
4.3.2.4	<i>Humeral Epi-Fluorescence Microscopy Results.....</i>	<i>118</i>
4.3.3	Femora Results	125
4.3.3.1	<i>Femoral Gross Morphology Results</i>	<i>125</i>
4.3.3.2	<i>Femoral Cross Sectional Area</i>	<i>127</i>
4.3.3.3	<i>Femoral Shape</i>	<i>129</i>
4.3.3.4	<i>Femoral Epi-Fluorescence Microscopy Results</i>	<i>132</i>
4.4	Discussion	137
4.4.1	Morphology	137
4.4.2	Microdamage	140
4.5	Conclusions.....	143

Chapter 5 Functional Adaptation to Altered Mechanical

Stimuli..... 145

5.1	Introduction.....	145
5.1.1	Biomechanical effects of unloading via spaceflight	146
5.1.2	Effect of unloading via HLS on Bone Mass and Maturation	147
5.1.3	Bone Mineral Density.....	147
5.1.3.1	<i>Measurement of Bone Mineral Density via pQCT and DEXA Scanners</i>	<i>147</i>
5.1.3.2	<i>Using Bone Mineral Density and Content as predictors of Mechanical Strength</i>	<i>148</i>
5.1.3.3	<i>Effect of unloading via Hindlimb Suspension on Bone Mineral Density.....</i>	<i>149</i>

5.1.4	Effect of unloading via Hindlimb Suspension on Biomechanical Strength	150
5.1.5	Research Questions	152
5.2	Materials and Methods	153
5.2.1	Experimental Set-up	153
5.2.2	pQCT Scans	154
5.2.3	Torsion Testing	155
	5.2.3.1 <i>Use of Torsion to determine whole bone strength</i>	155
	5.2.3.2 <i>Positioning Jig and Potting Bones</i>	156
	5.2.3.3 <i>Torsion Rig and Mechanical Testing</i>	157
5.2.4	Data Analysis	159
	5.2.4.1 <i>Correlation between Measured and Calculated Variables</i>	161
	5.2.4.2 <i>pQCT scan data as Predictors of Biomechanical Parameters</i>	164
5.2.5	Statistical Analysis	164
5.3	Results	165
5.3.1	pQCT Results	165
	5.3.1.1 <i>Total Bone Mineral Density</i>	165
	5.3.1.2 <i>Total Bone Mineral Content</i>	169
	5.3.1.3 <i>Cortical Area and Polar moment of Inertia, I_p</i>	173
5.3.2	Torsion Testing Results	176
	5.3.2.1 <i>Biomechanical parameters directly measured</i>	177
	5.3.2.2 <i>Biomechanical parameters indirectly measured</i>	179
	5.3.2.3 <i>pQCT scan data as Predictors of Biomechanical Parameters</i>	180

5.4	Discussion	184
5.5	Conclusions.....	189
Chapter 6 General Discussion		191
6.1	Conclusions.....	195
6.2	Future work.....	197
Bibliography		191
Appendices		219

List of Figures

	Page
Fig. 1.1	Schematic representation of the wall of a long bone diaphysis showing the four types lamellar bone (from Junqueira et al., 1992).....4
Fig. 1.2	Endochondral Ossification (from http://classes.aces.uiuc.edu).....6
Fig. 1.3	Resorption (-) and formation (+) processes in modelling during growth in length (from Jee et al., 1983)8
Fig. 1.4	Schematic representation of a BMU creating a new osteon.....9
Fig. 2.1	Hindlimb suspension cage detailing the 3 components allowing motion.....20
Fig. 2.2	Schematic of Protocol for the Sample Preparation and Use.....26
Fig. 3.1	Mechanism for adaptation for a single loading stimulus:30
Fig. 3.2	AP-1 binding to a DNA strand in order to regulate transcription (http://sitemaker.umich.edu/kerppola.lab/research_interests).....34
Fig. 3.3	Polymerase Chain Reaction (Watson et al., 1994).....51
Fig. 3.4	Osteocalcin PCR product electrophoresed in parallel with a molecular marker of known size (PBluescript & Hae III; lane 1).....52
Fig. 3.5	Demonstrates a gel electrophoresis of β -actin and osteocalcin product amplified up from rat single stranded cDNA.56
Fig. 3.6	Flow chart of SMART synthesis59
Fig. 3.7	Determining the optimal SMART cycle number:62
Fig. 3.8	Alterations to the SMART protocol: Total RNA is converted into single stranded SMART modified cDNA and amplified in a modified PCR.63
Fig. 3.9	Using the Typhoon gel imager to evaluate the storage phosphor screen (http://www1.amershambiosciences.com)67
Fig. 3.10	Balancing Hand loaded Trial dot blot probed with RNRPS9.....67
Fig. 3.11	Multi-blot Replicator flow chart.....69
Fig. 3.12	Gel electrophoresis of amplified PCR products for each of the candidate genes' transcripts.....70
Fig. 3.13	Determining the optimal object size and background correction.....72
Fig. 3.14	Normalised c-fos/RNRPS9 data Vs. Time for the Control and Suspended groups.....76

Fig. 3.15	Normalised c-fos/GAPDH data Vs. Time for the Control and Suspended groups.....	77
Fig. 3.16	Normalised c-fos/Housekeeping data Vs. Time for the Control and Suspended groups.....	78
Fig. 3.17	Normalised osteocalcin/RNRPS9 data Vs. Time for the Control and Suspended groups.....	79
Fig. 3.18	Normalised osteocalcin/GAPDH data Vs. Time for the Control and Suspended groups.....	80
Fig. 3.19	Normalised osteocalcin/housekeeping data Vs. Time for the Control and Suspended groups.....	81
Fig. 3.20	Normalised IGF-I/RNRPS9 data Vs. Time for the Control and Suspended groups.....	82
Fig. 3.21	Normalised IGF-I/GAPDH data Vs. Time for the Control and Suspended groups.....	83
Fig. 3.22	Normalised IGF-I/housekeeping data Vs. Time for the Control and Suspended groups.....	84
Fig. 4.1	Schematic of left upper limb bones; view of lateral surface:.....	99
Fig. 4.2	Schematic of right lower limb bones:.....	100
Fig. 4.3	Trace of femoral periosteal surface (bar = 500µm).....	103
Fig. 4.4	Mid-Diaphyseal transverse cross section of a rat femur under UV Epi-Fluorescence (Bar = 500µm).....	106
Fig. 4.5	Body weights Vs. Time for Control and Suspended groups.....	111
Fig. 4.6	Humeral Weight Vs. Time for Control and Suspended groups.....	112
Fig. 4.7	Humeral Length vs. Time for Control and Suspended groups.....	113
Fig. 4.8	Humeral Total mid-diaphyseal Cross-Sectional Areas Vs. Time.....	114
Fig. 4.9	Humeral Periosteal Cross Sectional Areas Vs. Time.....	114
Fig. 4.10	Humeral Endosteal Cross Sectional Areas Vs. Time.....	115
Fig. 4.11	Humeral Periosteal Circularity Vs. Time.....	116
Fig. 4.12	Humeral Periosteal Elongation Vs. Time.....	117
Fig. 4.13	Humeral Endosteal Circularity Vs. Time.....	117
Fig. 4.14	Humeral Endosteal Elongation Vs. Time.....	118
Fig. 4.15	Humeral Periosteal BFIs Vs. Time (* denotes n < 6).....	119
Fig. 4.16	Humeral Endosteal BFIs Vs. Time (* denotes n < 6).....	120
Fig. 4.17	Humeral Total Bone Formation Index Vs. Time (* denotes n < 6).....	121

Fig. 4.18	Oxytetracycline labelled microcrack (indicated) in the humerus of a suspended rat	122
Fig. 4.19	Calcein blue labelled microcrack in the humerus of a suspended rat.....	123
Fig. 4.20	Control and Suspended Femoral Weights Vs. Time	126
Fig. 4.21	Control and Suspended Femoral Lengths Vs. Time.....	126
Fig. 4.22	Femoral Total mid-diaphyseal Cross-Sectional Areas Vs. Time	127
Fig. 4.23	Femoral Periosteal Cross Sectional Areas Vs. Time.....	128
Fig. 4.24	Femoral Endosteal Cross Sectional Areas Vs. Time.....	129
Fig. 4.25	Femoral Periosteal Circularity Vs. Time.....	130
Fig. 4.26	Femoral Periosteal Elongation Vs. Time.....	130
Fig. 4.27	Femoral Endosteal Circularity Vs. Time.....	131
Fig. 4.28	Femoral Endosteal Elongation Vs. Time.....	132
Fig. 4.29	Femoral Periosteal BFIs Vs. Time (* denotes $n < 6$)	133
Fig. 4.30	Femoral Endosteal BFIs Vs. Time (* denotes $n < 6$)	134
Fig. 4.31	Femoral Total New BFIs Vs. Time (* denotes $n < 6$).....	134
Fig. 4.32	Oxytetracycline labelled <i>in vivo</i> microcrack (indicated) in the femora of a hindlimb suspended rat	136
Fig. 5.1	A drawing by the Italian Galileo Galilei (1564-1642) demonstrating the dimensions of bones from animals of differing weights.....	145
Fig. 5.2	Procedure for evaluating the effect of HLS on the mechanical and structural properties of rat femora	154
Fig. 5.3	Positioning a femur in the Jig and embedding the ends	157
Fig. 5.4	Bone in place in the torsion rig.....	159
Fig. 5.5	Each pQCT scan was used to create a hollow ellipse with equivalent I_p and area values using Matlab	160
Fig. 5.6	Correlation between I_p values measured via pQCT and those calculated in Matlab.....	162
Fig. 5.7	Correlation between Area values measured via pQCT and calculated in Matlab	163
Fig. 5.8	Total Density of Distal slice Vs. Time for Control and Suspended groups	166

Fig. 5.9	Total Density of Mid-Diaphyseal slice Vs. Time for Control and Suspended groups.....	167
Fig. 5.10	Total Density of Proximal slice Vs. Time for Control and Suspended groups.....	168
Fig. 5.11	Total Density of the three combined slices Vs. Time for Control and Suspended groups	169
Fig. 5.12	Total Mineral Content of the Distal Slice Vs. Time for Control and Suspended groups	170
Fig. 5.13	Total Mineral Content of the Mid-Diaphyseal Slice Vs. Time for Control and Suspended groups.....	171
Fig. 5.14	Total Mineral Content of Proximal Slice Vs. Time for Control and Suspended groups.....	171
Fig. 5.15	Total Mineral Content of the three combined slices Vs. Time for Control and Suspended groups.....	172
Fig. 5.16	Cortical Area the of the Mid-Diaphyseal Slice Vs. Time for Control and Suspended groups.....	174
Fig. 5.17	Polar Moment of Inertia of the Mid-Diaphyseal Slice Vs. Time for Control and Suspended groups.....	175
Fig. 5.18	A typical spiral fracture resulting from the destructive torsion test.....	176
Fig. 5.19	Torque Vs. Angular Rotation for 14 Day Control and Suspended Groups (14 day suspended #5 was excluded as it failed at the growth plate).....	176
Fig. 5.20	Maximum Torque Vs. Time for Control and Suspended groups	177
Fig. 5.21	Stiffness Vs. Time for Control and Suspended groups	178
Fig. 5.22	Angular Deformation Vs. Time for Control and Suspended groups.....	178
Fig. 5.23	Maximum Stress Vs. Time for Control and Suspended groups	179
Fig. 5.24	Linear Regression Analysis showing the significant relationship between Bone Mineral Density and Max. Torque ($p < 0.01$, $R^2 = 0.17$).....	181
Fig. 5.25	Linear Regression Analysis showing the relationship between Bone Mineral Content and Max. Torque ($p = 0.06$, $R^2 = 0.09$).....	181
Fig. 5.26	Linear Regression Analysis showing the significant relationship between Bone Mineral Content and Stiffness ($p < 0.05$, $R^2 = 0.13$)	182

- Fig. 5.27 Linear Regression Analysis showing the significant relationship between Mean Cortical Area and Stiffness ($p < 0.05$, $R^2 = 0.10$) 183
- Fig. 5.28 Linear Regression Analysis showing the significant relationship between Mean Ip and Angular Deformation ($p < 0.05$, $R^2 = 0.11$) 183

List of Tables

		Page
Table 3.1	Summary of Critical Factors regulating IGF-I and IGFBPs in Bone Cells (Rodan, 2002)	42
Table 3.2	Oligonucleotide Primer Sequences and their starting positions in their respective genbank sequences	53
Table 3.3	Optimised RT-PCR amplification conditions for candidate genes.	54
Table 3.4	PCR cycle time-points for extracting aliquots of product	57
Table 3.5	SMART primer sequences (V = A, G or C; N = A, G, C or T)	64
Table 3.6	Sequence of probes used for hybridisations	71
Table 3.7	Example demonstrating normalising the comparisons relative to the median of the control group.....	74
Table 3.8	Statistical analysis of the relationships between c-fos and the housekeeping genes with respect to Time and Treatment (ANOVA).....	78
Table 3.9	Statistical analysis of the relationships between osteocalcin and the housekeeping genes with respect to Time and Treatment (ANOVA).....	81
Table 3.10	Statistical analysis of the relationships between IGF-I and the housekeeping genes with respect to Time and Treatment (ANOVA).....	84
Table 4.1	Protocol for dehydration, infiltration and polymerisation of specimens according to Erben (1997)	101
Table 4.2	Concentrations and dosages of fluorochromes and colour under UV epi-fluorescence.....	104
Table 4.3	Fluorochrome sequence and administration schedule.....	105
Table 4.4	Criteria for identifying microcracks in bone (Lee et al., 1998, 2003).....	108
Table 4.5	Humeral crack data. All values are mean \pm standard deviation.	124
Table 4.6	Femoral crack data. All values are mean \pm standard deviation.	136
Table 4.7	Comparison of crack propagation data from various authors	142
Table 5.1	Statistical analysis of the pQCT scan data for BMD and BMC with respect to Time and Treatment.....	173

Table 5.2	Statistical analysis of the pQCT scan data for Ip and Area with respect to Time and Treatment.....	174
Table 5.3	Statistical analysis of the correlation between mean values of BMD, BMC, Ip and Area and the stiffness, maximum stress and maximum torque.....	180

Preface

Hardiman DA. Adaptation of growing bone to mechanical load: an interdisciplinary study. In: Fitzpatrick J, Mallon P (ed) Proceedings of the 3rd Annual Sir Bernard Crossland Symposium (ISBN 1-898012-52-0). Institution of Engineers of Ireland: Dublin 1999 p 45-58

Hardiman, D., Lee, T. and Croke, D. (2000) In vivo mRNA expression of osteocalcin, IGF-I and c-fos in the periosteum and cortex of rat long bones. *Ir J Med Sci* . **169**, 275.

Hardiman, D, Croke, D., Prendergast, P. and Lee, T. (2001) In: *Bioengineering in Ireland 7* (Eds, FitzPatrick, D. and Carr, A.) University College, Dublin, pp. 7. ISBN 1-902277-35-x

Hardiman, D., McWilliam, P., Croke, D. and TC, L. (2001) Analysis of altered gene expression in rat periosteal and bone cortex cells via a novel application of SMART cDNA synthesis. *J Ir Coll Phys Surg*, **30**, 168.

Hardiman, D., Croke, D., Prendergast, P. and Lee, T. (2002) Morphological change in a disuse osteoporosis model in rats: Hindlimb suspension. In: *Bioengineering in Ireland 8: Proceedings of the 8th Annual Conference of the Section of Bioengineering of the Royal Academy of Medicine in Ireland and the 16th Meeting of the Northern Ireland Biomedical Engineering Society* (ISBN 1-902277-57-0) (Eds, FitzPatrick, D., McCormack, B.A.O. and Dickson, G.) University College Dublin, p. 60.

Hardiman, D., Croke, D., Prendergast, P. and Lee, T. (2003) The SMART protocol and small scale cDNA arrays. In: *Bioengineering in Ireland 9: Proceedings of the 10th Annual Conference of the Section of Bioengineering of the Royal Academy of Medicine in Ireland* (Eds, FitzPatrick, D., McCormack, B.A.O. and McCormack, D.) (ISBN 1-902277-72-4) University College, Dublin, p. 22

Hardiman, D., Croke, D., Prendergast, P. and Lee, T. (2004) In *Bioengineering in Ireland 10: Proceedings of the 10th Annual Conference of the Section of Bioengineering of the Royal Academy of Medicine in Ireland* (ISBN 1-902277-) The Changing Faces Of Disuse Osteoporosis: Morphology, Structural Strength And Gene Expression University College, Dublin p 56

O'Brien, F.J., Hardiman, D.A., Hazenberg, J.G., Mercy, M.V., Mohsin, S., Taylor, D. and Lee, T.C. (2004) The behaviour of microcracks in compact bone. *European journal of Morphology* (In Press)

Acknowledgements

Well, I finally got there and as with anything difficult that takes this long, there are an innumerable amount of people who have helped me along the way. However, I would like to single out the following for special praise or remarkable perseverance:

First and foremost, I would like to thank Clive Lee for his constant unwavering support and generally constructive criticism over this long and circuitous route to finality. The book has arrived even if it's a little late for your daughter's birthday. Thanks a lot for everything over the last few years.

I am also indebted to everyone else who I've had the pleasure of working with in the department of Anatomy/Biology. I've been there so long it's a long list so I hope it's a complete one. Thanks to Peter K, Peter S, Terry, Vincent, Stanley, Fergal, Lorraine, Sinead, Alec Elliot and Alice.

As for the lads who I shared the post-graduate room with in my time here. Great craic was had. Thanks Jan, Matt, Johnny, Maeve, Conor, Paul Keogh, Oran, Noortje and Orlaith.

I'd also like to thank Raffaat for his help in the making of the histological slides and Johnny who helped with the animal work with such enthusiasm and speed. My gratitude also to Dr. Anthony Staines for his help with the statistical analysis.

To all those in the Biochemistry department of the Royal College of Surgeons: You have taken an engineer into your midst and tried your hardest to beat the mechanics out of him. In particular, thanks to David Croke who was always there, when I had yet another of my endless supply of basic molecular biology questions. Thanks for your patience and guidance. As for Orna, Donncha and Peter McWilliam, you guys were superb teachers and a great laugh. Thanks for all the 'Biochem' lessons. Thanks also to those, past and present, who've had the undoubted pleasure of working beside the flurry of annoyance that was me during my time in the lab. To those who beat me to the finish line: Eilis (Peahead) Foran, Freeley (who just beat me...well by a year), Flanagan, Olive, Sylvia (ooh lala), Catherine and Keith. And to those left behind who'll get there eventually: Heidi (full faith in ye), Frances (you can relax soon). Thanks also to the rest of Biochem: Aideen, Belinda, Jim and Paddy.

Despite my physical isolation from Trinity there are people there I also wish to thank. In particular I'd like to thank Paddy Prendergast for his help in the mechanical side of the

project and for asking awkward questions now and again to keep me on my toes. Thanks also to David Taylor, Peter O'Reilly and Gabriel for the help and assistance. Of course, thanks also to the lads both in Dublin and around the country and world. There's far too many of you to mention everyone so here's some that come to mind: Paddy, Neil, Cormac, Maz, Richie, Brian, Fionuala, Mick, Pauline, Al, Ed, Marcus, Helen, Ronan, Emma, Rowena, Michelle, Vinny, Phil, Aoife, Joanne, bella and Sara. In addition, thanks to Maeve, Jan, Matt, Heidi, Frances, Michael and Eilis, who have each in their individual ways made coming into work just that little bit easier. Hope to stay friends for a long time to come. Maeve and Jan deserve extra brownie points for always being there when needed and for knowing when to just let things lie. Of course I also want to thank my family for being there for me throughout this work. You made this possible. Thanks for everything Dad, Mam, Sue and Jay. And so it comes to Claire. What perseverance. Thanks for all the support, encouragement and for knowing when to just let me rant on about my 'love of Mol Biol'. You played a starring role! Thanks babe. In the end, I dedicate this thesis and all that's in it to Claire, my parents and especially to my two grans, Hardiman and Hudson, who passed away during the course of the PhD. Love always and R.I.P.

"If we knew what it was we were doing, it would not be called research, would it?"
Albert Einstein (1879-1955).

"If the study of all these sciences which we have enumerated, should ever bring us to their mutual association and relationship, and teach us the nature of the ties that bind them together, I believe that the diligent treatment of them will forward the objects into view, and that the labour, which otherwise would be fruitless, will be well bestowed."
Plato (BC427? – BC347?)

And something a little more low-brow:

"The average human has about one breast and one testicle."

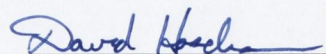
Statistics 101

I gratefully acknowledge the financial support of the Health Research Board and Department of Anatomy of the Royal College of Surgeons in Ireland

Declaration

I declare that I am the sole author of this thesis and that all the work presented in it, unless otherwise referenced, is my own. I also declare that this work has not been submitted, in whole or in part, as an exercise for a degree or qualification at any other University.

I agree that the library of the University of Dublin may lend or copy this thesis upon request.



David Hardiman

October 17, 2003

Summary

Osteoporosis, a condition characterised by a loss of bone mass, is of increasing clinical interest in an aging population. Bone formation and growth are controlled by genetic, hormonal and biomechanical factors. This multifactorial regulation is present *in utero* with mechanical loading critical in regulating skeletogenesis. After birth, growth and ossification are strongly influenced by physical activity and externally applied forces. Clinically, reduced loading may occur due to bed-rest, paralysis or stress shielding around implants while overloading may lead to differential growth and skeletal asymmetry.

This study investigated the effects of altering the mechanical load applied to the long bones of growing rats. An established rat disuse osteoporosis model, hindlimb-suspension, was used, whereby traction tape along the tail elevated and unloaded the hindlimbs while maintaining weight-bearing forces on the forelimbs. The main aims of this interdisciplinary study were to investigate the relationships between gene expression, bone formation and structural strength in unloaded bones. Differences in bone shape, quantity and quality were measured in the proximal halves of the right femora. This was achieved by labelling new bone with fluorescent agents, embedding the bone in PMMA and making cross sectional slides for histological analysis. The distal halves of the femora were used to detect gene expression in samples of periosteal tissue. Patterns of gene expression were assessed using the SMARTTM protocol to amplify all populations of mRNA to levels where they could be assessed using standard molecular biology protocols. This indicated which genes were 'switched on or off' as a result of the unloading. Finally, the left femora were assessed at three points along their lengths using a pQCT scanner prior to a destructive torsion test. Combining these data enabled the effect of unloading on the bones' structural and mechanical properties to be determined.

Hindlimb suspension reduced the periosteal bone formation rate and the total amount of bone present at the mid-diaphysis of the femora. *In vivo* microdamage was found in rat humeri and femora under control conditions using two fluorochromes, oxytetracycline and calcein blue. Unloading via suspension resulted in a site-specific reduction in bone mineral density, measured via pQCT, in the femora. Loss of density was greatest at the distal scan site, which contained most trabecular bone. In addition, following the torsion tests, there was a significant reduction in the maximum torque and stiffness values in the suspended femora. The relationships between the pQCT scan parameters and the mechanical properties were also assessed, with BMD found to best predict mechanical strength while I_p and area best predicted stiffness. A new method of gene expression analysis, involving the creation of SMARTTM cDNA arrays, was successfully implemented. Gene expression patterns of three candidate genes, c-fos, osteocalcin and IGF-I, were assessed in periosteal tissue. Altered gene expression patterns were identified and tracked over the suspension period with altered levels in osteocalcin and c-fos found consistent with the changes observed in the histological analysis.

This system allowed the hypothesis of functional adaptation to be tested i.e. that altered load results in a drive for adaptation, which in turn results in altered gene expression patterns that alter the cellular phenotype and thus change in the bones morphology and structural properties. This study acts as a template for further research into the effects of altered load on the skeleton and enables tissue specific analysis to be conducted.

Nomenclature

α	= Alpha
ψ	= Angular deflection [Radians]
β	= Beta
κ	= Effective torsional constant of non-prismatic hollow ellipse
π	= Pi = 22/7
μm	= metre x 10^{-6}
μg	= gram x 10^{-6}
τ_{max}	= Maximum shear stress [Nmm^2]
ANOVA	= Analysis of variance
BFI	= Bone formation index
BMC	= Bone mineral content [mg/cm^3]
BMD	= Bone mineral density [mm^3]
Ca	= Calcium
cm	= metre x 10^{-2}
CSA	= Cross sectional area
CSMI	= Cross sectional moment of inertia
DEXA	= Dual energy X-ray absorptiometry
g	= gram
G	= Shear modulus [N/mm^2]
HCl	= Hydrochloric acid
HLS	= Hindlimb suspension
IGF-I	= Insulin-like growth factor I
I_p	= Polar moment of area [mm^4]
K	= Torsion constant
Kb	= Kilo bases (~ nucleotide bases X 10^3)
L	= Length of bone segment to be tested [mm]
l	= litre
m	= metre
mg	= grams x 10^{-3}
MgCl_2	= magnesium chloride
ml	= litre x 10^{-3}

mm	= metre x 10^{-3}
NaOH	= Sodium Hydroxide
nm	= metre x 10^{-9}
pM	= Molar x 10^{-12}
pQCT	= Peripheral quantitative computed tomography
T	= Torsional moment [Nmm]
vCTBMD	= volumetric cortical bone mineral density [mm^3]

Chapter 1 Introduction

1.1 Overview

A commonly held misconception is that bone is a simple and dead material. The truth is that bone is a complex multifunctional tissue, which is constantly changing. Allied to this is an in-built ability to adapt to changing mechanical environments and to repair itself when necessary (Lee and Taylor, 1999). This intrinsic capacity to change shape is vital if the bone is to fulfil its constantly changing structural role over the life of an individual and was first described in 1892 by a German called Julius Wolff (1836 – 1902)(see section 1.3). This process by which bone adapts to its mechanical history is now generally known as functional adaptation, a term proposed by Roux (1895). Mechanically, adaptation works to continually tailor the bone to the loads placed upon it, an example of which would be the increased bone mass in tennis players' dominant arms (Jones et al., 1977).

Clinically, this causes problems when the mechanical force necessary to maintain bone mass is removed. This commonly occurs in illness (bed rest, paralysis) or when bone around prosthetic implants is stress shielded. In these cases, the loads applied to the bones are significantly reduced and resorption occurs to adapt the bone to this new loading regime. In extreme cases this can lead to the prosthesis becoming loose and needing to be revised. A further complication occurs when normal loading is resumed following prolonged periods of bed rest and paralysis, where fractures can take place (Kavanagh et al., 1989, Krolner et al., 1983).

The effects of altering the load on bones have been extensively studied. Underloading causes a reduction in cross-sectional area (Spengler et al., 1983, Uthoff and Jaworski, 1978) but has little effect on bone length (van der Meulen et al., 1995). Studies on overloaded bones have been equivocal, with some showing an increase and others a decrease in mechanical strength (Biewener and Bertram, 1994, Lee et al., 2002, Matsuda et al., 1986). However, these differences may be due to the large variety of test set-ups, types of bones and subjects used to create a situation of overload. Despite this work, the mechanisms by which bone adapts to altered mechanical load remains

unclear. In this study the relationships between mechanical load, gene expression and morphological change within growing long bones were examined.

1.2 Introduction to Bone

Bone is the main constituent of the human skeleton and it plays a number of vital roles:

- Support. Bones provide structural support and act as a framework for the attachment of soft tissues and organs.
- Leverage. By providing sites of attachment for muscles, bones act as levers that multiply the forces generated in muscle contraction and allow movements ranging from the delicate motion of a fingertip to movements of the entire body.
- Protection. Bones protect soft tissues and organs from injury. For example, the ribs protect the heart and lungs, the skull protects the brain and vertebrae shield the spinal cord.
- Storage and release of minerals and lipids. Bone contains a large amount of valuable minerals such as calcium, carbonate and phosphorus, which must be kept at critical levels within the body. In order to maintain the correct mineral balances within the body, bone can act as a storehouse releasing these minerals into or absorbing them from the blood. In addition the bones store lipids in areas of yellow marrow as energy reserves.
- Site of cell production. Within certain bones, the red marrow that fills the internal cavities of bones produces blood cells.

Bone is a supporting connective tissue and contains specialised cells and a matrix consisting of extracellular protein fibres and a ground substance. Bone is comprised of four cell types and an intercellular calcified matrix made up of organic matrix, mainly collagen, and inorganic hydroxyapatite (Schiller, 1994). The four cell types are the osteoprogenitor cell, the osteoblast, the osteocyte and the osteoclast. The first three have the same embryological origin and transform from one to the other in relation to their functional activity. Osteoprogenitor cells line the bone surfaces and differentiate into osteoblasts in response to an appropriate signal, such as increased mechanical loading. Osteoblasts are responsible for the formation of new bone tissue, or osteoid, and communicate via gap junctions. Approximately 10–20% of osteoblasts surround themselves with newly secreted osteoid and their level of activity diminishes. These cells communicate via cell processes in canaliculi in the mineralised osteoid and are

termed osteocytes. Because of this network of cells within the matrix, osteocytes are thought to be the primary sensors of mechanical loading in bone (Lanyon, 1993, Cowin et al., 1991, Skerry et al., 1989). The fourth cell type is the osteoclast. These are large motile cells involved in bone resorption (Schiller, 1994).

1.2.1 Bone Structure

Bone can be simply subdivided based on its apparent density or volume fraction, the ratio of bone mass to total volume, with bone greater than 0.7 units termed cortical or compact bone while that less than 0.7 is termed trabecular or cancellous bone (Gibson and Ashby, 1988). The biochemical composition of cortical and trabecular bone is the same and they are differentiated on the basis of density and three-dimensional arrangement of lamellae, canaliculi and osteocytes.

Histologically bone can be divided into two main types, woven and lamellar bone (Schiller, 1994). The rate of bone formation determines which type is laid down. Primary or woven bone contains numerous osteocytes, has a disorganised or random structure of collagen fibres and thus fairly isotropic material properties. Woven bone is rapidly deposited and this immature bone is also the first type of bone laid down during fracture healing. During maturation, woven bone is replaced in a process called remodelling. This mature bone has an obvious lamellar structure (see Figure 1.1) and thus has anisotropic material properties.

There are four types of lamellar bone:

- Circumferential bone: consists of lamellar sheets of bone arranged around the outer periosteal and inner endosteal surfaces.
- Concentric bone: consists of concentric rings of lamellar bone arranged around a central canal. An osteon consists of a central canal, which contains the vasculature and nerves, surrounded by concentrically arranged lamellae containing embedded osteocytes.
- Interstitial bone: represents the remnants of old circumferential or concentric bone which are situated between existing osteons.
- Trabecular bone: consists of a network of struts called trabeculae. The osteocytes within these trabeculae receive nutrients by diffusion along canaliculi

that open to the surface of the bone and therefore the thickness of the trabeculae is controlled by their need for nourishment.

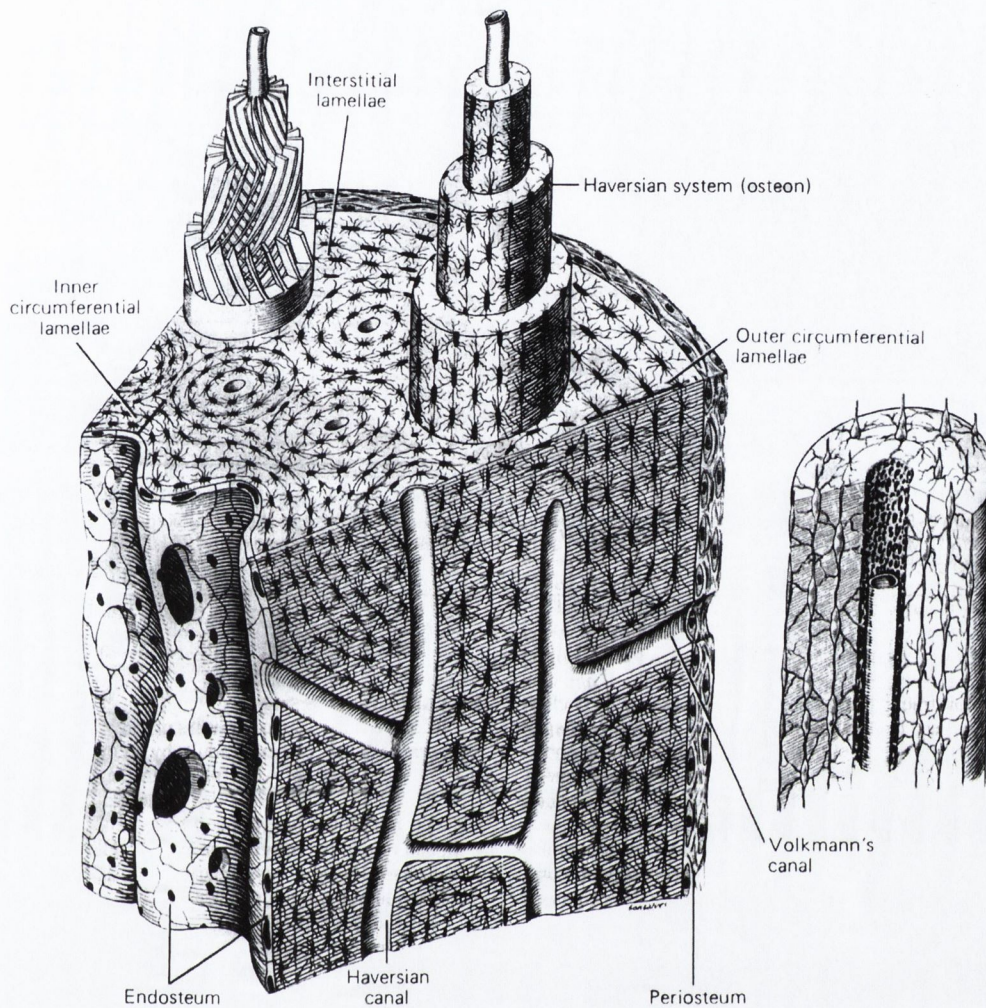


Fig. 1.1 Schematic representation of the wall of a long bone diaphysis showing the four types lamellar bone (from Junqueira et al., 1992)

The first three types of lamellar bone form within the bone cortex, with osteons only forming when an appropriate stress is present or when the bone has grown to a size where the bone wall thickness requires a secondary vascular structure to get nutrients into the cells. In this sense, rodent bone can often be described as acting as a single osteon. Osteons are normally aligned parallel to each other along the plane of principal stress, so in the diaphysis of long bones the osteons are arranged parallel to the long axis of the bone. In general, compact bone is found along the diaphysis or shafts of long

bones where stresses arrive from a limited number of directions. In addition, trabecular bone sites are encased in a thin cortical bone shell.

Trabecular bone is generally located in regions of bone where the stresses are low and where the stresses are coming from many different directions. Trabeculae are formed during the ossification of the growth plate and are associated with increases in bone length following the division and hypertrophy of enlarged chondrocytes. Trabecular bone is lighter than cortical bone and so reduces the weight of the skeleton making it easier to move and also provides a framework for red bone marrow to produce blood cells. Skeletally, trabecular bone is found in the vertebrae, the pelvis and at the metaphyses and epiphyses of long bones such as the femur. Trabecular bone is always covered with a thin cortical bone shell.

With the exception of joint cavities, the outer surfaces of all bones are covered with a tissue layer known as the periosteum. The periosteum is made up of two layers, a fibrous outer layer and a cellular inner layer, and separates the bone from the surrounding tissues. It also participates in circulatory and nervous supply and plays an active role in bone growth and repair. A cellular layer called the endosteum also covers the inner surface of bone. Both the periosteum and endosteum are made up of a layer of flattened osteoprogenitor cells, osteoblasts and occasionally osteoclasts. When the periosteum and endosteum are active during bone growth, repair and remodelling, the osteoclasts or osteoblasts in these layers can act to either resorb or deposit bone. Osteoprogenitor cells also line the canals at the centre of osteons running parallel to the bones long axis (Haversian canals) and tangential canals (Volkmann's canals) (see Figure 1.1).

1.2.2 Bone development and Growth

Ossification is the process by which other tissues in the body are replaced by bone. Calcification, the deposition of calcium salts, occurs in ossification but can also occur in other tissues (such as calcified cartilage). Bone can be formed in two ways, intramembranous and endochondral ossification.

In intramembranous ossification, bone forms directly from a vascularised connective tissue membrane. It is initiated when mesenchymal cells cluster together to form a dense cellular membrane. Blood vessels then invade the space within the membrane and

an ossification centre forms in this newly vascularised region. These cells initially differentiate into osteoblasts, which form a layer of osteoid, which is later mineralised. Examples of bones formed by intramembranous ossification include the bones of the skull and the clavicle (Schiller, 1994).

Endochondral ossification is the process by which most of the bones in body, including those involved in this study, are formed. This is best explained by using the embryonic development of a limb as an example (see Figure 1.2).

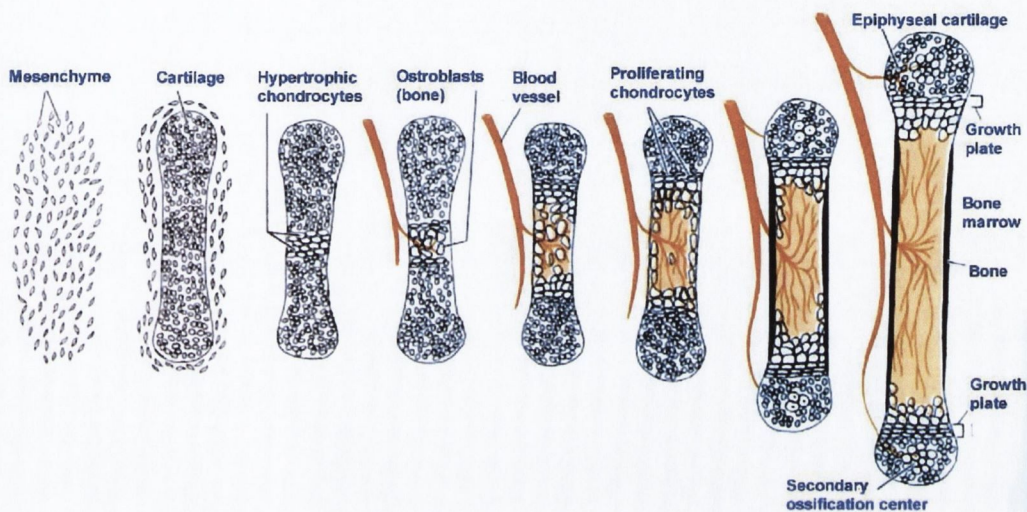


Fig. 1.2 Endochondral Ossification (from <http://classes.aces.uiuc.edu>)

At approximately 5 weeks gestation a model of the bone, called the anlagen, is formed entirely of hyaline cartilage. This cartilage model grows by expansion of the cartilage matrix already present, interstitial growth, and by the laying down of new cartilage at the surfaces, appositional growth. As the anlagen grows, the chondrocytes (cartilage cells) in the centre enlarge or hypertrophy. These enlarged cells expand their lacunae and the matrix is reduced to a number of struts, which then calcify depriving the cells of nutrition and starving them to death. Blood vessels enter the perichondrial layer around the cartilage and the inner osteoprogenitor cells from the perichondrium differentiate into osteoblasts. The perichondrium is now referred to as the periosteum and the osteoblasts soon produce a thin layer of bone around the shaft of cartilage. Blood vessels and stem cells now penetrate the calcified cartilage core from the periosteum. Endochondral ossification now occurs whereby the calcified cartilage matrix is resorbed by osteoclasts and newly differentiated osteoblasts replace it with woven bone. This site

is known as the primary ossification centre and ossification spreads out from this centre towards the ends. As the ossification front approaches the metaphysis, a secondary ossification centre will often form in the centre of the cartilaginous epiphyseal ends and a new ossification front will begin to move towards the primary front. During growth the model is not completely ossified and a region of cartilage at the physis or growth plate, where the two ossification fronts meet, continues to grow. As the bone diameter enlarges, the central region of the shaft is eroded away by osteoclasts and replaced by vasculature and bone marrow (Schiller, 1994).

After this initial embryonic development, further growth in long bones involves two distinct processes, increasing the length and enlarging the diameter. The presence of this cartilaginous growth plate allows growth in length by endochondral growth i.e. continual growth of cartilage and its subsequent replacement by bone. Growth in diameter or radial growth is achieved intramembranous ossification under the periosteum. As this bone is being added at the periosteum, resorption of the endosteal surface also occurs resulting in a larger internal diameter.

1.2.3 Modelling

As bones develop, their shafts must grow in length and diameter. However, it is not sufficient to simply add material to make the bones longer and wider, the bones gross shape must be controlled. This means bone must be added in some regions by the action of osteoblasts, and removed in others by osteoclastic action. This process is called modelling (see Figure 1.3).

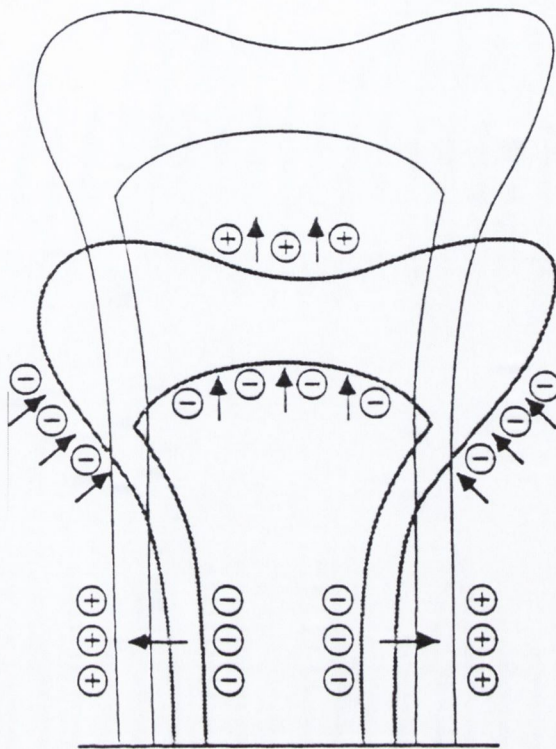


Fig. 1.3 Resorption (-) and formation (+) processes in modelling during growth in length (from Jee et al., 1983)

During growth and development modelling involves rapid bone turnover which leads to the required changes in shape and size. However, once the skeleton is mature the rate of modelling slows down to very low levels. The exception to this is fracture healing which by necessity requires a rapid response. It is important to note that modelling can be a prolonged process involving the independent actions of osteoclasts and osteoblasts at different sites.

1.2.4 Remodelling

Remodelling is a coupled action of osteoclasts and osteoblasts, which results in the removal of a portion of old or damaged bone and replacing it with newly formed bone. Initially the function of remodelling is to replace immature woven bone with mature structured lamellar bone. Once this has been done, remodelling continues but its function now is to repair and maintain the bone. This process prevents the accumulation of fatigue damage, which could lead to a fatigue fracture. In addition to this,

remodelling acts to adapt the bones internal microstructure to adapt to changing loading conditions (Martin et al., 1998).

Remodelling is a coupled action of a number of osteoclasts and osteoblasts, which collectively are known as a basic multi-cellular unit, BMU. A BMU remodelling cycle has three principal stages, activation, resorption and formation, ARF (Frost, 1987, Frost, 1986). Activation involves a signal being sent which causes osteoclasts to form and begin to resorb an area of bone around 200 μm in diameter on the surface of the bone. In trabecular bone the hollow (Howship's lacuna) moves along the surface, while in cortical bone the osteoclasts erode a tunnel (cutting cone) into the bone cortex (see Figure 1.4). The BMU erodes bone at a rate of around 40 μm a day. After a region has been resorbed and the osteoclasts have moved on, osteoblasts differentiate from mesenchymal cells and start to lay down new bone to replace the bone previously resorbed by the osteoclasts. However resorption is a faster process taking around three weeks compared to the three months for the osteoblasts to refill the site. In cortical bone, a BMU must maintain a supply of nutrients to the eroding osteoclasts deep within the cortex and so the osteoblasts do not completely fill in the hole eroded by the osteoclasts. As a result each newly laid down region of lamellar bone, or osteon, has a canal at its centre which contains blood vessels.

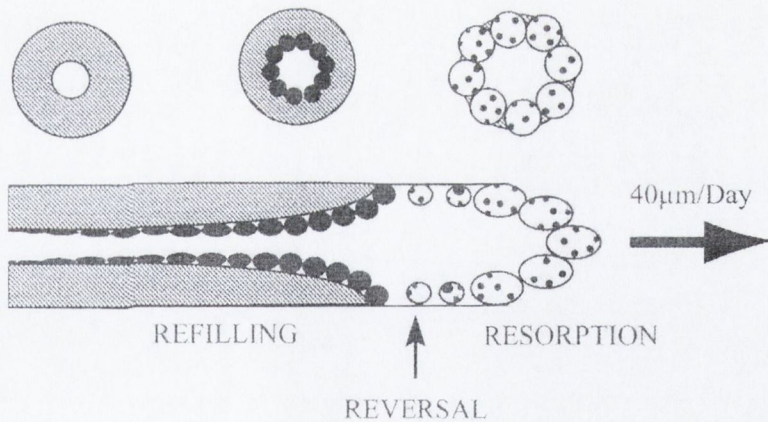


Fig. 1.4 Schematic representation of a BMU creating a new osteon. The large multinucleated cells to the right are osteoclasts; smaller cells (in black) are osteoblasts. Cross-sectional views are shown above. Not to scale (Martin et al., 1998).

In healthy young bones there is no net loss in bone mass as a result of remodelling. However in older individuals the volume of bone produced is often less than that resorbed leading to a net loss in bone mass. This is one of the mechanisms involved in osteoporosis (Parfitt et al., 1996).

1.2.5 Microdamage

A large number of mechanisms have been proposed as the stimulus for remodelling and adaptation. These include strain magnitude (Frost, 1992) and rate (O'Connor et al., 1982, Mosley and Lanyon, 1998), piezoelectric currents (Bassett, 1968), shearflow (Weinbaum et al., 1992), strain energy density (Huiskes et al., 1987) and microdamage (Burr and Martin, 1993, Martin, 2000, Lee et al., 1999, Lee et al., 2002, Schaffler et al., 1995, Prendergast and Taylor, 1994). The idea of microdamage, in particular, has a number of positive attributes in that it should produce an optimal level of remodelling, by balancing the need to maintain mechanical integrity while removing dangerous microcracks. In addition, microdamage would allow for targeted repair, where resorption can be stimulated to initiate at sites where microdamage is reaching critical levels. In fact, Martin and Burr (Martin and Burr, 1989) have shown, by observing the location of microdamage and resorption cavities, that it is 4-6 times more likely that microdamage triggers targeted repair than that of a random distribution of resorption cavities. Bentolila *et al.* (1998) showed in cyclicly loaded rats ulnae produced microdamage which in turn was associated with the creation of resorption cavities. In fact, all 14 of the 16 animals which had microdamage also had an increased number of resorption cavities, while the 2 remaining animals which had no microdamage also had no increase in resorption cavities. Finally, work by Noble et al. (2003) has suggested that regions of cellular apoptosis are found in regions of bone containing microdamage. One possible theory then, is that microdamage results in the apoptosis of adjacent cells, which in turn serves as a trigger for osteoclasts activity and remodelling.

1.2.6 Cell signalling and gene expression

Fundamental to the idea of controlled remodelling and adaptation is the concept that cells are directed and controlled by both systemic factors and local effects, such as mechanical loading and microdamage. As a result of these factors, cells respond by altering their gene and protein expression patterns and consequently their phenotype is altered (see section 3.1.1). This response could take the form of a positive signal or a negative one. In the positive case, following a signal, such as a reduced mechanical load, cells in the immediate environment will react by signalling osteoclasts to come and resorb unnecessary bone. The alternative is that the cells are constantly sending out an inhibitory or controlling signal to inhibit osteoclasts activity. Following the signal, these cells stop producing this inhibitory signal and osteoclasts move into the area and resorb unnecessary bone. Determining what stimulatory or inhibitory signals are being produced by the cells is vital to gaining a greater insight into the interactions between cells and their environment. This requires the gene and protein expression patterns of cells undergoing an altered environment to be assessed relative to those of a control group.

1.3 Clinical Applications

As described earlier, functional adaptation can lead to clinical problems such as the loosening of prostheses. Joint prostheses, are among the most successful orthopaedic procedures performed, with 541,245 total hip and knee replacement operations performed in the United States alone in 1999 (Mendenhall, 2000). In total hip replacement, a metal femoral stem is inserted into the medullary cavity of the proximal femur. This results in a stress reduction of around 60% in the proximal femur (Jacob and Huggler, 1980). As a result of this reduced stress, bone is resorbed from this region and the metal stem can become loose. This is substantiated by radiographic evidence of resorption at the bone-cement interface reported as early as 13 months post-operative.

Unfortunately, in cases where this resorption becomes advanced, the prosthesis may cease to function correctly and revision may be required. The size of the problem is evident from a study by Poss et al. (1984), who reported that up to 25% of total hip arthroplasties had femoral component loosening five years after the operation. In a 15 year review, carried out at the Mayo clinic, the probability of loosening of Charnley

total hip arthroplasty was estimated at 26% with around 10.9% requiring revision (Kavanagh et al., 1989). With a ageing world population, demographic trends predict the number of hip fractures in the US will triple by 2040 from an estimated 1.7 million in 1990 to 6.3 million in 2050 (Melton, 1996). Consequently, a significant rise in the number of hip arthroplasties can be expected.

1.4 Wolff's Law

The skeleton is able to withstand the external loading placed upon it because the modelling and remodelling processes ensure that each bone is functionally adapted to the loads placed upon it. Since bone is not simply a structural material, this adapted shape must be a compromise between structural properties (mass, strength and stiffness), metabolic functions (mineral storage and release) and tissue economy (reduced energy expenditure and weight). This relationship between form and function was described in 1892 by a German surgeon called Julius Wolff (1836 – 1902). In his book, *Das Gesetz der Transformation der Knochen* (Wolff, 1892) Wolff outlined his law of bone adaptation as:

“the alterations of the internal architecture clearly observed and following mathematical rules, as well as secondary alterations of the external form of the bones following the same mathematical rules, occur as a consequence of primary changes in the shape and stressing... of the bones” (Wolff, 1892, Lee and Taylor, 1999).

The structural behaviour of a long bone is a function of both its geometry and material properties. Although there has been some debate (Woo et al., 1981) it is now generally accepted that adaptation due to altered *in vivo* loads result in changes in geometry (cross sectional area, cortical thickness) material properties (bone mineral density) and mechanical properties (such as stiffness) (Amtmann and Oyama, 1976, Amtmann and Oyama, 1973).

Skeletal adaptation has been reviewed by a number of authors (Currey, 1984, Fyhrie and Carter, 1986, Lanyon, 1984, Rubin, 1984) and a variety of models have been proposed to explain it. Most of these models work on the premise that the bone responds by adaptation in order to keep some variable within set limits. When the variable moves outside the limits as a result of a change in the mechanical loading pattern a local signal is sent out to begin a remodelling cycle and adapt the bone to bring

the variable back within acceptable limits.(Gross and Rubin, 1993, Rubin and McLeod, 1994, Rubin et al., 1990). However, until the fundamental mechanisms by which bone responds to mechanical stimulation are known, it will be impossible to create a conclusive model to predict changes in bone properties.

In a normal skeleton adaptation due to changes in loading continues throughout life. However in a growing skeleton, the large increase in body size and the forces this generates must be taken into account and added to the forces experienced during normal physical activity. During growth, a bone's response to altered mechanical loading is more evident and occurs more quickly due to the fact that the bone is already biologically active (Carter, 1984). Once skeletal maturity has been reached, and body size stabilises, changes in loading conditions due to exercise become more important. If, as Wolff's Law predicts, bone adapts to the loading scheme placed upon it then bone mass should reflect loading history.

1.5 Observational studies

The belief that mechanical load is a prerequisite for maintaining bone mass has been substantiated by a number of experiments comparing levels of in groups with different functional activity. One approach has been to compare elite or chronic exercisers with sedentary age-matched controls. Compared to sedentary controls, chronic long distance runners have increased calcaneal bone mineral density, BMD, (Dalen and Olsson, 1974) and vertebral trabecular BMD (Lane et al., 1986, Marcus et al., 1985). Researchers have also investigated the effect of more moderate activity levels on bone mass but found only small differences between moderate exercisers and sedentary controls (Heinonen et al., 1995). For example, when casual runners were compared to sedentary controls there was only a limited effect on bone mineral density (Kirk et al., 1989).

Contrary to this, a number of reports document increased bone mass in subjects with lifetime physical activity patterns compared to sedentary controls (Greendale et al., 1995, Astrom et al., 1987). For example, Greendale et al. (1995) reported a significant increase in BMD at the hip in a group of older men and women who had higher levels of exercise in their youth, compared to a more sedentary group. One of the main problems with evaluating moderate changes in loading levels is ascertaining exactly what the current and raised activity levels are. Cross-sectional comparisons of athletes

compared to sedentary controls must also be viewed with caution. Since no measurements of bone mass are made prior to the exercise program, the increased bone mass cannot be conclusively linked to an increase in exercise and it is possible that these individuals are more likely to succeed at athletic sports because they have higher bone density. In addition, this simplified view takes no account of healthier diets and increased aerobic fitness and circulatory function.

An interesting case for examining different loading states can be seen in comparing the dominant to non-dominant limbs of athletes involved in sports with unilateral loading. A number of different researchers have examined the dominant forehands of professional tennis players and reported increases in humeral cortex thickness of around 30% (Dalen et al., 1985, Jones et al., 1977, Heinonen et al., 1995).

Studies of reduced mechanical load in humans have centred on two groups: Those confined to bed rest for long periods of time and astronauts. The effect of removing weight-bearing forces by confining patients to bed rest has been examined in a number of studies. There is considerable evidence that bed rest can result in deleterious, negatively balanced bone adaptation. Bed rest studies have consistently shown increased urinary and faecal calcium producing a negative calcium balance within the body which reaches a plateau between 4 and 6 weeks (~180mg/day) and remains negative as long as bed rest continues (up to 36 weeks) (LeBlanc et al., 1995). Concomitant measurements of the bone mineral density in the spine, femur neck, trochanter and pelvis showed a reduction of between 0.9% and 1.3% per month (LeBlanc et al., 1995). This figure rose to a 0.9% reduction per week in vertebral bone mass in a similar study on confined bed rest by Krolner et al. (1983).

Early on in the space program it was recognised that, as a result of reduced gravity in space, the bones of astronauts lost mass. However since it was seen to be a relatively slow process, it is only with the prospect of long duration space flights that research into its effects was initiated. During the three manned Skylab flights lasting 29 to 84 days, crew members demonstrated negative calcium balance which reached around 300 mg/day by 84 days of weightlessness (Rambaut et al., 1979, Rambaut and Johnston, 1979). Using a device designed by Vogel and Anderson (1972) to measure bone mineral density, it was shown that bone mass was not lost equally from all parts of the skeleton and that large differences were to be found between individuals. Later joint studies between NASA and the Russian space agency demonstrated mean bone mineral density

losses in the spine, femur neck, trochanter and pelvis of 1% to 1.6% per month and 0.3 to 0.4% per month from the legs and body although large differences were again noted between individuals (LeBlanc et al., 1996). More recent flights do not show the substantial losses in bone mineral content found earlier but flights now always include countermeasures such as resistance training. These limited data are however, enough to demonstrate that over long periods of weightlessness a significant reduction in skeletal mass can occur. This could result in renal problems, primarily stone formation, and also providing insufficient structural support following reloading in a normal gravity environment.

1.6 Experimental studies

The effects of mechanical loading have been extensively examined in long bones. Most researchers have used young but skeletally mature animals as immature bones are more sensitive to changes in load than mature bones (Jaworski et al., 1980). Loading has been increased by a variety of methods including removal of an adjacent bone (bone resection), externally applied forces, centrifugation and exercise regimes. Decreasing loading has been studied using two main methods, immobilisation and unloading. Immobilisation can be achieved via surgical or drug induced paralysis and by non-invasive casting. Unloading has been achieved by space flight and hindlimb suspension. It must be noted that when decreased or increased loading is applied during skeletal development the underlying growth related changes must be taken into account. Therefore, a basal control group must also be included in any experiment using growing animals, in order to determine whether a reduction in a measured parameter is due to an actual decrease or a reduction in the normal level of growth.

1.6.1 Increased loading

Researchers have generated increased load by a variety of different methods. These have included exercise, externally applied static and dynamic loads, overloading a bone by surgically removing an adjacent bone (resection) and by centrifugation. Studies of increased loading in young, growing animals have yielded mixed results with some showing enhanced (Saville and Whyte, 1969, Biewener and Bertram, 1994) and others diminished (Gordon et al., 1989, Li et al., 1991) mechanical properties. Exercise has its

advantages in that it will load the bone in a physiological manner (direction and magnitude). However, the exact loading is not known and thus it is difficult to relate loading to changes in the bone. The loading must also be significantly greater than that normally experienced and the animals' level of activity post exercise should not be diminished. For example, Woo et al. (1981) ran young adult swine every second day for a year and found a significant increase in bone quantity but no change in material properties in the femora of exercised pigs, when compared with controls

Externally applied load allows various load magnitudes and application type (static and dynamic) to be examined. However, in order for a true comparison to be made with controls, care must be taken to ensure that the loads are physiological in direction and magnitude and that the application of the load itself does not damage the bone locally and elicit a healing response. A number of researchers have applied known loads, *in vivo*, to growing bone. Hillam and Skerry (1995) mechanically loaded rat ulnae at 10 Hz with a peak force of 7 Newtons for four minutes a day for six days. This force was chosen to induce approximately double the surface strain previously measured *in vivo*. In the loaded ulnae bone formation was stimulated and bone resorption inhibited on the periosteal surface. Similarly, Pederson et al. (1999) applied an external load (4 point bending) to the right tibia of mice and found increased periosteal bone formation. Finally, Schaffler et al. (1995) and Bentolila et al. (1998) fatigued rat ulnae and demonstrated that this resulted in intracortical remodelling.

Increased load can also be induced via invasive surgery by removing a section of bone in order to increase the loading on a neighbouring bone (resection). An example of this would be the resection of the ulna in order to overload the radius. However the traumatic effect of the invasive surgery may elicit a further response with no link to the increased load. Goodship et al. (1979) resected the ulnae in growing swine, a process which doubled the strains in the radius and within three months the cross sectional area of the radius had doubled resulting in the strains returning to their pre-resection levels. In a similar experiment Lee (Lee, 1995) subjected the radii of sheep to either a sham operation or ulnar osteotomy (removal of the ulna) and found increased bone formation on the periosteal surface and resorption on the endosteal surface compared with the sham radii. Burr et al. (1989) found similar results in dogs.

Finally, centrifugation increases the gravitational forces but factors such as reduced activity levels and high physiological stress must be taken into account. Consequently,

results from centrifugation are difficult to interpret. In a series of experiments carried out by Amtmann and co-workers (Amtmann and Oyama, 1973, Amtmann and Oyama, 1976, Amtmann et al., 1976, Jaekel et al., 1977, Kimura et al., 1979), rats and dogs were chronically centrifuged at up to 2.76 G for up to 810 days. Compared to age matched controls they reported a reduction in femoral length (-6.6%), decreased cortical cross sectional area (-15.1%), increased density (+4.2% when differences in cross sectional area were taken into account) and increased compressive strength (+10% when adjusted to body mass).

Despite the differences in techniques and the shortcomings of the models, the general consensus is that adaptation occurs by both surface modelling and matrix remodelling. Goodship et al. (1979), Lanyon et al. (1982), Burr et al. (1989) and Lee (1995) all found bone formation on the periosteal surface and bone resorption on the endosteal surface in bones subjected to increased loading. The result is a bone with an increased mass distributed around a larger diameter, which increases the moment of inertia making it stronger as a structural unit. Furthermore, the existing bone cortex underwent remodelling (Lee et al., 2002).

1.6.2 Decreased Loading

Decreased loading has been studied using two main methods, immobilisation and unloading. Surgery to denervate or immobilise a limb has been used by a number of researchers. Lanyon (1980) observed significant decreases in the mechanical properties (bone mass, width and curvature) in the right hindlimb of rats which had undergone denervation compared to both the contra-lateral limb and those of controls. However, trophic effects that nerves exert on bones have been removed and this may influence results. Also in this study and others (Uthoff and Jaworski, 1978, Uthoff and Finnegan, 1983, Carter et al., 1981), the contra-lateral limb was used as a control, despite the fact that it is not independent of the experiment and therefore could be significantly overloaded. Finally, the traumatic effect of the invasive surgery may elicit a further response with no link to the reduced load. Uthoff & Jaworski (1978) also studied bone's response to non-traumatic immobilisation, by encasing the right forelimb of young dogs in plaster. After 32 weeks, bone mass stabilised after a reduction of 30 -

40%. In a later study on mature dogs, similar disuse caused an approximately 33% reduction in bone mass.

Unloading has been achieved in experiments using hindlimb suspension and via the microgravity associated with space flight. Following periods in space, rats were found to have a site specific and age-related reduction in mechanical properties of their bones (Morey and Baylink, 1978, Martin, 1990, Wronski and Morey, 1983, Shaw et al., 1988, Spengler et al., 1983). Following the long duration spaceflights of the Skylab series, mineral studies indicated that urinary calcium levels were approximately double the pre-flight level after 30 days in the microgravity of space . These initial data were compatible with bone mineral loss and in subsequent flights aboard Russian Cosmos spacecraft, decreased trabecular bone was noted in the metaphyses of rats after 22 days in space (Yagodovsky et al., 1976). Other work carried out has also confirmed that long term exposure to hypogravity in space may result in loss of bone mass due to suppression of bone formation and increased resorption . These effects are discussed in more detail in section 5.1.1.

However, due to the logistical and cost problems associated with space flight, a ground-based model was required to simulate weightlessness. In 1979, Emily Morey (1979) developed a ground-based model using rats in the National Aeronautics and Space Administration (NASA) Ames Research Centre. This model satisfied the following criteria: (1) the system should not stress the animal, which can be evaluated using weight gain and glucocorticoid levels (markers of systemic stress); (2) The model should unload the limb without constraint by paralysis (3) The animal should be allowed to maintain health by eating, grooming and moving. Initially two different methods of suspension were proposed: tail suspension and back harness suspension. However, a study by Wronski and Morey-Holton (1987) compared tail and back harness suspension techniques and found that back harness suspension induced more stress and resulted in skeletal abnormalities. Tail suspension was seen to be less traumatic and produced no significant skeletal abnormalities relative to control animals. Consequently, tail suspension was used in this study and is discussed in detail in chapter two.

1.7 Aims and Objectives

The main aim of the project was to use a suspension model for disuse osteoporosis to investigate the relationship between gene expression, morphology and mechanical strength.

Within this overall aim the following objectives were identified:

- To subject growing bone to conditions of normal load (controls), weight bearing suspended (humeri) and underload (femora) for periods up to 2 weeks.
- To assess the effect of unloading via suspension on the formation patterns of young growing bone.
- To quantify the degree of periosteal modelling, intracortical microcracking and remodelling using fluorochrome dyes under these loading conditions.
- To assess the structural and material properties of normal and underloaded bone by pQCT imaging and mechanical testing.
- To extract and purify RNA from periosteal cells (largely osteoblasts and bone lining cells) under these loading conditions .
- To study osteoblast gene-expression patterns by means of a candidate-gene strategy.

Chapter 2 Hindlimb Suspension

2.1 Introduction

In hindlimb suspension, either traction tape along the tail elevates and unloads the hindlimbs while the forelimbs remain loaded. A system of overhead rollers allow the animal to move in all directions while a fish-line swivel provides for rotational motion (see Figure 2.1). When suspended, the animal is still able to use its forelimbs for locomotion, eating and grooming. As a result, tail suspension is now accepted as the appropriate model for evaluating the effects of simulated weightlessness on skeletal homeostasis.

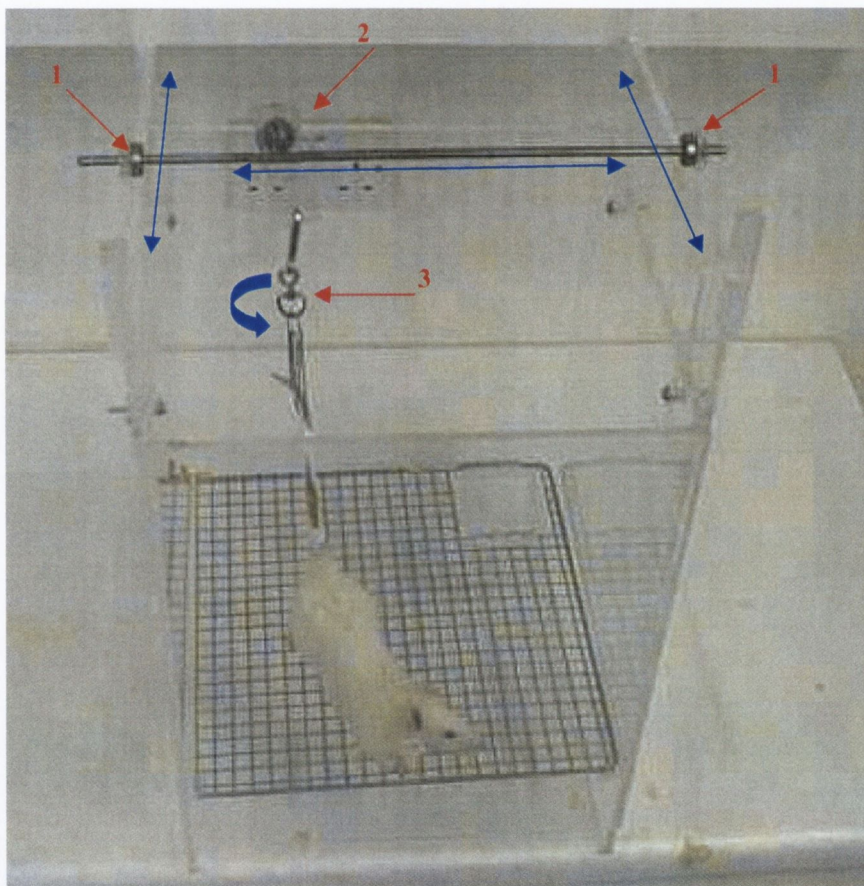


Fig. 2.1 Hindlimb suspension cage detailing the 3 components allowing motion

(1: Rollers allowing motion from front to back; 2: Roller to allow motion from left to right; 3: Swivel for rotation) —→ direction(s) of motion —

The hindlimb suspension model provides the opportunity to evaluate the physiological and cellular mechanisms of the skeletal response to altered load. Although the exact forces on the hindlimbs are unknown, a study by Hargens et al. (1983) found that the forelimbs were similarly loaded to those of a normal weight-bearing rat. A further study by Shaw et al. (1987), showed that weight-bearing forces are eliminated although some inertial and muscle forces remain. A large body of work has been conducted using the hindlimb suspension model encompassing changes in metabolic markers such as calcium, osteocalcin, parathyroid hormone and 1,25-dehydroxyvitamin D, 1,25D (Halloran et al., 1986, Bikle et al., 1987, Gallop et al., 1980, Patterson-Buckendahl et al., 1989), bone mass and maturity (Globus et al., 1986, Halloran et al., 1986, Bikle et al., 1987, Shaw et al., 1987), bone formation and resorption rates and mechanical properties (van der Meulen et al., 1995, Machwate et al., 1994, Matsumoto et al., 1998, Sessions et al., 1989). Work has also been carried out to attempt to reverse the effects of unloading (via infusion with growth hormone, insulin like growth factor 1 and 1,25D (Bikle et al., 1994, Halloran et al., 1986, Bikle et al., 1995) and on the effect of reloading following periods of suspension (Vico et al., 1995, Matsumoto et al., 1998, Sessions et al., 1989, Westerlind et al., 1994).

2.1.1 Calcium and other metabolic markers

A number of systemic markers have been used to chart the absorption or release of proteins and minerals from the bone as it is either formed or resorbed. Following periods of hindlimb suspension there is a small transient increase in the serum level of calcium (Halloran et al., 1986). This parallels a significant decrease in calcium content in the bone (Bikle et al., 1987, Halloran et al., 1986). Systemic levels of osteocalcin, an extracellular matrix (ECM) protein accounting for nearly 10% of the non-collagenous proteins of bone ECM (Gallop et al., 1980)(see section (5.3.2), fall by 25% during the first week of hindlimb suspension (Patterson-Buckendahl et al., 1989). In addition, although osteocalcin protein content is reduced after 7 days, it returns to normal after 28 days of continued suspension. Serum levels of 1,25D also fall (Halloran et al., 1986). However after 5 to 15 days of continued unloading serum levels of calcium, osteocalcin and 1,25D return to control levels (Halloran et al., 1986, Patterson-Buckendahl et al., 1989).

2.1.2 Bone mass and mineralization

The effects of HLS on the mass and mineralization of unloaded bone are discussed in detail in Chapter 5. Commonly researchers have found a reduction in the bone mass of the un-weighted limbs which parallels reductions in the bone mineral content and calcium levels (Halloran et al., 1986, Bikle et al., 1987). However, in young growing animals this reduction in accretion of mass and mineral content is transient with the rate of accretion rising towards that of the controls by the fourth week of continued unloading, although bone mass remains significantly lower (Globus et al., 1986). This reduction in bone mass occurs in both cortical (diaphysis) and trabecular (metaphysis) sites although it is more pronounced in metaphyseal sites (Globus et al., 1986). Finally, density-gradient fractionation has also shown that the level of mineralisation is also retarded in hindlimb unloaded bones (Bikle et al., 1987).

2.1.3 Bone formation and resorption rates

The effects of HLS on the bone formation and resorption rates of unloaded bone are discussed in detail in chapter 3. Overall, investigators have found that HLS resulted in a transient suppression of bone deposition at the periosteal surface. There was no effect on the endosteal surface where bone resorption is predominant in young growing animals (van der Meulen et al., 1995, Globus et al., 1986). This reduction in bone formation occurs in both cortical and trabecular regions (Globus et al., 1986, Machwate et al., 1994, Matsumoto et al., 1998, Sessions et al., 1989, Sakata et al., 1999). However, studies have shown that bone length remains unaffected by suspension (van der Meulen et al., 1995, Vailas et al., 1988, Shaw et al., 1987). Finally, the above investigators found that the reduction in bone formation rates following HLS to be transient, with growth rates returning to control levels by the end of the second week.

2.1.4 Biomechanical properties

The effects of HLS on the biomechanical properties of bone are discussed in detail in chapter 5. On the whole, suspension has been shown to result in a reduction in the structural properties of bone. Following various periods of suspension a number of investigators have established evidence of reductions in directly measured parameters such as stiffness, strength and maximum torque, and derived values based on the measured shape and structure and the assumption of homogeneous material properties such as maximum derived stress and the effective elastic modulus in the unloaded bones relative to controls (Abram et al., 1988, Shaw et al., 1987, van der Meulen et al., 1995, Bloomfield et al., 2002). The reasons given for the loss of strength found in most studies have been varied with researchers attributing it to either reduced cross sectional area or reductions in both cross sectional area and derived material properties. This may be due to differences in test set-ups and the ages of the animals used.

2.1.5 Summary

Hindlimb suspension has been accepted as an effective model for evaluating skeletal responses to mechanical loading. As a result of unloading, mass, mineralization and biomechanical properties are reduced in the unloaded bones. In both trabecular and cortical bone there is a reduction in bone formation rates, while periosteal bone mineralisation is also retarded in cortical bone. Levels of resorption do not seem to be overly affected due to hindlimb suspension. Ultimately, unloading reduces the mechanical strength of the affected bones, which could pose a increased risk of fracture following reloading.

2.1.6 Aims

The aims of this section of the project were as follows:

- To set up and test the HLS model in our laboratory based on the version first created by Morey (1979) and modified later by Van der Meulen (1995)
- To successfully suspend rats for periods of up to 2 weeks concurrently with age matched pair fed controls
- To collect and store genetic, morphological and mechanical samples of the femora and humeri following periods of HLS

2.2 Materials and Methods

2.2.1 Experimental Design

Groups of male Sprague-Dawley rats were obtained from the Biological Research Facility, Beaumont Hospital, under Irish government license (Ref. B100/2195). Following five days of acclimatisation, groups (age 39 days) were randomly assigned to basal control (B), age matched control (C) or hindlimb suspended (S) groups (all groups n=6). All animals were weighed at the onset of the experiment. Group B were sacrificed at the onset by over-anaesthetisation with CO₂ followed by cervical dislocation. Since all the animals were young growing rats this basal control group reveals whether a measured decrease in a particular parameter is an actual decrease or a reduction due to diminished or inhibited growth. In order to reduce the effect of body weight, age matched controls were pair fed with those of the experimental group, whereby each day group C were fed the mean amount of food eaten by the experimental group the previous day. As result differences in body weight between experimental and age matched control groups were minimised. Group S were hindlimb suspended using a system of overhead pulleys to elevate and unload the hindlimbs while maintaining load on the forelimbs.

Gene expression of a number of genes have been shown to be altered within hours but return to normal within two weeks following altered load (Bikle et al., 1994a, Bikle et al., 1994b, Matsumoto et al., 1998). Alternatively, morphological and mechanical changes would take a number of weeks to be evident. Therefore, in order to obtain the most information from the candidate genes while still getting meaningful morphological and mechanical data, it was decided to sacrifice the suspended and age matched control groups at 1, 3, 7 and 14 days. In addition, since changes in morphology and structural properties would take a number of days to become apparent, it was decided to eliminate the 1 day groups' samples from the morphological and mechanical studies.

2.2.2 Conditions of altered load

Skeletal unloading of the hindlimbs was achieved using the rat hindlimb suspension model first designed in NASA by Morey (1979) and used since by a large number of authors (Globus et al., 1984, Globus et al., 1986, Bikle et al., 1994a, van der Meulen et al., 1995). Rats were held loosely in a towel while their tails were cleaned using warm soapy water and then wiped clean using water. The tails were then 'degreased' by using 70% ethanol and cotton wool. Tincture of Benzoin (Friars Balsam, Prices Dental, Ireland) was then applied to the tail and it was allowed to dry. Benzoin is an anti-inflammatory and also helps by providing a sticky surface. A 1cm wide strip of adhesive tape (Zinc oxide plaster B. P., Paragon, Smith & Nephew Medical Limited, England) was then applied laterally, for approximately 5 – 10 cm, along both sides of the tail to form a small loop near the end of the tail. This tape was then secured by wrapping stockinette (Stockinette B. P., Seton Healthcare Group Plc., England) around the tail and securing it in place using more adhesive tape. The loop of adhesive tape was then attached to a series of overhead pulleys allowing the animals hindlimbs and pelvic region to be elevated off the ground. This system of pulleys allows the animal to use its front paws to move freely in any direction around the cage and is vital for maintaining health. Also, as the animals grew, the sides of the cages were raised to ensure the hind limbs remained unloaded. In this model of hindlimb suspension, rear-limbs, pelvis and caudal region of the spine are unloaded while the forelimbs remain loaded. In previous studies and in this study, this model of unloading was well tolerated by the rat. In this study, the level of stress induced by HLS was assessed by monitoring levels of feeding and weight gain. In addition, levels of grooming and activity were assessed qualitatively.

2.2.3 Sample Preparation

The right humeri and femora were used to detect changes in morphology and gene expression while the left femora were used in a destructive torsion test to determine any changes in biomechanical properties (see figure 2.2). After sacrifice, both loaded humeri and unloaded femora were disarticulated and cleaned of excess tissue. The periosteum was then dissected away from the mid-diaphysis of the right femur using a sterile scalpel. The right periosteal and full bone samples were then placed in separate

sterile cryo-vials (Nalgene cryogenic vials, Nalgene Company, USA) filled with RNALater (Ambion Inc., Texas, USA), snap-frozen in liquid nitrogen and stored at -70°C. This process protected the samples' mRNA from degradation. Total time from sacrifice to snap-freezing of all samples was less than ten minutes. Later the frozen right bones were measured using a vernier calliper on a bed of dry ice and their midpoints determined using standard anatomical points (see section 5.2.2). Once the point was identified a scalpel was used to mark the point by making a small incision. The bones were then sectioned transversely into two halves across the mid-diaphysis using an electric circular saw (miniplex Triplex, Miniplex France) transferred to two new cryo-vials and re-stored at -70°C for later analysis. The distal halves of both right long bones were stored for later gene and protein expression analysis in another study while the proximal halves of the femora and humeri were used to make histological slides for morphological studies. The left femur was stored at -20 °C and used in a destructive torsion test. The left humeri were not used in the torsion experiments as the morphological results suggested no widespread changes were to be found in the normally loaded humeri.

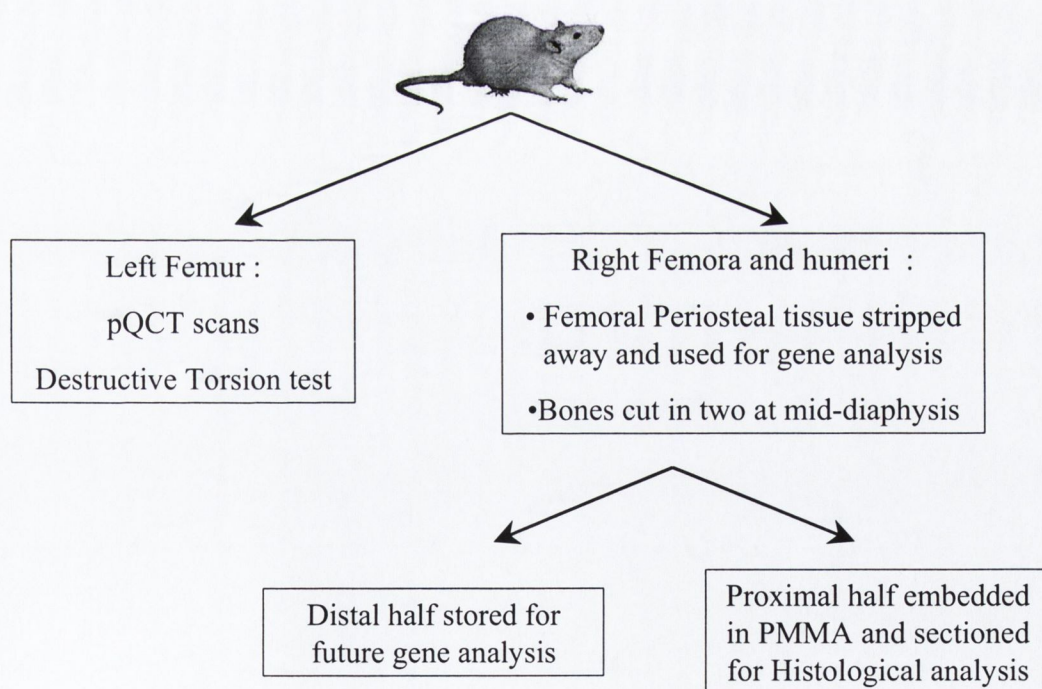


Fig. 2.2 Schematic of Protocol for the Sample Preparation and Use

2.2.4 Statistical Analysis

A Power Analysis based on existing data (van der Meulen et al., 1995) showed that 6 animals were required in each group to achieve greater than 90% power. All data measured were statistically analysed using standard methods for longitudinal studies (Diggle et al., 1994) using the statistics software Intercooled STATA (StataCorp. 2001. Stata Statistical Software: Release 7.0. College Station, TX: Stata Corporation). Linear regression analysis and ANOVA (Analysis of Variance) were performed on all data sets. The choice of which statistical method to use was governed by the following premise. In cases where it is assumed that there is a linear effect on a particular data set (e.g. for an increase in the independent variable, such as time, there is a linear response in the dependent variable) both ANOVA and linear regression analysis were used. In these cases, ANOVA and linear regression analysis will yield similar results. However, if a pulsatile effect was thought likely (e.g. in cases where for an increase in the independent variable, such as time, there is a transient response in the dependent variable) only ANOVA was used to analyse the data. In addition, when ANOVA and Linear regression gave contrasting answers the trend of the graphed data was assessed and the strengths of the two tests (R^2 value) were taken into account in deciding the answer. Finally, although both ANOVA and linear regression are insensitive to reasonable degrees of variance, in cases where the data appeared skewed a robust linear regression analysis and Kruskal-Wallis ANOVA were performed to check the previously obtained results. For $p < 0.05$, the difference were considered significant, while $p < 0.01$ were noted.

2.3 Results

Following consultation with Professor Van der Meulen in Cornell University, twelve cages were built, 6 HLS and 6 control cages. Sprague-Dawley rats were acclimatised in individual cages for 5 days prior to the experimental period. During this time normal levels of feeding, activity and grooming were assessed qualitatively.

Following this period of acclimatisation the rats were randomly assigned control or experimental. The experimental animals were then tail suspended for periods of time. The times chosen were 1, 3, 7 and 14 days. During the suspension period the animals were monitored for signs of excessive stress. Throughout the experiment the animals

tolerated suspension well, in that levels of feeding, activity and grooming were maintained at control levels. All animals, experimental and control, also gained weight over the experimental period.

2.4 Conclusions

In summary, the following aims were accomplished:

- Rats were suspended for periods of up to 2 weeks concurrently with age-matched pair-fed controls
- HLS did not result in any change in the body weight following periods of suspension
 - This implies any differences in the measured variables are as a result of the change in mechanical load rather than any excessive stress experienced by the animals
- The following samples were collected for analysis
 - Periosteal femoral samples
 - Femoral and humeral bone for histological analysis
 - Femoral and humeral bone for later protein analysis (subsequent study)
 - Femoral bone for destructive mechanical tests

Chapter 3 Gene Expression Analysis following Altered Mechanical Load

3.1 Introduction

It is clear that bone formation and resorption during both development and remodelling necessitate stringent control of osteoblast and osteoclast proliferation and differentiation. Regulation of these biological processes involves the sequential expression of both systemic (e.g. hormones and growth factors under the control of the central nervous system) and cell specific genes (e.g. locally controlled proteins produced by and acting upon specific cell types) in response to an integrated series of regulatory signals. These are in turn mediated by physiological factors such as mechanical loading. Consequently, it is vital that a greater understanding is found of the parameters that control the expression of these genes during bone formation and remodelling.

Mechanically, adaptive control of bone structure requires a feedback mechanism. This requires a network of cells communicating with each other in order to guide the remodelling action to the correct region of bone (see Figure 3.1). Cells of the osteoblast lineage are distributed on the surface and throughout the matrix (osteocytes). It is this network of osteocytes which seems ideal to both perceive alterations in the matrix (increased loading, microdamage) and to direct adaptive modelling and remodelling to the site. This belief that osteocytes are the mechano-sensors in bone has growing experimental support.

In a study by Skerry et al. (1989) bones from skeletally mature male turkeys were exposed to short term dynamic loading, which had previously been shown to result in increased new bone formation. The activity of Glucose 6-Phosphate dehydrogenase (G6PD), an enzyme involved in biosynthetic processes such as the production of RNA was investigated. Following loading, an increase in the activity of G6PD in periosteal cells was observed. In osteocytes, the G6PD activity per cell was not significantly increased by loading, but the number of cells showing activity was twice that of the controls. This study shows that intermittent loading of bone tissue results in a rapid response in the metabolism of both osteocytes and periosteal cells. Other authors have also suggested that osteocytes are the primary sensors of mechanical load in bone

(Cowin et al., 1991, Lanyon, 1993, Noble et al., 2003, Burger and Klein-Nulen, 1999). However, there is only limited scientific evidence that osteocytes perform this function. One of the main obstacles to increased understanding of the role of osteocytes is that they are not easily accessible for study. It is possible to extract and culture osteocytes from neo-natal bones, but the gene expression of these cultured cells may be very different from that of older bones *in situ*.

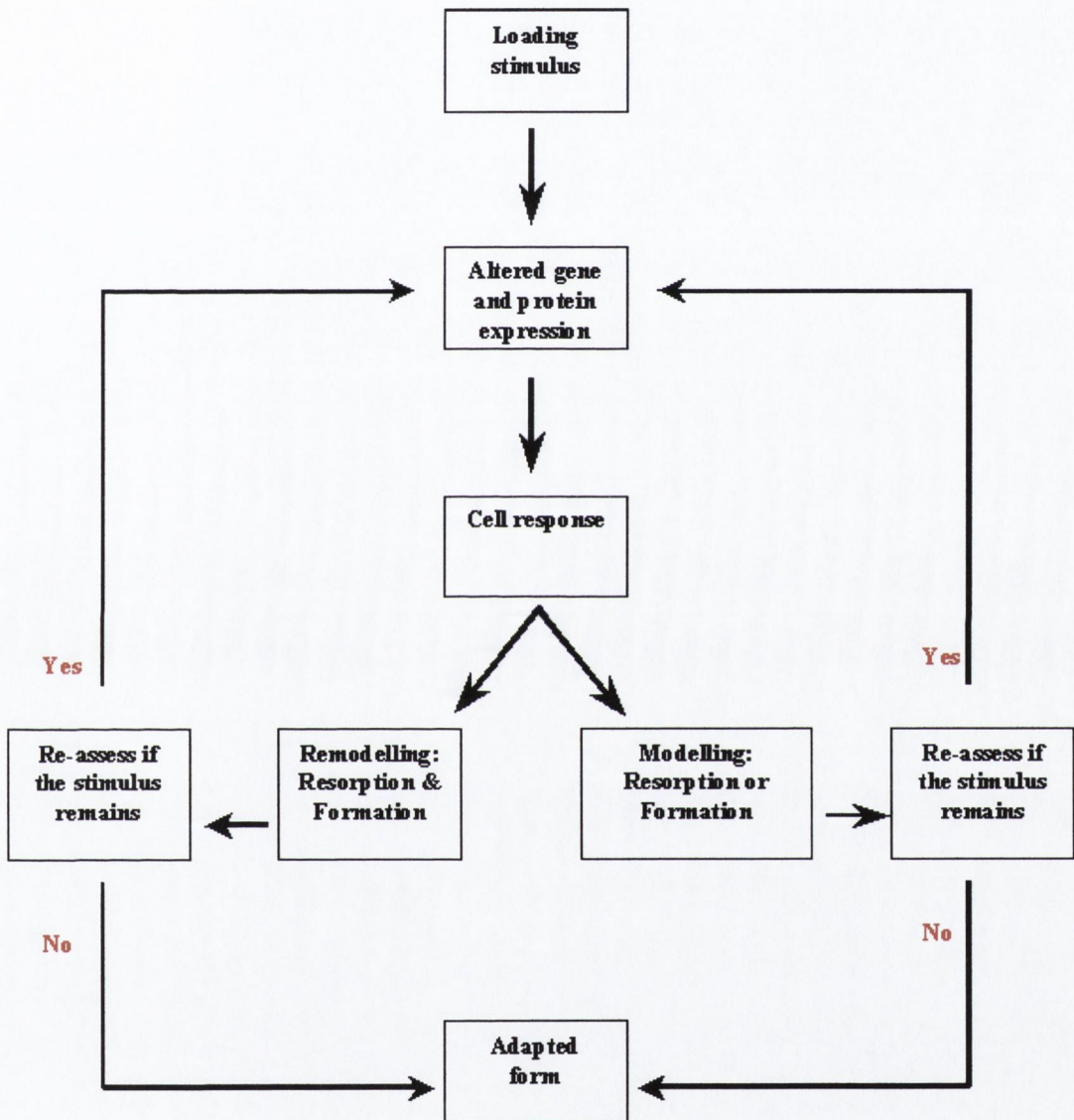


Fig. 3.1 Mechanism for adaptation for a single loading stimulus: Altered load acts as a mechanical stimulus. In response, genes within the bone cells are expressed and they either form new osteoid or resorb bone or both. As a result, the bone is adapted to its new state of loading (remodelling is rare in rats).

3.1.1 Gene Expression

Deoxyribonucleic acid, DNA, is the most important substance in the human body, as it carries all the hereditary information needed to form proteins, the building blocks of life. The instructions for cells to grow or divide are encoded within it and the differentiation required to produce the large number of specialised cells in higher life forms, such as humans, are made possible by its ability to produce such a vast array of proteins. In fact, proteins are the most abundant organic molecules in the cell with at least 100,000 different types in the human body.

Proteins are folded linear polymers of amino acids, called polypeptides. The order of amino acids determines the folding and hence the shape and function of the protein. The particular sequence of nucleotides in a region of DNA strand codes for a corresponding sequence of amino acids in the protein. There are two types of nucleic acids, DNA, which fulfils the storage of information function and Ribonucleic acid, RNA, which processes that information to make proteins (Alberts et al., 1994).

Organisms differ because their cells contain DNA molecules with a different nucleotide sequence. With four possible bases, the number of different sequences in a DNA chain n nucleotides long is 4^n . This information on a DNA chain can be separated into specific regions, with each region containing the sequence or coding for a particular protein being known as a gene. In order for DNA to transfer its information to synthesise protein, the coding sequence of the gene must be copied into RNA in a process called transcription, which in turn is translated into a protein. A molecule of RNA is single stranded and relatively small compared to DNA as each RNA molecule only codes for a specific protein.

Not all genes are expressed to the same degree in cells, with different cells expressing different RNAs and hence, different proteins. The type and quantity of RNA expressed is indicative of what proteins are being synthesised and the proteins present in a cell relate to the function of the cell at that time. There are a number of methods currently available to detect the type and quantity of RNA being expressed in tissues. This study initially sought to utilise the method of Semi-Quantitative Reverse Transcriptase-Polymerase Chain Reaction (Semi-Quantitative RT-PCR). In this technique, total RNA is copied into copy DNA (cDNA), and then specific cDNA corresponding to the target gene is synthesised and amplified by Polymerase Chain Reaction (PCR). Comparing the quantity amplified of the target gene to that of a housekeeping or reference gene, in this

case β -actin, GAPDH or RNRPS9, will give an insight into whether RNA is being expressed at different levels in different cellular tissue. A housekeeping gene is a gene that is expressed in all cells at all times at the same level. However, to reduce chances of spurious results, it is better practice to use a panel of housekeeping genes to assess changes in gene expression levels. This means that the technique is only semi-quantitative, as it does not measure directly the amount of the gene transcripts (Alberts et al., 1994).

3.1.2 Candidate genes

Most of the data on the effects of hormones and other growth factors have been obtained from experiments with small laboratory animals, mainly rats and mice. There are reasons to believe that this basic data is to some extent applicable to other species and to man. There are of course species differences (Olsson and Reiland, 1978) and although rats do not normally develop secondary osteons it has been shown that under extreme conditions remodelling does occur (Bentolila et al., 1998). Also Wang et al. (2001) has shown that bone loss in aged male Sprague-Dawley rats is comparable to that experienced by man in old-age.

In assessing potential candidate gene suitability for this study, emphasis was placed on genes being chosen such that either expression or inhibition of the genes would encompass the full experimental period. In particular, genes that had been previously examined in relation to changing loads were considered. In this regard, a large number of potential genes were identified from the literature and evaluated for suitability. Bone cells respond to systemic levels of growth hormone (GH), glucocorticoids, parathyroid hormone (PTH), sex hormones and 1,25-dihydroxy vitamin D₃ (1,25D) (Rodan, 1992). They also produce, and respond to, many growth factors that have been implicated in bone development, bone remodelling and repair. These include IGF-I and II, c-fos, c-jun, Osteocalcin, Osteopontin, Prom-1, TGF- β , TRAP (Rodan, 1992). Due to limited time, money and the expected low yield of RNA to be obtained from rat bone in this model, three genes were chosen for their suitability and interaction with other growth factors. The three genes chosen were c-fos, osteocalcin and insulin-like growth factor 1 (IGF-I). Although these genes will be discussed in detail in the subsequent sections, the following is a brief overview of their relative merits.

c-fos is expressed by many cells including: osteocytes, osteoblasts and chondroblasts *in vivo* (McCabe et al., 1995, 1996). Its expression is elevated within hours following increased loading. It is triggered by osteotropic hormones such as parathyroid hormone (PTH) (Chow et al., 1998) and prostaglandins. In certain *in vitro* models, and *in vivo*, PTH has also been shown to induce c-fos expression in osteoblasts, chondroblasts and osteoclasts in a specific temporal manner. A number of genes responsive to c-fos expression have also been identified. These include interstitial collagenase and osteocalcin (Schule et al., 1990, Angel and Karin, 1991) with c-fos expression being shown to down-regulate osteocalcin expression (McCabe et al., 1995). In general, these data suggest that c-fos is an early response gene with an important transcriptional role in bone cell differentiation and function (Stein and Lian, 1993). Despite these studies, the precise biological function of c-fos on osteoblasts *in vivo* remains poorly understood.

Osteocalcin is produced by osteoblasts primarily during the mineralisation of bone and acts as both an inhibitor of bone formation (Ducy et al., 1996) and an active recruiter of osteoclast pre-cursors (Glowacki and Lian, 1987). A number of factors have been shown to regulate osteocalcin expression. These include PTH, glucocorticoids, tumour necrosis factor α , 1,25D and c-fos (Hauschka and Gallop, 1977). Following unloading, osteocalcin expression is reduced, while overload results in an increase in osteocalcin gene expression.

IGF-I is a growth factor which is expressed by osteocytes, osteoblasts and osteoclasts and can be induced by PTH, prostaglandin E₂, interleukin-6 and estrogen (McCarthy et al., 1989, 1991, Franchimont et al., 1997). Following either reduced or increased load IGF-I is up-regulated. However the growth promoting effects of the growth factor are transiently resisted in unloaded bone (Bikle et al., 1994c).

3.1.2.1 c-fos

The c-fos gene encodes a 2.2 kb mRNA and is a member of the cellular early response gene family. It is expressed at high levels in a few tissues such as amnion, yolk sac, placenta, neural tissue and bone marrow (Muller, 1986). In the majority of other cell types, the basal level of c-fos expression is quite low, but can be rapidly and transiently induced by a large number of agents and stimuli including growth factors, serum, parathyroid hormone (PTH), as well as mechanical stimulation (Angel and Karin, 1991, Pearman et al., 1996, Kostenuik et al., 1997, Matsumoto et al., 1998). To account for

the diversity of situations and cells upon which c-fos acts, it has been suggested that it may be involved as an early response gene, which acts to turn on other genes.

The c-fos gene encodes a protein that is a member of the basic/leucine zipper (bZIP) family of transcription factors, Fos (see Figure 3.2). Other members of the Fos family include: FOSB (Zerial et al., 1989), the Fos related antigens, Fra-1 and Fra-2 (Cohen et al., 1989, Matsui et al., 1990); other Jun like proteins including c-jun, JunB and JunD (Clohisy et al., 1992, Nakabeppu et al., 1988, Hirai et al., 1989). When Fos heterodimerizes with a member of the Jun family it forms an active complex that can bind to DNA in a sequence specific manner and regulate transcription. It is the interaction of the two leucine zippers that enables the amino-terminal basic regions of the bZIP domain to form a competent DNA binding region (see Figure 3.2). This Fos/Jun heterodimer is often referred to as the activator protein 1 (AP-1) complex.

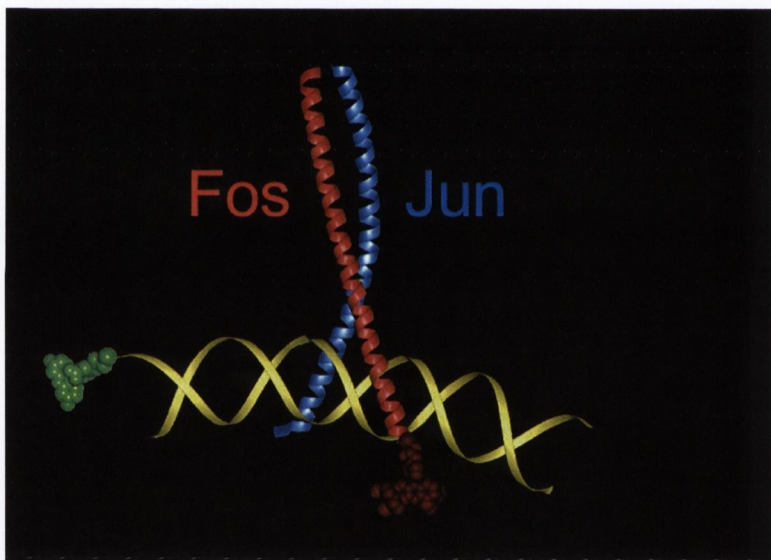


Fig. 3.2 AP-1 binding to a DNA strand in order to regulate transcription (http://sitemaker.umich.edu/kerppola.lab/research_interests)

3.3.1.1 Effect of c-fos expression on osteoblasts and osteoclasts

In osteoblast cells *in vitro*, levels of c-fos are enhanced during the proliferative period of osteoblast development, fall to minimal levels post-proliferatively and are enhanced late in the developmental sequence when apoptosis is evident in the mature osteoblast cells (McCabe et al., 1995). Interestingly when c-fos is elevated during either proliferation or apoptosis there is a reciprocal decrease in osteocalcin expression (McCabe et al., 1995). The suppression of osteocalcin by c-fos may be explained by c-fos occupying AP-1

sites, which overlap binding domains for element-specific transcription factors within the osteocalcin promoter.

There is also evidence that suggests that members of the AP-1 family are involved in the regulation of osteoblast differentiation:

- AP-1 binding sites are located in the promoter regions of several genes expressed in osteoblasts including alkaline phosphatase, $\alpha 1(I)$ collagen and osteocalcin (McCabe et al., 1996)
- Extracellular signalling molecules such as TGF β and PTH, have been shown to induce expression of AP-1 and some of its common components, c-fos and c-jun, in osteoblast cells, as is typical of early response genes (Clohisy et al., 1992, Lee et al., 1994, McCauley et al., 1997)
- AP-1 family are expressed in osteoblastic cultures at sites of active bone formation *in vivo* (Dony and Gruss, 1987).

With the advent of transgenic mice came the ability to analyse the effect of over and under expressing c-fos function using genetic manipulations *in vivo*. Over expression of c-fos in transgenic mice eventually leads to osteochondromas and osteosarcomas (Ruther et al., 1989). As these arise from osteoblasts it was originally assumed that c-fos would play an important role in the regulation of osteoblast proliferation. However, deletion of the c-fos gene in transgenic mice does not affect osteoblasts function, with normal levels of osteoblast proliferation found. Thus, the phenotype of c-fos deficient mice argues against the proposed role, as regulators of osteoblast proliferation. Conversely, in these c-fos knockout mice osteoclast differentiation is dramatically inhibited and the mice exhibit several skeletal abnormalities related to osteoclast dysfunction, including severe osteopetrosis (Johnson et al., 1992, Wang et al., 1992, Grigoriadis et al., 1995, Popoff and Marks, 1995). Although these two results seem to contradict one another, there are two possible explanations for these gain-of-function and loss-of-function experiments:

- There could be functional redundancies, with other members of the AP-1 family fulfilling the functions of c-fos in the knockout mice
- The over expression of c-fos in the transgenic mice could perturb the function of another unidentified bZIP transcription factor that is required to regulate osteoblast proliferation

Consequently, the role of c-fos in osteoblast differentiation and proliferation is not fully determined with some of the ambiguity in the transgenic mice experiments resulting from the possibility of its osteoblastic functions being substituted by another related AP-1 family member (Grigoriadis et al., 1995).

In addition, although traditionally viewed as a regulator of cell proliferation and oncogenesis, significant evidence has shown c-fos to be an important regulator of bone remodelling via its action on osteoclasts (Angel and Karin, 1991, Grigoriadis et al., 1995). It is considered that c-fos expression is required for osteoclast differentiation.

3.3.1.2 Effect of altered mechanical load on c-fos expression

A number of studies have attempted to identify the mechanisms involved in the induction of stretch-mediated transcriptional activity in the c-fos promoter of bone using a series of promoter-reporter constructs (Peake and El Haj, 2003, Peake et al., 2000). Instead of the discovery of a single mechanoresponse element, a more complex and interactive picture is emerging. Within the 400 bp region located directly upstream of the transcriptional start site, there are the serum response element (SRE), calcium/cAMP response element(s) (CREs), shear stress response element (SSRE), Fos-AP-1 binding sequence (FAP) and the sis-inducible element (SIE). Deletion of a number of these elements reduces, but does not inhibit mechanoinduction, implying that mechanical induction of c-fos in osteoblastic cells is mediated by multiple response elements along a number of pathways.

While the effect of skeletal unloading on the expression of c-fos at the cellular level *in vivo* has not been reported, some work has been done on its effect on c-fos levels *in vitro*. Kostenuik et al. (1997) compared levels of c-fos expression *in vitro* between bone marrow stromal cells extracted from control rats and rats that had undergone five days of skeletal unloading. After 15-20 days of culture, there was a 50% drop in the expression of c-fos in the unloaded animals' cells. This was accompanied by a corresponding decrease in bone marrow stromal cell proliferation. Chambers et al. (1999) mechanically loaded rat tail vertebrae and found elevated levels of c-fos expression throughout the bone. This also indicates that mechanical loading is a necessary factor for the normal expression of the early response c-fos gene.

In two experiments, Mikuni-Takagaki et al. (1996, 1998) isolated osteoblastic cells from rat frontal and parietal bones and incubated them in culture dishes coated with

0.5% type I collagen in order for them to develop into young osteocytes. These cultures of primary osteocytes were then stretched for 3 hours using flex I plates. They reported that following stretching, elevated levels of two early response genes, cyclooxygenase 2 (COX-2) and c-fos, were recorded as well as elevated levels of osteocalcin and IGF-I. Interestingly the changes in mRNA levels of COX-2, osteocalcin and IGF-I appeared in a biphasic manner with a small but prolonged rise and fall over the first few hours. This was followed by secondary peaks of increased expression, of COX-2 after 8 hours and IGF-I and osteocalcin after 24 hours. Furthermore these secondary peaks were blocked by the use of NS398, a specific inhibitor of the inductive cyclooxygenase, during the mechanical stretching. These results implied that the mechanical loading induced bone formation through young osteocytes in two ways: direct anabolic reaction of the osteocytes to produce matrix proteins such as osteocalcin; and indirect effects on osteoblasts by the increased levels of growth factors such as IGF-I which are known to lead to proliferation of osteoblasts and bone formation. They also suggested that the long lasting effects of mechanical load *in vivo* could be explained by a secondary anabolic reaction through the renewed upregulation of COX-2 mRNA.

A study by Matsumoto et al. (1998) showed that c-fos expression in rat periosteal cells was increased within two hours of reloading following 14 days unloading. They suggested that mechanical unloading impairs periosteal bone formation by impairing the expression of c-fos in periosteal cells.

A number of authors have examined the effect of low intensity pulsed ultrasound (US) on the mRNA response of various bone-forming cells. Naruse et al. (2000) used US on bone marrow stromal cells (ST2 cells) and demonstrated transiently elevated c-fos and increased mRNA expression of insulin like growth factor 1 (IGF-I) and osteocalcin (OC); all changes consistent with a bone-forming response. Warden et al. (2001) used isolated bone-forming cells (UMR-106) and found stimulated mRNA expression of the early response genes c-fos and COX-2 along with elevated expression of the bone matrix protein OC.

Finally, Yamaguchi et al. (2002) mechanically loaded cultures of human periodontal ligament under cyclic tensile forces. Following loading c-fos expression was transiently elevated with a peak 30 minutes after the application of mechanical forces. Interestingly there was no change in the levels of osteocalcin expression reported.

Overall, it is clear that c-fos appears to play a critical role in regulating the development and activities of the osteoblasts, osteocytes and osteoclasts that ultimately form and maintain the skeleton.

3.1.2.2 Osteocalcin

Osteocalcin, or bone Gla protein, is a member of a large family of mineral binding extracellular matrix proteins collectively called the Gla proteins (Esmon et al., 1975). Gla proteins contain glutamic acid residues which confer on these proteins a high affinity for mineral ions such as Ca^{2++} and for hydroxyapatite crystals, the mineral component of the bone extracellular matrix (Suttie, 1985). Among the non-collagenous proteins produced by osteoblasts, osteocalcin is one of the most abundant (Hauschka et al., 1989). Osteocalcin levels in urine or serum have long been used as a bone formation marker. Studies which have followed untreated postmenopausal women for two to four years found serum osteocalcin to be the best single biochemical marker of bone loss (Johansen et al., 1988). However it is generally accepted that combinations of serum total alkaline phosphatase and osteocalcin and other markers are more effective and reliable than serum osteocalcin alone (Slemenda et al., 1987). However, this approach was not pursued, as it was not within the perceived scope of the project.

Celeste et al. (1986) reported the structure of the osteocalcin cDNA in rat, as well as humans and mice. The gene is relatively small, with less than one thousand bases of genomic sequence, with four exons. Although a lot of work has been done on the processing and structure of these proteins since their discovery twenty five years ago, it is only with the advent of modern molecular biology techniques that investigators have been able to ask questions about their gene expression regulation.

3.3.2.1 Effect of osteocalcin expression on osteoblasts and osteoclasts

Because osteocalcin gene expression is inhibited late during osteoblast differentiation, it is not an obligatory component of the regulatory mechanism associated with commitment to the osteogenic phenotype. Formation of bone with a mineralised extracellular matrix will still occur in animals with an ablated osteocalcin gene (Ducy et al., 1996). Consequently, the biological activity of osteocalcin appears to be linked to sustaining the structural and/or functional properties of bone tissue. As a result its

involvement in the process of remodelling is a distinct possibility (Glowacki et al., 1991).

Over the years it has been shown that a number of factors can influence osteocalcin synthesis. Hormones such as glucocorticoids and tumour necrosis factor α as well as 1,25-dihydroxy Vitamin D₃ can regulate the expression. *In vitro* the transition from brushite [Ca₄(HPO₄)₂6H₂] to hydroxyapatite [Ca₁₀(PO₄)₆(OH)₂] is inhibited by low concentrations of osteocalcin (Hauschka and Gallop, 1977). When bone particles were prepared from rats almost totally devoid of osteocalcin (following six weeks of treatment with warfarin) and implanted subcutaneously in normal rats, the implanted bone particles were found to be resistant to resorption (Lian et al., 1984). A decreased ability to recruit and differentiate osteoclast progenitors compared to control bone particles was also noted (Glowacki and Lian, 1987). These results imply that osteocalcin may regulate bone resorption by recruiting cells of the osteoclast lineage. However, experiments using warfarin must be interpreted carefully since the warfarin affects the γ -carboxylation of glutamic residues present in matrix Gla protein, osteocalcin and possibly other as yet unknown skeletal proteins. Therefore the phenotype observed, cannot be conclusively attributed to a decrease in the level of just one protein.

In a study by Ducy et al. (1996) mutant mice were generated with true loss of function of osteocalcin (i.e. total absence of osteocalcin in blood or bone). They found that there was increased bone formation in both cortical and cancellous bone. This indicates that in mice, *in vivo*, osteocalcin is an inhibitor of bone formation.

3.3.2.2 Effect of altered mechanical load on osteocalcin expression

In vitro, Tanaka et al. (2003) seeded osteoblast MC3T3-E1 cells into collagen gels, and applied combinations of sinusoidal strain (S) and cyclic broad frequency vibrations (V). Sinusoidal stimulation alone did not affect the cell responses. Following both S and V, cellular proliferation was repressed and osteocalcin mRNA was upregulated after 7 days.

A number of studies have been conducted to try to elucidate the response in osteocalcin gene expression to altered load. Lean et al. (1995) mechanically loaded the eight caudal vertebrae of 13 week old rats and found an increase in the proportion of trabecular bone

surfaces on which transcripts for osteocalcin were detectable from < 3 to 25%, 72 hours after loading.

Bikle et al. (1994b) found decreased levels of osteocalcin mRNA in the tibiae of rats which had been unloaded via space flight or hindlimb suspension. This was consistent with the shift towards reduced maturation. In a study by Patterson-Buckendahl et al. (1989) the femurs of rats, which had been hindlimb suspended for periods of up to 4 weeks, were examined. The osteocalcin protein content of the femur diaphysis was reduced after 1 week but returned to normal by 28 days of continued unloading. This reduction was mirrored by a reduction of 25% in the serum osteocalcin levels measured, which is consistent with a decreased rate of bone growth.

In a study by Kostenuik et al. (1997) rats were hindlimb suspended for 2 or 5 days after which their tibial bone marrow was harvested and the bone marrow stromal cells (BMSCs) cultured. BMSCs from 5 day suspended rats had 35% less osteocalcin mRNA, after 20 days culture, than BMSCs from control rats. This mirrored a reduction in the mineralisation of the cultured cells from suspended rats. This result contrasts with that of Machwate et al. (1993) who reported that after 14 days unloading the osteoblast phenotype was unchanged. However this could be explained since studies have shown that bone formation has returned towards normal following 12 – 14 days continued unloading (Globus et al., 1986b).

Finally, in an interesting experiment by Sasaguri et al. (1998), groups of young mice were fed either hard pellets or soft food and their mandibular condyles examined. In the group eating soft food, as a result of the reduced mandibular loads involved, the condyles were found to under-developed with a thinner layer of cartilage and fewer bone trabeculae. Northern hybridisation of the total RNA extracted from these condyles also exhibited a significant 77% decrease in expression of osteocalcin compared to that of the mice eating hard food.

3.1.2.3 Insulin-Like Growth Factor-1

One of the most important factors in bone formation and its vitality is the growth promoting activity of the insulin-like growth factors (IGFs). This key role in the local regulation of bone is demonstrated by the finding that around 50% of basal bone cell proliferation can be blocked by inhibiting the actions of IGFs in serum free cultures (Mohan, 1993). IGF-I is a member of the family of anabolic peptides, which are structurally and functionally related to insulin (Daughaday and Rotwein, 1989). Although IGFs are not unique to bone, they are actively synthesised by osteoblasts and are important in cell recruitment and differentiation (Rosen et al., 1994). Bone is the second largest depot for IGFs (besides liver) and IGF-I is found in very high concentrations in the skeletons of most mammals (Bautista et al., 1990). IGFs are made available to skeletal tissues by active synthesis by osteoblasts or by the release of IGFs, which have previously been produced and bound to proteins within the stores of hydroxyapatite. These IGFs are released during the process of resorption. However the possible role of IGFs in remodelling is unclear. IGFs produced by osteoblasts, or released from the bone matrix via resorption, have the potential to stimulate proliferation and enhance the activity of bone cells. The effect of this separate pool of IGFs in the vascular system on osteoblasts is unknown.

IGF-I expression can be stimulated via a number of systemic hormones, regulatory agents, growth hormone, parathyroid hormone, prostaglandin E₂ and estrogen (see table 3.1).

IGFs also have a number of binding proteins, which modulate its activity, and these binding proteins are also produced by bone cells in response to growth hormone and IGF itself. Approximately 99% of all circulating IGFs are bound to six specific high-affinity IGF binding proteins (IGFBP 1-6) that modulate IGF action in a positive or negative manner. IGFBPs appear to modify IGF action by either inhibiting or promoting IGF bioactivity.

In a recent clinical study (Jehle et al., 2003), the levels of serum IGF system components were assessed in patients with various forms of osteoporosis. Compared with age and sex matched controls, osteoporosis patients showed a 73% decrease in free IGF-I, a 29% decrease in total IGF-I, a 10% decrease in IGFBP-3 and a 52% decrease in IGFBP-5 levels; they had higher levels of IGFBP-1 (4.1 fold), IGFBP-2 (1.8 fold), IGFBP-4 (1.3 fold) and IGFBP-6 (2.1 fold). This study shows that in osteoporosis there

is a deficiency in serum levels of stimulatory IGF components (IGF-I both free and total, IGFBP-3 and IGFBP-5) and an excess of inhibitory IGFBPs (IGFBP-4 and IGFBP-6). The study also found evidence that this imbalance was aggravated further in osteoporitic patients who had recently suffered bone fractures.

A further study demonstrated a significant positive correlation between serum IGF-I levels and the osteoblastic surface measured by histomorphometric techniques (Reed et al., 1995). The evidence that the serum levels of IGF system components are altered during physiological or pathological states when bone metabolism is distorted, in diseases such as osteoporosis, provide indirect evidence for an important role for IGF components in bone remodelling.

Limited trials investigating the effectiveness of using IGF-I for the treatment of bone defects have been performed. In a recent trial Meinel et al (2003) trapped IGF-I protein inside biodegradable microspheres and injected them into a 8mm metaphyseal drill hole and a 10mm tibial defect. Administration of IGF-I resulted in an increase of 12% newly formed bone in the drill hole and bridging of the defect by 8 weeks. In addition inflammatory marker gene expression was also found at the site of the bone injury.

Regulatory Agent	Effect on IGF-I	Effect on IGFBP-4	Effect on IGFBP-5
PTH	Increase	Increase	Increase
Estrogen	Increase	Increase	Not determined
PGE ₂	Increase	Increase	Increase
Glucocorticoids	Decrease	Decrease	Decrease
TGFβ	Increase/Decrease	Decrease	Decrease
FGF	Decrease	Decrease	Decrease
PDGF	Decrease	Not determined	Decrease
BMP-7	Increase	Decrease	Increase/Decrease
Il-6	Increase	Not determined	Increase
IGFs	Decrease	Decrease	Increase

Table 3.1 Summary of Critical Factors regulating IGF-I and IGFBPs in Bone Cells (Rodan, 2002)

3.3.3.1 Effect of IGF-I expression on osteoblasts and osteoclasts

Andrew et al. (1993) examined IGF gene expression during human fracture healing. It was reported that both IGF-I and IGF-II mRNA were expressed in plump osteoblasts on active osteoid. On the other hand flat bone lining cells in trabecular bone showed no apparent IGF expression. This differential expression among cells of the osteoblast lineage strongly implicates IGFs in bone adaptation. Osteoclasts actively engaged in bone resorption have also been shown to express IGF-I mRNA. In vitro, IGF-I has been shown to promote formation of osteoclasts from mononuclear precursors and to stimulate existing osteoclasts (Slootweg et al., 1992). However a study by Hill et al. (1995) suggests that these effects are an indirect action on osteoclastic activity via its effects on osteoblast cells.

3.3.3.2 Effect of mechanical load on IGF-I expression

Lean et al. (1995) mechanically loaded caudal vertebrae in 13-week-old rats. Following this single episode of loading there was a significant increase in the extent of trabecular surface exhibiting IGF-I mRNA transcripts, which peaked 72 hours after loading. Furthermore IGF-I expression was detected in osteocytes in both trabecular (between 6 and 24 hours after loading) and cortical bone (between 6 and 72 hours after loading). In particular the mid-diaphyseal region showed strong hybridisation for IGF-I mRNA.

Machwate et al. (1994) demonstrated that hind limb suspended adult rats having been given continual infusion of rhIGF-I (1.3 or 2.0 mg/kg. per day) showed enhanced recruitment of osteoblastic cells, increased trabecular bone formation by histomorphometric indices and at least partially reduced trabecular bone loss. Contrary to that, in a series of studies Bikle et al. (1994a, 1994b, 1994c, 1994d) examined levels of IGF-I in rats. In charting levels of IGF-I mRNA from prenatal to 28 months post birth, mRNA levels of IGF-I were found to be high up to birth, to fall post nately reaching a nadir in weeks 3 – 6, and then to recover to levels observed at birth. The authors linked this rise and fall to the bone's development from foetal to post-natal life and from rapid growth in adolescence to the slower bone remodelling characterising older bone.

Bikle et al. (1994c) also showed that despite IGF-I being a well known mediator of osteoblast proliferation and function, infusion of IGF-I failed to prevent the loss of bone associated with hindlimb suspension. Infusion of IGF-I (200 µg/day) during 1 week of

hindlimb suspension doubled the increase in bone mass of the controls but failed to reverse the cessation of bone growth in suspended animals. The skeletal unloading seemed to result in a resistance to the growth promoting effects of IGF-I despite elevated mRNA and protein levels of IGF-I and its receptor (IGF-IR) in the tibiae and femora of rats undergoing hindlimb suspension for 2 weeks. The explanation proposed for this reciprocal relationship is that the unloaded bones develop resistance to the growth promoting effects of IGF-I and that its subsequent rise is a compensatory response by the bone in an effort to overcome the resistance. Much of the anabolic action of growth hormone is mediated through IGF-I, although growth hormone can act independently of IGF-I on bone formation. Increasing circulating IGF-I however inhibits the growth hormone production by virtue of a negative feedback. In a recent follow-up study, by the same investigators, in an attempt to separate the effects of IGF-I from those of growth hormone, growth hormone deficient dwarf rats (dw-4 rats) were hindlimb suspended. The animals were once again infused with either vehicle or 2.5mg/kg body weight/day recombinant human IGF-I throughout the experimental period. Once more, IGF-I resulted in increased periosteal bone formation at the tibio-fibular junction of normally loaded rats. Unloading blocked this ability of IGF-I to increase bone formation at the tibio-fibular junction while it increased the bone formation at the midpoint of the normally loaded humerus.

Bikle et al also isolated and cultured bone marrow osteoprogenitor cells from the suspended and control growth hormone efficient dwarf rats. Infusion with IGF-I resulted in significantly increased osteogenic colony number, total alkaline phosphatase activity and total mineralisation in cells from normally loaded rats. Unloading reduced all these parameters although there were no differences in levels per cell. These results suggest that IGF-I stimulates the proliferation of osteoprogenitor cells. Unloading suppresses proliferation of these cells and blocks the effects of IGF-I. Finally, since this resistance persists when the cells are evaluated *in vitro*, this indicates an ability of these cells to remember their loading history.

3.1.3 Translation from mRNA to protein

This study examines the effect of altering mechanical load on the gene expression levels in periosteal tissue by quantifying mRNA expression levels. This methodology assumes that mRNA expression levels directly relate to protein expression levels, and hence to the cell response. This is a simplified viewpoint, and in reality there are several possibilities preventing the translation of mRNA into its' corresponding protein. For example, mRNA may be 'masked' by associated proteins to form ribonucleoprotein particles, thereby preventing the mRNAs' association with the ribosomes that are present. Consequently, to fully understand what is happening in the cell, both mRNA and protein expression levels need to be assessed. However, due to the minute quantities of tissue available (which makes protein quantitation from periosteal tissue difficult) it was decided that quantitation at the level of protein expression in addition to the genomic work was outside the scope of this project.

3.1.4 Research Questions

The aim of this section of the project was to investigate the effect of altered mechanical loading, via hindlimb suspension, on the gene expression patterns of the right femoral periosteum of young rats. Changes, due to unloading, in the gene expression pattern of the rats' right femora were assessed by a candidate gene approach. The genes chosen were osteocalcin, Insulin-like growth factor I and c-fos. Initially, the method of RT-PCR was used to assess changes in gene expression. Ultimately, gene expression levels were quantified by amplifying the mRNA using SMART technology and then creating cDNA arrays using this amplified cDNA. These cDNA arrays were then probed using radioactively labelled gene sequences.

The following research questions were asked:

- Using RT-PCR can individual mRNA samples be consistently assessed for altered gene expression patterns?
- Can SMART technology be used to generate cDNA arrays to analyse gene expression patterns in samples with limited RNA volumes
 - Can this protocol be applied to future *in vivo* work on small animals
- Does HLS result in a change in the gene expression pattern in the periosteum of the unloaded femora?

- Does HLS result in a change in the gene expression of osteocalcin, IGF-I and c-fos in the periosteal tissue of unloaded femora?
 - Are the changes transiently induced or consistently altered over the course of the experiment?

3.2 Molecular Biology Materials

The following analar grade chemicals were obtained from Sigma Chemical Company Ltd., UK: Agarose, Low melting point Agarose, Ammonium Persulphate, Bromophenol Blue, Diethyl Pyrocarbonate (DEPC), Ethidium Bromide, Formaldehyde, IsoAmyl Alcohol, Magnesium Chloride, Ficol, Sodium Hydroxide (NaOH), Sodium Citrate, Sodium dodecyl sulphate (SDS), Ethylenediaminetetraacetic acid (EDTA), Dithiothreitol (DTT) and Mineral Oil.

The following analar grade chemicals were obtained from B.D.H. Ltd., UK: Acrylamide, Chloroform, Ethanol, Hydrochloric Acid, Isopropanol, Tris-HCl and N-hexane.

The following reagents were obtained from BD Clontech Laboratories Inc., USA: Advantage II Polymerase Kit, Proteinase K.

The following reagents were obtained from Gibco/BRL, UK: Random Primers, Superscript II RT kit, 10X TBE (1.0M Tris, 0.9M Boric acid, 0.01 M EDTA), 20X SSC (3.0M NaCl, 0.3M Sodium Citrate), 10X TAE (10mM EDTA pH 8.0, 400mM Tris-acetate).

The following were obtained from Promega Corporation, USA: RnasIN and *Taq* DNA Polymerase, MgCl₂, Promega Wizard PCR preps DNA purification kit.

The following reagents were obtained from Biotecx Labs Inc., USA: Ultraspec II RNA isolation system.

Sybr Green RNA & DNA stains was obtained from Boehringer Mannheim GmbH, Germany.

Redivue αP^{33} and αP^{32} dCTP (>2500 Ci/mmol, 370 MBq/ml), Whatman 3MM filter paper and Hybond N+ nylon membrane were obtained from Amersham Pharmacia Biotech, UK.

The primers for RNRPS9, osteocalcin, IGF-I and GAPDH were synthesised by Pharmacia Biotech (Amersham Pharmacia Biotech, Great Britain).

The primers for c-fos were synthesised by MWG-Biotech AG, Germany.

The primers for the SMART protocol were synthesised by Sigma-Genosys.

All-in one random primer labelling kit was obtained from Sigma-Aldrich Chemie GmbH, Germany.

Nalgene cryogenic vials were obtained from Nalgene Company, USA.

RNALater and Expresshyb were obtained from Ambion Inc., Texas, USA.

The Multi-blot Replicator was obtained from V & P Scientific, INC., San Diego, USA.

Polaroid 665 photographic film was obtained from Polaroid Corporation, USA.

Stock Solutions

The following stock solutions were made up as follows:

10X SSC: 3.0M NaCl, 0.3M Sodium Citrate.

10% SDS: 100g of Sodium Dodecyl sulphate was dissolved in 1 litre of sterile H₂O.

10 X Print dye: containing 25% Ficol, 0.1% Bromophenol blue in sterile H₂O.

1.6M NaOH: containing 32g of NaOH in 500ml of H₂O.

10% APS: 10g of Ammonium Persulphate in 100ml of sterile H₂O.

Wash Solutions

Hybridisation wash solution 1: 2X SSC, 0.1% SDS

Hybridisation wash solution 2: 0.1X SSC, 0.1% SDS

3.3 Molecular Biology Methods

Sections 2.2.1 and 2.2.2 detail the experimental set-up. Briefly, groups of young growing rats ($n = 6$) were nominated as either experimental or control. The experimental rats were hindlimb suspended for periods of up to two weeks concurrently with the age-matched pair fed controls.

3.3.1 Tissue Harvesting

Mason et al. (1996) outlined a technique by which RNA from periosteal cells, mainly bone lining cells and osteoblasts, and intracortical osteocytes could be extracted. This protocol has been implemented in this study. Following the experimental period outlined above all animals were euthanised via over-anaesthetisation with CO₂ gas. Immediately after death the skin and muscle tissue was dissected away from the right humerus and femur. Following disarticulation of the joints the bones were excised. A sterile scalpel blade was used to strip away a 5mm zone of periosteum from the mid-diaphysis. These periosteal samples were then stored in aliquots of RNALater (Ambion Inc., Texas, USA), snap-frozen in liquid nitrogen and stored at -70°C before extraction. The remainder of the bones were then frozen by immersion in n-hexane at -20°C (BDH Supplies) and cooled using dry ice to -70°C. Later the frozen right bones were measured using a vernier calliper on a bed of dry ice and their midpoints determined using standard anatomical points (see section 4.2.2). Once the midpoint was identified a scalpel was used to mark the point by making a small incision. The bones were then sectioned transversely into two halves across the mid-diaphysis using an electric circular saw (miniplex Triplex, Miniplex France) transferred to two new cryo-vials and re-stored at -70°C for later analysis. The distal halves of both right long bones were stored for later gene and protein expression analysis in a subsequent study while the proximal halves of the femora and humeri were used to make histological slides for morphological studies.

3.3.2 RNA Isolation

Total RNA was harvested from cells using the Ultraspec RNA isolation system (Biotecx Labs Inc., USA). The cells and bone matter and a small amount of Ultraspec (1 ml) were gently homogenised using a hand held glass-Teflon homogeniser before being

transferred to sterile microcentrifuge tubes. The nucleoproteins and other bone matter were allowed to dissociate or separate out for five minutes. An aliquot (0.2 ml) of chloroform: isoamyl alcohol (24:1) was added and the tubes were shaken vigorously prior to centrifugation at 12,000 rpm for 15 minutes at 4°C. This separates out an aqueous phase which contains the RNA which was then carefully transferred to a sterile microcentrifuge tube. Half the volume of isopropanol and 0.05 volume of RNA Tack™ Resin were added. This resin binds to the isolated RNA, making it easier to visualise. This mixture was then vortexed and centrifuged for one minute at 12,000 rpm. The supernatant was removed and the solid pellet containing the isolated total RNA was washed twice using 1 ml of 75% ethanol and suspended in 30µl of DEPC treated RNase free water and stored at -70°C.

3.3.3 Polymerase Chain Reaction

The polymerase chain reaction (PCR) has become a powerful, yet standard, tool for the analysis of gene expression. PCR is a cyclic chemical reaction whereby the number of copies of a DNA sequence is doubled in every cycle (see Figure 3.3). In order to amplify the DNA from a particular gene, at least part of its nucleotide sequence must be known. This allows the design of two synthetic nucleotide primers, around twenty bases long, one complementary to each strand of the DNA double helix. A typical PCR cycle then involves denaturing the DNA at high temperature (94°C), binding the primers to the region of DNA in question (temperature dependant on the primer sequences) and then using the enzyme *Taq* DNA polymerase to extend the DNA sequences between the primer positions on the original DNA strand (94°C) (Sambrook, 1989).

A typical PCR reaction would have around 30 cycles resulting in an exponential increase in the numbers of copies of target sequence.

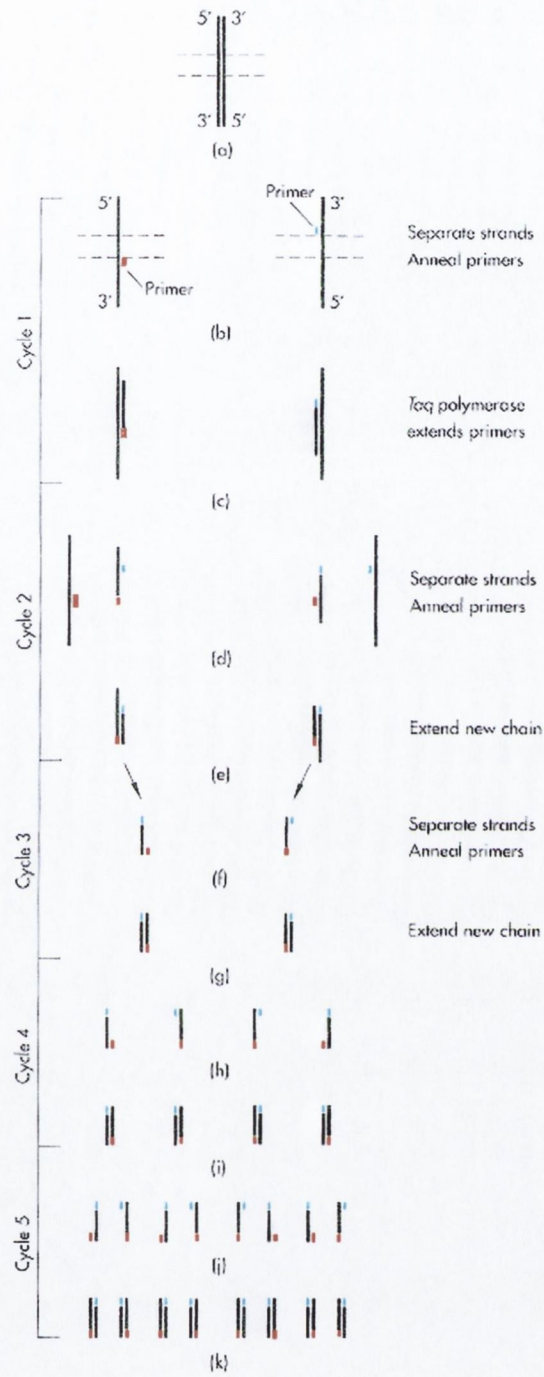


Fig. 3.3 Polymerase Chain Reaction (Watson et al., 1994)

3.3.3.1 Optimising PCR Conditions for Candidate genes

Specific oligonucleotide primers were designed using a software package (Oligo 4, National Biosciences Inc., USA). The primers were designed using the gene sequences for β -actin (Nudel et al., 1983), RNRPS9 (Rattus Norvegicus Ribosomal protein Subunit 9) (Chan et al., 1993), GAPDH (Glyceraldehyde-3-phosphate dehydrogenase)(Piechaczyk et al., 1984), osteocalcin (Yoon et al., 1988), Insulin-like growth factor-1 (Roberts et al., 1987) and c-fos (Curran et al., 1987)(see table 3.2). In order to detect any DNA contamination in the isolated RNA, the primers for some of the genes were designed to span an intron (DNA sequences that are present in genomic DNA that are spliced out in RNA). As a result if, for example, any DNA was present in the purified RNA sample the osteocalcin PCR product length would be 328 bp (amplifying across an intron) whereas using only RNA the PCR product length is 99 bp (see Figure 3.4).

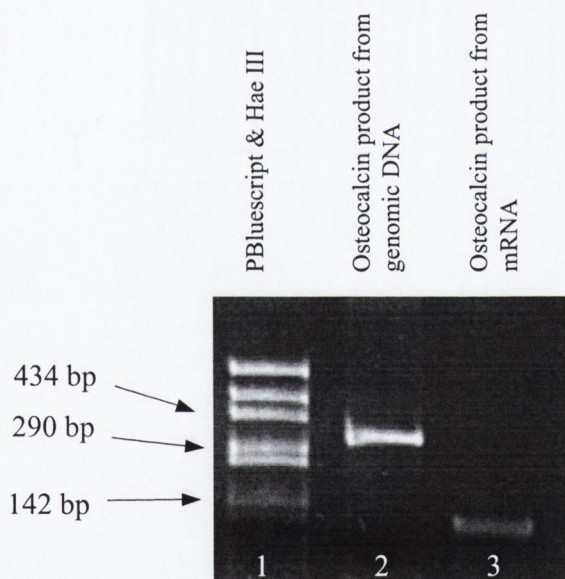


Fig. 3.4 Osteocalcin PCR product electrophoresed in parallel with a molecular marker of known size (PBluescript & Hae III; lane 1).

Lane 2 contains osteocalcin product amplified from genomic DNA (designed to span an intron. Genomic product size: 328 bp). Lane 3: osteocalcin product amplified from total RNA extracted from periosteal tissue (designed size: 129 bp)

Primer Transcripts	Nucleotide start position (genbank)	5'.....3'
RNRPS9 Forward	34	TCG CCA GAA GCT GGG TTT GTC
RNRPS9 Reverse	512	TTC TCC TTA TGG TGG TGG CCG
GAPDH Forward	80	GTG AAG GTC GGT GTC AAC GGA TTT
GAPDH Reverse	611	CAC AGT CTT CTG AGT GGC AGT GAT
Osteocalcin Forward	1559	CCG GCG CTA CCT CAA CAA TG
Osteocalcin Reverse	1868	GCG TCC TGG AAG CCA ATG TG
c-fos Forward	853	CCC TGC CTC TTC TCA ATG
c-fos Reverse	944	GCC GGA AAC AAG AAG TCA
IGF-I Forward	528	TGG GGG AAA GGA TGG ACT C
IGF-I Reverse	647	TGG GTG GGG TTT GTG AAA G

Table 3.2 Oligonucleotide Primer Sequences and their starting positions in their respective genbank sequences

PCR amplification conditions were optimised, individually for each candidate gene, using rat genomic DNA isolated from rat muscle as follows:

200 mg of fresh muscle tissue was frozen at -20°C. The frozen rat tissue (200mg) was homogenised in 1ml buffer containing 0.05M Tris, 0.1M EDTA (pH 8.0) to break open the cells. A further 8ml of this solution with 1ml of 10% SDS and 200µl of proteinase K (10 mg/ml) was added. The solution was incubated overnight at 37°C. The following day, 10ml of phenol: chloroform (1:1) was added, the solution mixed and then centrifuged at 12000 rpm for 15 minutes to separate the phases. The aqueous phase was transferred to a new clean tube and the phenol: chloroform extraction was repeated twice more, followed by a chloroform extraction. DNA was precipitated in a final concentration of 0.2M NaCl and twice the volume of ethanol. The sample was centrifuged at 3000rpm for 2 minutes and the supernatant discarded. The DNA pellet was washed in 70% ethanol, air dried and re-dissolved in 2ml de-ionised H₂O. The concentration of DNA was assessed using a spectrophotometer by measuring the absorption of light at 260nm wavelength.

Using this isolated DNA the PCR reactions for each candidate gene were optimised, using concentration curves for primer sets, MgCl₂ and DNA. Later, once RNA had been

isolated, cDNA was created. The PCR reactions were further adjusted for amplification using cDNA created from isolated RNA.

Candidate gene	Product Size [bp]	Forward & Reverse primer Conc.	MgCl ₂ volume	cDNA volume	Annealing Temperature
β-actin	190	50 pM	1.5µl	3µl	56°C
Osteocalcin	129* ⁽³²⁸⁾	50 pM	2.5µl	3µl	54°C
c-fos	109	50 pM	2.5µl	3µl	54°C
IGF-I	138	50 pM	2.4µl	3µl	53°C
GAPDH	555	50pM	3µl	5µl	55°C
RNRPS9	499	50pM	2.5µl	3µl	54°C

Table 3.3 Optimised RT-PCR amplification conditions for candidate genes.

*(Product designed to span an intron. E.g. osteocalcin product size for genomic DNA template is 328 bp. Final PCR reaction volume 50µl.)

3.3.4 Semi-Quantitative Reverse Transcription PCR

The hypothesis underlying this section of the proposed research is that alteration in osteocyte and osteoblast phenotype in response to mechanical loading is driven by alteration in patterns of gene expression. These alterations could be measured via the application of one or other of the relatively recently developed methods for "gene-expression profiling" (Dunican et al., 1997) such as gene arrays as well as more traditional methods such as Northern blotting. However, due to the low yield of RNA from bone, many of these techniques were not possible to implement in this case. As an alternative, the method of semi-quantitative reverse transcriptase PCR (RT-PCR) (He et al., 1995) was initially employed. This had the advantage of working directly from total cellular RNA, thus avoiding the necessity of further purification. RT-PCR studies on RNA extracted from bone cells subjected to altered mechanical loading were carried out according to a "candidate-gene" approach (see section 3.1.2). That is, a survey of the literature describing recent gene-expression studies in bone cells was used to guide our selection of RNA transcripts/genes for study.

Semi-quantitative RT-PCR is an extension of the standard PCR technique used to detect the relative expression of specific genes. Semi-quantitative RT-PCR makes it possible to detect very low levels of mRNAs in cells. In fact, RT-PCR has been shown to be 1,000-10,000 fold more sensitive than traditional Northern blotting techniques in detecting gene expression (Cance et al., 1992). In semi-quantitative RT-PCR, cDNA (complimentary DNA) is generated from total RNA. The cDNA generated is used as a template in PCR reactions with primers designed and optimised for the genes to be examined. It is then possible to detect and analyse the quantity of mRNA being expressed by a particular gene relative to the expression of a panel of housekeeping genes, GAPDH, RNRPS9 and β -actin. A housekeeping gene is a gene which has been shown to have the same level of expression in all cells at all times.

3.3.4.1 cDNA synthesis

cDNA was produced from the isolated RNA using the superscript II Reverse Transcription Kit (Gibco/BRL, UK). Random primers were used to prime first strand synthesis. Due to the expected low yield of total RNA from bone tissue, 10 μ l of total RNA was mixed with 1 μ l of random primers and incubated at 70°C for ten minutes to anneal the primers to the RNA, followed by 2 minutes on ice to end the reaction. Random primers are short segments of single-stranded DNA (ssDNA) called oligonucleotides, or oligos for short. These oligos are only 8 nucleotides long (octamers) and they consist of every possible combination of bases, which means there must be $4^8 = 65,536$ different combinations in the mixture. Because every possible hexamer is present, these primers can bind to any section of DNA.

The following was then added to each synthesis solution to a final volume of 20 μ l: 4mM Tris-HCl (pH. 7.5), 10mM DTT, 0.625mM dNTPs, 200U RnasIN (Promega Corporation, USA) and 0.25 μ l DEPC treated water. The cDNA reaction was incubated for two minutes at 37°C. Finally 200U of Moloney Murine Leukaemia Virus (MMLV) Reverse Transcriptase was added and cDNA was synthesised for 90 minutes at 37°C. The synthesis reaction was stopped by heating to 95°C for 5 minutes prior to storage at -20°C.

3.3.4.2 Optimising Semi-Quantitative RT-PCR

The semi-quantitative RT-PCR amplifications were based on the method of He et al. (1995). cDNA was synthesised as detailed earlier. Specific oligonucleotide primers were designed using primer analysis software Oligo 4 (National Biosciences, Plymouth, MN) for β -actin, RNRPS9, GAPDH, osteocalcin, c-fos and IGF-I (see table 3.2). The specific amplification conditions for each gene were optimised on rat genomic DNA isolated from muscle tissue. PCR reactions were carried out on a Hybaid™ thermal cycler or a DNA engine (MJ Research, USA) in a final volume of 50 μ l containing: 1mM dNTPs, 5mM Tris-HCl (pH 8.3), 7.5mM KCl, 2.5U *Taq* DNA polymerase. Added to this were the optimised volumes of MgCl₂, Primers and cDNA (see Table 3.3). The cycling conditions used were: 95°C for 1 minute, the relevant annealing temperature for 1 minute (see table 3.3), 72°C for 1 minute, for roughly 30 cycles, followed by 2 minutes at 72°C. To ensure that comparisons were made within the exponential stage of the PCR reaction, amplifications were paused and aliquots (12 μ l) were taken out of the reaction at particular cycle points specific for each gene (See table 3.4 and Figure 3.5).

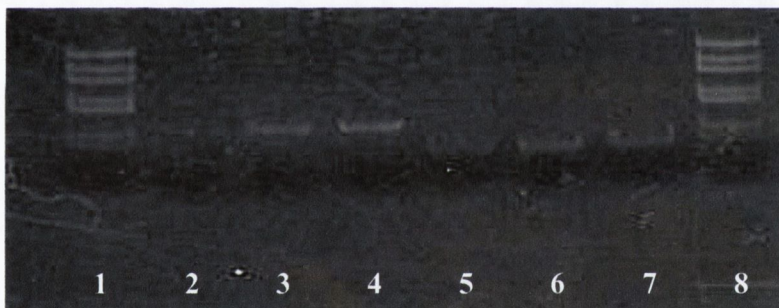


Fig. 3.5 Demonstrates a gel electrophoresis of β -actin and osteocalcin product amplified up from rat single stranded cDNA.

Lanes 1 & 8 contain a DNA marker of known product sizes (PBluescript & Hae III). Lanes 2 – 4 contain β -actin PCR product amplified 19, 20 and 21 cycles. Lanes 5 – 7 contain osteocalcin PCR product amplified 28, 29 and 30 cycles

Gene	Typical cycle number to extract aliquot of product		
GAPDH	22	25	28
β -actin	19	22	25
Osteocalcin	28	31	34
c-fos	30	33	36
IGF-I	35	38	41

Table 3.4 PCR cycle time-points for extracting aliquots of product

One of the main tenets of semi-quantitative RT-PCR is getting a varied set of RNA samples balanced so that the samples remain within the exponential phase of the PCR while also identifying differences in the candidate genes compared with the balanced housekeeping genes cycles. This is done in two main ways:

- By varying the amount of input total RNA in each PCR reaction it is possible to balance out the resultant sample smears. The level of total RNA can be assessed via electrophoresis on a 1% formaldehyde agarose gel and visualized using an RNA stain such as SYBR Green TM. Using these new generation genomic stains and a gel imaging system such as the Typhoon (see section 3.6.2.6) allows as little as 20ng of total RNA to be visualized. Once visualized all samples can be balanced to match the sample with the least volume of total RNA.
- Each amplification cycle (within the exponential phase) leads to a two-fold increase in the number of copies of the PCR's target mRNA transcript. Therefore, by using different numbers of amplification cycles in each sample reaction it is possible to make large manipulations to balance the sample set.

However the downside to both of the above methods is that each time you do an iteration of balancing (either via input RNA or using a cycle curve for each transcript) you have to use up some of the initial template (total RNA isolated from rat tissue). In this study the amount of total RNA isolated from the periosteal tissue in a 6 mm mid-diaphyseal region varied widely. This meant that, at the extremities, there was a ten-fold difference in the amount of total RNA recovered (50ng – 500ng). These large variances in the volume of RNA recovered can be attributed to a number of variables including:

- Volume of tissue obtained in the dissection
- Variation involved in the RNA extraction technique

As a result, in order to balance the sample set, a large number of balancing iterations had to be performed. This had the effect of using up large amounts of template (total RNA). Consequently, it was decided that SQ RT-PCR was too wasteful of template and that with such a widely ranging sample set it would not be possible to get a balanced set of samples.

As a result of the problems detailed above it was decided to move to a new method of gene expression analysis. Following an analysis of newly available methods, SMART (Switching Mechanism at 5' end of RNA Transcript) technology was chosen as an appropriate technique as it works on very little starting template (anything over 20ng) and allowed for analysis of expression patterns by a large number of methods.

3.4 Switching Mechanism at 5' end of RNA Transcript (SMART)

All mRNAs have a number of general properties. In particular they have a 'cap' at the 5' end and a poly A⁺ tail at the 3' end. SMART is a technique developed by BD Clontech Laboratories Inc. (USA). SMART is based on a standard PCR but takes advantage of the general properties of mRNA in a modified PCR reaction to amplify non-specifically all mRNAs present in a sample. It has been shown to be able to create high quality cDNA from nanograms of RNA while retaining relative levels of mRNA transcripts. SMART cDNA synthesis starts with either total or poly A + RNA. A modified oligo(dT) primer (the 3' SMART CDS III Primer) primes the first-strand synthesis reaction (see table 3.5 and figure 3.6). When RT reaches the 5' end of the mRNA, the enzyme's terminal transferase activity adds a few additional nucleotides, primarily deoxycytidine, to the 3' end of the cDNA. The SMARTTM oligonucleotide, which has an oligo(G) sequence at its 3' end, base-pairs with the deoxycytidine stretch, creating an extended template. RT then switches templates and continues replicating to the end of the oligonucleotide (Chenchik et al., 1996, Matz et al., 1999, Zhu et al., 2001, Zhumabayeva et al., 2001). The resulting full-length, single-stranded (ss) cDNA contains the complete 5' end of the mRNA, as well as sequences that are complementary to the SMART oligonucleotide. In cases where RT pauses before the end of the template, the addition of deoxycytidine nucleotides is much less efficient than with full-length cDNA-RNA hybrids, thus preventing base-pairing with the SMART Oligonucleotide. The SMART anchor sequence and the poly A sequence serve as

universal priming sites for end-to-end cDNA amplification. Therefore, cDNA without these sequences due to prematurely terminated cDNAs caused by incomplete RT activity, contaminating genomic DNA, or cDNA transcribed from poly A- RNA, will not be exponentially amplified. This results in all full length mRNA sequences being faithfully copied and transcribed into single stranded cDNA. Once the mRNA has been copied into cDNA it can then be used as a template to be amplified in a PCR using specifically designed primers (binding to the previously added SMART primers) to amplify all mRNA subsets. In order to ensure that the amplification is still within the exponential phase (and therefore all relative ratios between transcripts is being maintained) the PCR is brought to a previously determined cycle number. This amplified cDNA can then be used to ascertain if a particular gene has an altered expression pattern relative to a housekeeping gene using standard techniques.

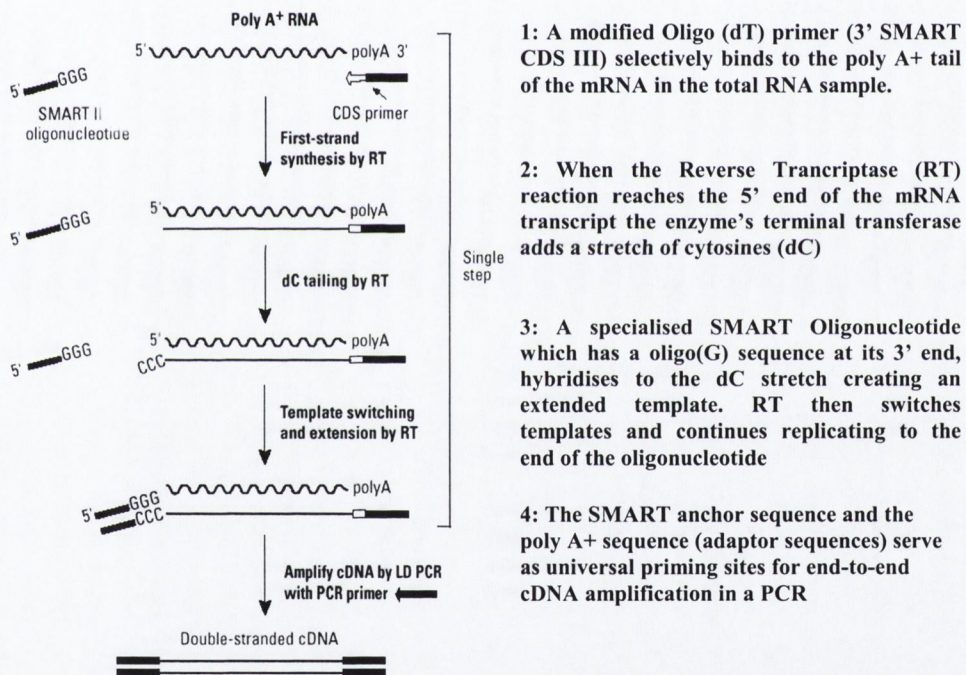


Fig. 3.6 Flow chart of SMART synthesis

3.4.1 Standard SMART Protocol

The SMART cDNA synthesis can be broken up into two steps: first-strand synthesis and SMART amplification.

Total RNA was isolated according to the protocol described in section 3.5.2. All thermal cycles were performed on a Perkin-Elmer Thermal cycler (PE 480, Perkin-Elmer Life and Analytical Sciences, USA).

The first strand synthesis for each sample was carried out by combining the following reagents in a sterile 0.5-ml reaction tube:

- 3µl of total RNA
- 1µl of CDS III/3'PCR primer (~10µM)
- 1µl SMART III oligonucleotide. (~10µM)

The tubes contents were incubated at 70°C in a thermal cycler for 2 minutes. The following was then added to each reaction tube:

- 2µl 5X First-strand buffer
- 1µl DTT (20mM)
- 1µl dNTP (10mM)
- 1µl MMLV reverse Transcriptase (200 units/µl)

The tubes were briefly vortexed, spun down and incubated at 42°C for 1 hour under mineral oil on a thermal cycler. Following the hour incubation 40µl of TE buffer was added to give a final volume of 50 µl of single stranded first strand cDNA. Finally, to terminate the reaction the tubes were heated to 72°C for 7 minutes.

SMART amplification was performed in a 100µl reaction volume. This was made up by adding the following to each 0.5-ml reaction tube:

- 10 µl of diluted single stranded first strand synthesis cDNA
- 74 µl deionised water
- 10µl 10X cDNA PCR buffer
- 2µl dNTP (10mM)
- 2µl SMART PCR primer (~10µM)
- 2 µl Advantage II polymerase mix

The tubes were then overlaid with two drops of mineral oil and placed in the preheated (95°C) thermal cycler. After an initial 95°C for 2 minutes the following cycle conditions used were: 95°C for 15 seconds, 65°C for 30 seconds, 68°C for 6 minutes, for 15 cycles. At this point the cycling was stopped and an 80µl aliquot was taken from each tube and stored at 4°C. The remaining samples were then cycled for a further 10 cycles, with a

4µl aliquot taken out and stored in a fresh micro-centrifuge tube every 2 cycles. These aliquots were then used to assess the optimal cycle number for each sample via gel electrophoresis (see section 3.6.1.1). When the optimal cycle numbers were determined additional thermal cycles were performed to bring the remaining 80µl of each sample up to its optimal cycle number.

3.4.1.1 Assessing the optimal cycle number

When mammalian total RNA is amplified using the SMART method the resultant cDNA can be visualised using a genomic stain and a 1.2% agarose gel. The resultant synthesised cDNA should appear as a moderately strong smear from 0.5 – 6 kb with some distinct bands. These bands correspond to highly expressed RNAs in the original tissue and hence the position and number of bands is specific for each tissue type. Choosing the correct number of cycles ensures that the double stranded cDNA remains in the exponential phase of amplification. Over amplification must be avoided as it results in the relative ratios between different mRNA transcripts becoming distorted. On the other hand, under-cycling results in a low yield of PCR product. The optimal cycle point is therefore one or two cycles less than what is required for the PCR reaction to reach the exponential plateau. In practice, aliquots were taken from the PCR reaction every two cycles between 15 and 25 cycles. These were then electrophoresed on a 1.2% agarose gel and stained using SYBR green. The plateau cycle point was that at which the yield of PCR products ceased to increase visually. This in turn corresponded to the appearance of a product smear in the high molecular weight region of the gel. Consequently, in this experiment the optimal cycle point for the particular reaction would then be taken as two cycles less than this point (see Figure 3.7).

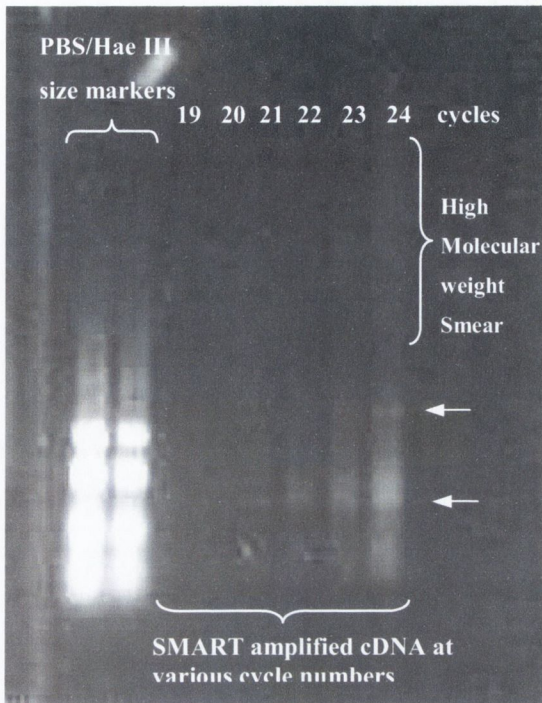


Fig. 3.7 Determining the optimal SMART cycle number:

A 4 μ l aliquot of the amplified cDNA product at each cycle point was electrophoresed on a gel and visualised using SYBR green RNA stain. The high molecular weight smear in lane 24 implies that this is over cycled by this point. Therefore, the optimal cycle number for this sample was taken as 22. The arrows indicate highly expressed mRNA transcripts

3.4.2 Alterations to the SMART protocol

Although SMART was available as a kit containing everything necessary for 6 reactions it would have proved costly to use kits due to the large sample size in this study. Consequently, it was decided to synthesise the primers ourselves. Following primer synthesis the system was optimised and the resultant SMART products compared with those created using the commercial kit. Finally, to analyse our amplified SMART cDNA for altered gene expression cDNA arrays were created using the multiblot replicator kit to create cDNA arrays. This protocol from mRNA to amplified SMART cDNA to cDNA array to data analysis is summarised in figure 3.8 and described in detail in sections 3.4.2.1 to 3.4.2.6.

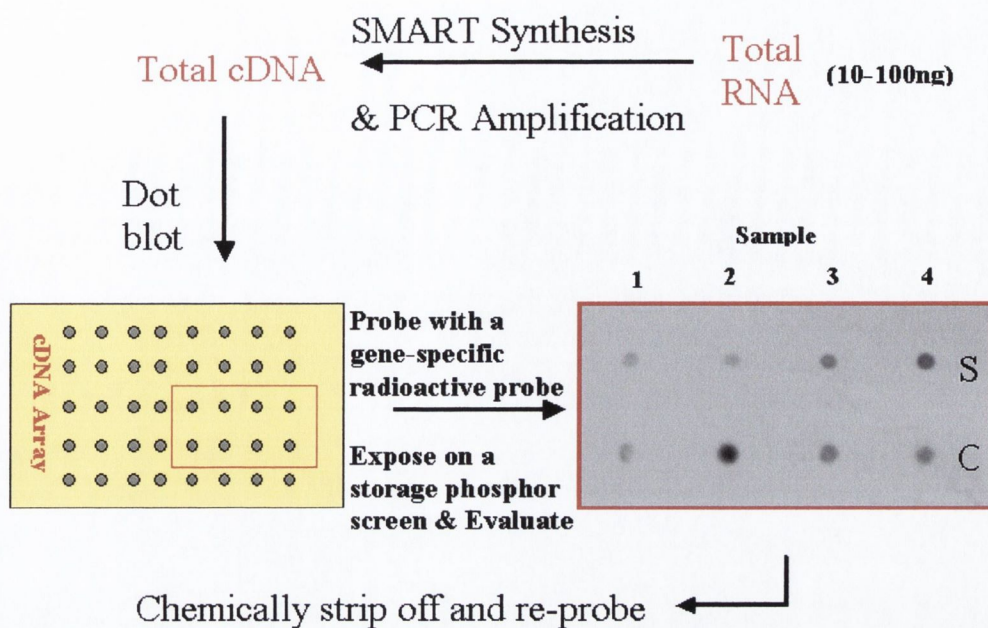


Fig. 3.8 Alterations to the SMART protocol: Total RNA is converted into single stranded SMART modified cDNA and amplified in a modified PCR.

This total cDNA is then transferred onto the cDNA array/Dot blot using the multi-blot Replicator Kit and fixed in place. The array is then probed with a gene specific radioactive probe and exposed to a storage phosphor screen. The resulting image is evaluated and the intensity of each 'dot' calculated. The array is then chemically stripped and a different radioactive probe used.

3.6.2.1 Synthesising Primers

The SMART primer sequences for each of the three primers were identified (see table 3e.5) and synthesized by Sigma-Genosys (Sigma-Genosys Ltd., U.K.). The enzyme (Advantage 2 polymerase) and its accompanying buffer solution were purchased directly from BD Clontech (BD Clontech Labs. Inc., USA).

Primer	Nucleotide Sequence
CLONTECH SMART CDS III/3'PCR primer	ATTCTAGAGGCCGAGGCCGACATGTTTTT TTTTTTTTTTTTTTTTTTTTTTTTVN
CLONTECH SMART III Oligonucleotide	AAGCAGTGGTATCAACGCAGAGTGGCCATTAT GCCGGG
CLONTECH SMART cDNA PCR primer	AAGCAGTGGTAACAACGCAGAGTACTTTTTT TTTTTTTTTTTTTTTTTTTTTTTTVN

Table 3.5 SMART primer sequences (V = A, G or C; N = A, G, C or T)

The SMART reactions were optimised in the same way as any other PCR, i.e. MgCl₂ and primer concentration curves. To aid in this process a small quantity of commercially obtained primers were used to balance the input primer concentrations.

The smears of cDNA, which were produced using the synthesized primers, were compared to those achieved using the commercial kit to ensure that the resultant products were similar in product size and intensity. To ensure that the smears contained full-length mRNA transcripts a previously optimised standard PCR for osteocalcin was performed using amplified SMART product as starting template. The osteocalcin primers had been designed so that the resulting transcript would span an intron, therefore this PCR would also check that the SMART amplification was amplifying from mRNA and that there was no genomic contamination. However, since SMART amplification from genomic and poly A⁻ RNA is far less efficient than that of poly A⁺ mRNA, genomic contamination was not envisaged as a problem.

3.4.2.2 Balancing Steps

SMART first strand synthesis is strongly dependent on the input RNA. In this experiment the quantity of total RNA recovered from the rat periosteal tissue is too low for spectrometry determination. Therefore the total RNA for each sample was balanced to the other samples in its group by running an aliquot (1 μ l) out on a denaturing 1% agarose gel. Since the volume of total RNA was so limited it was necessary to use SYBR Green RNA stain TM to stain the RNA so that it could be visualized on a multipurpose gel imager (Typhoon 8600, Amersham Biosciences, USA). The Typhoon works by shining a laser of a known wavelength across the stained gel and measuring the light emitted at the wavelength specific to the genomic stain used (in this case SYBR green). This emitted light is then converted to a grey-scale image format (.gel) where the intensity of a pixel (on a scale from 0 (white) to 100,000 (black)) is directly related to the intensity of the emitted lights signal. Each sample's two ribosomal bands were used to assess the volume of RNA present using the ImageQuant software (Molecular Dynamics, USA). Essentially an object box is drawn around the ribosomal bands corresponding to 18s and 28s. The median value for all the pixels along the box edge is calculated and denoted the background value. All pixels within the object box with a value above that of the background are then summed to give a intensity value for any particular sample band (See section 3.4.2.6 for more detail on how ImageQuant calculates band intensity).

Running the total RNA out on a denaturing gel also provides an opportunity to assess the quality of the samples. In all cases little to no degradation was observed and the 28s bands signal was observed to be approximately twice that of the 18s band.

Following the initial balancing of the input RNA, the samples were further, more stringently balanced in the amplifying stage. As described in section 3.4.1.1 the optimal cycle number was assessed for each sample in batches of twelve. This enabled twelve samples at a time to be balanced relative to each other.

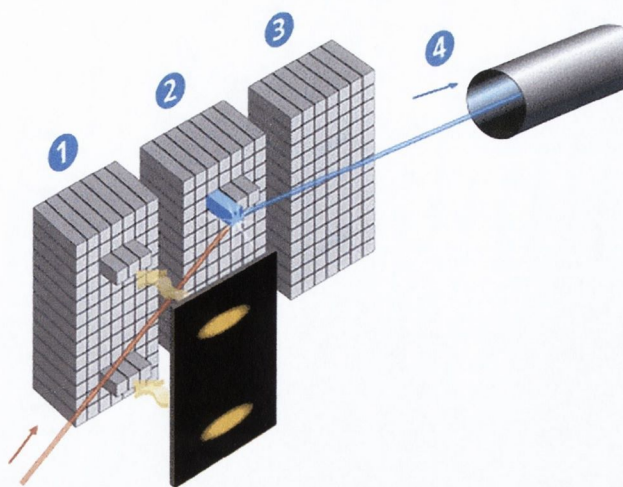
3.4.2.3 Balancing via a Trial 'Dot Blot'

In addition to these balancing steps it was decided to use a trial dot blot to ensure that the maximum balancing of the samples occurred. Consequently, 2 μ l of amplified product was denatured in a fresh print mix, containing final concentrations of 0.16 Molar NaOH, 1 X Print dye (containing Ficol and bromophenol blue) and cDNA for a

final volume of 6 μ l. This solution was then hand loaded using a pipette onto a positively charged nylon membrane (Hybond N⁺). The cDNA was then permanently fixed to the membrane by baking it at 80°C for 2 hours.

A radioactive probe for RNRPS9 was created firstly by performing a standard PCR using the previously optimised conditions, using first strand cDNA synthesis as starting template. This PCR product was then electrophoresed on a 1.2% low melting point agarose TAE gel and visualised using ethidium bromide stain. The PCR band was then excised out using a sterile scalpel and the cDNA extracted and purified using the Promega Wizard PCR preps DNA purification kit. Radioactive isotope, ³²P, was incorporated into the purified RNRPS9 product using the random primer kit (Sigma-Aldrich, Germany), to create a radioactive gene specific probe.

The trial blot was pre-hybridised in a rotating hybridising oven at 65°C in 10ml of the commercial hybridisation buffer Expresshyb for 30 minutes. Following this, the Expresshyb was replaced with 10 ml of fresh solution, which had been mixed together with the radioactive probe. The blot was then left to hybridise with the radioactive probe overnight at 65°C. When the hybridisation was complete the blot was washed using 50ml of hybridisation wash solutions at room temperature for 20 minutes each (Wash 1: 2X SSC, 0.1% SDS; wash 2: 0.1X SSC, 0.1% SDS). Following washing the blot was bound in cellophane and placed in a cassette with a storage phosphor screen on top of it for at least 4 hours. Care was taken to ensure the screen did not come into contact with any moisture as this results in irreparable damage to the screen. The storage phosphor screen was then evaluated using the Typhoon scanner by shining a laser across its surface and measuring the output in the form of light (see Figure 3.9). These results gave a more accurate estimation of how much cDNA was loaded for each sample. Sets of samples could then be finally balanced relative to each other. The trial blot also provided an opportunity to balance loaded cDNA between sample sets (with each set comprising a group of six controls and six suspended animals samples).



1. Exposure of the storage phosphor screen to ionizing radiation induces latent image formation
2. During laser scanning, the BaFBR:EU⁺² crystals in the screen release energy as blue light
3. And return to ground state
4. Blue light is collected and measured to form a quantitative representation of the sample

Fig. 3.9 Using the Typhoon gel imager to evaluate the storage phosphor screen (<http://www1.amershambiosciences.com>)

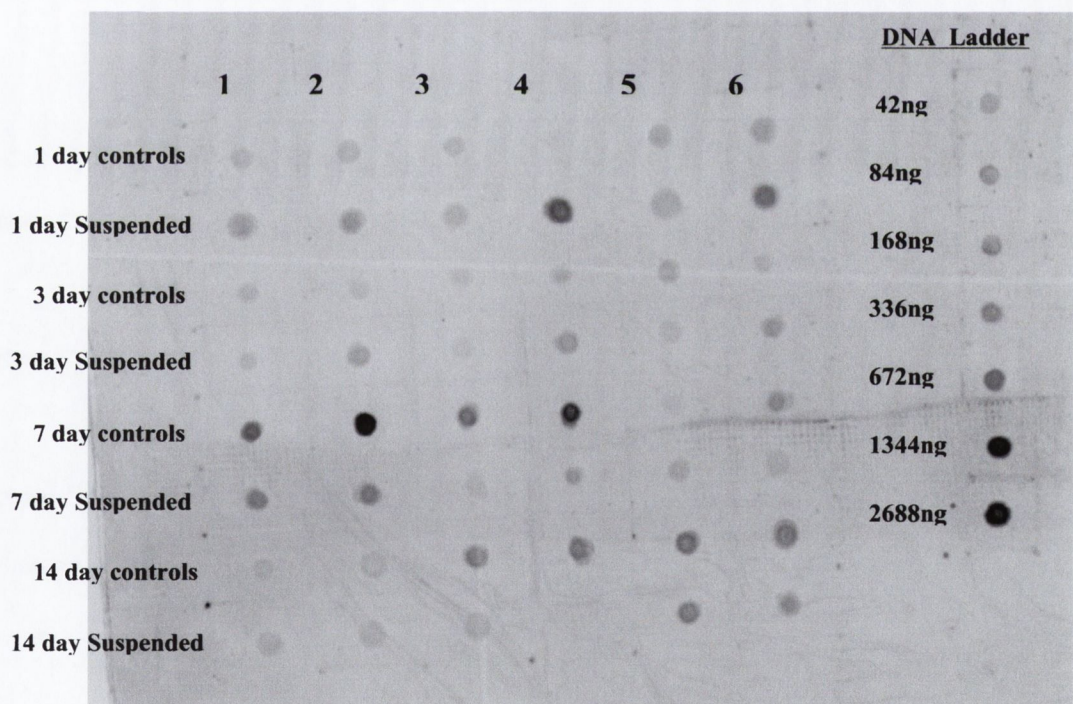


Fig. 3.10 Balancing Hand loaded Trial dot blot probed with RNRPS9

3.4.2.4 Multi-blot Replicator Kit

At the end of the SMART reactions the cDNA was concentrated down using a simple ammonium acetate precipitation from 80µl starting volume to 12.5µl. Two micro-litres were used during the preparation of the trial blot leaving 10.5µl of amplified cDNA. A fresh print mix was prepared (as over time the bromophenol lost its colour) containing final concentrations of 0.16 Molar NaOH, 1 X Print dye and cDNA in a final volume of 12.5 µl. Half the mix was used for a single hand loaded dot blot while the remaining 6.25µl was used to create two duplicate pin-loaded blots using a Multi-blot Replicator (V & P Scientific, INC., San Diego, USA). The Pin-loaded dot blots were prepared as follows (see Figure 3.11)

Two pieces of nylon membrane (Hybond N+, Amersham Pharmacia) were placed on top of 3 sheets of Whatman 3MM blotting paper. Using double-sided sticky tape the multi-print accessory was attached to the centre of the membrane and one corner of the Hybond was marked for orientation purposes (this step was done for each duplicate membrane). The SMART cDNA samples were added to the fresh print mix and transferred to a sterile 96 well source plate. The source plate was then centred and fixed into the Library copier accessory. The 96 solid Pin Replicator was then dipped into an alcohol reserve and flamed to sterilise the pins. Holding the replicator at a 45° angle to the source plate library copier, the left and right guide pins were placed into the corresponding alignment/positioning holes. The replicator was then rotated forward slowly until the guide pins lined up and slid into the alignment holes. This brought the replicator pins into contact with the reservoirs of cDNA and Print mix in the 96 well plate. Each time the replicator's pins came into contact with the solution at the bottom of the wells (print mix and cDNA), a hanging droplet of 0.1µl was picked up on the end of the pin. The replicator was then removed from the library copier and again at a 45° angle positioned into the top left guide hole on the left and right sides of the first multi-print replicator. It was then rotated into place and the pins lowered into contact with Hybond N+ membrane. This transfers the hanging droplet of print mix and cDNA at the end of the solid pin to the membrane. These two steps were then repeated for the duplicate membrane. The process was then repeated until all of the print mix had been transferred to the duplicate membranes. In addition to the SMART cDNA amplified from periosteal tissue, a DNA ladder, consisting of serial dilutions ranging from 2 micrograms to 42 nanograms, was transferred to each blot.

All membranes were then neutralised by placing on 2 sheets of 3MM Whatman paper that had been soaked in 2x SSC for 2 minutes and fixed by baking at 80°C for 45 minutes. Once the cDNA had been fixed the membranes were wrapped in cellophane and stored in a cool dry container prior to use.

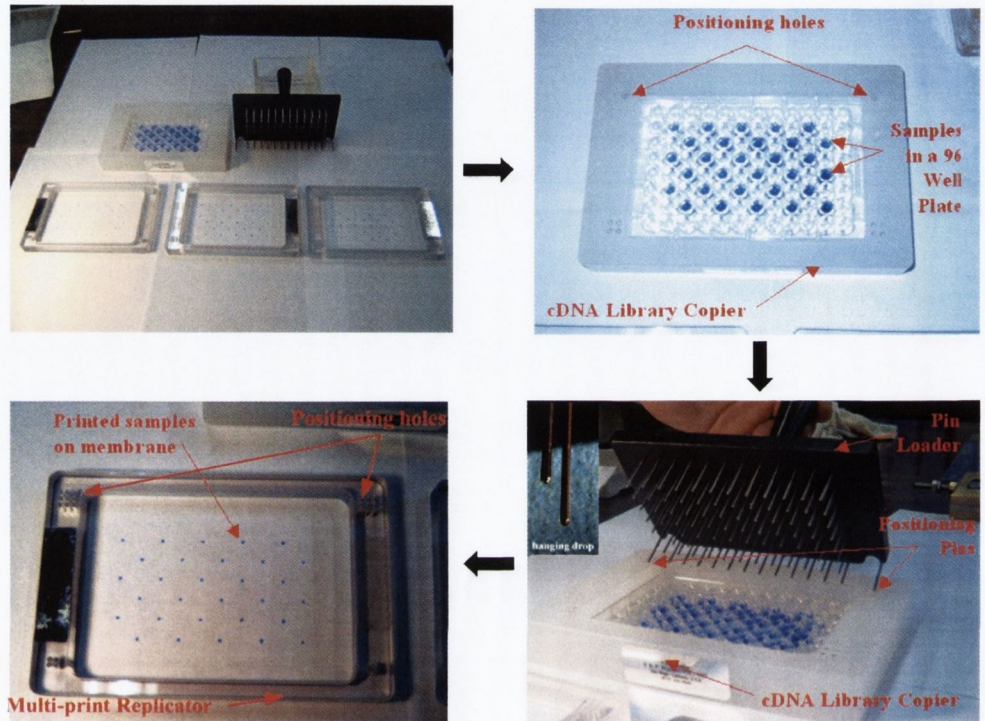


Fig. 3.11 Multi-blot Replicator flow chart

Individual samples of cDNA are mixed with 1X print mix and loaded into individual wells in the 96 well plate. The 96 well plate is then placed into the library copier. This has guide holes so that each of the 96 individual pins on the pin loader will fit into its corresponding well. Each pin will then pick up a hanging droplet of 0.1µl of the sample. This droplet is then printed onto up to 4 duplicate membranes, which are held in place using the multi-print positioning plates. This is then repeated until the entire sample has been transferred.

3.4.2.5 Gene specific Radioactive labelling and Probing protocol

Radioactive probes, for each gene of interest (RNRPS9, GAPDH, IGF-I, c-fos and osteocalcin), were created by performing a standard PCR, using the previously optimised conditions, using first strand synthesis as starting template. These PCR

products was then electrophoresed on a 1.2% low melting point agarose TAE gel and visualised using ethidium bromide stain.

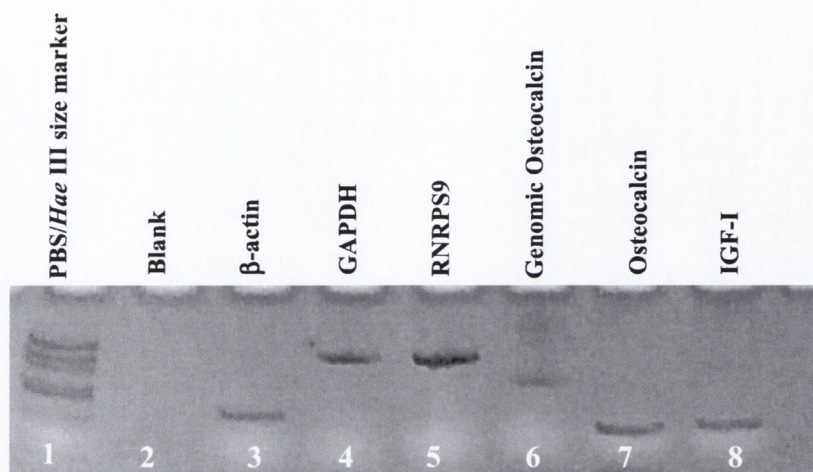


Fig. 3.12 Gel electrophoresis of amplified PCR products for each of the candidate genes' transcripts.

Lane 1: PBS/*Hae* III genomic size marker; Lane 2: empty; Lane 3: β -actin; Lane 4: GAPDH; Lane 5: RNRPS9; lane 6: Genomic osteocalcin; Lane 7: cDNA osteocalcin; Lane 8: IGF-I

The PCR band for each gene transcript was then excised using a sterile scalpel and the cDNA extracted and purified using the Promega Wizard PCR preps DNA purification kit. The purified product was then labelled with the radioactive isotope, ^{32}P , using the random primer kit, to create a radioactive gene specific probe. Each gene transcript used was also assessed for cross-reactivity by running the sequence of nucleotides amplified through the 'Blast' Search engine on the national Institute of Health's website (<http://www.ncbi.nlm.nih.gov/blast>). This checks the sequence inputted against those of all other known gene transcripts for cross-reactivity. No highly conserved regions were found in any of the gene transcripts used.

The three blots, 2 pin-loaded and one hand loaded, were then probed in a rotating hybridising oven at 65°C as described in section 3.4.2.3 with one of the radioactive probes. The blots were then washed, bound in cellophane and placed in a cassette with a storage phosphor screen on top of it for series of exposures. In this experiment, 3 exposure lengths were used, 4 hours, 1 day and 4 days. The storage phosphor screen was evaluated using the Typhoon scanner by shining a laser across its surface and measuring the output in the form of light (see Figure 3.9 and section 3.4.2.6).

Once the different exposures had been carried out the radioactive probe was stripped from the blot by pouring 100ml of boiling 0.05% (95 °C) SDS over the blot and allowing the solution to cool. This was repeated twice more or until the radioactivity had reduced to background levels. To ensure previous radioactive probes had no effect on subsequent probing the sequence of different probes was carefully chosen to start with the gene with the expected weakest expression and finish with the gene with strongest expression (see table 3.6). In addition, since the amplified transcript size of the two housekeeping genes chosen were similar to the range of the amplified candidate genes, any effect of amplifying different size transcripts in the SMART PCR was negated.

Candidate Gene	Size of full mRNA Transcript	Probed in order of
c-fos	2116	1st
IGF-I	1346	2nd
Osteocalcin	480	3rd
RNRPS9	498	4th
GAPDH	1233	5th

Table 3.6 Sequence of probes used for hybridisations

3.4.2.6 Data Analysis and Data Cleaning

The storage phosphor screens were assessed using a multipurpose gel imager (Typhoon 8600, Amersham Biosciences, USA) to create a greyscale image (.gel) for the three exposure times, 4 hours, 1 day, 4 days, for each gene of interest. These ‘.gel’ files were then analysed using the ImageQuant software (Molecular Dynamics, USA). Before the scans dots can be quantified, ‘objects’ are created around each dot within the array. ImageQuant allows the user to specify the size and shape of the object as well as allowing a choice of methods for calculating the background level (none, local median and histogram peak). The volume is then calculated for each dot. Essentially, this is the integrated intensity of all the pixels in the spot less the background. This is calculated by subtracting the background pixel intensity value from each pixel value and summing the resultant answers.

$$Volume = \sum_{y=1}^M \sum_{x=1}^N [f(x, y) - background] \quad (1)$$

Since, the volume calculated is influenced by the objects' position and size a number of tests were carried out to determine the optimal configuration. To determine the optimal method of quantifying a spots volume the DNA ladder was used in a preliminary quantification. Circular objects of varying size (denoted small, medium and large) were centred on each dot in the DNA ladder. For each object size, the volume quantification was performed using each of the three background correction methods (none, local median and histogram peak) (see Figure 3.13). Each combination of object size and background was assessed and the ratios between the each successive point on the ladder found. The mean and standard deviation for each combination was then calculated. Since the quantities of DNA loaded in each dot of the ladder were known, a two-fold increase between successive spots was expected and the combination of medium object size with local median as the background correction was found to produce the best results (1.88 ± 0.53). The local median background value is denoted as the median value for all the pixels along the object edge. This means that even if there are differences across the blots the background is specific to each area on the blot.

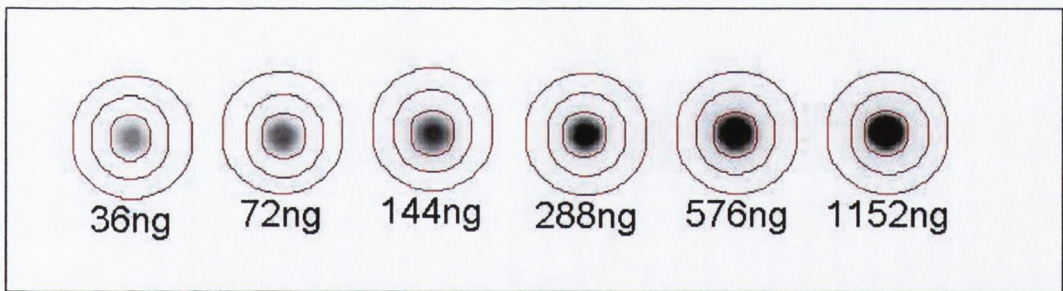


Fig. 3.13 Determining the optimal object size and background correction

To assess which exposure time was optimal, once again the relative ratios of the DNA ladders were assessed for the three exposure times for each gene of interest and the one with the mean ratio closest to a two-fold increase chosen. In all of the blots and gene combinations, the longest exposure (4 days) was found to be the optimal.

This uniform object size was then centred on the middle of each dot on the .gel files for the 4-day exposure for each gene of interest on each of the arrays (two pin loaded and

one hand-loaded). Volume quantification was then performed giving a database containing 48 values corresponding to the 12 rats (6 control and 6 suspended) at 1, 3, 7 and 14 days for each of the three cDNA arrays for all five genes (3 candidate and 2 housekeeping). Comparisons were then calculated to give the relative ratio of each candidate gene to each housekeeping gene for each spot. For example, if a particular dot's volume was found to be 'x' in its c-fos probe and 'y' in its GAPDH probe, then the relative ratio would be x/y. Finally, once these comparisons (3 candidate genes compared to 2 housekeeping) were completed each ratio was divided by the median value of its equivalent control group (see table 3.7). This process of normalising each set of data to the median of its equivalent (in time) control group results in the controls at each time point having a median of one while maintaining their distribution. As a consequence, it is possible to then more easily compare different groups which would have similar distributions but whose median value was different.

Finally, to prevent any misleading readings resulting from dots that were too weak, the following rules were applied to each dot on each array:

- If the average pixel value was not at least five percent greater than the background value the dot was ruled out (10% in the case of 'dirty' blots)
- If over 10 of the possible 18 'gene of interest/housekeeping gene comparisons' were invalid following the first rule all of the remaining comparisons were discounted.

To see a full spreadsheet detailing which data points were ruled out see appendix A3.

Sample #	c-fos Volume	GAPDH Volume	c-fos/GAPDH Ratio	Median of Control Ratios	Normalised Ratios
Control 1	200	1000	0.20	0.37	= (0.20 / 0.37) = 0.55
Control 2	100	800	0.13	-	0.34
Control 3	400	1000	0.40	-	1.09
Control 4	800	2000	0.40	-	1.09
Control 5	300	600	0.50	-	1.36
Control 6	400	1200	0.33	-	0.91
Suspended 1	100	800	0.13	-	0.34
Suspended 2	180	750	0.24	-	0.65
Suspended 3	250	900	0.28	-	0.76
Suspended 4	300	600	0.50	-	1.36
Suspended 5	200	1000	0.20	-	0.55
Suspended 6	150	750	0.20	-	0.55

Table 3.7 Example demonstrating normalising the comparisons relative to the median of the control group

3.5 Statistical Analysis

All data measured were statistically analysed using the statistics software Intercooled STATA (StataCorp. 2001. Stata Statistical Software: Release 7.0. College Station, TX: Stata Corporation). Since a pulsatile effect was thought likely in the genetics data (e.g. in cases where for an increase in the independent variable, such as time, there is a transient response in the dependent variable), ANOVA (Analysis of Variance) was performed on all data sets. In the previous sections an increase or decrease in a particular parameter as a result of HLS would be still present at subsequent time points (i.e. a decrease in new bone formation after three days is still present at later time points). In contrast in the genetics analysis, a transient response at a time point is likely to have completely dissipated by the subsequent time points (i.e. in response to a stimulus new mRNA transcripts are produced at day three, these transcripts are likely to have degraded by day seven). Consequently, the interaction term between the treatment

(control and suspended) and time effects was also analysed in order to ascertain where particular terms significance was derived from. This looks at the effect of treatment over time and, and if a significant treatment by time interaction is found, it determines at which time point the effect originates. Finally, although both ANOVA and linear regression are insensitive to reasonable degrees of variance, in cases where the data appeared skewed a robust linear regression analysis and Kruskal-Wallis ANOVA were performed to check the previously obtained results. For $p < 0.05$, the difference were considered significant, while $p < 0.01$ were noted.

3.6 Results

In this section, the results of the gene expression analysis are presented for the three genes of interest, c-fos, osteocalcin and IGF-I. For each gene the normalised data from all three arrays are pooled. Each candidate gene's data is presented and analysed for each of the two housekeeping genes separately. The two sets of data (relative to the two housekeeping genes) are then pooled and analysed collectively. This acts as a further check to prevent spurious false positives, as a significant alteration in gene expression should be present in all three comparisons (relative to the two individual housekeeping genes and in combination). Any differences found would therefore indicate a level of variability and hence doubt in the results.

3.6.1 c-fos

Figure 3.14 shows the normalised data for c-fos/RNRPS9 for the periosteal samples from the control and suspended femora over the experimental period. There was a statistically significant effect of time on the ratio between c-fos and RNRPS9 (ANOVA, $P < 0.001$). Overall, there was no significant effect of the treatment (HLS) on the c-fos/RNRPS9 normalised data (ANOVA, $P = 0.82$). There was also a significant treatment by time interaction (ANOVA, $P < 0.05$) with this significant effect originating in a significant increase in c-fos/RNRPS9 in the suspended group after 7 days (ANOVA, $P < 0.01$).

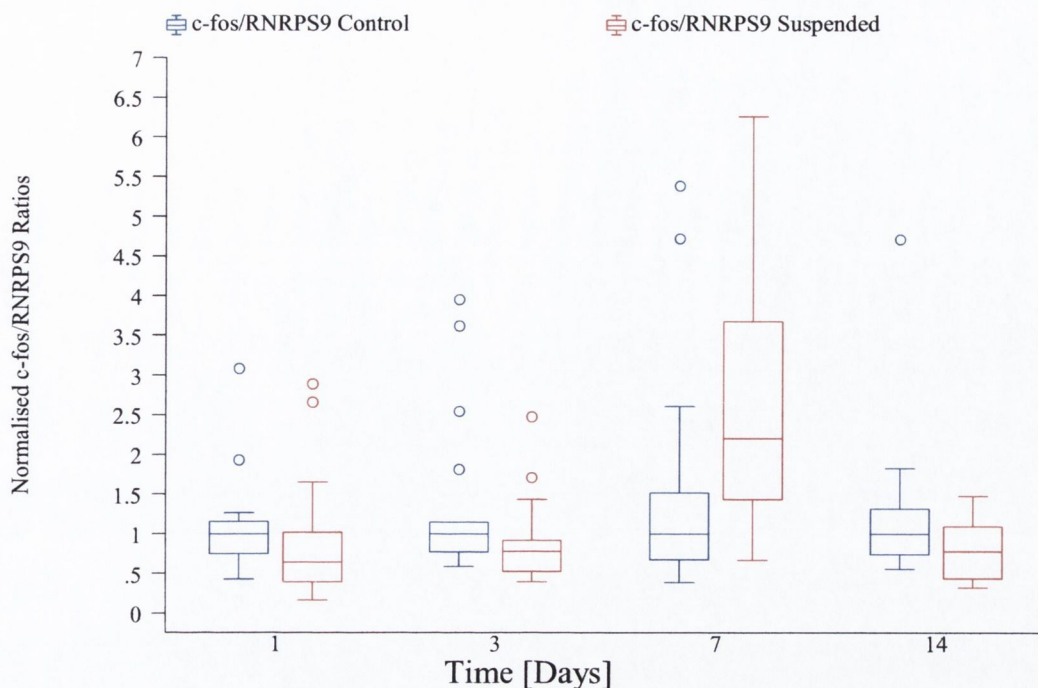


Fig. 3.14 Normalised c-fos/RNRPS9 data Vs. Time for the Control and Suspended groups

(Box Plot Explanation: The line in the middle of the box represents the median or 50th percentile of the data. The box extends from the 25th percentile, $x_{[25]}$, to the 75th percentile, $x_{[75]}$, the so-called interquartile range, IQR. The lines or ‘whiskers’ emerging from the box extend to the upper and lower adjacent values. The upper adjacent value corresponds to the largest data point less than or equal to $x_{[75]} + 1.5 \cdot \text{IQR}$. Conversely the lower adjacent value is defined as the smallest data point greater or equal to $x_{[25]} - 1.5 \cdot \text{IQR}$. Any values more extreme than the adjacent values are plotted individually.)

This picture is mirrored in Figure 3.15, which shows the normalised data for c-fos/GAPDH for the periosteal samples from the control and suspended femora over the experimental period. There was a statistically significant effect of time on the ratio between c-fos and GAPDH (ANOVA, $P < 0.05$). Overall there was again no significant effect of the treatment (HLS) on the c-fos/GAPDH normalised data (ANOVA, $P = 0.27$). There was a significant treatment by time interaction (ANOVA, $P < 0.05$) with this significant effect originating in an increase in c-fos/GAPDH in the suspended group after 7 days that approached significance (ANOVA, $P = 0.067$).

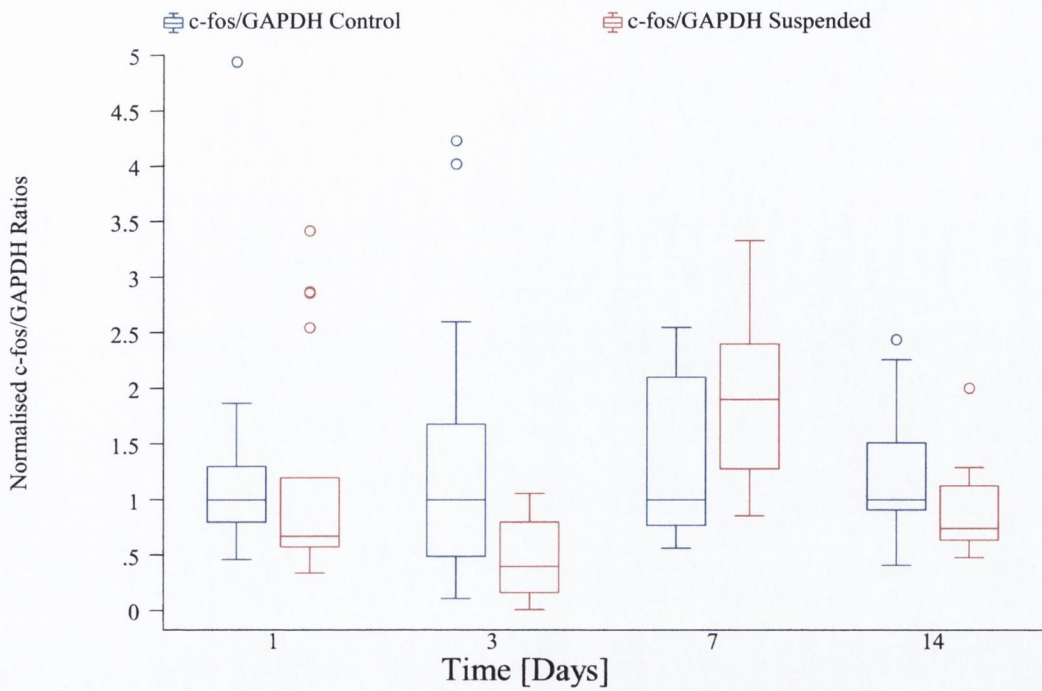


Fig. 3.15 Normalised c-fos/GAPDH data Vs. Time for the Control and Suspended groups

Figure 3.16 shows the combined normalised data for c-fos/housekeeping for the periosteal samples from the control and suspended femora over the experimental period. There was a statistically significant effect of time on the ratio between c-fos and the housekeeping genes (ANOVA, $P < 0.0001$). Overall there was no significant effect of the treatment (HLS) on the c-fos/housekeeping normalised data (ANOVA, $P = 0.37$). There was a significant treatment by time interaction (ANOVA, $P < 0.001$) with this significant effect originating in a significant increase in c-fos/housekeeping in the suspended group after 7 days (ANOVA, $P < 0.005$). Finally, Table 3.8 summarises the statistical relationship between c-fos levels and time and treatment.

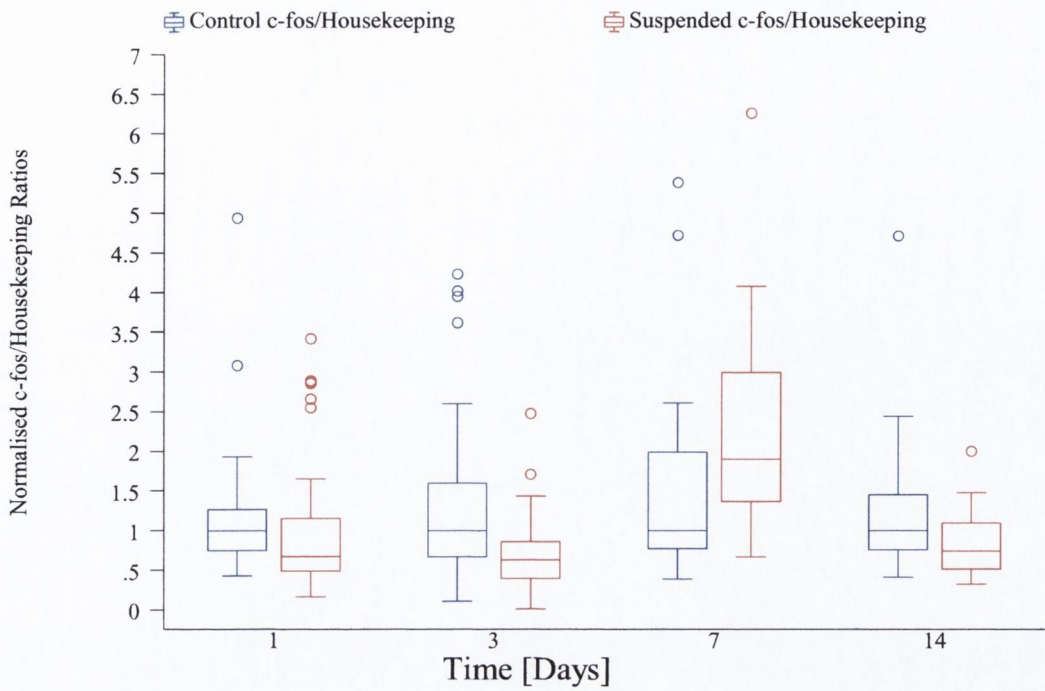


Fig. 3.16 Normalised c-fos/Housekeeping data Vs. Time for the Control and Suspended groups

	Days	Treat	Interaction Treat*days
c-fos/both	p = 0.0000	p = 0.37	p = 0.0003
c-fos/RNRPS9	p = 0.0001	p = 0.82	p = 0.02
c-fos/GAPDH	p = 0.011	p = 0.27	p = 0.017

Interaction Term	1 Days	3 Days	7 Days
c-fos/both	p = 0.453	p = 0.443	p = 0.001
c-fos/RNRPS9	p = 0.659	p = 0.990	p = 0.009
c-fos/GAPDH	p = 0.527	p = 0.234	p = 0.067

Table 3.8 Statistical analysis of the relationships between c-fos and the housekeeping genes with respect to Time and Treatment (ANOVA)

3.6.2 Osteocalcin

Figure 3.17 shows the normalised data for osteocalcin/RNRPS9 for the periosteal samples from the control and suspended femora over the experimental period. There was a statistically significant effect of time on the ratio between osteocalcin and RNRPS9 (ANOVA, $P < 0.001$). Overall there was a significant effect of the treatment (HLS) on the osteocalcin/RNRPS9 normalised data (ANOVA, $P < 0.05$). There was also a significant treatment by time interaction (ANOVA, $P < 0.01$) with this significant effect originating in a significant increase in osteocalcin/RNRPS9 in the suspended group after 7 days (ANOVA, $P < 0.01$).

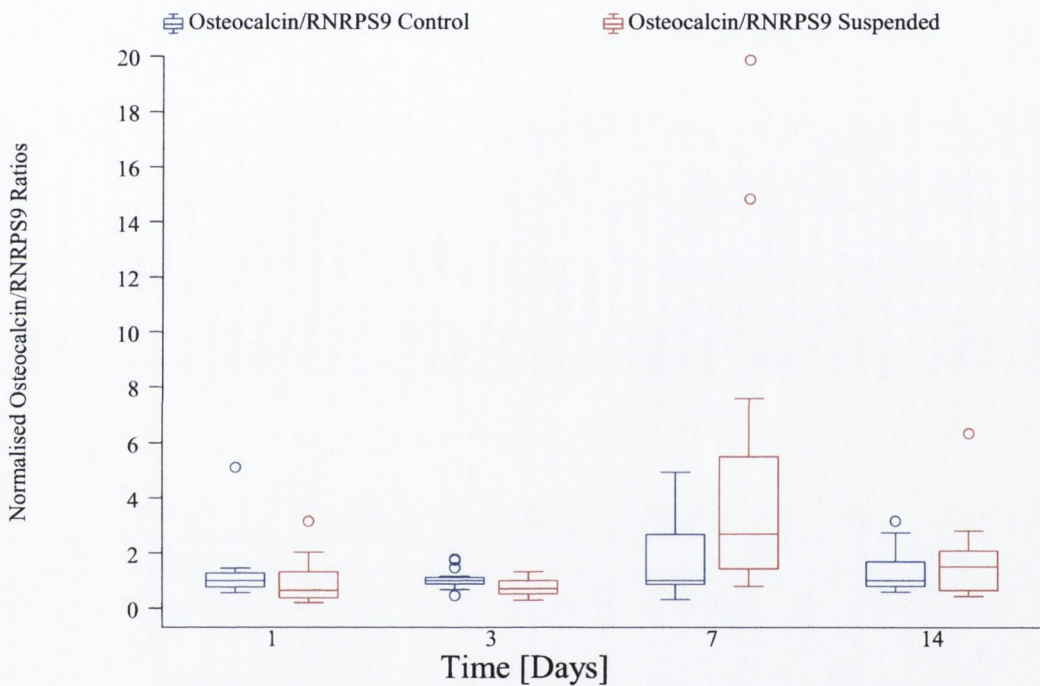


Fig. 3.17 Normalised osteocalcin/RNRPS9 data Vs. Time for the Control and Suspended groups

This picture is mirrored in Figure 3.18, which shows the normalised data for osteocalcin/GAPDH for the periosteal samples from the control and suspended femora over the experimental period. There was a statistically significant effect of time on the ratio between osteocalcin and GAPDH (ANOVA, $P < 0.001$). Here there was no significant effect of the treatment (HLS) on the osteocalcin/GAPDH normalised data (ANOVA, $P = 0.11$). There was a significant treatment by time interaction (ANOVA, P

< 0.001) with this significant effect again originating in a significant increase in osteocalcin/GAPDH in the suspended group after 7 days (ANOVA, $P = 0.005$).

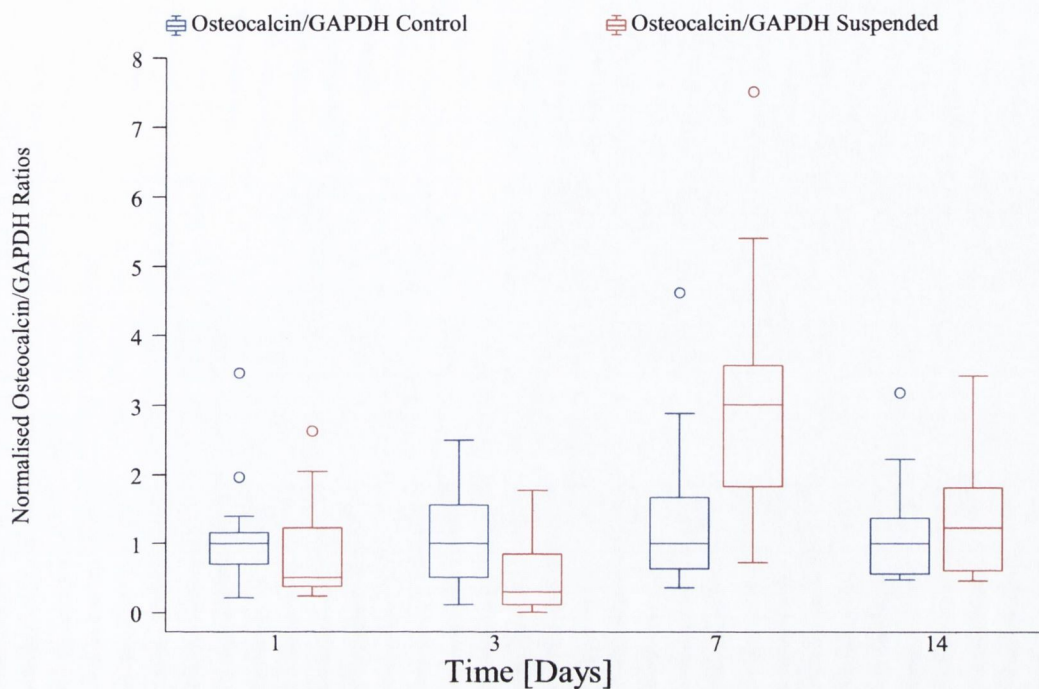


Fig. 3.18 Normalised osteocalcin/GAPDH data Vs. Time for the Control and Suspended groups

Figure 3.19 shows the combined normalised data for osteocalcin/housekeeping for the periosteal samples from the control and suspended femora over the experimental period. There was a statistically significant effect of time on the ratio between osteocalcin and the housekeeping genes (ANOVA, $P < 0.0001$). Overall there was a significant effect of the treatment (HLS) on the osteocalcin/housekeeping normalised data (ANOVA, $P < 0.05$). There was a significant treatment by time interaction (ANOVA, $P < 0.001$) with this significant effect originating in a significant increase in osteocalcin/housekeeping in the suspended group after 7 days (ANOVA, $P < 0.001$). Finally, Table 3.9 summarises the statistical relationship between the levels of osteocalcin and the parameters time and treatment.

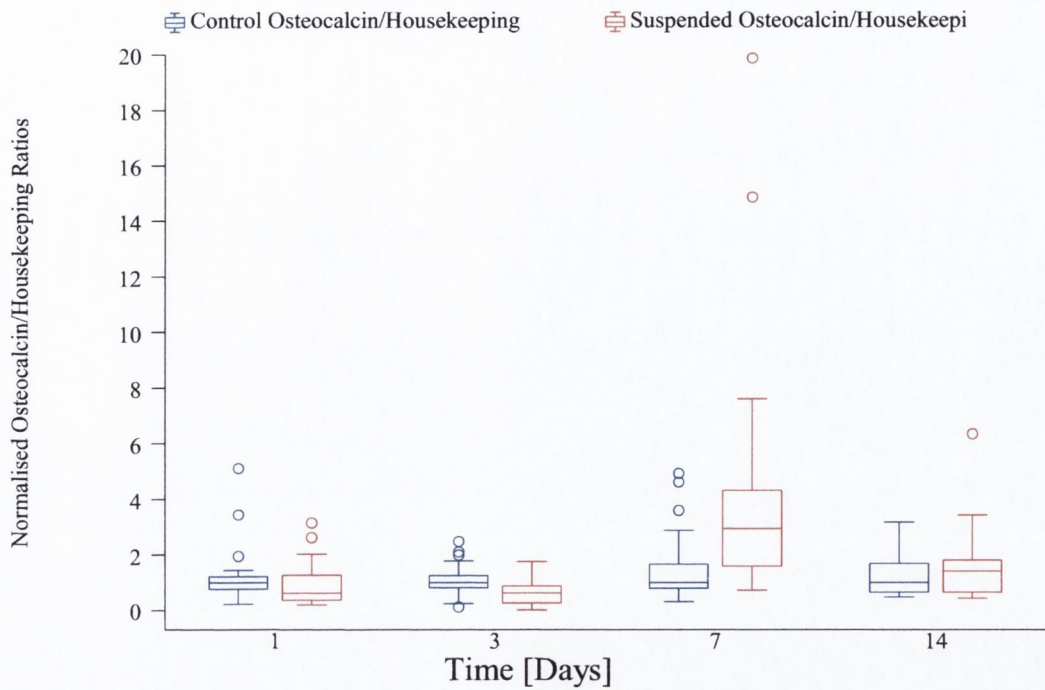


Fig. 3.19 Normalised osteocalcin/housekeeping data Vs. Time for the Control and Suspended groups

	Days	Treat	Interaction Treat*days
Oc/both	p = 0.000	p = 0.012	p = 0.000
Oc/RNRPS9	p = 0.000	p = 0.039	p = 0.002
Oc/GAPDH	p = 0.000	p = 0.112	p = 0.000

Interaction Term	1 Days	3 Days	7 Days
Oc/both	p = 0.312	p = 0.203	p = 0.000
Oc/RNRPS9	p = 0.492	p = 0.516	p = 0.006
Oc/GAPDH	p = 0.347	p = 0.096	p = 0.002

Table 3.9 Statistical analysis of the relationships between osteocalcin and the housekeeping genes with respect to Time and Treatment (ANOVA)

3.6.3 Insulin-like Growth Factor I

Figure 3.20 shows the normalised data for IGF-I/RNRPS9 for the periosteal samples from the control and suspended femora over the experimental period. There was no statistically significant effect of time on the ratio between IGF-I and RNRPS9 (ANOVA, $P = 0.10$). Overall there was also no significant effect of the treatment (HLS) on the IGF-I/RNRPS9 normalised data (ANOVA, $P = 0.90$). There was also no significant treatment by time interaction (ANOVA, $P = 0.47$).

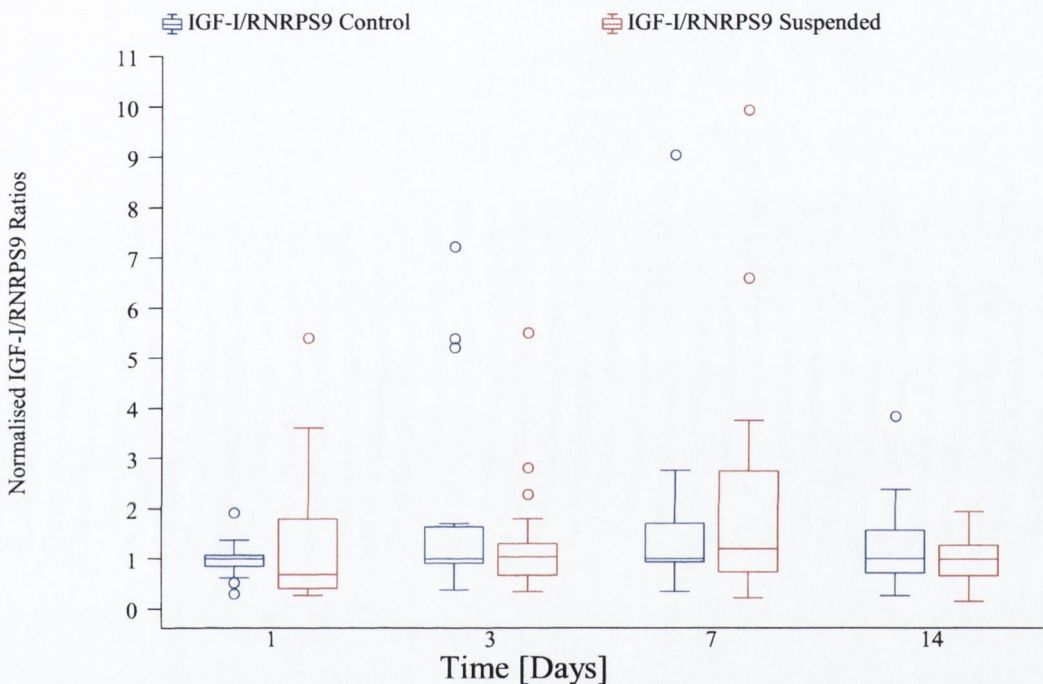


Fig. 3.20 Normalised IGF-I/RNRPS9 data Vs. Time for the Control and Suspended groups

This picture is different in Figure 3.21, which shows the normalised data for IGF-I/GAPDH for the periosteal samples from the control and suspended femora over the experimental period. There was again no statistically significant effect of time on the ratio between IGF-I and GAPDH (ANOVA, $P = 0.50$). There was also no significant effect of the treatment (HLS) on the IGF-I/GAPDH normalised data (ANOVA, $P = 0.19$). There was however a significant treatment by time interaction (ANOVA, $P < 0.05$) with this significant effect again originating in a significant decrease in IGF-I/GAPDH in the suspended group after 3 days (ANOVA, $P < 0.05$).

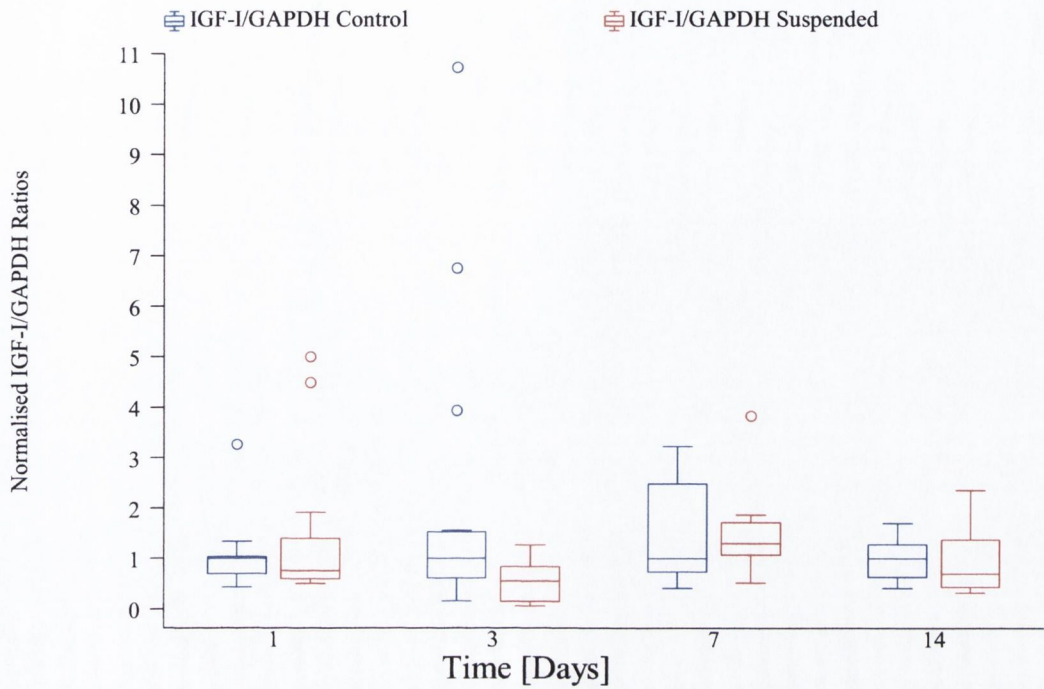


Fig. 3.21 Normalised IGF-I/GAPDH data Vs. Time for the Control and Suspended groups

Figure 3.22 shows the combined normalised data for IGF-I/housekeeping for the periosteal samples from the control and suspended femora over the experimental period. Overall, there was a statistically significant effect of time on the ratio between IGF-I and the housekeeping genes (ANOVA, $P < 0.05$). There was no significant effect of the treatment (HLS) on the IGF-I/housekeeping normalised data (ANOVA, $P = 0.47$). There was however a significant treatment by time interaction (ANOVA, $P < 0.05$) although there was no significant effect at any of the time points (ANOVA, $P < 0.001$). Finally, Table 3.10 summarises the statistical relationship between the levels of insulin-like growth factor-I and the parameters time and treatment.

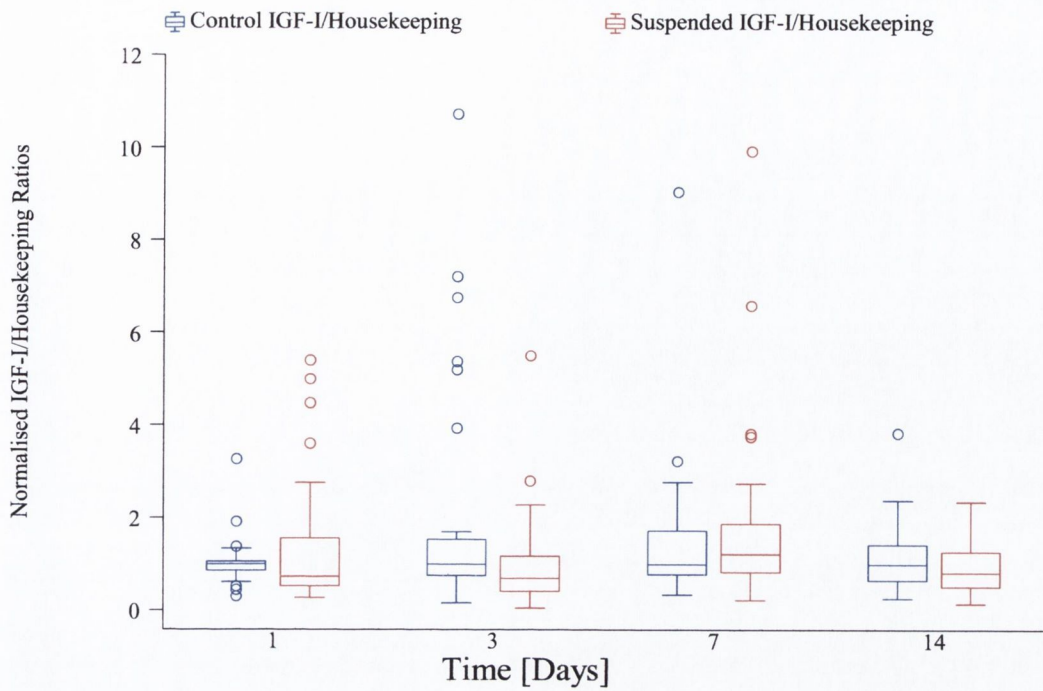


Fig. 3.22 Normalised IGF-I/housekeeping data Vs. Time for the Control and Suspended groups

	Days	Treat	Interaction Treat*days
IGF-I/both	p = 0.043	p = 0.47	p = 0.039
IGF-I/RNRPS9	p = 0.0966	p = 0.90	p = 0.4662
IGF-I/GAPDH	p = 0.4994	p = 0.1847	p = 0.0363

Interaction Term	1 Days	3 Days	7 Days
IGF-I/both	p = 0.351	p = 0.142	p = 0.317
IGF-I/RNRPS9	p = 0.452	p = 0.821	p = 0.259
IGF-I/GAPDH	p = 0.579	p = 0.040	p = 0.854

Table 3.10 Statistical analysis of the relationships between IGF-I and the housekeeping genes with respect to Time and Treatment (ANOVA)

3.7 Discussion

Disuse osteoporosis, due to lack of exercise or bed-rest, is characterised by a loss of bone mass following the unloading of bones. This loss of bone mass has both genetic and epigenetic components. The genetic component is a systemic factor involved in determining the size and shape of all the bones in the body, and is particularly strong in growing animals. The epigenetic factor that is of most interest in disuse osteoporosis is the effect of altering the mechanical forces imparted to the bone. Experimentally, disuse osteoporosis can be induced via hind limb suspension. HLS in young growing animals, as used in this research project, is characterised by a cessation or reduction in the cross-sectional growth in the unloaded limbs. However this cessation/reduction is transient and growth returns towards normal by two weeks of continued unloading (Globus et al., 1986b). This implies that at least two forces are at work on the system. In young growing animals there is a strong age-related growth potential driven by a genetic component. There is also an epigenetic component, which in this case is the mechanical stimulus required by the cells for normal growth. The unload induced by HLS seems to transiently interfere with or override the genetic growth potential and bone growth ceases. This in turn implies that a signalling pathway is present linking the cells recognition of reduced mechanical load and its reduced bone formation function. When considering a timeframe for this signalling response, one approach could be to compare the rate of response with that achieved in cases of overload. In overload there is a rapid transient response, which occurs within 20 minutes and peaks at around 4 hours (Matsumoto et al., 1998). However since growth is resumed after around a week, at some point the growth potential must override this epigenetic factor and the bone cells begin forming new bone. Cells have been shown to have a memory of their previous mechanical loading history. Bone marrow stromal cells extracted and cultured from the marrow cavities of bones which had been unloaded via HLS had a reduced proliferation and bone forming rate (Kostenuik et al., 1997, Machwate et al., 1993, 1999). Consequently, it would seem likely that cells which had reduced function due to an epigenetic signal, following reduced mechanical load, would require a secondary systemic signal to stimulate the cells to resume normal levels of bone formation. In addition, researchers have shown that dynamic loads are required to elicit a bone response (Lanyon and Rubin, 1984). Consequently, in designing the project timeframe it was felt that the time points chosen (1, 3, 7 and 14 days) would be sufficient to pick

up the response to unloading, at the earlier timepoints, and the restoration of the growth signal. In addition the choice of candidate genes reflected this need to assess the response of the cells over the full timeframe, with c-fos being an early response gene while osteocalcin and IGF-I have been closely linked with bone formation.

Rats are a commonly used model in osseous research, as they are a fast growing, cost effective model for the analysis of osseous dysfunction. However, due to the small size of the animals, the volume of bone tissue samples obtainable is also small. For example, in this project, stripping the periosteum from a 5 mm region of mid-diaphysis of a rat femur yielded between 50ng and 1µg of total RNA. As a result of this low yield of RNA, many standard molecular biology techniques are incapable of working unless samples are to be pooled. Northern blot analysis, for instance, requires at least 10µg of total RNA in each sample to be analysed.

In chapters four and five the effect of unloading, via HLS, on the growth rates and structural properties of the unloaded femora was examined. The aim of this section of the research project was to investigate the effect of unloading, via HLS, on the gene expression patterns of the femoral periosteal tissue of young rats. Initially, RT-PCR was employed to analyse the gene expression patterns. However after a number of trials, it was decided to modify a commercially available product, SMART, to create small-scale cDNA arrays. SMART is a modified PCR, which amplifies non-specifically all the mRNAs within a sample while preserving the relative ratios between transcripts. This amplified product was then pin-loaded onto positively charged nylon membranes in much the same manner as commercial arrays are created. Gene specific radioactive probes were then hybridised to the cDNA arrays in a candidate study to assess gene expression patterns relative to those of a housekeeping genes. Candidate studies by their nature have a number of positive and negative attributes. The benefits are that by reviewing the literature and through understanding of the biology of the traits of interest, the researcher can use good judgement to select candidate genes of interest. It also takes advantage of, and uses, the previously published literature and allows referencing with these previous results to validation of results. In addition, it is cheaper (in total) and easier to use by a small lab such as ours interested in a specific gene(s) expression response. The main drawbacks include the risk of missing gene expression changes in crucial genes of interest, which comprehensive techniques, such as

GeneChip™ array technology, would pick up. Finally, the candidate gene approach reveals little information about the regulatory elements of the candidate genes.

Overall, the system used here is considered a quick and reproducible method of analysing the gene expression patterns of a relatively large number of samples. In particular it is of use in cases where RNA yield is low and variable in quantity and quality. As such this system is proposed as a first step analysis to determine what genes and time points might be of interest for further study. This further study would likely take the form of a quantitative technique such as real-time PCR. The system employed in this study has a number of positive attributes. The use of array technology is a well accepted model for gene expression analysis. SMART works from as little as 25ng total RNA, which enables work to be done on very small tissue samples such as biopsies or periosteal samples. Use of the Multiblot replicator allows for the analysis of a large number of samples (up to 144) simultaneously. The process is also relatively easy and inexpensive to set-up, allowing the opportunity to use the method in smaller labs without expensive specialised equipment. Finally, multiple copies of a cDNA array can be created at the time of sample collection and stored for later analysis. On the other hand, this system is semi-quantitative as gene expression levels are measured relative to the expression level of a panel of housekeeping genes. In this study a number of the commercial kits components were replicated/synthesised externally to reduce the cost. However, since this study was initiated the cost of the commercial kit has vastly reduced and been simplified. Consequently, future studies would be encouraged to use the commercially available kits¹ rather than replacing components. This would result in a simpler amplification process and need less optimisation when setting up the system. The main drawback of this gene array approach is that it is still only semi-quantitative and hence further quantitative study may be necessary.

The hypothesis at the start of the gene expression analysis was that unloading would result in a transient drop in genes associated with bone formation. Therefore it was expected that the expression of c-fos, osteocalcin and IGF-I, genes previously linked with a bone forming response, would be transiently reduced immediately following HLS (Kawata and Mikuni-Takagaki, 1998, Kostenuik et al., 1997). This response to the

¹SMART kit primers post 2001 also contain a t4 gene 32 protein. This protein increases the yield from RT-PCR products and greatly raises the efficiency of the SMART amplification cycles (Biotechniques 31:81-86 (July 2001))

epigenetic factor, reduced load, must at some point be overridden by the growth potential in these young animals as bone growth returns to normal within 14 days of continued unloading. Therefore, at some point the signal for bone formation and growth must be reinstated.

In this experiment, for each dot on the array, the expression of each candidate gene was assessed as a ratio of the value of the housekeeping gene(s) for the same dot. This ratio was then in turn expressed relative to the median value of its corresponding age-matched control group. This allowed the data from each cDNA array to be directly compared to each other. The data for each candidate gene was then statistically assessed relative to the two housekeeping genes, independently and in combination. The gene expression patterns of *c-fos* and osteocalcin were found to be very similar regardless of whether they were compared against the housekeepers individually or in combination. Interestingly, the variance found in the *c-fos* data was substantially greater than that found in the osteocalcin or IGF-I data. There is no methodological reason for this discrepancy and the answer may be due to the nature of the gene in question, with *c-fos* being involved in numerous transcription pathways unrelated to the effects of mechanical load. In the case of both *c-fos* and osteocalcin, there was a drop in the suspended groups expression level at 1 and 3 days, although this was not found to be statistically significant. After 7 days there was a significant increase in the expression of both these genes in the suspended groups relative to the controls. However, by day 14 there was once again no difference between their expression levels. These elevated levels of *c-fos* and osteocalcin are indicative of a bone formation response. One explanation is that this rise is related to the reinstating of the normal age-relating growth pattern. Indeed, when the bone formation index and mid-diaphyseal periosteal area data from chapter three are studied, it is clear that between days 7 and 14 there is a reversal of effects. After 7 days the periosteal formation rate in the suspended animals is lower than that of the controls. However, after 14 days this pattern changed with new bone being laid down at the periosteal surface at a level at least that of bone formation seen in the controls. The 7 day time frame here is also comparable to that observed by Bentolila et al. (1998) who overloaded rat bones to create microdamage and saw a resorption response around 10 days later.

The gene expression pattern of IGF-I was found to be different to that of *c-fos* and osteocalcin. When compared against GAPDH there was a significant transient decrease

in IGF-I levels after three days of suspension. However this decrease was not present when compared against RNRPS9 or when the data sets were combined. Consequently, based on this dichotomy in the data, this effect of suspension on the gene expression of IGF-I in femoral mid-diaphyseal periosteal tissue cannot be conclusively established. However it is clear that the elevated levels of IGF-I expression found in previous experiments in total bone mRNA extractions has not been found in this study (1995, Bikle et al., 1994b, 1994c, 1994d).

The belief that c-fos and osteocalcin expression would be down regulated following HLS stems largely from work carried out on overload bones, although some work has been done on gene expression patterns in underload. Since morphologically bone formation is reduced following HLS, a reduction in the expression of genes associated with the proliferation and activation of osteoblasts was expected. A number of researchers have overloaded bone or bone cells by a variety of methods. For example, *in vivo*, bones have been mechanically loaded using metal pins inserted into the bones and the response assessed at the surface using methods like *in situ* hybridisation or for the entire bone using Northern Blot analysis (Chambers et al., 1999, Chow et al., 1998). However, *in situ* hybridisation can only be done on trabecular bone, which may not respond the same way as cortical bone. Northern blot analysis requires large amounts of RNA. This generally requires the researcher to either homogenise full bones prior to extracting the RNA or pooling of samples to generate the required amount of genomic material. Obviously, using the entire bone means that any measured RNA pattern is that of a mix of cell types, consisting largely of osteocytes and osteoblasts, although there would also be epithelial and vascular cells. Furthermore, data from pooled samples is sensitive to extreme values. Despite the variation in techniques the results have been similar with overload resulting in a bone forming response. This is preceded by a transient upregulation in the expression of c-fos and osteocalcin, with elevated levels reported as early as 20 minutes post application of the load.

Another approach has been to culture cells either on a flexible plate or within a gel. These cells can then be stretched to mechanically load them and the response measured via a large number of standard molecular biology techniques (Kawata and Mikuni-Takagaki, 1998, Yamaguchi et al., 2002, Nakayama et al., 1996, Peake et al., 2000, Peake and El Haj, 2003). Another approach is to pass ultrasound through cultures of cells in order to mechanically stimulate them (Warden et al., 2001, Naruse et al., 2000).

Again, the general response to these varying loads is for the cells to elicit a bone forming response, which once again is preceded by a transient upregulation of c-fos and osteocalcin. However, care must be taken in extrapolating these data to *in vivo* models, as the mode, magnitude and directions of loading are unlikely to be physiological.

A number of researchers have also examined the effects of underload on the gene expression patterns in rats. In a series of experiments, Bikle et al (1995, Bikle et al., 1994a, 1994b, 1994c, 1994d) examined the effect of HLS and spaceflight on gene expression patterns in the unloaded limbs. They found reduced expression levels of osteocalcin and elevated IGF-I mRNA levels in the tibiae of rats following spaceflight. This picture was mirrored in experiments using HLS where decreased osteocalcin levels and elevated levels of IGF-I mRNA, in the proximal tibia and distal femur of growing rats, were measured after 2 weeks of hindlimb elevation. However, in these experiments the mRNA isolated was from the homogenate of the entire bone or bone section after the marrow cavity had been flushed out. Again, the distinction must be made that this expression pattern is therefore that of a mix of cell types of which osteoblastic cells are in the majority. In later experiments by the same research group (1999, Kostenuik et al., 1997), rat osteoprogenitor cells (BMSCs) were isolated and cultured from primary cells flushed from the medullar cavities of rat bones that were unloaded for 5 days via HLS. BMSCs from 5-day unloaded rats expressed 50% less c-fos and 35% less osteocalcin mRNA compared with controls. These data demonstrate that cultured osteoprogenitor cells retain a memory of their *in vivo* loading history and indicate that skeletal unloading inhibits proliferation and differentiation of osteoprogenitor cells *in vitro*.

Finally, in a study conducted by Matsumoto et al. (1998) the periosteum was also isolated and analysed separately following HLS. In this experiment, samples were only taken at the end of the two weeks and no differences were found. Although the required information is not stated in the published paper, since Northern blot analysis was performed it must be assumed that periosteal samples from a number of animals were pooled in order to generate the required 20µg of total RNA. In addition, the choice of statistical test (Students t test) for the analysis is questionable as it is more likely to result in a false positive significant result.

Although the initial hypothesis of a transient down regulation in c-fos and osteocalcin has not been validated, it is not possible to discount it yet. There are a number of possible explanations as to why the expected reduction in c-fos and osteocalcin was not

detected. Firstly, in overload the response is swift and transient (detectable within 20 minutes, peaking after a couple of hours and returning to normal within 6 hours (Chambers et al., 1999, Peake and El Haj, 2003, Warden et al., 2001, Peake et al., 2000). If the response to underload is of a similar timeframe then it is likely that taking measurements at the first time point, after one day, would have been too late to detect a transient response peak. Secondly, the response to underload is likely to have a less easily quantified signal than that to overload. Consequently, it may be necessary to use a quantitative method instead of a semi-quantitative method to detect a reduction in gene expression levels in lowly expressed genes. Finally, an important point to note is that in this study only the periosteal tissue was analysed whereas in most other studies either a different type of bone was used or the full bone was crushed to isolate the mRNA, resulting in a mixture of mRNA from various types of cells.

3.8 Conclusions

The aim of this section of the project was to investigate the effect of altered mechanical loading, via hindlimb suspension, on the gene expression patterns of samples of periosteal tissue from the right femora of young rats. In order to do the analysis an existing commercial product, SMART, was modified to create a new simple system for creating small-scale cDNA arrays. A candidate gene approach was employed to assess alterations in gene expression due to mechanical unloading. The genes chosen were osteocalcin, Insulin-like growth factor I and c-fos. The cDNA arrays were then probed sequentially with gene specific radioactive probes to determine the levels of expression for each gene in each periosteal sample.

To conclude, the following research questions have been answered:

- The use of RT-PCR to analyse the gene expression pathways in individual mRNA samples with limited RNA volumes from rat periosteal tissue of varying quantity is problematic
- SMART technology was used to generate small-scale cDNA arrays by using the Multiblot replicator to create a quick, reproducible and relatively inexpensive system for mRNA analysis:
 - SMART works from as little as 25ng total RNA, which enables work to be done on samples with low RNA volumes.
 - A large number of samples (up to 144) can be analysed simultaneously.
 - The process is also relatively easy and inexpensive to set-up, allowing the opportunity to use the method in smaller labs without expensive specialised equipment.
 - Finally, multiple copies of a cDNA array can be created at the time of sample collection and stored for later analysis.
- These cDNA arrays created from periosteal tissue were analysed for changes in gene expression patterns following various periods of HLS
 - Following HLS there was a consistent drop (not statistically significant) in the levels of c-fos and osteocalcin measured at one and three days.
 - After seven days there was a significant increase in the levels of c-fos and osteocalcin

- This increase is consistent with the bone forming response which was observed between seven and fourteen days in chapter three at the mid-diaphysis
- This bone forming response could be the systemic/genetic factors reasserting control in these young fast growing rats
- The data for the gene expression levels of IGF-I was contradictory with a drop in expression seen after 3 days relative to GAPDH but not when compared against RNRPS9 or the two housekeeping genes combined
 - Consequently further study may be necessary to elucidate the real response
- Overall further study is required at this more specific tissue level. This could be accomplished in part using the array technique described here to determine the optimal time points and genes of most interest. The further study should then take advantage of newer quantitative techniques, such as real-time PCR,

Chapter 4 Morphological Change and Microdamage

4.1 Introduction

Wolff's law states that a bone's form reflects its function. This implies that if the mechanical function of a long bone is altered by the removal of the weight bearing forces, the form or shape of the bone will change. In this experiment, hindlimb suspension (HLS) was used to unload the femora of young growing rats in order to examine the effects of altered load. Young animals were used as the effects of unloading are more marked in animals whose bones are growing (Jaworski et al., 1980).

4.1.1 Previous work

HLS of growing rats has been shown to result in a decrease in both bone mass and maturity. However, studies have shown that this reduction in the weight of the bones is transient and appears to be restricted to the unloaded bone (Globus et al., 1986b, Arnaud et al., 1995, Roer and Dillaman, 1990).

Contrary to the effect on bone mass, HLS has no effect on the length of either the humeri or femora (Spengler et al., 1983, van der Meulen et al., 1995, Vailas et al., 1988, Shaw et al., 1987). Since bone length remains unaffected it is also evident that factors other than applied loading, such as genetic factors, appear to determine bone length.

In growing rats, the periosteal and endosteal diameters are increasing, with bone formation occurring predominantly at the periosteal surface and bone resorption predominantly at the endosteal surface. Studies have shown that following hindlimb suspension the effect on cross sectional area is also different in the loaded and unloaded bones. In the loaded humeri, there were no significant differences reported in the humeral cross sectional area (periosteal, endosteal or total) of the suspended animals (Bikle et al., 1994b, Globus et al., 1986a, Morey et al., 1979). In the unloaded femora a number of studies have shown the periosteal diaphyseal diameter is reduced relative to controls whereas the endosteal diameter remains unaffected (van der Meulen et al., 1995, Globus et al., 1986b, Morey et al., 1979). This implies that the reduction in the rate of accretion of bone mass due to unloading by hindlimb suspension seems to be

largely the result of a reduced bone formation rate rather than an increased resorption rate.

In cortical bone, Sessions et al. (1989) showed that in the tibiae of rats, hindlimb suspended for 28 days, osteoblast surface was reduced by 29% and bone formation rate at the tibio-fibular junction was reduced by 34%. Globus et al. (1986b) found that the bone formation rate at the tibio-fibular junction decreased to 49% of control levels in the first week of hindlimb suspension but returned to control levels by the end of the second week. In trabecular bone, hindlimb suspension also causes a decrease in bone formation rate relative to controls in rats (Matsumoto et al., 1998, Machwate et al., 1994). These studies found the reduction in bone formation rate to be transient and to return to control levels by the end of the second week.

There is only limited evidence of *in vivo* labelling of microcracks prior to the animals sacrifice with, to this authors knowledge, only one paper published showing *in vivo* microdamage in horses using a fluorochrome, calcein green (Stover et al., 1992). However, a number of authors have stained *in vivo* microdamage in other animals using bulk staining in basic fuchsin (Muir et al., 1999, O'Brien et al., 2000, Lee et al., 1998, Schaffler et al., 1989, Burr and Martin, 1993, Lee et al., 2002) and with fluorochromes (Alizarin) post-mortem (O'Brien et al., 2003).

4.1.2 Fluorescent Markers

The use of fluorescent agents to bind to and label exposed calcium in bone is well established (Rahn, 1977, Lee et al., 2003). Fluorochromes chemically bind to the exposed calcium on various surfaces in the bone matrix. Calcium is exposed in bone as it is being mineralised during formation, demineralised in resorption or on the walls of microcracks. When these bound fluorochromes are exposed to light of a specific wavelength, electrons in the inner shell are excited and move to an outer shell. On returning to the inner shell they release energy in the form of light of longer wavelength and characteristic colour. When administering a series of agents at specific intervals, each dye will label bone formation as well as resorption sites and microcracks in the matrix. However since bone resorption is a relatively rapid process, estimated at 40-50 $\mu\text{m}/\text{day}$ in cortical bone longitudinally, or 5 $\mu\text{m}/\text{day}$ radially (Martin and Burr, 1989), if more than three days elapse between administration and sacrifice, the labels in the resorption sites will have been removed. Successive sites of newly formed bone retain

the dyes. By knowing the time of administration of each agent, and by measuring the distances between labelled sites, bone formation and periosteal expansion rates can be calculated. In this study all animals received fluorescent labels according to a dosage regime developed by Rahn (1977)(see section 4.2.5).

4.1.3 Research Questions

The aim of this section of the project was to investigate the effect of altered mechanical loading, via hindlimb suspension (HLS), on the morphology and growth patterns of the long bones of young rats. Morphological changes due to altered load were assessed by measurements of bone dimensions and by histological analysis of slides made from the mid-diaphysis of the animals' femora and humeri. Intra-peritoneal injections of fluorescent dyes were given to all animals to mark sites of new bone formation at the time of administration. These fluorescent dyes were then used to identify the effect of altered loading on the formation patterns during the experimental period.

The following research questions were asked:

- Would HLS result in an altered gross morphology, bone length and weight, in humeri and femora?
- What is the effect of HLS on growth patterns across the mid-diaphyses of the loaded humeri and unloaded femora?
 - Does HLS affect the amount of bone present (encompassing measurements of periosteal, endosteal and total cross sectional areas)?
 - Does HLS result in a change in the shape of the bones at the mid-diaphysis (encompassing measurements of circularity and elongation)?
 - Is this response due to altered formation, resorption or a coupled response of the two?
- Does the altered loading due to HLS cause microcracking or the formation of secondary osteons/Haversian systems?

4.2 Materials and Methods

4.2.1 Measuring Bone Length and Weight

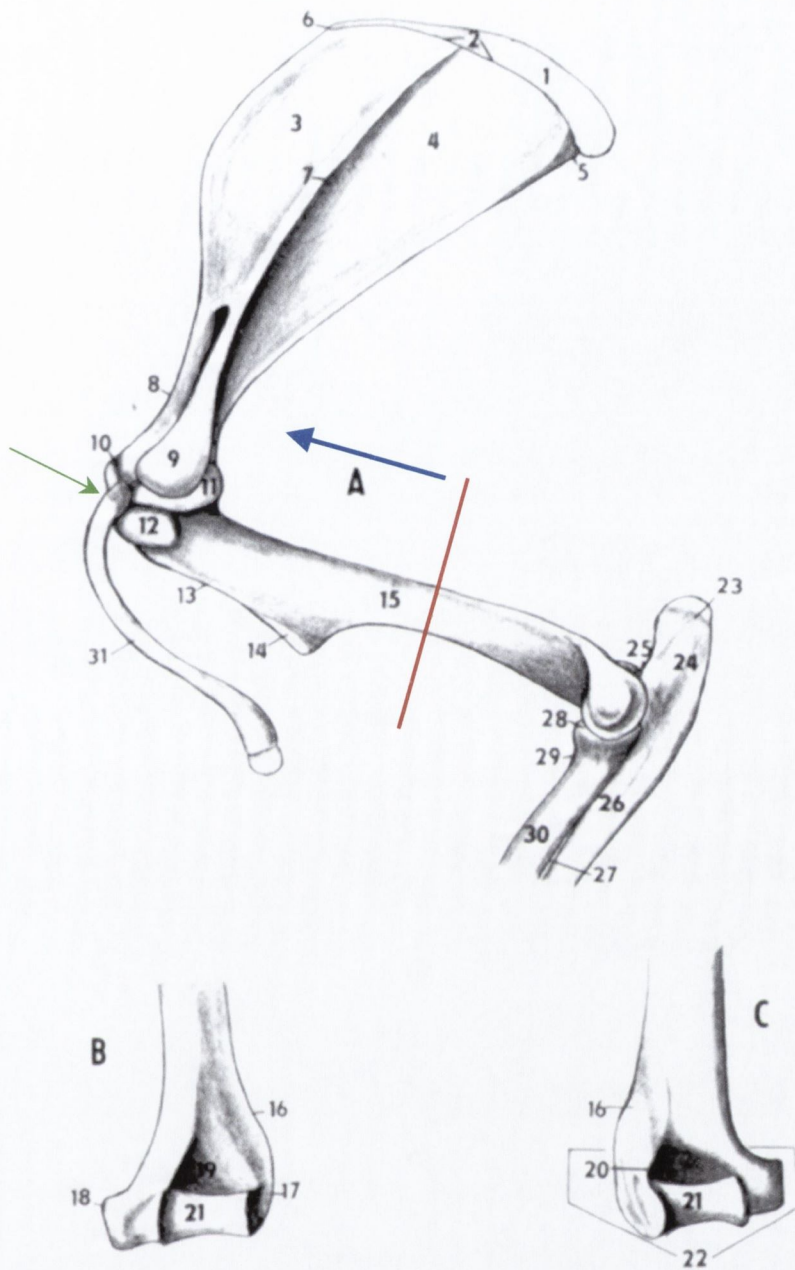
Prior to the experiment, all animals were weighed using a standard weighing scales. Following periods of HLS, the animals were sacrificed and the long bones excised (see section 2.2). Once the soft tissue was cleaned away from the bones, they were weighed and their lengths measured using standard vernier calipers. In the humeri the length measured was from the distal surface of the trochlea to the proximal surface of the humeral head, while in the femora from the distal surface of the condyles to the superior surface of the greater trochanter (See Figures 4.1 & 4.2).

4.2.2 Tissue Infiltration and embedding

In order to produce high quality thin sections and hence, slides, the bones were embedded in poly-methyl methacrylate (PMMA). Whilst cutting thin sections, PMMA serves to support the structure by filling the medullary cavity and any voids within the bone. The method selected to embed the bone tissue for histological sectioning was based on that of Erben (1997). This process was chosen, to allow for later immunohistochemical analysis in a related study, as at no stage does the temperature rise to a degree where proteins are denatured. Denaturation is the process by which, with the addition of heat, a protein's shape and functionality is altered, sometimes irreversibly. Standard embedding techniques (Frost, 1958, Lee, 1995, O'Brien et al., 2000) cause denaturation and so destroy the ability of the fluorescent immuno-histochemical markers to bind to the protein.

In the humeri, the bones were prepared by drilling a small hole proximally between the humeral head and the greater tuberosity (see Figure 4.1). In the femora, the holes were made proximally between the femoral head and the greater trochanter (see Figure 4.2). Water under low pressure was then used to flush out the contents of the marrow cavity. The bone samples were then fixed, dehydrated (Schenk et al, 1984) and infiltrated according to the schedule in Table 4.1. All steps of fixation, dehydration and infiltration were carried out at 4°C and all MMA solutions were stirred for at least 1 hour before use. Polymerisation was carried out in 7 ml glass vials. In order for the bone specimen to be located in the centre of the PMMA block, the infiltrated tissue was placed on a

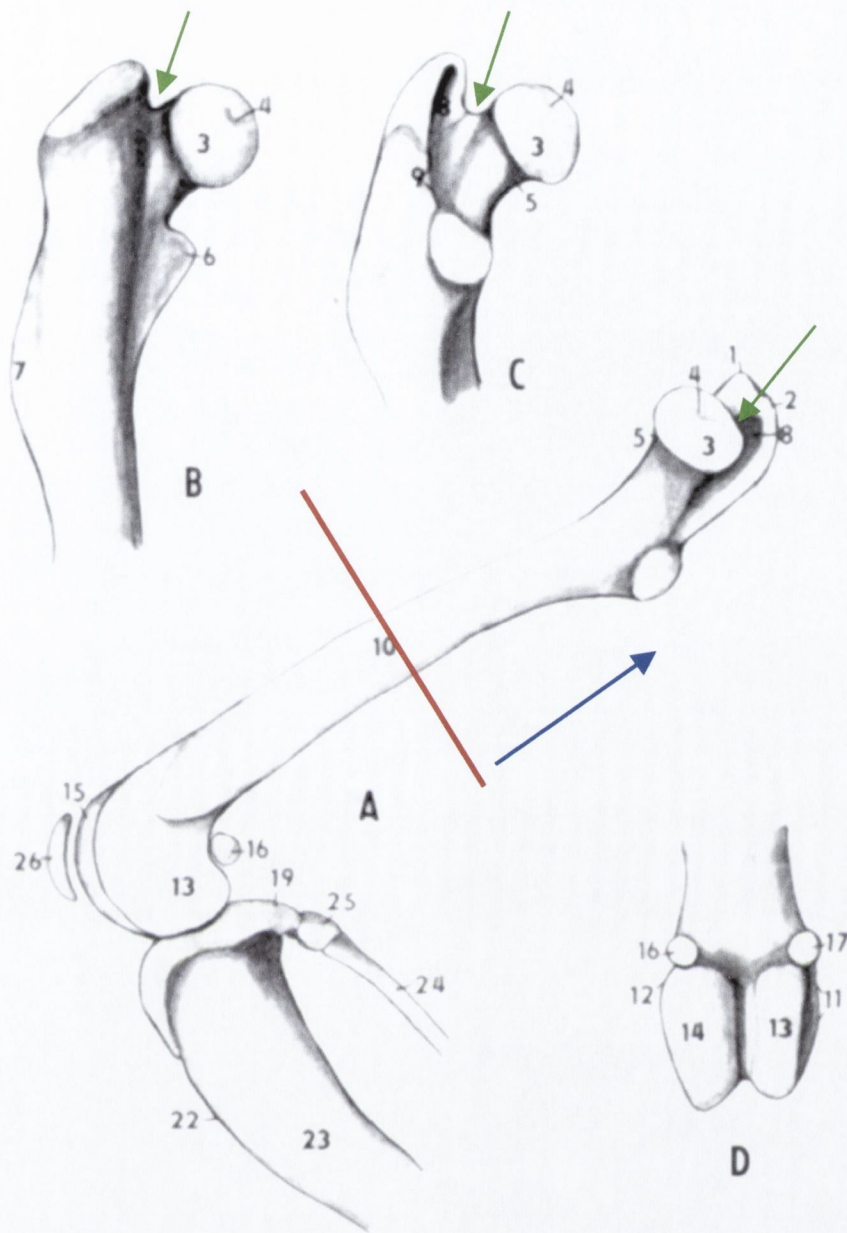
polymerised layer of plastic in the bottom of the glass vials and the vials then filled. To prepare the plastic bases, 2 ml of the final polymerisation mixture was poured into each glass vial. Since the polymerisation process is sensitive to oxygen (bases do not polymerise in the presence of oxygen) each vial was then thoroughly gassed with N₂, capped and polymerised within 1 day at 4°C. After the addition of the accelerator, care was taken that the polymerisation mixture was kept cold at all times. Polymerisation was carried out at -18°C to -20°C and was complete within 3 days. Polymerised blocks were stored at -20°C.



1-10: Scapula 11: Head of humerus 12: Greater Tubercle 13: Crest of humerus 14: Deltoid Tuberosity 15: Main humeral shaft 16: Lateral supracondylar crest 17: Lateral condyle 18: Medial condyle 19, 20: Fossae 21: Trochlea of humerus 22: distal epiphysis 23-26: Tibia 28-30: radius

Fig. 4.1 Schematic of left upper limb bones; view of lateral surface: clavicle, humerus, radius and ulna (A). Distal end of the humerus: cranial surface (B), caudal surface (C) (from Popesko et al., 1992).

— Cut transversely across the mid-diaphysis
 → Direction of serial sectioning → Direction of drilled hole



1, 2: Greater trochanter 3: Head of femur 4: Fovea of head 5: Neck of femur 6: Lesser trochanter 7: Third trochanter 8: Trochanteric fossa 10: Mid-shaft 11, 12: Epicondyles 13: Medial condyle 14: Lateral condyle 15: Trochlea of femur 16-23: Tibia 24, 25: Fibula

Fig. 4.2 Schematic of right lower limb bones:

Medial plane view (A). Proximal end of the femur: cranial surface (B), proximal surface (C). Distal end of the left femur: caudal surface (D) (from Popesko et al., 1992).

- Cut transversely across the mid-diaphysis
- ➔ Direction of serial sectioning
- ➔ Direction of drilled hole

Step	Duration	Temperature	Solution
Fixation	2 days	4°C	40% ETOH
Dehydration	2 days	4°C	70% ETOH
	2 days	4°C	95% ETOH
	Twice for 1 day	4°C	100% 2-Propanol
	Twice for 2 days	4°C	100% Xylene
Infiltration I	3 days	4°C	60 ml MMA (Merck, Germany) + 35 ml Butylmethacrylate (Sigma, USA) + 5 ml Methylbenzoate + 1.2 µl polyethylene glycol 400
Infiltration II	3 days	4°C	60 ml MMA (Merck, Germany) + 35 ml Butylmethacrylate (Sigma, USA) + 5 ml Methylbenzoate + 1.2 µl polyethylene glycol 400 + 0.4g dry benzoyl peroxide
Infiltration III	3 days	4°C	60 ml MMA (Merck, Germany) + 35 ml Butylmethacrylate (Sigma, USA) + 5 ml Methylbenzoate + 1.2 µl polyethylene glycol 400 + 0.8g dry benzoyl peroxide
Polymerisation	Within 3 days	-20°C	60 ml MMA (Merck, Germany) + 35 ml Butylmethacrylate (Sigma, USA) + 5 ml Methylbenzoate + 1.2 µl polyethylene glycol 400 + 0.8g dry benzoyl peroxide + 400µl N, N-dimethyl-p-toluidine.

Table 4.1 Protocol for dehydration, infiltration and polymerisation of specimens according to Erben (1997)

4.2.3 Slide preparation

After trimming of the plastic blocks to remove any excess, the embedded bone segments were oriented in the grips of the diamond saw (Minitom, Struers, USA) to ensure the cut was at 90 degrees to the mid-diaphysis. Three serial sections of 200 μm thickness were cut at room temperature using the diamond saw. The sections were then hand ground using silicon paper to a thickness of 100 μm (Lee, 1995, Frost, 1958). The thickness of each section was checked with a standard micrometer screw before being transferred to baths containing 40% alcohol and water. The sections were then air dried and mounted on slides using Xan mounting media (Sigma Aldrich, Ireland) and left to dry at room temperature for 24 hrs. The slides were labelled and then studied under both transmitted light and epi-fluorescence microscopy (Nikon Eclipse E800, Nikon Optical, Japan).

4.2.4 Morphological Analysis (transmitted light)

Images of each slide were obtained using a digital video camera (Nikon DXM1200, Japan) and transferred to a Dell Dimension 4100 PIII personal computer (Dell Corporation, Ireland) using an integrated software package called Lucia measurement (Lucia Measurement 4.71, Laboratory Imaging Ltd., Czech Republic). Lucia Measurement was used to capture all images with each image saved (*.LIM format) along with its own accompanying calibration factor. This calibration factor was established and checked using a standard graticule prior to each image capture session. Once captured, all images were orientated so that the medial aspect of the section was to the left and the posterior aspect at the top. Measurements were made on both humeri and femoral cross-sections by tracing a line around both the inner and outer surfaces of the bones cross-section (see Figure 4.3).

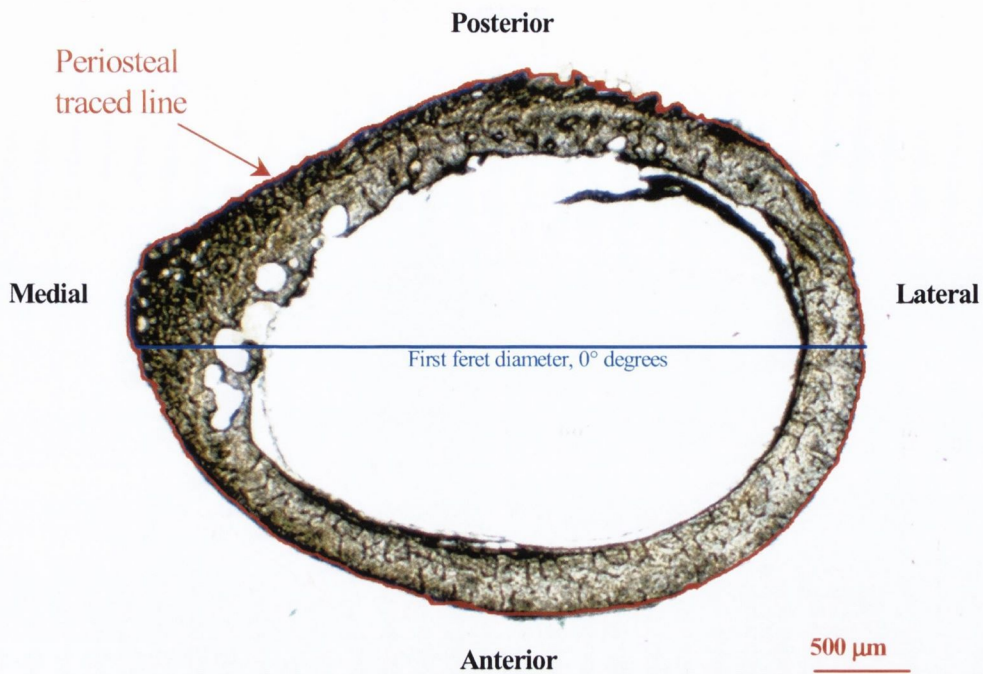


Fig. 4.3 Trace of femoral periosteal surface (bar = 500μm)

Lucia image is an integrated measurement package and outputs values for the following parameters for the traces of both the inner medullary cavity and the outer periosteal surface:

- Perimeter
- Area
- Maximum/Minimum feret (ferets diameter is calculated by projecting a line through the centroid horizontally, 0°, until it hits the traced line. This is then repeated at 10° intervals between 0° and 180° and the maximum and minimum values noted)

Lucia image also outputs a number of derived shape measurements calculated from these directly measured parameters including:

- Circularity ($4\pi \cdot \text{Area} / [\text{Perimeter}]^2$)
- Elongation (Maximum feret/Minimum feret)
- Total cross sectional area (CSA) of the bone, Periosteal CSA – Medullary canal/Endosteal CSA).

All data were exported to Microsoft Excel (Microsoft Excel, Microsoft Corporation, USA) and analysed statistically (see section 4.2.6).

4.2.5 Morphological Analysis (UV epi-fluorescence)

Rahn (1977) developed a regime (dosage and sequence order) for the administration of five fluorochrome dyes (calcein blue, xylenol orange, calcein, alizarin complexone and oxytetracycline) to facilitate interpretation of histological images of bone. This sequence and dosage regime was used subsequently to label bone remodelling under conditions of altered mechanical load (Lanyon et al., 1982, Lee et al., 2002, Burr et al., 1989, Lee, 1995). In order to quantify the degree of periosteal modelling, intracortical microcracking and remodelling in this study two fluorochromes were utilised, calcein blue and oxytetracycline.

Each fluorochrome was prepared by dissolving in sterile water (BK Veterinary Products, Bury St. Edmunds) and mixed using a magnetic stirrer to achieve the required concentration (Table 4.2) (1977). The pH was measured using a Lennox 3010 pH metre (Lennox Laboratory Supplies, Ireland) and adjusted to physiological level (pH 7.2 – 7.4) using concentrated HCl or NaOH solutions.

Fluorochrome	Colour	Concentration (mg/ml)	Dosage (mg/kg)
Oxytetracycline	Yellow	30	30
Calcein Blue	Blue	30	30

Table 4.2 Concentrations and dosages of fluorochromes and colour under UV epi-fluorescence

To obtain a sterile solution, the prepared fluorochrome solutions were then mechanically filtered through a Millipore filter system (Millipore, Bedford, MA, USA) to remove any bacteria (0.22 µm disposable filter). These filtered sterile solutions of fluorochromes were then kept sealed until use.

The animals' body weights were measured to calculate the volume of the standard fluorochrome solution (30 mg/ml) required to give an individual dosage of 30 mg/kg. All fluorochrome markers were administered via intraperitoneal injections. In all groups oxytetracycline was given at day -1 to label new bone formation (see Table 4.3). Following preliminary experiments it was determined that at least one week must pass in order to ensure that successive fluorochrome dyes did not overlap. As a result only in

the two week groups was a dose of calcein blue given the day prior to sacrifice to label any microcracks and resorption sites present.

Group	Fluorochrome	Administered on day	Sacrificed on day
B	Oxytetracycline	-1	0
C and S	Oxytetracycline	-1	3
C and S	Oxytetracycline	-1	7
C and S	Oxytetracycline	-1	14
	Calcein Blue	13	

Table 4.3 Fluorochrome sequence and administration schedule (B: Basal control; C: Experimental control; S: Suspended)

4.2.5.1 Bone Formation Index and formation rates

The response of bone to HLS is not uniform around the periosteal surface, with sites of muscle attachment, such as the posterior eminence on the tibia, least affected by unloading. Many current methods use a coordinate or angular system whereby the growth is only assessed at various points around the circumference. In this study, a new parameter was introduced which takes the total cross sectional area growth into account. Fluorochrome labelled formation sites were identified and used to calculate a bone formation index ($BFI = \text{Area of new bone formed} / \text{Total bone cross sectional area}$). In order to do this the periosteal and endosteal surfaces from day zero were identified as rings of oxytetracycline labelled bone. New bone formed was determined to be any bone lying outside a labelled day zero periosteal surface or inside a day zero endosteal surface (see Figure 4.4).

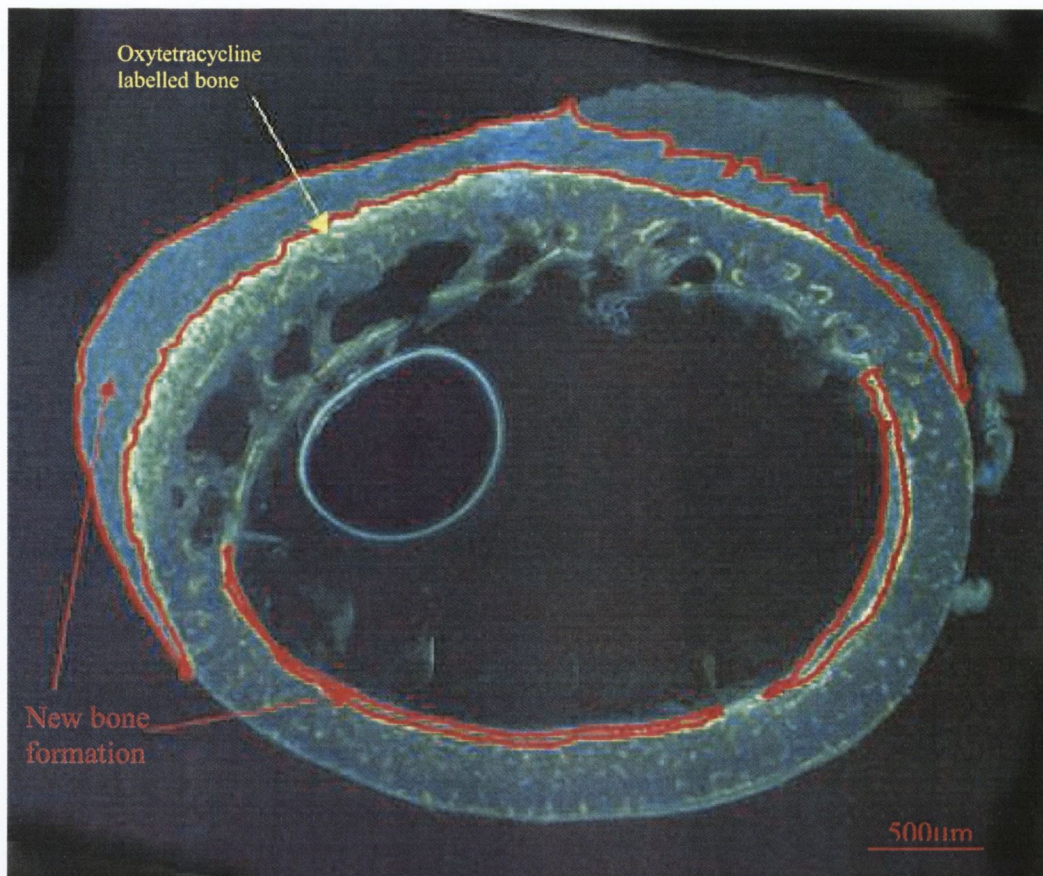


Fig. 4.4 Mid-Diaphyseal transverse cross section of a rat femur under UV Epi-Fluorescence (Bar = 500µm)

This bone formation index is a method of examining the effect of unloading on the growth of long bones that isolates the formation response from that of resorption. Unfortunately, using this method it is impossible to calculate a resorption index, as it is impossible to measure how much bone has been resorbed since day 0. However, when the results from the bone formation index are examined in conjunction with the bone cross sectional area results, it is possible to infer the resorption response to altered mechanical loading.

The results for the UV epi-fluorescence work on the bones was broken up into 4 main parts:

- Periosteal Bone Formation Index calculations, BFI: all new bone formed outside the oxytetracycline labelled periosteum from day 0 as a percentage of total bone.

- Endosteal BFI: all new bone formed inside the oxytetracycline labelled endosteum from day 0 as a percentage of total bone.
- Total BFI: the sum of the periosteal and endosteal BFIs.
- Formation of secondary osteons and microcracks.

Unfortunately, experimental error resulted in seven of the twelve 14-day animals not receiving their correct dosage of oxytetracycline (14-day animals: 3 control and 4 suspended). These animals were the first group to be hindlimb suspended and hence the first to be given intraperitoneal injections of fluorochrome. The likely cause of the experimental error was that the injections were not administered correctly with the fluorochrome being injected too deeply, into the lower bowel, and hence passed out in the faeces. As a result, it was not possible to calculate a bone formation index from these seven animals' cross-sections, as the oxytetracycline label is not present to create a baseline position of the periosteum. As a result, the limited 14-day groups data (5 animals) were excluded from the statistical analysis but were included in the graphs for comparison purposes.

4.2.5.2 Detection of Haversian systems and microcracking

Following sacrifice the mid-diaphysis of the distal half of the right femora and humeri were sectioned using a diamond saw and viewed under the microscope (see sections 4.2.2 to 4.2.4). Under transmitted light the bones' cross sectional areas were examined while under UV epi-fluorescence, the presence of Haversian systems and fluorochrome labelled microcracks were sought.

Lee et al. (1998, 2003) detailed a method of using agents to label microdamage accumulation using fluorochromes and this protocol was used here (see Table 4.4).

Step 1	Fluorescence microscopy - green incident light (G – 2A filter block, $\lambda=546$ nm), x125 magnification: Candidate crack should be intermediate in size, being larger than canaliculi but smaller than vascular canals
Step 2	Fluorescence microscopy - green incident light (G – 2A filter block, $\lambda=546$ nm), x125 magnification: Candidate crack should have a sharp border, with fluorescence of the agent within crack borders evident
Step 3	Fluorescence microscopy - UV incident light ($\lambda=365$ nm), x125 magnification: Candidate crack should be stained through the depth of the section

Table 4.4 Criteria for identifying microcracks in bone (Lee et al., 1998, 2003)

Once cracks were located the crack lengths were measured and the following parameters calculated:

- Crack Density: Number/Area [no./mm²]
- Surface Density: Total crack length/Area [$\mu\text{m}/\text{mm}^2$]
- Mean crack length: [μm]

Cracks stained with oxytetracycline were *in vivo* cracks present' in the bones microstructure prior to the experimental period. Cracks stained with calcein blue in the 14-day groups were formed during the course of the experimental period and could be examined for the effect of HLS.

For the purpose of data analysis the cracks were subdivided into four groups as follows:

- Combined data 0, 3, 7 day groups: these oxytetracycline labelled cracks are normal *in vivo* cracks found in the sections from both control and suspended 0, 3 and 7 day groups
- Control 14-day group: these cracks were stained with calcein blue and were either formed during the suspension period (in the case of those with oxytetracycline staining) or before and during suspension (when there was no oxytetracycline) in the sections from both control 14-day groups

- Suspended 14-day group: these cracks were stained with calcein blue and were either formed during the suspension period (in the case of those with oxytetracycline staining) or before and during suspension (when there was no oxytetracycline) in the sections from suspended 14-day groups
- Combined data 14-day groups: this is the sum/combination of the control and suspended 14-day groups

4.2.6 Statistical Analysis

All data measured were statistically analysed using the statistics software Intercooled STATA (StataCorp. 2001. Stata Statistical Software: Release 7.0. College Station, TX: Stata Corporation). Linear regression analysis and ANOVA (Analysis of Variance) were performed on all data sets. The choice of which statistical method to use was governed by the following premise. In cases where it is assumed that there is a linear effect on a particular data set (e.g. for an increase in the independent variable, such as time, there is a linear response in the dependent variable) both ANOVA and linear regression analysis were used. In these cases, ANOVA and linear regression analysis will yield similar results. However, if a pulsatile effect was thought likely (e.g. in cases where for an increase in the independent variable, such as time, there is a transient response in the dependent variable) only ANOVA was used to analyse the data. Also, when ANOVA and Linear regression gave contrasting answers the trend of the graphed data was assessed and the strengths of the two tests (R^2 value) were taken into account in deciding the answer. Finally, although both ANOVA and linear regression are insensitive to reasonable degrees of variance, in cases where the data appeared skewed a robust linear regression analysis and Kruskal-Wallis ANOVA were performed to check the previously obtained results. For $p < 0.05$, the difference were considered significant, while $p < 0.01$ were noted.

4.3 Results

All data in are displayed in the form of box plots (See below Figure 3.14 for explanation of box plots). Boxplots display the median, inter quartile range and any outliers. The median (the middle value of a set of numbers) is used, as it is a more robust indicator of the central tendencies than the mean of the data. In each graph there are two boxes (each corresponding to a group of 6 animals) at each time point, with the exception of day 0 as there was only one (basal) control group. In all cases control groups are coloured blue while suspended groups are red.

4.3.1 Body Weight Results

All animals were weighed at the beginning of the experiment and no statistically significant difference was found between the initial bodyweight of the control and suspended groups. There were six animals in each control and experimental group (totalling 18 suspended animals and 24 controls in the morphological study).

Normal levels of feeding, grooming and activity were maintained throughout the experimental period indicating hindlimb suspension was well tolerated by all the animals. All animals increased their body weight with increasing age over the experimental period (see Figure 4.5). At each successive time point both control and suspended groups' body weights had increased and over the time period both experimental and control groups' weights had grown significantly (Linear Regression analysis, $P < 0.01$; ANOVA, $P < 0.001$). Finally, although the two groups were pair-fed, at all time points the median value of the suspended groups' body weight was less than that of the controls. Nonetheless, there was no statistically significant effect of HLS on the body weight of the two groups at any point (ANOVA, $P = 0.1944$; Linear Regression Analysis, $P = 0.594$).

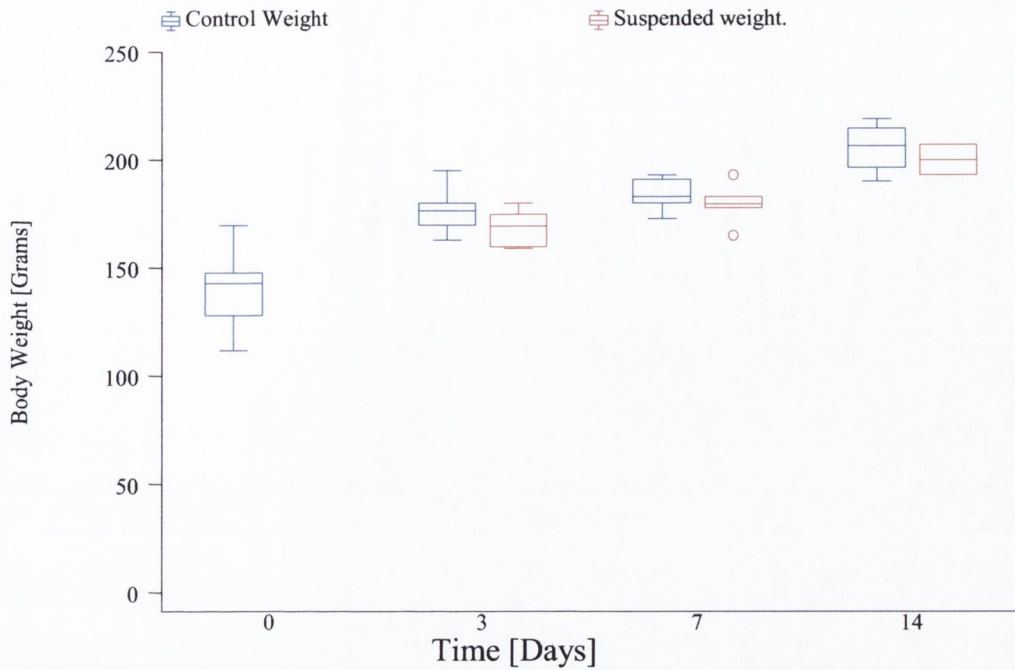


Fig. 4.5 Body weights Vs. Time for Control and Suspended groups

4.3.2 Humeri Results

In this section the morphological results are presented for the loaded humeri. In order to first ascertain whether the HLS had resulted in any large-scale morphological changes, humeral weight and length were examined.

4.3.2.1 Humeral Gross Morphology Results

Figure 4.6 shows that the weight of the humeri increased in all the suspended and control groups throughout the experimental period. This increase over time was statistically significant (ANOVA, $P < 0.001$; Linear Regression Analysis, $P < 0.001$). There was no statistically significant difference between the humeral weight of suspended and control groups (ANOVA, $P = 0.76$; Linear Regression Analysis, $P = 0.87$).

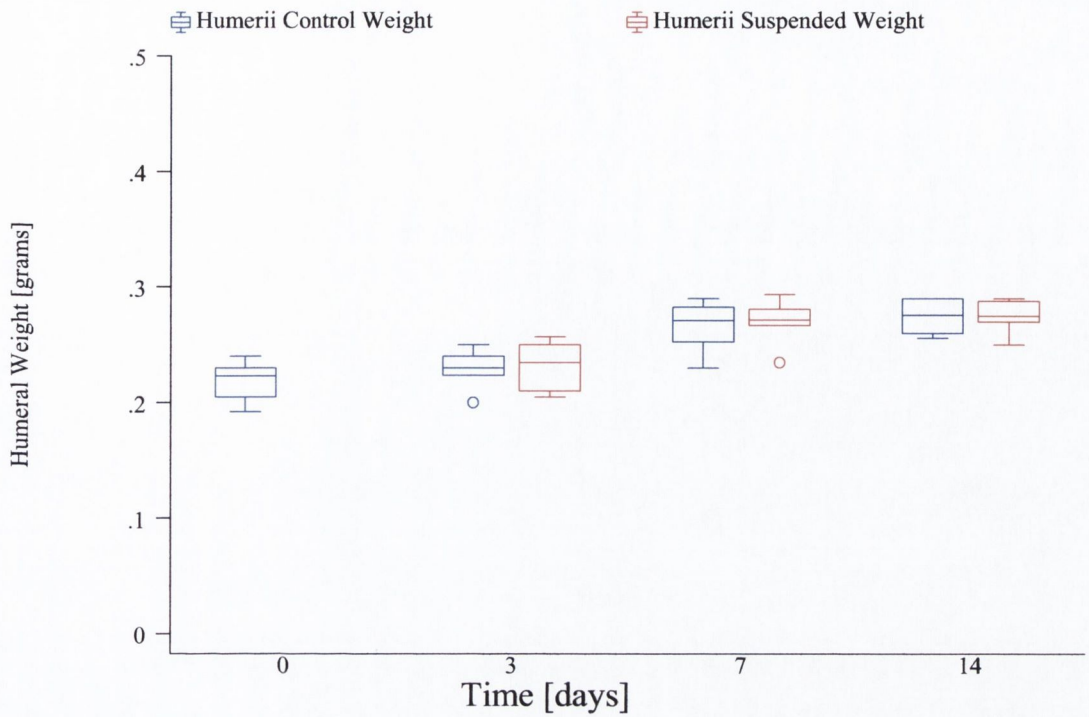


Fig. 4.6 Humeral Weight Vs. Time for Control and Suspended groups

Figure 4.7 shows the humeral length in the suspended and control groups. There is growth throughout the experiment, with the humeral length at each successive time point greater than that of the previous point. This time effect was significant (ANOVA, $P < 0.001$; Linear Regression Analysis, $P < 0.001$). When the humeral lengths were examined, no statistically significant differences were found as a result of the HLS (ANOVA, $P = 0.10$; Linear Regression Analysis, $P = 0.10$).

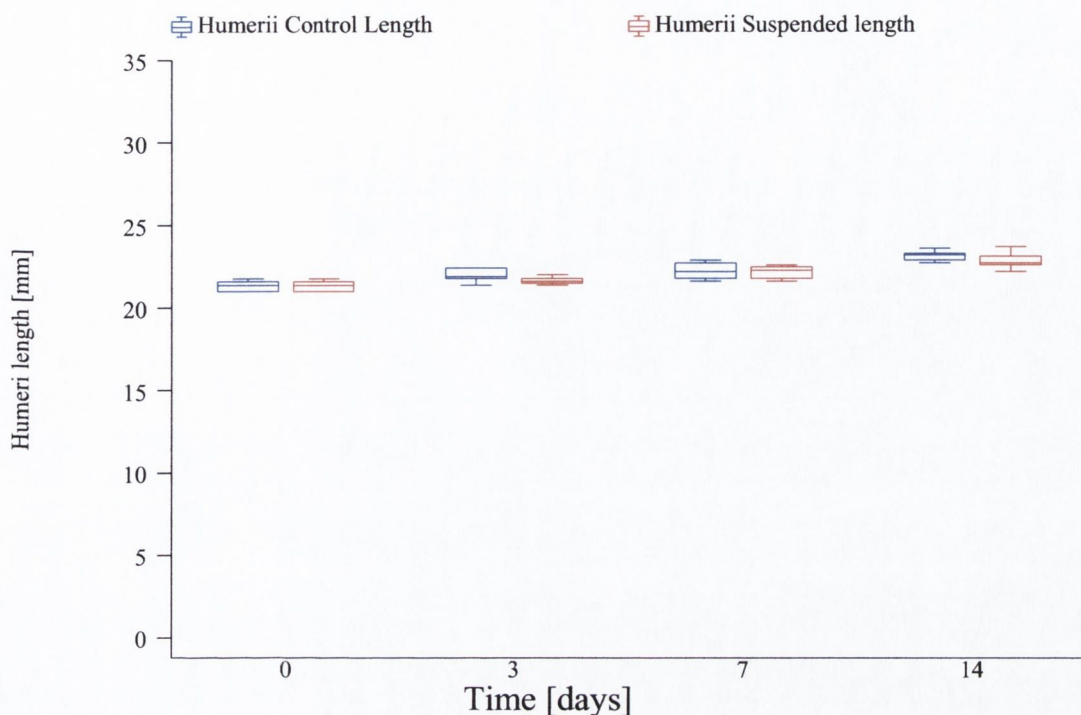


Fig. 4.7 Humeral Length vs. Time for Control and Suspended groups

4.3.2.2 Humeri Cross Sectional Area

Next, the effect of hindlimb suspension was examined on the cross sectional area of a transverse section across the mid-diaphysis of the loaded humeri. Figure 4.8 shows the total mid-diaphyseal CSA in both the control and suspended groups. Total CSA was calculated by taking away the endosteal area (marrow cavity area) from the periosteal area. Although there is a small increase in both suspended and control total cross sectional areas, it is not consistent over the full experimental period. However, the effect of time on the total CSA was statistically significant (ANOVA, $P < 0.001$; Linear Regression Analysis, $P < 0.01$) it is not clear what this time-effect is and it could be simply due to the young animals varying growth patterns. There were no statistically significant differences between the suspended and control groups' cross sectional areas following HLS (ANOVA, $P = 0.36$).

Figure 4.9 shows that the periosteal areas of the humeri increased in both the suspended and control groups throughout the experimental period. This increase over time was statistically significant (ANOVA, $P < 0.001$; Linear Regression Analysis, $P < 0.001$) and

again reflects growth rapidly. While suspended animals tend to have a larger periosteal CSA at the end of the experimental period, overall there was no statistical significance between the control and suspended groups (ANOVA, $P = 0.07$).

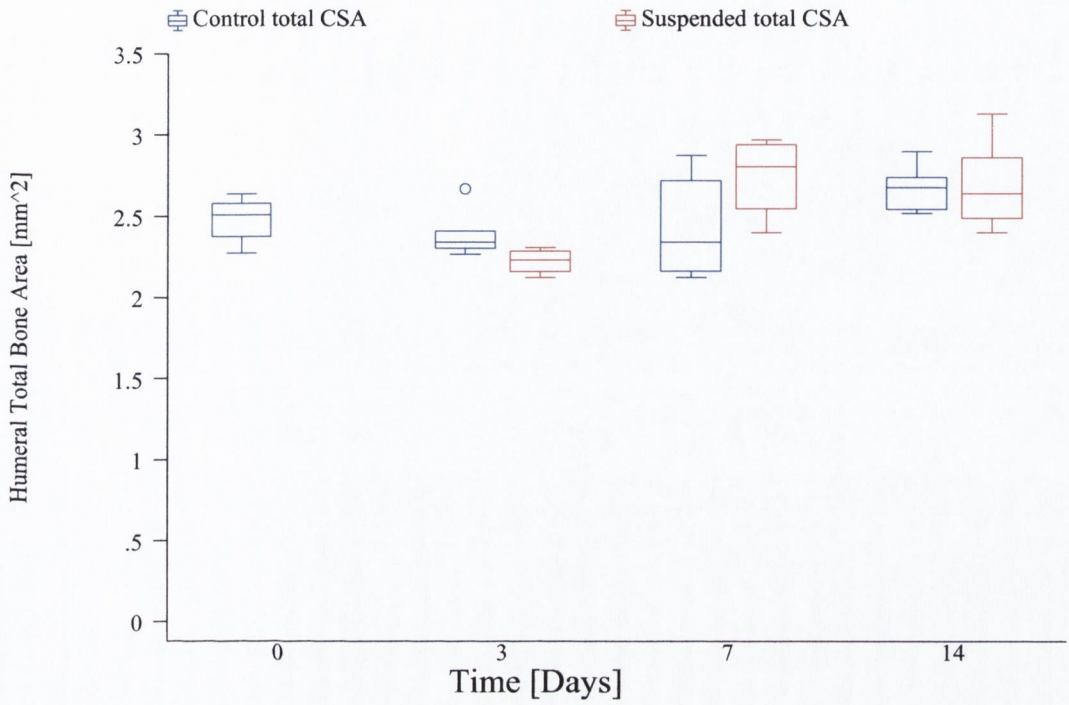


Fig. 4.8 Humeral Total mid-diaphyseal Cross-Sectional Areas Vs. Time

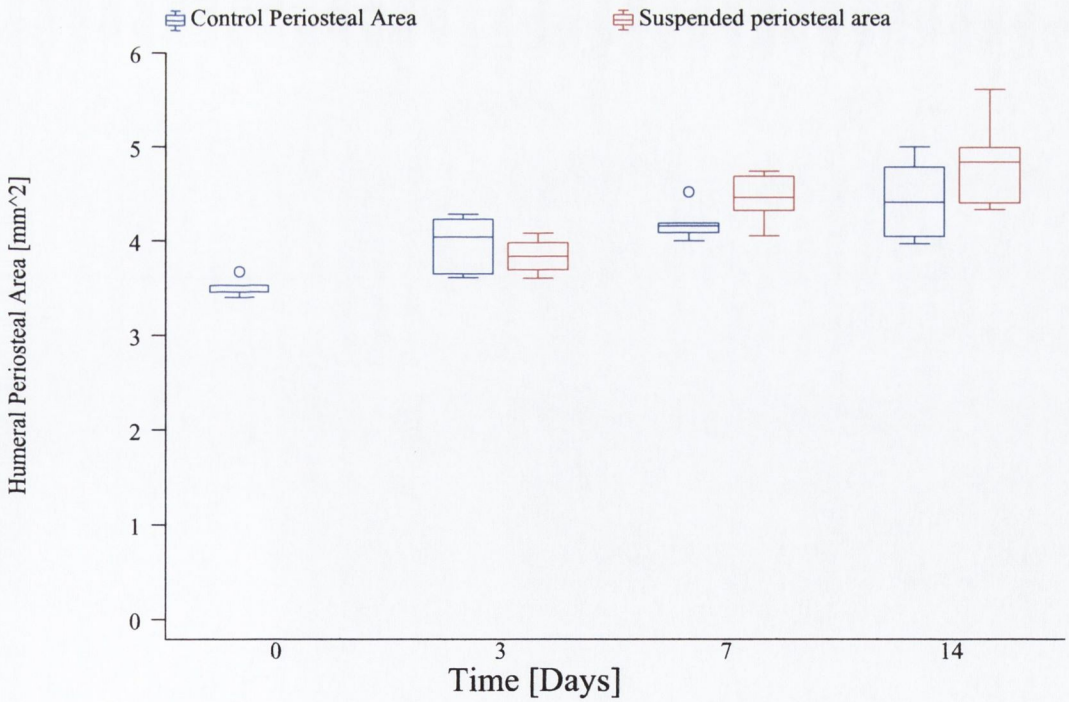


Fig. 4.9 Humeral Periosteal Cross Sectional Areas Vs. Time

Figure 4.10 shows the endosteal area, or area of the medullary canal, in the suspended and control groups. The endosteal areas of the humeri increased in both groups throughout the experimental period and this was statistically significant (ANOVA, $P < 0.001$; Linear Regression Analysis, $P < 0.001$). There was no statistical difference in endosteal cross sectional areas between the control and suspended groups (ANOVA, $P = 0.19$).

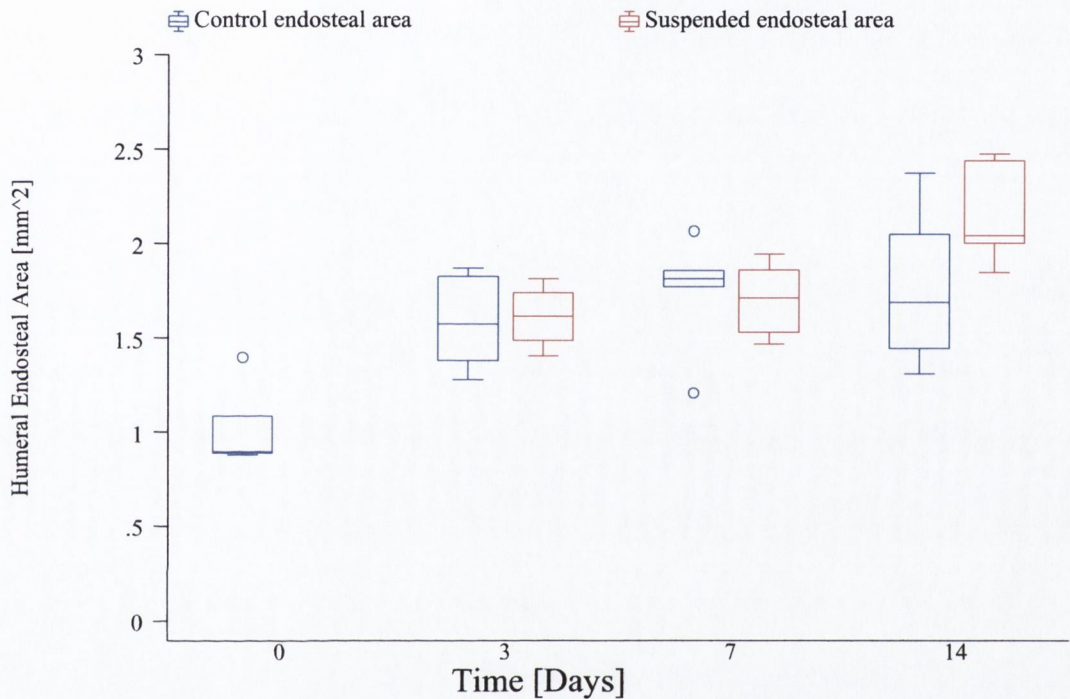


Fig. 4.10 Humeral Endosteal Cross Sectional Areas Vs. Time

4.3.2.3 Humeral Shape

The bone cross sections were analysed for changes in shape as a result of the hind limb suspension. Two geometric variables were calculated for each bone's cross-section (see section 4.2.4): circularity (a function of the perimeter and area) and elongation (a function of the maximum and minimum feret values).

Figure 4.11 shows periosteal circularity values for the control and suspended groups' humeri. There was no statistically significant effect of time on the circularity values for the two groups (ANOVA, $P = 0.30$; Linear Regression Analysis, $P = 0.26$). HLS was found to have a statistically significant effect on the periosteal circularity values for the

two groups, with the suspended groups humeri being more circular than the controls (ANOVA, $P < 0.01$).

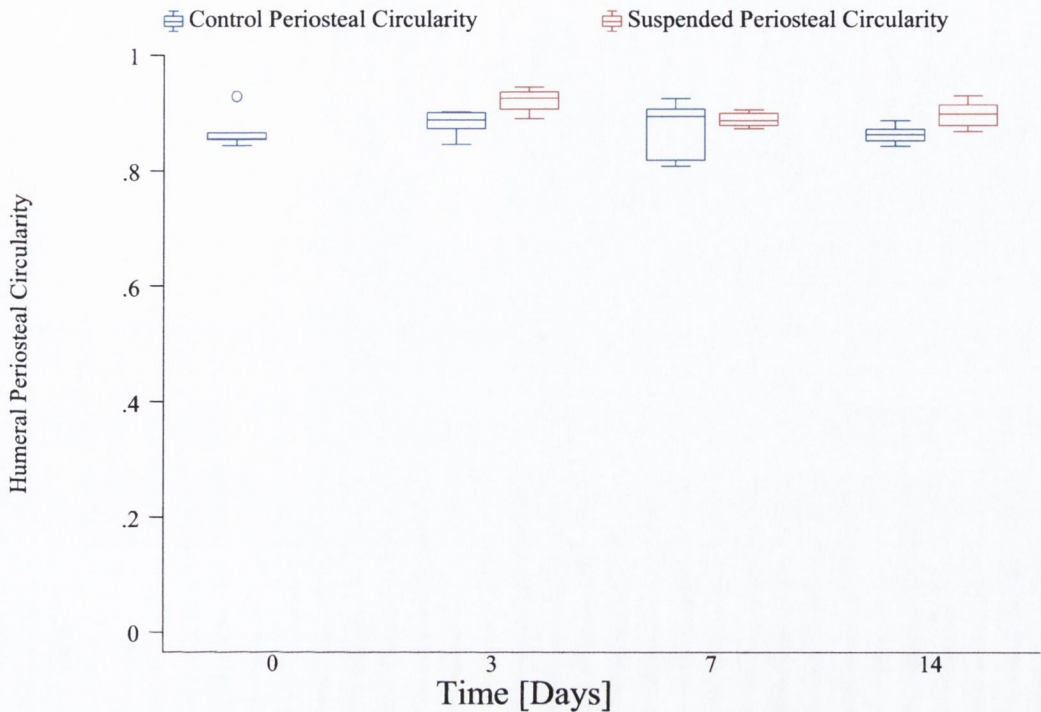


Fig. 4.11 Humeral Periosteal Circularity Vs. Time

Figure 4.12 shows the humeral periosteal elongation data for the control and suspended groups. There was a statistically significant effect of time on the elongation values for the two groups (ANOVA, $P < 0.01$; Linear Regression Analysis, $P < 0.01$). Periosteal elongation differed significantly with the suspended groups humeri being more circular than the controls (ANOVA, $P < 0.01$).

Figure 4.13 shows endosteal circularity data for the control and suspended groups. There were a large number of voids and other irregularities at the endosteal surface, which resulted in a large degree of variance in the data. These irregularities had a large effect on the perimeter term, which is squared in the geometric variable 'circularity'. Neither time (ANOVA, $P = 0.66$) nor HLS (ANOVA, $P = 0.26$) had a statistically significant effect on endosteal circularity.

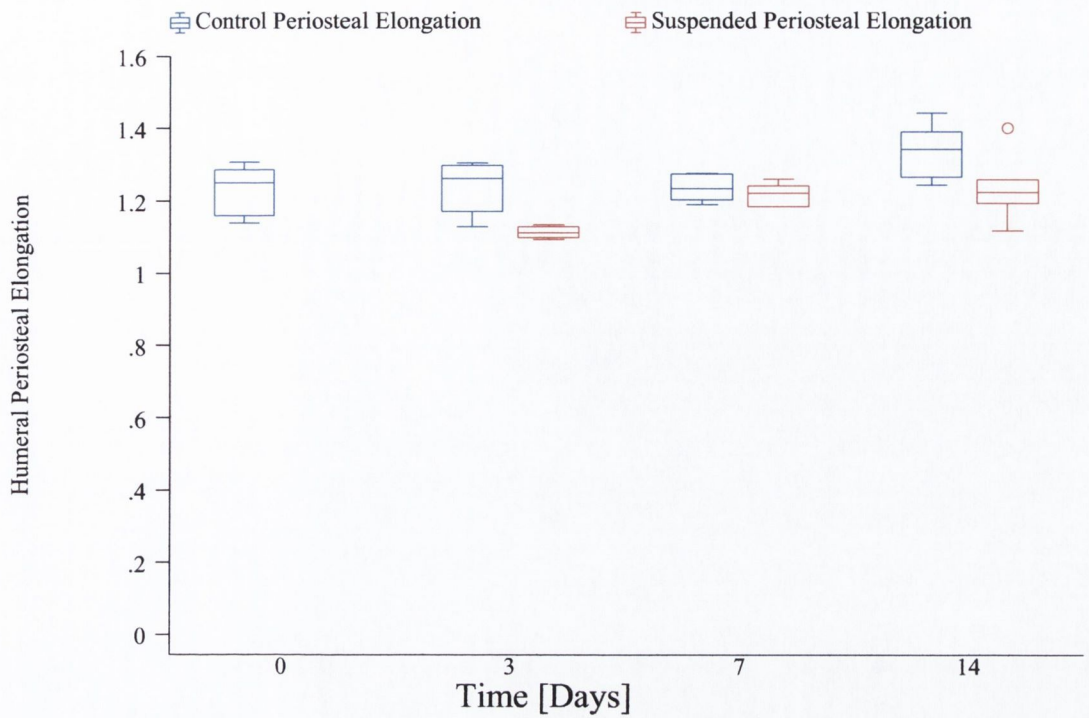


Fig. 4.12 Humeral Periosteal Elongation Vs. Time

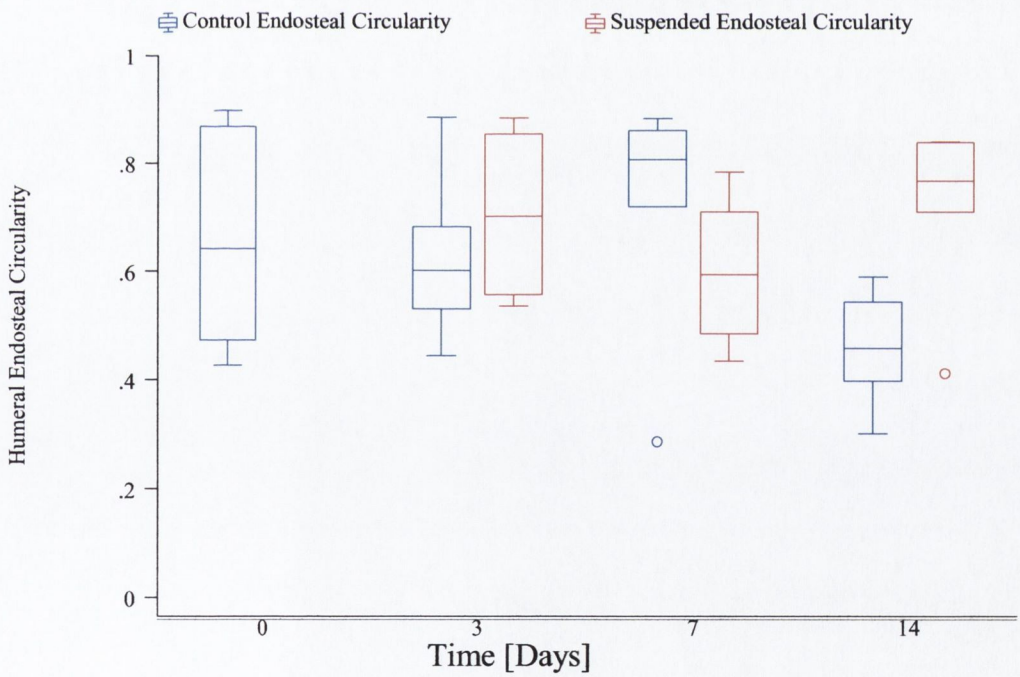


Fig. 4.13 Humeral Endosteal Circularity Vs. Time

Figure 4.14 shows endosteal elongation data for the control and suspended groups. Statistically there was no significant effect of time on the endosteal elongation (ANOVA, $P = 0.06$). Similarly, there was no statistically significant effect of HLS on the suspended animals endosteal elongation data (ANOVA, $P = 0.05$).

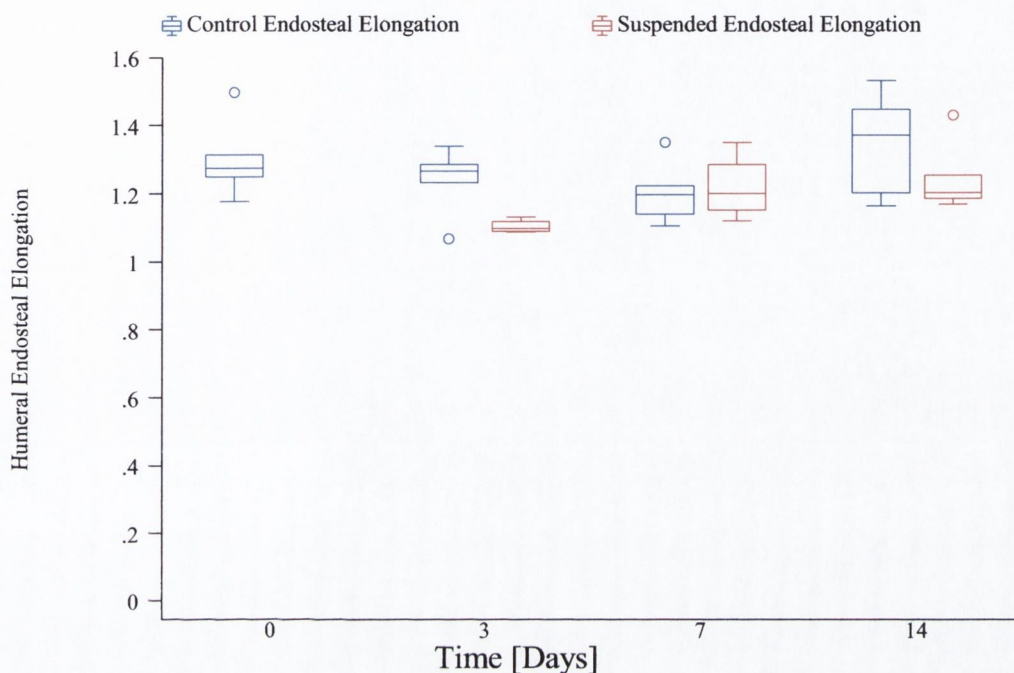


Fig. 4.14 Humeral Endosteal Elongation Vs. Time

4.3.2.4 Humeral Epi-Fluorescence Microscopy Results

In Figure 4.15 the data for the humeral periosteal bone formation index for the two groups are presented. As expected in young growing animals, the amount of new bone increased in both groups from 3 to 7 days. This increase over time was statistically significant (ANOVA, $P = 0.001$). The amount of new periosteal bone formation was unaffected in the suspended animals. This effect of HLS was not found to be statistically significant (ANOVA, $P = 0.90$).

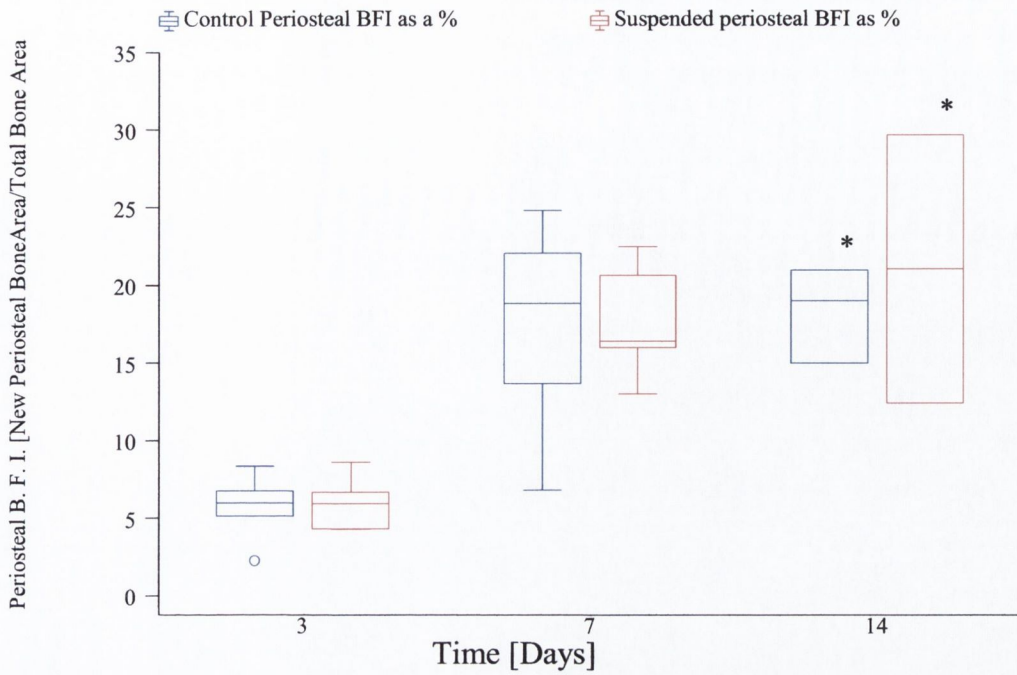


Fig. 4.15 Humeral Periosteal BFIs Vs. Time (* denotes n < 6)

Figure 4.16 details the endosteal BFI for the humeri. Growth resulted in an increase in new bone formation in both groups over the experimental period. This increase in the endosteal BFI over time was not statistically significant up to 7 days (ANOVA, $P = 0.08$). HLS caused a significant increase in the amount of new bone formation at the endosteal surface in the humeri of the suspended groups (ANOVA, $P < 0.01$).

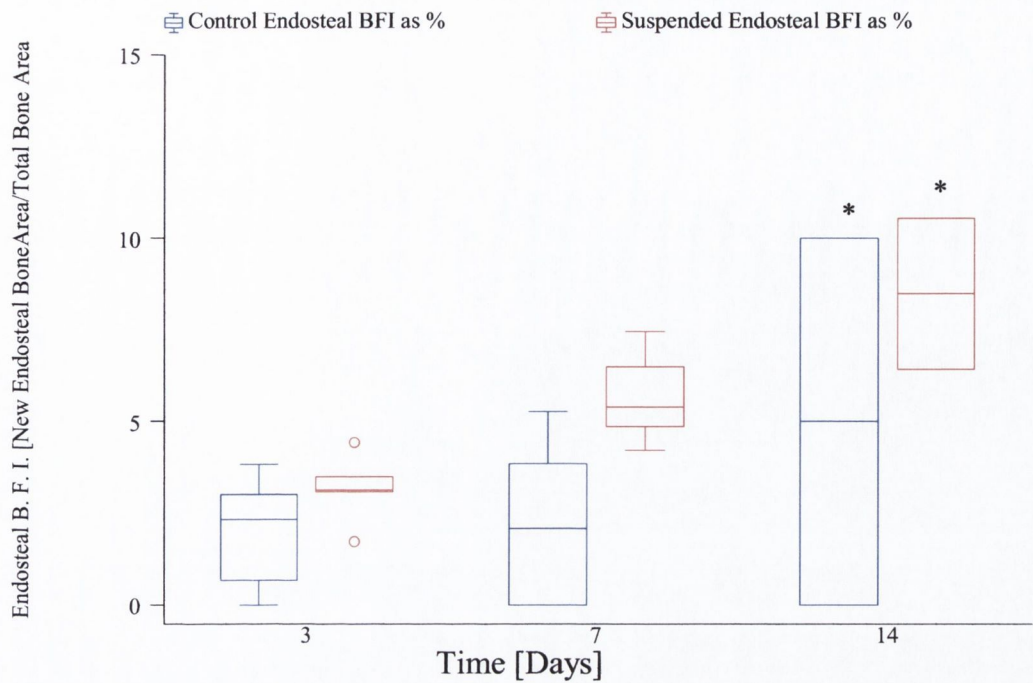


Fig. 4.16 Humeral Endosteal BFIs Vs. Time (* denotes $n < 6$)

Figure 4.17 shows the total BFIs for the two groups. There was a significant effect of time on the data with both groups increasing significantly over the experimental period (ANOVA, $P < 0.001$). HLS caused no significant change in the total BFI of the suspended animals relative to the controls (ANOVA, $P = 0.17$).

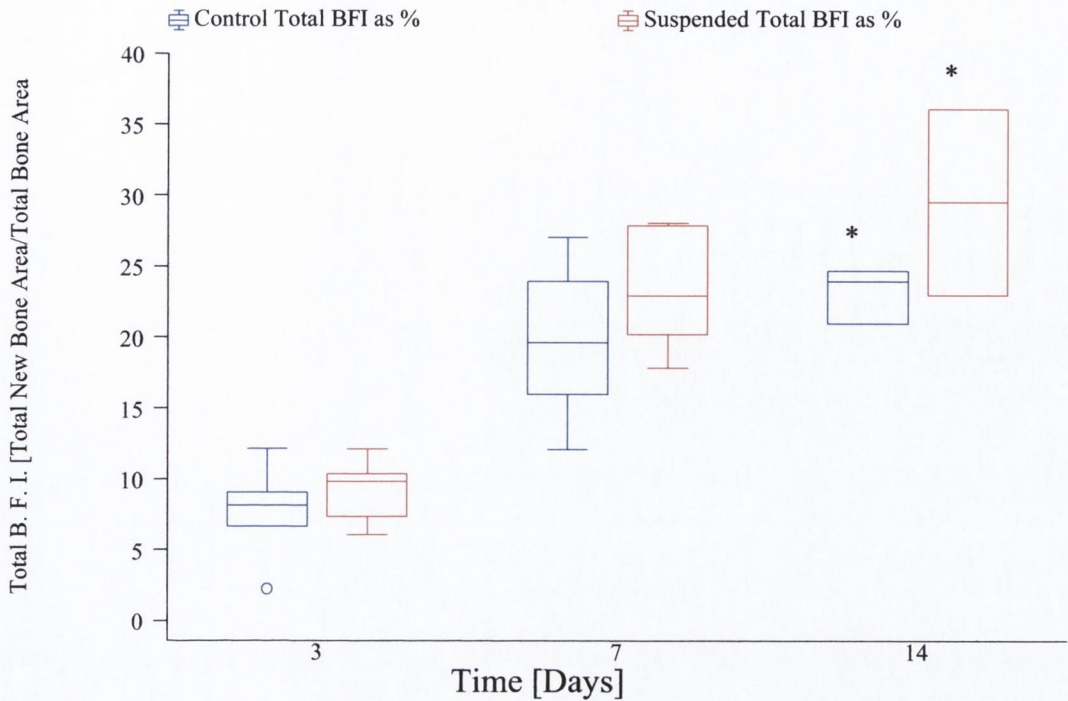


Fig. 4.17 Humeral Total Bone Formation Index Vs. Time (* denotes n < 6)

Each humeral section was also examined for the presence of either Haversian systems or microcracking. Unsurprisingly, no Haversian systems were located in any of the transverse sections of the loaded humeri in this experiment.

In the humeri, cracks were found in half of the animals (18 of the 36 animals) and in just under a third of all sections examined (Total: 30 out of 106 slides; Control: 16 out of 58; Suspended: 14 out of 48). This resulted in 44 measured cracks of which 24 were in control humeri and 20 in suspended. Due to the experimental error outlined in section 4.2.5.1 the 14-day groups data is divided into those sections containing oxytetracycline and those without. In the sections from those animals that received oxytetracycline, cracks stained with oxytetracycline were formed prior to the experimental period and indicate that microdamage is normally present *in vivo*. Cracks stained with calcein blue were formed during the course of the experimental period and could be due to HLS. When there is no oxytetracycline in the section it was not possible to determine whether the crack was formed prior or during the experiment.

All the cracks in the 0, 3 and 7 day groups were stained with oxytetracycline, while all those found in the 14-day groups were stained with calcein blue. No oxytetracycline stained cracks were found in the 14-day groups regardless of whether or not the animals had received the correct oxytetracycline dosage. Many of the cracks were also observed to be located near the endosteal surfaces. In summary, 20 out of the 24 control cracks and 17 of the 20 suspended cracks were located near the endosteal surface (see Figures 4.18 & 4.19).

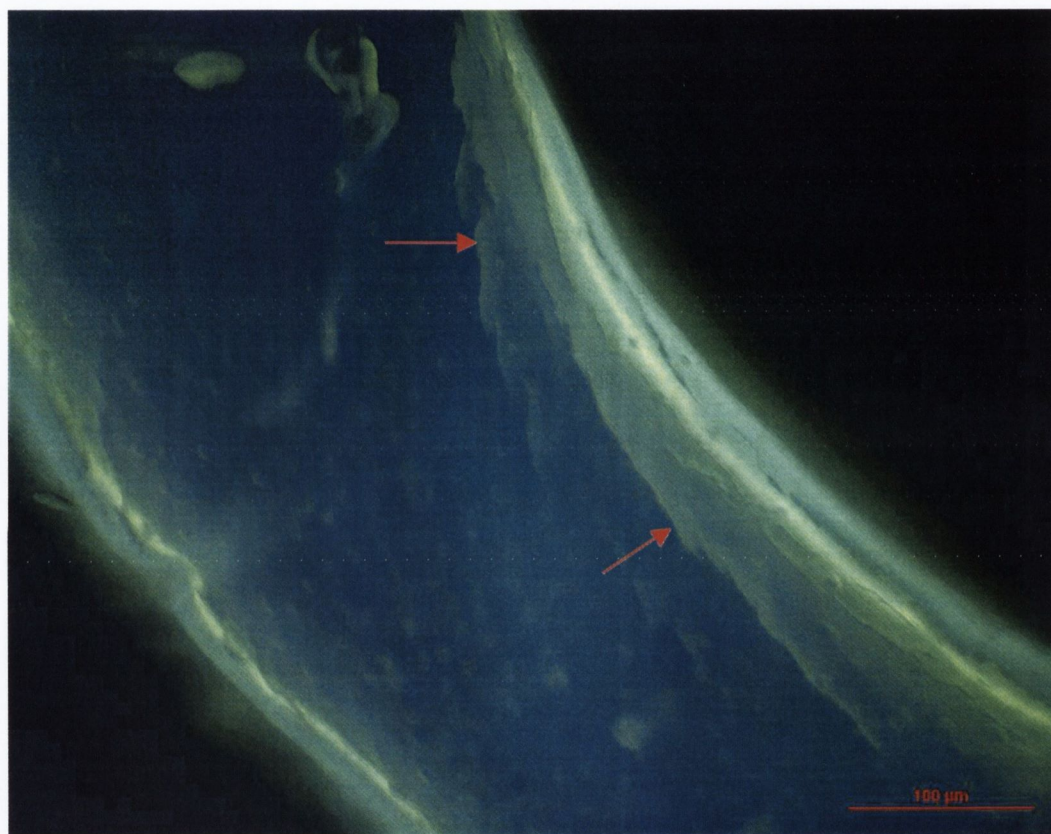


Fig. 4.18 Oxytetracycline labelled microcrack (indicated) in the humerus of a suspended rat

Specimen 3 day suspended # 6 (Bar=100μm)

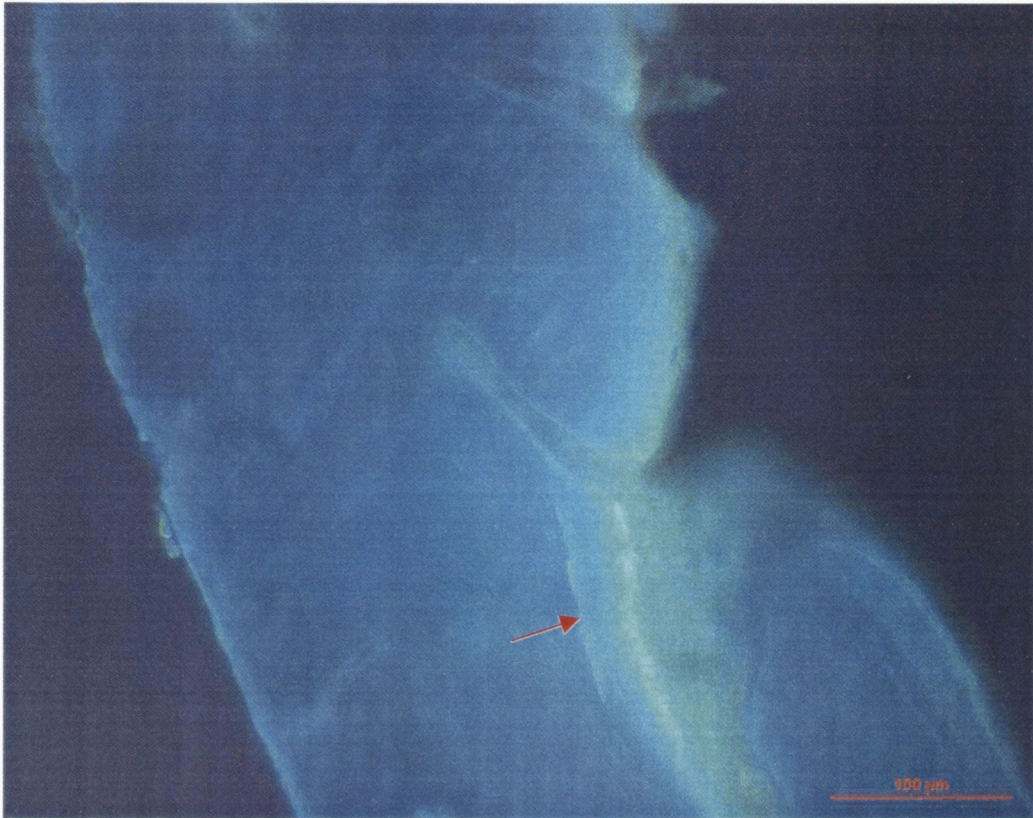


Fig. 4.19 Calcein blue labelled microcrack in the humerus of a suspended rat Specimen 14 day suspended # 2 (Bar = 100 μ m)

Table 4.5 below details the crack data for the transverse sections through the mid-diaphysis of the humeri. No statistical analysis was performed on the crack data as in the 0, 3 and 7 day groups the cracks in both control and suspended groups were *in vivo* cracks, while there was not enough data points remaining in the 14-day groups to merit further comparative study. Finally, all the microcrack data are presented as mean \pm standard deviation in order to allow comparison with previously published data on *in vivo* microdamage levels in various animals and in humans (O'Brien et al., 2003, O'Brien et al., 2000, Muir et al., 1999).

	Crack density [number/ mm ²]	Crack Surface density [μm/ mm ²]	Crack length [μm]
Combined data 0, 3, 7 day groups	0.17 ± 0.35	30.2 ± 63.5	62 ± 92
Control 14-day group	0.22 ± 0.29	34.8 ± 46.1	80.3 ± 97.5
Suspended 14-day group	0.22 ± 0.41	57.1 ± 110.4	121.5 ± 169.6
Combined data 14-day groups	0.22 ± 0.34	44.7 ± 80.6	99 ± 134.8

Table 4.5 Humeral crack data. All values are mean ± standard deviation.

4.3.3 Femora Results

In this section, the morphological results are presented for the mechanically unloaded femora. Throughout suspension, the femora experience no mechanical forces as a result of weight bearing, although they do experience some muscle loads. The premise here is that as a result of the reduced mechanical load the bones' morphology would be altered. This adaptation could take the form of a reduced formation rate, increased resorption rate, or a combination of the two.

4.3.3.1 Femoral Gross Morphology Results

In order to ascertain whether HLS had resulted in any large-scale morphological changes, the femoral weights and lengths were examined for each group. These data are presented below in Figure 4.20 and Figure 4.21. Unfortunately, part of the distal condyles was lost whilst dissecting out three femora (2 of the three-day suspended animals (3 day suspended #3, #4) and one of the 14 day control animals (14 day control #2)). This error would distort the three day suspended and 14-day control animals' femoral weight and length data. Hence these data have been excluded from the length and weight analysis and graphs.

There was growth throughout the experimental period, and this time effect was significant for both the femoral weight and length (ANOVA, $P < 0.001$; Linear Regression Analysis, $P = 0.001$).

Figure 4.20 presents the femoral weight data for the control and suspended groups. There was no statistically significant effect of HLS on femoral weights (ANOVA, $P = 0.27$).

Figure 4.21 shows the femoral lengths for the suspended and control animals. The femoral lengths in both groups increased throughout the experimental period. No significant differences were found between suspended and control groups (ANOVA, $P = 0.16$).

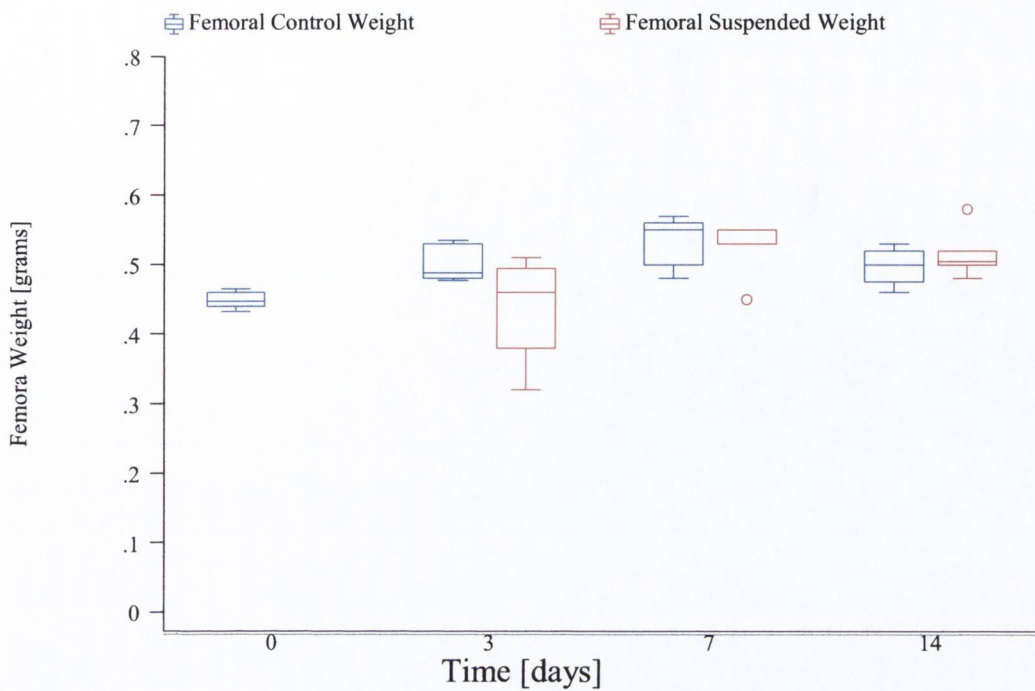


Fig. 4.20 Control and Suspended Femoral Weights Vs. Time

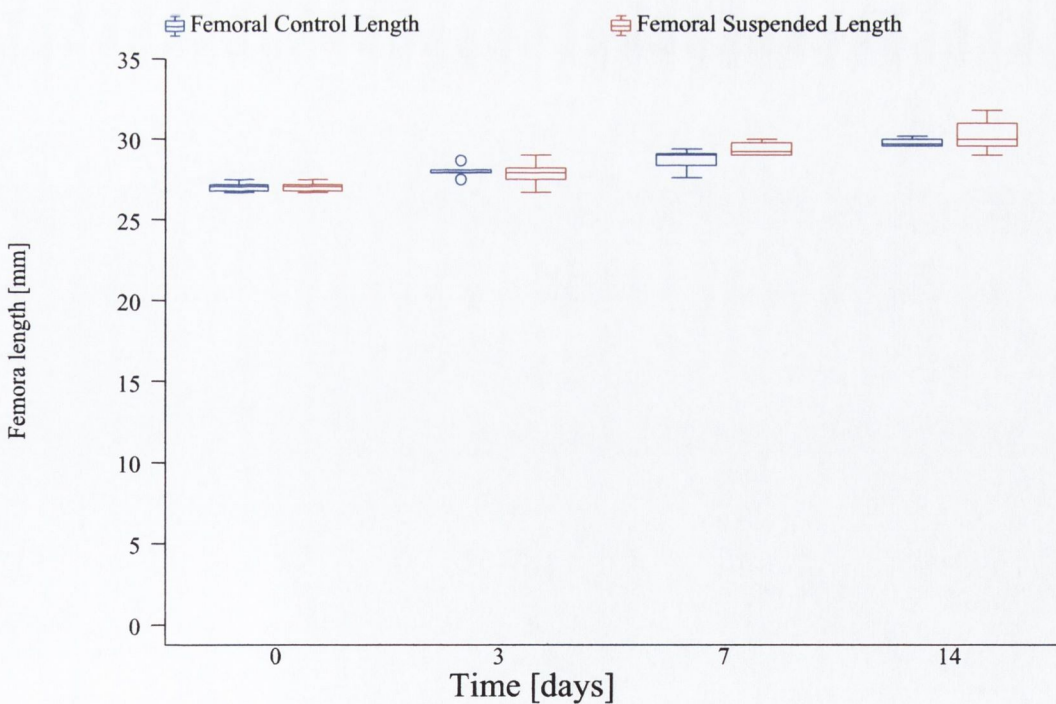


Fig. 4.21 Control and Suspended Femoral Lengths Vs. Time

4.3.3.2 Femoral Cross Sectional Area

In figure 4.22 there are two values displayed for both the control and suspended groups' total CSA. The corrected value corresponds to the normal value minus the sum of the areas of any large resorption cavities in the bone. As can be seen from the graphs the effect of this correction is to slightly reduce the total cross sectional area in each group. In both the corrected and uncorrected data there is a statistically significant effect of time for all groups (ANOVA, $P < 0.001$, Linear Regression Analysis < 0.01). However, while the cross sectional area increases over time, the increase is small.

As a result of the HLS there is a statistically significant difference in the total cross sectional areas of the suspended animals relative to the controls in both the uncorrected data set (ANOVA, $P < 0.01$) and corrected data set (ANOVA, $P < 0.01$). At all times in both the corrected and uncorrected data sets the suspended animals' CSA values were smaller than those of the controls.

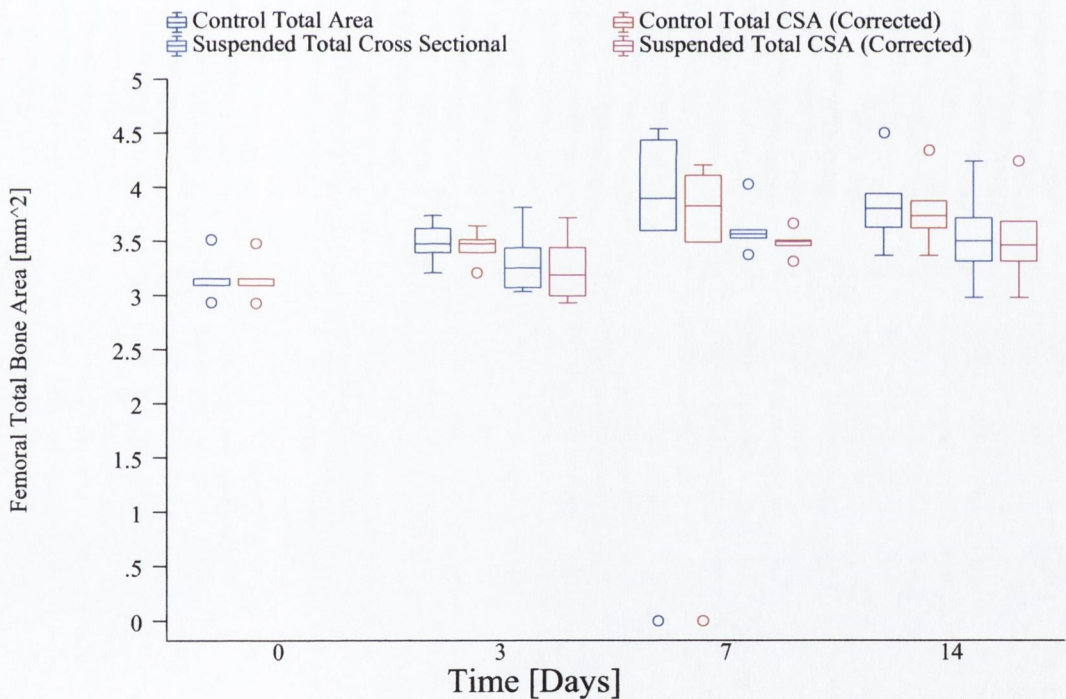


Fig. 4.22 Femoral Total mid-diaphyseal Cross-Sectional Areas Vs. Time

Figure 4.23 shows the periosteal cross sectional areas for the control and suspended groups. The femoral periosteal CSA increased significantly over time (ANOVA, $P < 0.001$; Linear Regression Analysis, $P < 0.001$). In the first three days, there is a reduction in growth in the suspended animals' periosteal cross sectional area. After this, the suspended animals' periosteal area began to increase and surpassed that of the controls by day 14. Statistically there was no significant effect of HLS on the periosteal areas of the femora in the suspended and control groups (ANOVA, $P = 0.70$).

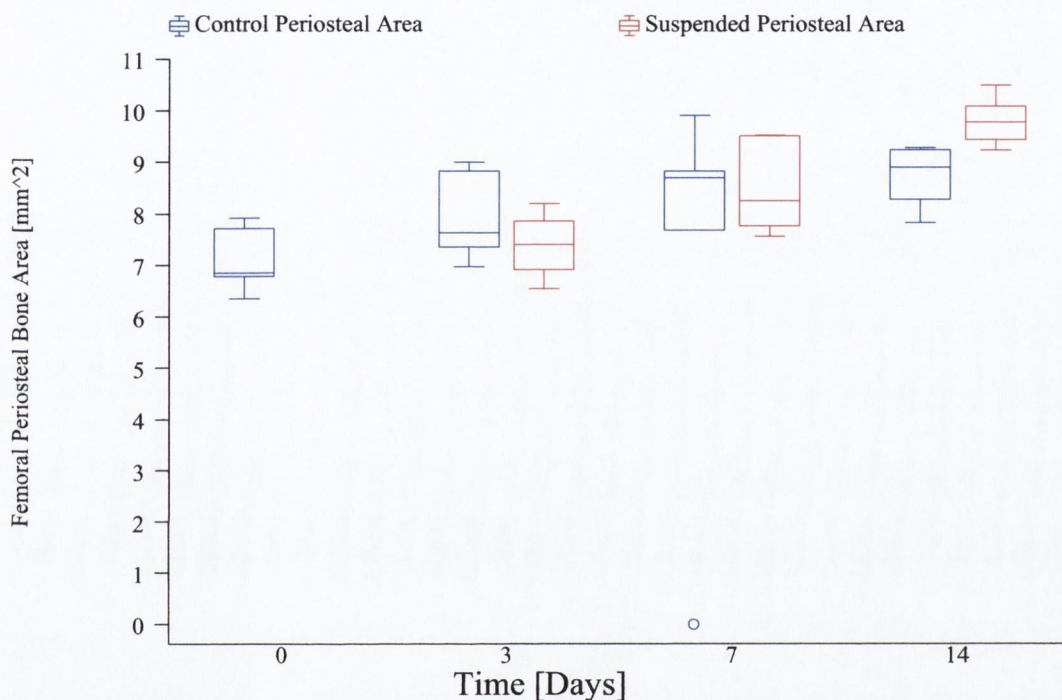


Fig. 4.23 Femoral Periosteal Cross Sectional Areas Vs. Time

Figure 4.24 shows the endosteal CSA area for the two groups. There was a significant increase in femoral endosteal CSA over time (ANOVA, $P < 0.001$; Linear Regression Analysis, $P < 0.001$). There was no statistical significance between the control and suspended periosteal areas (ANOVA, $P = 0.14$).

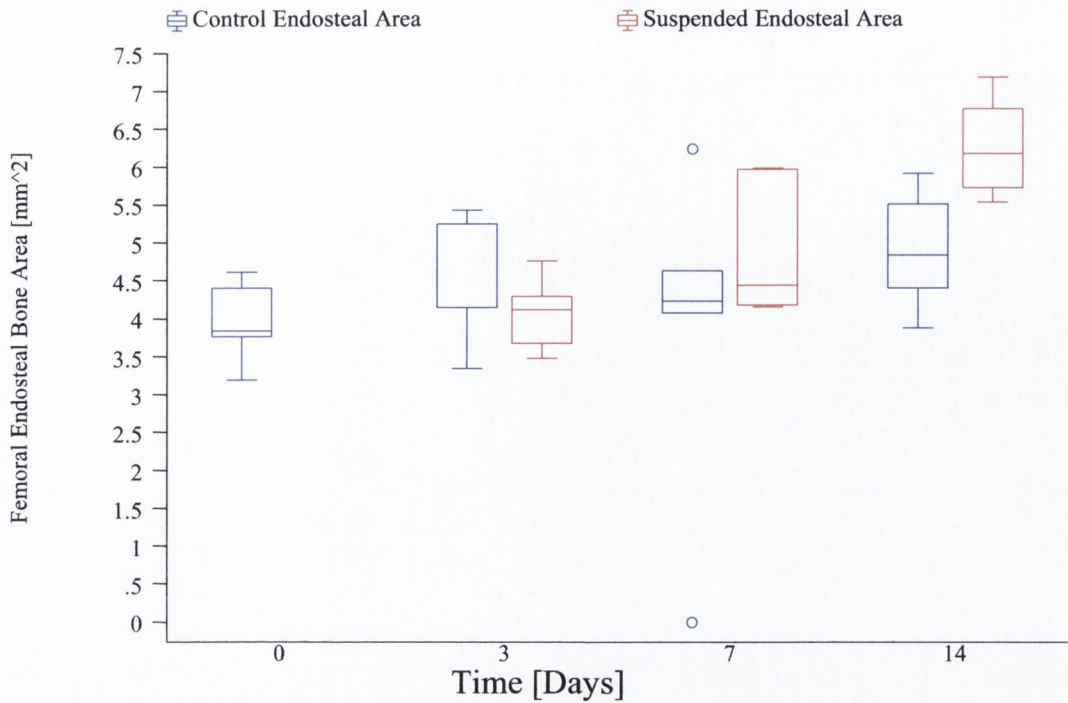


Fig. 4.24 Femoral Endosteal Cross Sectional Areas Vs. Time

4.3.3.3 Femoral Shape

Figure 4.25 shows the periosteal circularity data for the control and suspended groups' femora. Over the course of the experiment there was a significant effect of time on the femoral periosteal circularity (ANOVA, $P < 0.01$). The suspended animals' femoral periosteal circularity values tended to be greater than those of the control groups and this HLS effect was statistically significant (ANOVA, $P < 0.01$).

Figure 4.26 shows the equivalent femoral periosteal elongation values for the two groups. There was a statistically significant effect of time on the elongation values for the two groups (ANOVA, $P < 0.05$; Linear Regression Analysis, $P < 0.05$). There were no significant differences in the periosteal elongation data of the two groups (ANOVA, $P = 0.86$).

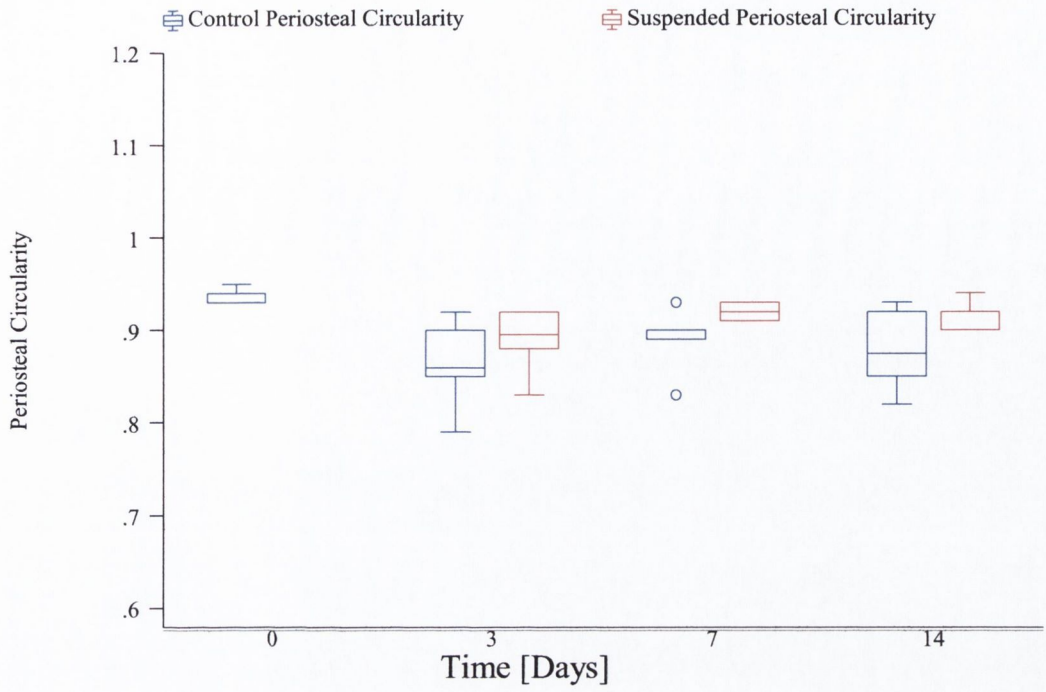


Fig. 4.25 Femoral Periosteal Circularity Vs. Time

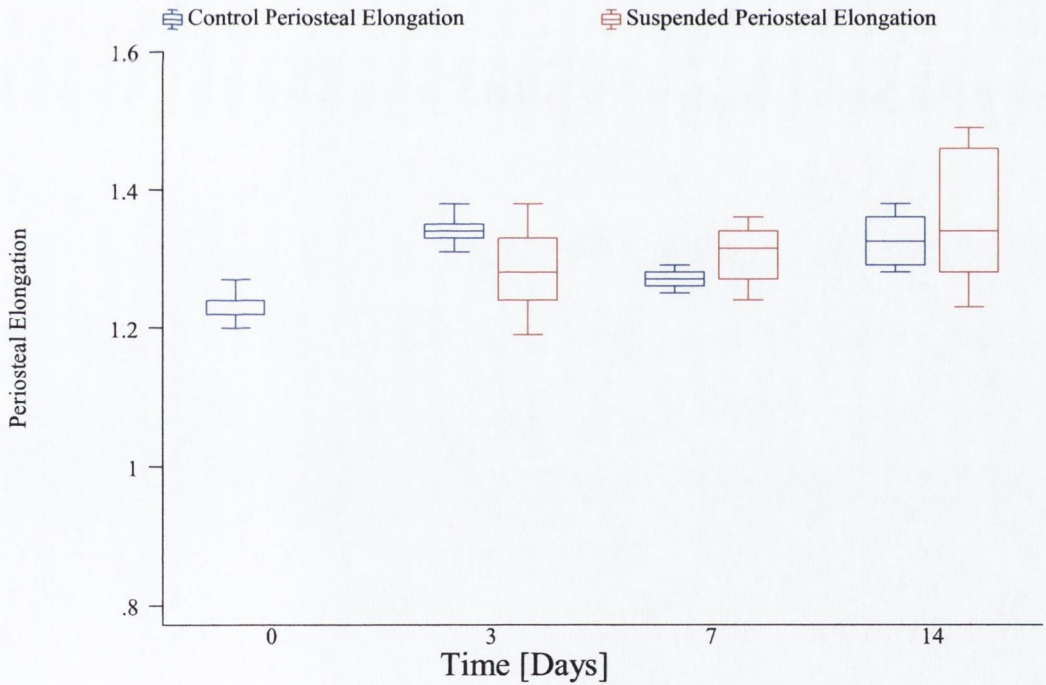


Fig. 4.26 Femoral Periosteal Elongation Vs. Time

Figure 4.27 shows the femoral endosteal circularity data for the two groups. There were large numbers of voids and other irregularities, which resulted in a large degree of variance in the data. This variance has a particularly large effect on the perimeter term, which is squared in the geometric variable 'circularity'. Neither time (ANOVA, $P = 0.15$) nor HLS (ANOVA, $P = 0.27$) had a statistically significant effect on femoral endosteal circularity.

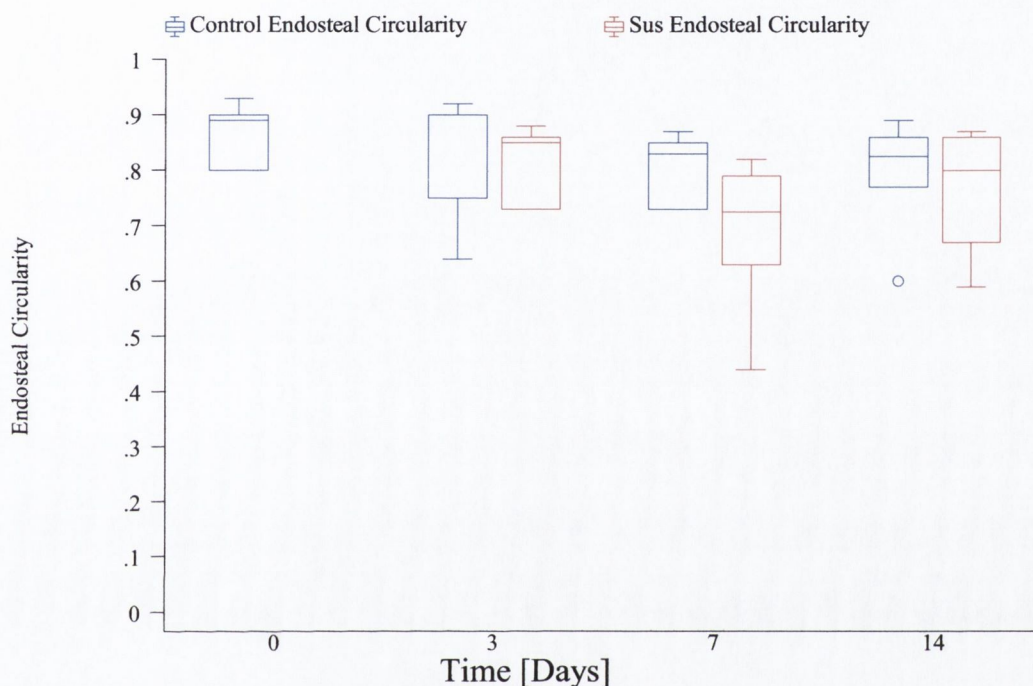


Fig. 4.27 Femoral Endosteal Circularity Vs. Time

Figure 4.28 shows the femoral endosteal elongation data for the control and suspended groups. Over time there is an upward trend in the values for elongation at the endosteal surface of the femora, which was statistically significant (ANOVA, $P < 0.01$). Hind limb suspension had no statistically significant effect on the endosteal elongation values of the suspended animals relative to the controls (ANOVA, $P = 0.54$).

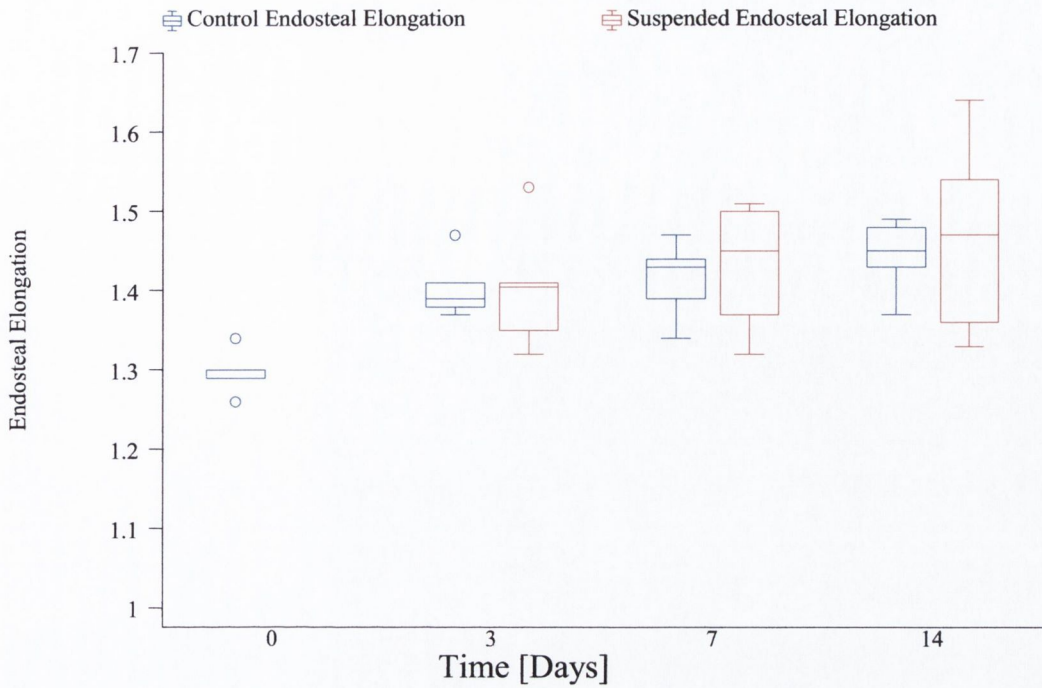


Fig. 4.28 Femoral Endosteal Elongation Vs. Time

4.3.3.4 Femoral Epi-Fluorescence Microscopy Results

Figure 4.29 shows the periosteal bone formation index data for the two groups. The amount of new bone increased in both groups from 3 to 7 days. This increase over time is statistically significant (ANOVA, $P = 0.001$). As a consequence of the HLS, the amount of new periosteal bone formation was reduced in the suspended animals. This loss was particularly evident in the 3 day suspended group. This effect of HLS was found to be statistically significant (ANOVA, $P < 0.05$).

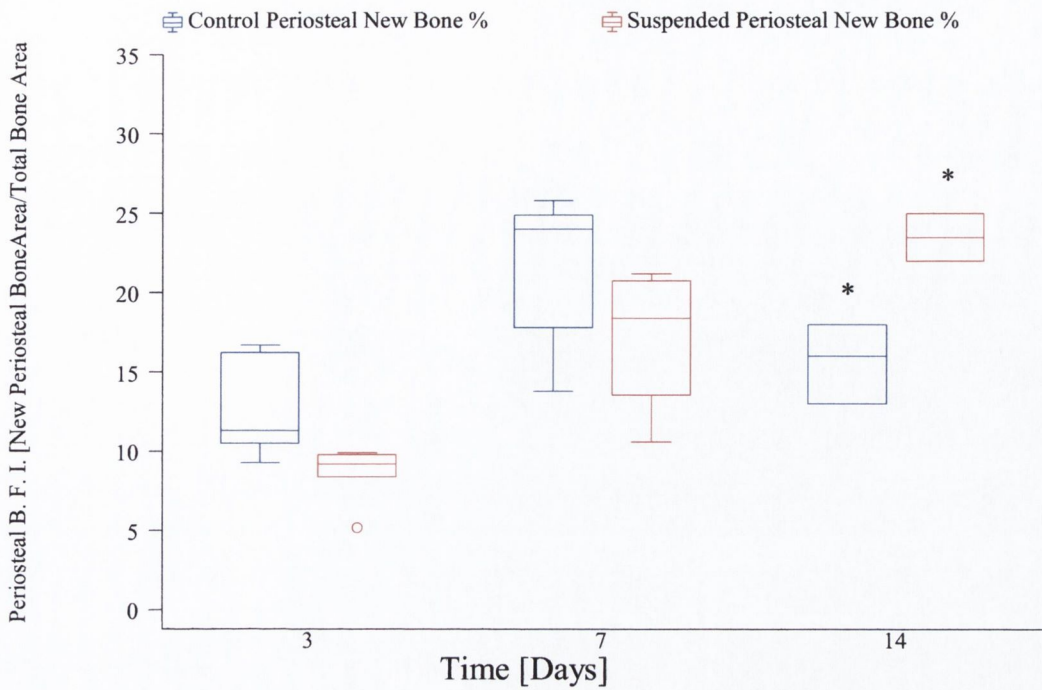


Fig. 4.29 Femoral Periosteal BFIs Vs. Time (* denotes $n < 6$)

Figure 4.30 shows that the endosteal bone formation rates are lower than those at the periosteum. Growth resulted in an increase in new bone formation in both groups over the experimental period and this increase over time was statistically significant up to 7 days (ANOVA, $P < 0.01$). When the effect of HLS was examined there was no significant difference between the two groups endosteal BFIs (ANOVA, $P = 0.45$).

Figure 4.31 shows the data for the total periosteal bone formation index for the two groups are presented. There was a significant effect of time on the data with both groups increasing significantly over the experimental period (ANOVA, $P < 0.001$). Also, as a result of HLS there was a significant reduction in the total BFI of the suspended animals relative to the controls (ANOVA, $P < 0.001$).

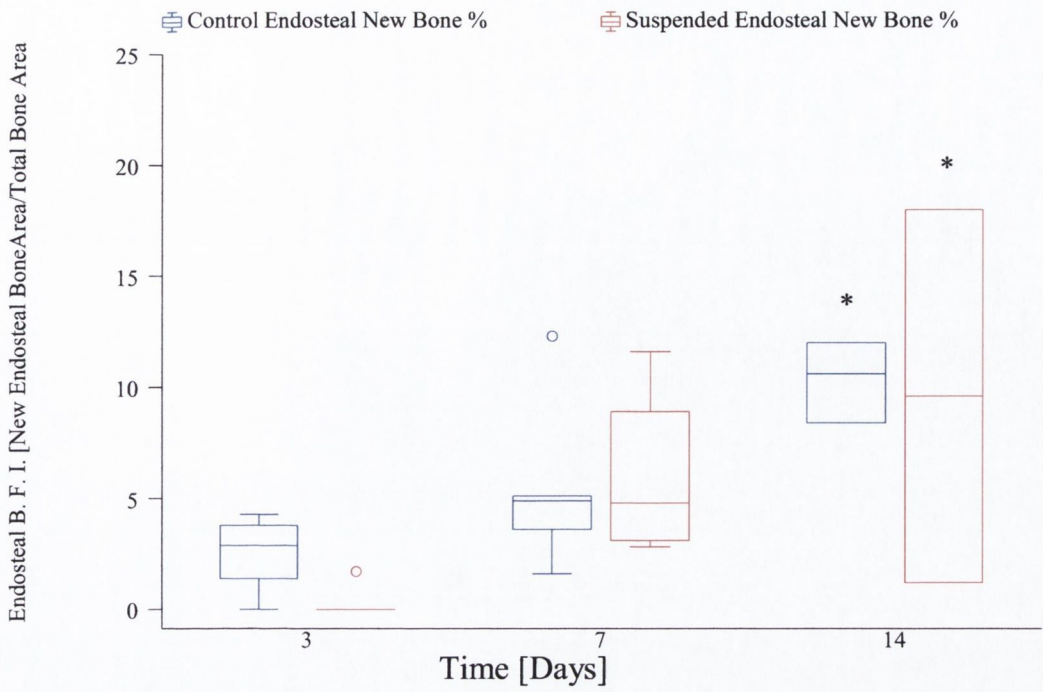


Fig. 4.30 Femoral Endosteal BFIs Vs. Time (* denotes n < 6)

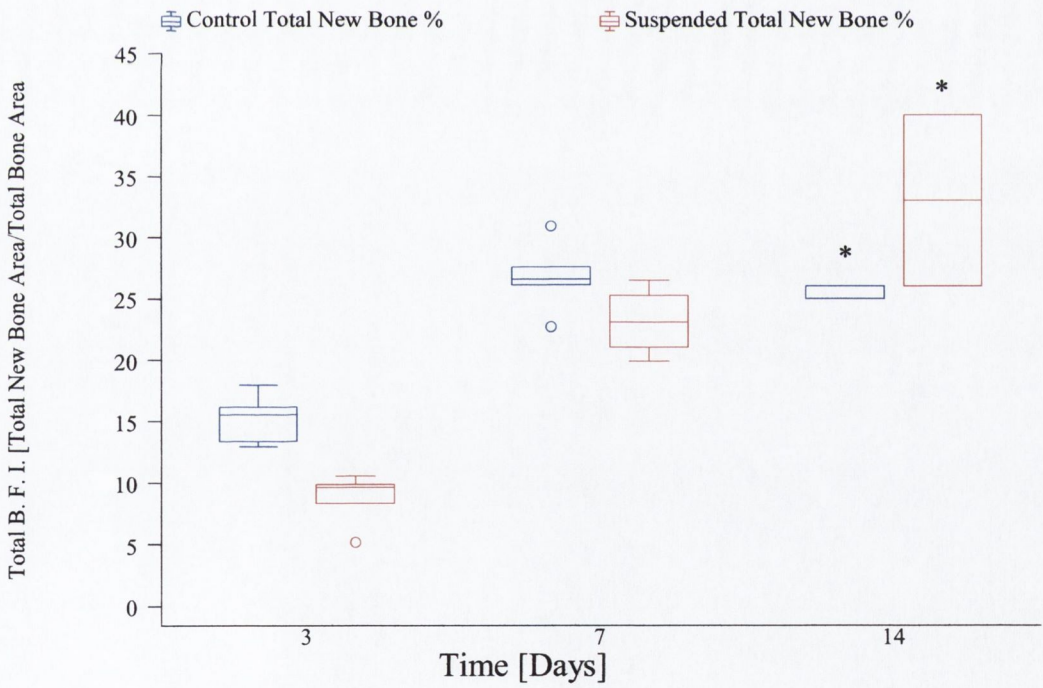


Fig. 4.31 Femoral Total New BFIs Vs. Time (* denotes n < 6)

Each femoral section was also examined for the presence of either Haversian systems or microcracking. No Haversian systems were located in any of the transverse sections of the unloaded femora.

In the femora, cracks were found in two thirds of the animals and in a quarter of all sections examined (Total: 33 out of 138 slides; Control: 19 out of 77; Suspended: 14 out of 61). This resulted in 45 measured cracks of which 23 were in control humeri and 22 in suspended. Again, due to the experimental error outlined in section 4.2.5.2, the 14-day groups data is divided into those sections containing oxytetracycline and those without. In the sections from those animals that received oxytetracycline, cracks stained with oxytetracycline were formed prior to the experimental period and therefore indicate the levels that microdamage is normally found *in vivo*. Cracks stained with calcein blue were formed during the course of the experimental period and may be related to HLS. When there is no oxytetracycline in the section it is unfortunately not possible to confirm whether the crack was formed prior to the experiment.

All the cracks in the 0, 3 and 7 day groups were stained with oxytetracycline while all those found in the 14-day groups were stained with calcein blue. No oxytetracycline labelled cracks were found in the 14-day groups sections regardless of whether the animal had received its correct oxytetracycline dosage or not.

The majority of the cracks were again observed to be located near the endosteal surfaces. In summary, 21 out of the 23 control cracks and 17 of the 22 suspended cracks were located near the endosteal surface (see Figures 4.32).

The microcrack data was once again divided into the four groups described earlier (see section 4.2.5.1). Table 4.6 outlines the crack data for the transverse sections across the mid-diaphysis of the control and suspended femora.

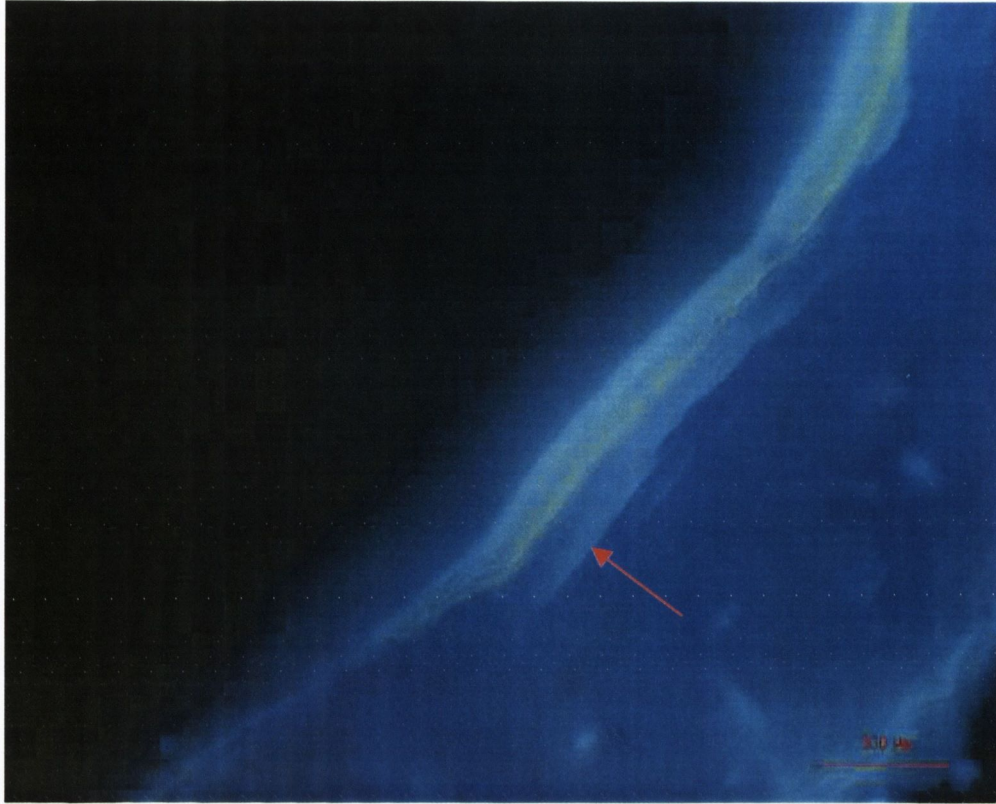


Fig. 4.32 Oxytetracycline labelled *in vivo* microcrack (indicated) in the femora of a hindlimb suspended rat

Specimen 3 day suspended # 2 (Bar=100 μ m)

	Crack density [number/mm ²]	Surface density [μ m/mm ²]	Crack length [μ m]
Combined data 0, 3, 7 day groups	0.11 \pm 0.2	20.2 \pm 40.6	62.2 \pm 102
Control 14-day group	0.06 \pm 0.12	13 \pm 26.9	41.6 \pm 91.8
Suspended 14-day group	0.11 \pm 0.23	24.2 \pm 46.6	72.4 \pm 120.2
Combined data 14-day groups	0.08 \pm 0.17	17.2 \pm 36.4	56.2 \pm 105.7

Table 4.6 Femoral crack data. All values are mean \pm standard deviation.

4.4 Discussion

HLS did not result in any changes in the grooming or activity levels in the suspended animals. However, this assessment is a qualitative one and thus subject to individual assessment. Quantitatively the animals' feeding patterns were monitored and controlled throughout the suspension period. As expected in growing animals, all the rats gained weight. Since glucocorticoid levels in the rats were not investigated, the stress levels of the rats were not directly measured. Hence, the stress effect of HLS was assessed via the weight gain data taken throughout the experiment and the qualitative assessment of the animals' behavioural patterns.

Hindlimb suspension is a well-documented and accepted method of inducing underload in the hindlimbs of rats and mice. As a result of suspension the suspended animals will gain weight at a slightly reduced rate than ad libitum non-suspended controls (Morey et al., 1979). To negate this effect, which would influence results, the control groups were pair fed with the suspended groups in this experiment. This ensured that the controls were only able to eat, at most, the same amount as had the suspended animals on the previous day. Consequently, there was no statistically significant difference in the body weights between the two groups. Allied to the fact that the animals maintained normal levels of grooming and activity and gained weight throughout, this indicates that the animals were not overly stressed and that any measured differences in the bones of the suspended animals were taken to be as a result of altered load, although this was not definitively proved.

4.4.1 Morphology

The first effect investigated in this experiment was that of HLS on the gross morphology of the humeri. Following HLS, no significant differences were found in either the bone length or weight for the mechanically unloaded humeri as compared with controls. This was expected and is consistent with previous studies (Shaw et al., 1987, Spengler et al., 1983, Vailas et al., 1988, van der Meulen et al., 1995).

Following HLS, no significant differences were found in either the bone length or weight of the unloaded femora. Therefore there was no significant effect of HLS on the gross morphology in the suspended animals' femora. This differs from other authors'

findings who found no change in length but a significant difference in the weight of the suspended animals femora (van der Meulen et al., 1995).

Throughout the experimental period the suspended animals' femora experience reduced mechanical load. To investigate if this altered loading pattern resulted in changes in the bones' shape and microstructure, slides of transverse sections across the mid-diaphysis were examined. In the femora, there was an increase in the periosteal, endosteal and total cross sectional areas over time. These increases were directly attributable to normal age related growth and in the case of both periosteal and endosteal areas the increase over time was statistically significant. Following HLS there was a transient cessation of growth in the suspended animals femora up to 3 days. Growth then resumed and the suspended animals' periosteal area increased and even surpassed that of the controls by day 14. Despite this cessation of growth, neither the periosteal nor endosteal cross sectional areas were statistically significantly different between the two groups. Interestingly, the total cross sectional areas of the suspended animals' femora were significantly reduced in comparison to the normally loaded controls. This implies that the difference in total cross sectional area measured is a function of both formation, which predominates at the periosteal surface, and resorption, which is dominant at the endosteal surface. This again differs from some studies, which showed a decrease in total cross sectional area to be as a result of the inhibition of bone formation alone (van der Meulen et al., 1995, Morey et al., 1979, Globus et al., 1986b).

To investigate if HLS resulted in changes in the bones' cross sectional area, shape and microstructure, slides of transverse sections across the mid-diaphysis were examined. In the humeri there was a significant increase in the periosteal, endosteal and total cross sectional areas over time due to growth. However, HLS had no statistically significant effect on any of these areas. This is similar to previous studies (van der Meulen et al., 1995, Morey-Holton and Globus, 1998) and with the premise normal weight bearing forces are present in the humeri.

The shape of the humeri was examined using two geometric parameters, circularity and elongation, for both periosteal and endosteal surfaces. As a result of HLS both periosteal circularity and elongation were found to be significantly different from the controls. In the suspended animals, circularity values were increased while the elongation data showed a decrease compared to controls. Both results indicate that the suspended animals' mid-diaphyseal cross sections have become more circular as a result

of suspension. At the endosteal surface, there was no significant effect of HLS on the suspended animals' endosteal circularity data. However, as previously explained, the circularity geometric parameter was strongly affected by the irregularities at the endosteal surface. The effect of HLS on endosteal elongation approached critical significance (ANOVA, $P = 0.0517$) with the endosteal area of the suspended animals being more circular than that of the controls. There is little work done on changes in shape but these results are consistent with the hypothesis that although the humeri continue to experience weight-bearing loads, the actual loading pattern may be altered in hindlimb suspension, which results in an altered humeral shape.

The shape of the femora was examined using two geometric parameters, circularity and elongation, at both the periosteal and endosteal surfaces. As a result of HLS, periosteal circularity was significantly increased relative to the controls while there was no significant difference in elongation. However, since the periosteal surface is relatively smooth with no large irregularities and this parameter, circularity, encompasses all the data points along the edge, it would be expected to yield an accurate answer. In comparison, the elongation data is made up from 18 measurements of feret diameter at 10° increments around the bone edge and thus is a less accurate measurement of bone shape. At the suspended animals' endosteal surfaces, there was no significant effect of HLS on the endosteal circularity or elongation. Overall, this implies that there was only a limited effect of HLS on the shape of the suspended animals femora due to unloading. These results are consistent with the underlying hypothesis that the femora experience reduced mechanical loads as a result of HLS.

To investigate the effect of HLS on humeral formation alone, intraperitoneal injections of oxytetracycline were administered before the experimental period, which labelled bone forming at the time of the injection. This fluorochrome labelled the bone at the endosteal and periosteal surfaces, resulting in two rings of stained bone (See Figure 4.4). Therefore, any bone inside the endosteal ring or outside the periosteal ring, was bone formed after the start of the experiment. This new bone was expressed as a percentage of the total bone present, and was termed 'Bone Formation Index' (BFI). The BFI in turn was subdivided into periosteal, endosteal and total BFIs to denote where the new bone was located. In the humeri there was no effect of HLS on the suspended groups' periosteal BFI. Unfortunately, as a result of the experimental error detailed in section 4.2.5.1 the 14 day groups could not be included in the BFI statistical

analysis. At the endosteal surface there was a statistically significant effect of suspension on the formation rate, with more new bone laid down in the suspended animals. However the total amount of bone formed at the endosteum was still very small as this is largely a resorbing surface. Unsurprisingly therefore, there was no statistically significant effect of HLS on the total BFI, as the amount of bone formed at the periosteum far exceeds that at the endosteum.

When the pattern of femoral formation was examined in isolation, via the bone formation indices, there was a large reduction in the amount of new bone formed at the periosteum. This effect of suspension on periosteal formation in the suspended animals was statistically significant up to seven days. At the endosteum, there was a virtual cessation of bone formation from day zero to day three in the suspended animals. However, as expected in growing animals, the total amount of endosteal bone formation was very small in both groups, and overall there was no statistically significant effect of HLS on the endosteal BFI. Unsurprisingly, as the periosteal formation far exceeds that at the endosteum, the effect of HLS on the total BFI was also significant, with a large reduction in the new bone formed in the suspended animals. These data are consistent with work by Sessions (1989) where the bone formation rate at the tibio-fibular junction was reduced by 34%, and Globus (1986a) who found a decrease of 49% at the same junction relative to controls.

4.4.2 Microdamage

All sections in the loaded humeri and unloaded femora were examined for the presence of Haversian systems and microcracks. No Haversian systems were found in any of the mid-diaphyseal sections of either the humeri or femora. This was expected, as the humeri either did not experience a greatly increased load in HLS or were normally loaded. Similarly, the femora were either underloaded via HLS or normally loaded. Furthermore, Bentolila et al. (1998) suggested that rat bone would need to be highly loaded in order to initiate secondary remodelling and create Haversian systems. Finally, since the animals' bones are growing rapidly, bone can readily be added at the outer surfaces where needed, to reduce any local excess loads, thus alleviating the need for remodelling via secondary osteon formation.

This study showed that *in vivo* microdamage is present in both rat humeri and femora. This *in vivo* microdamage was labelled with two fluorochromes: oxytetracycline and

calcein blue. The only other evidence of *in vivo* labelling, prior to the animals sacrifice, was a study by Stover (1992) using calcein green to label microcracks in race horses.

From examination of microcrack levels in both the humeri and the femora (see Table 4.5), it is clear that there are large differences between the two microdamage populations. Cracks were found in a higher percentage of humeral than femoral sections. As a result, humeral crack density and surface density values were roughly 50 percent greater relative to the femoral values in the 0, 3 and 7 day groups. In the case of the various 14 day groups this picture was mirrored with the humeral values being greater. However, care must be taken when looking at the 14-day data due to the labelling problem with oxytetracycline discussed earlier. Unfortunately, this also prevented us from using the 14 day groups to determine the effect of HLS on microcrack propagation in the humeri and femora.

The majority of the cracks (84% in both humerii and femora) were observed to be located near the endosteal surfaces (see Figures 4.18, 4.19 & 4.32). The reason for this is not known but a number of possibilities include:

- The bone at the endosteal surface is older and has therefore experienced more loading cycles.
- The endosteal surface is predominantly a resorbing surface and has a large number of resorption cavities which may act as stress concentrators.
- The bone at the endosteal surface may be less mineralised as a result of the resorption activity present.

The last possibility could be tested using nano-indentation to determine whether the level of mineralization had been altered following HLS. In addition, histologically the relationship between the location of microcracks and stress concentrators such as resorption cavities could be assessed.

No oxytetracycline labelled cracks were found in the 14 day groups regardless of whether they had received the correct dosage. However the medullary canal is growing rapidly by resorption and since the majority of all cracks found were located at the endosteal surface, it is likely that any cracks stained with oxytetracycline were removed by the time calcein blue was administered.

A number of studies into *in vivo* microdamage have been done and these data are presented in Table 4.7. These studies were performed on a number of different animals and on a variety of bones. O'Brien et al. (2000) studied and reconstructed, in 3-D, *in*

in vivo microcracks from longitudinal sections of human rib. These researchers also looked at *in vivo* microcrack levels in bovine tibia (O'Brien et al., 2003) Another study by Muir et al. (1999) looked at microcracking in the left central tarsal bones of greyhounds.

	Crack length [μm]	Crack density [Cracks/ mm^2]	Surface density [$\mu\text{m}/\text{mm}^2$]
This study (0, 3 & 7 days): Rat humeri	62 \pm 92	0.17 \pm 0.35	30.2 \pm 63.5
This study (0, 3 & 7 days): Rat femora	62.2 \pm 102	0.11 \pm 0.2	20.2 \pm 40.6
O'Brien et al. (2000) Human rib	97 \pm 38	0.16 \pm 0.13	36.8 \pm 33.3*
O'Brien et al. (2003) Bovine tibia	65.8 \pm 9.6	0.014 \pm 0.005	0.9 \pm 0.16
Muir et al. (1999) Canine central tarsal bone (left)	68 \pm 21	0.046 \pm 0.056	3.1 \pm 4.2

Table 4.7 Comparison of crack propagation data from various authors

(* Data obtained via personal correspondence with author).

When the crack data found in this study are compared against these other studies a number of observations can be made. Firstly mean crack lengths are similar in all the experiments. The crack and surface density values in this experiment for both humeri and femora were similar to those found in human rib. However, they are considerably greater than those found in either bovine tibia or canine central tarsal bone. In the case of surface density the values found in this experiment were substantially greater than those reported elsewhere. Nonetheless, it is important to realise that these experiments are not directly comparable. For example, in the case of bovine tibia the bones microstructure (highly organised with numerous secondary osteons) and indeed microstructural properties (stiffness, strength and mineralisation) would be vastly different to the rat bones in this experiment.

4.5 Conclusions

To conclude, the following research questions have been answered:

In the humeri:

- HLS had no effect on the gross morphology, bone length and weight, of the humeri.
- HLS resulted in a limited change in growth patterns across the mid-diaphysis of the loaded humeri:
 - HLS had no effect on the amount of bone present in the humeri with no significant differences between suspended and control groups periosteal, endosteal or total cross-sectional areas.
 - HLS resulted in a change in the shape of the humeri with an altered periosteal shape seen in both circularity and elongation periosteal values in the suspended animals as compared to controls.
 - At the humeral endosteal surface there was also increased bone formation in comparison to the controls although the amount of bone formed was small in contrast to the periosteal bone formation.
 - It is unclear whether this change in shape is the result of a change in formation, resorption or a coupled response of the two.

In the femora:

- HLS had no effect on the gross morphology, bone length and weight, of the femora.
- HLS resulted in a large change in growth patterns across the mid-diaphysis of the unloaded femora:
 - HLS resulted in a reduction in the total amount of bone present with significantly less bone present in the total femoral CSA values of the suspended animals as compared to controls.
 - HLS had no significant effect on the femoral endosteal and periosteal CSA values.
 - HLS resulted in a change in the femoral periosteal circularity values but not the periosteal elongation values or either of the endosteal shape parameters.

- HLS resulted in a reduced periosteal bone formation rate in the suspended animals (evidenced by the BFI study) although this did not result in an altered periosteal CSA.
- Therefore the response to unloading seems to be a coupled response of formation and resorption although in growing animals formation is by far the predominant force.

Microcracking and formation of Haversian systems:

- No Haversian systems were found in any of the sections from either the humeri and femora.
- *In vivo* microcracks were found under normal conditions in rat bones and were labelled via intraperitoneal injections of two fluorochromes, oxytetracycline and calcein blue, in both the humeri and femora.
 - There were more *in vivo* microcracks present in the humeri than the femora with both mean crack density and surface density values greater in the humeri than the femora.
 - The mean crack lengths were similar in the humeri and femora.
- Unfortunately, due to experimental error, the effect of HLS on microcrack initiation and propagation could not be assessed.

Chapter 5 Functional Adaptation to Altered Mechanical Stimuli

5.1 Introduction

Four centuries ago, Galileo Galilei (1564-1642) recognised that the rigidity of the skeleton of terrestrial animals was related to its load bearing function, which in turn was associated with the animal's size and mass (Galileo, 1638)(see Figure 5.1). This link between mechanical load and form was later observed by Ward, who noted that the trabecular arrangement within the femoral head, now known as Ward's triangle, had patterns comparable to those found in the crossbeam structures of nineteenth century streetlights (Ward, 1876). Nearly 30 years later Julius Wolff postulated his 'law' in his book, *'Das Gezetz der Transformation der Knochen'* (Wolff, 1892). In this, he wrote in more detail on how the structure of bone reflects its mechanical usage history. The process of bone formation and bone remodeling according to its mechanical history is now generally known as functional adaptation, a term proposed by Roux (1895).



Fig. 5.1 A drawing by the Italian Galileo Galilei (1564-1642) demonstrating the dimensions of bones from animals of differing weights.

It is clear that the length-to-width ratio is remarkably different between light and heavy animals. (After G. Galilei, 1638, *Two new Sciences*, translated by Stillman Drake, The University of Wisconsin Press, 1974.)

This idea that a bone's form reflects its function has been observed clinically in cases of underload via prolonged bed-rest, immobilisation, spaceflight and HLS and in the case of overload in athletes and military recruits (see sections 1.6.1 & 1.6.2 and chapter 2). In chapter 4 the effect of HLS on the amount of bone present in rat humeri and femora was examined via mid-diaphyseal transverse slides. This section of the project deals with the effect of HLS on the structural properties of the contra-lateral femora. Consequently, the material and geometric properties of the control and suspended groups' femora were assessed along the bones' lengths using peripheral quantitative computed tomography, pQCT. The mechanical properties of the femora were assessed via destructive torsion tests and a number of mechanical parameters measured. These data were then combined to assess the effect of HLS on the biomechanical properties of the unloaded femora.

5.1.1 Biomechanical effects of unloading via spaceflight

Changes in the material properties of astronauts' bones as a result of reduced loading in space were noted as early as 1967 following work based on astronauts in the Gemini-Titan IV, V and VII missions (Mack et al., 1967, Mack and LaChance, 1967) and in Macaca monkeys in the biosatellite III project (Mack, 1971). The authors reported demineralisation and a reduction in bone density in the foot and hand of astronauts and a loss in bone density in the monkeys at a number of scan sites. Further studies on the SKYLAB series of flights (1973-1975), which lasted 28-84 days, provided more detail on these losses and hypothesised that the bone loss mostly affected weight-bearing bones (Vogel and Whittle, 1976, Smith et al., 1977). Long-term spaceflight on the MIR space station found decreases in bone mineral ranging from 3% to 10% in cosmonauts following 75 to 185 day missions. Once again this loss of bone mineral density was limited to the weight bearing tibiae with no loss found in the radius (Stupakov et al., 1984, Vico et al., 2000, Collet et al., 1997). These studies also suggested that the time required to replace the lost tibial bone far exceeded that which caused the reduction in the first place. Rats flown for 19 days in the Cosmos-1129 developed osteoporosis in the trabecular regions of long bones before returning to normal 29 days after their return (Rogacheva et al., 1984). Finally, recent observations made during MIR long duration missions suggests that redistribution of bone mineral content occurs, with loss of

mineral in the lumbar vertebrae and lower limbs, and increased mineralisation of cervical and cephalic areas (Schneider et al., 1995). Due to the logistical difficulties and expense involved in spaceflight, the ground-based model, hind limb suspension, has also been used extensively to study reduced load on the mechanical properties of bone (Abram et al., 1988, Bikle et al., 1987, Vailas et al., 1988, Shaw et al., 1987, Bloomfield et al., 2002, van der Meulen et al., 1995, Morey et al., 1979). More recently spaceflight data does not show substantial losses in BMD but flights now always include countermeasures.

5.1.2 Effect of unloading via HLS on Bone Mass and Maturation

Bikle et al. (1987) hindlimb suspended rats for periods of up to 15 days and determined maturation levels by analysing the uptake of ^3H proline and ^{45}Ca in the tibia via density fractionation. They concluded that following HLS the maturation of bone was inhibited leading to an accumulation of less-well mineralised tissue. This reduction in maturity was mirrored by a reduction in the fat free bone mass in the unloaded bones which paralleled a reduction in bone calcium content (Globus et al., 1986b, Vico et al., 1995). However the concentrations of several matrix and mineral components such as calcium, collagen, phosphorus and DNA remained unchanged following unloading (Shaw et al., 1987, Vailas et al., 1988). Work done by Jain et al. (2000) determined that the loss in bone mass resulted from proportional reductions in both the organic matrix and total mineral content, with the reduction in mineral content solely due to a reduction in calcium in the bone. Furthermore this reduction in mass occurs only in the unloaded bones (Arnaud et al., 1995, Globus et al., 1986b, Roer and Dillaman, 1990) and at both the predominantly cancellous metaphyses and the predominantly cortical diaphysis, although the losses in bone mass are greater in the metaphyses (Globus et al., 1986b).

5.1.3 Bone Mineral Density

5.1.3.1 Measurement of Bone Mineral Density via pQCT and DEXA Scanners

The effects of various therapeutic measures and mechanical loading/unloading on bone mineral density (BMD) have been well documented via dual energy x-ray photon absorptiometry, dual energy x-ray absorptiometry (DEXA), peripheral quantitative

computerised tomography (pQCT) and micro computerised tomography (μ CT). Measurements with dual energy x-ray photon absorptiometry and DEXA result in values which reflect an areal BMD (g/cm^2), calculated as a quotient of bone mineral content (BMC; g) to a two-dimensional projected corresponding area, rather than a volumetric density (g/cm^3). In studies where there are little changes in size, in adult bone, areal BMD is a good substitute for volumetric bone mineral density, vBMD, however in studies where an experimental factor may affect growth and density, or where there is a disparity in the bone size, the validity of using areal BMD from DEXA rather than vBMD must be questioned (Ashizawa et al., 1999, Seeman, 1997, Bhudhikanok et al., 1996). For example in young animals with growing bones there are small changes in vBMD but increases in bone size result in a substantial increase in areal BMD (Lu et al., 1996, Schonau et al., 1993, Schonau et al., 1994).

5.1.3.2 Using Bone Mineral Density and Content as predictors of Mechanical Strength

Classically, mechanical tests have been used to determine the mechanical properties of bones. Often these tests result in the destruction of the bones, which is clearly not applicable to most clinical situations. More recently, a large number of studies have attempted to use the density and geometry parameters obtained in both DEXA and pQCT scanners to determine and predict the mechanical properties of bones. The ability to do this has obvious clinical benefits in treating diseases such as osteoporosis. Researchers have used both DEXA and pQCT scanners of various resolutions on different bones and bone types from a number of different species, ranging from human second metatarsal to rat and mouse long bones. Bones have been tested using a variety of mechanical tests including torsion, cantilever and three-point bending. As a result of the wide range of experimental set-ups and perhaps the variability inherent in bone, the findings have been inconsistent, with some authors finding geometric parameters and some finding bone mineral density parameters to have the greatest correlation with mechanical properties. The difficulty in making direct comparisons due to the wide variety of experimental set-ups is evident in the following examples.

Jämsä et al. (1998) used three-point bending tests to evaluate the ability of pQCT scan parameters to predict mechanical strength of mouse femora and tibiae. They found that individually, cross sectional moment of inertia, CSMI ($r = 0.86$, $p < 0.0001$), and cross sectional area, CSA ($r = 0.94$, $p < 0.0001$), best predicted the breaking force for the

femora and tibiae respectively while for the elastic modulus it was CSA ($r = -0.80$, $p < 0.0001$) and CSMI ($r = -0.70$, $p < 0.001$) respectively. When the parameters were combined using stepwise linear regression analysis, the following relationships were found. Breaking force of the femur was best explained by a combination of CSMI and volumetric cortical BMD, vCtBMD ($r^2 = 0.84$, $p < 0.0001$). Stiffness of the femur was best explained by CSMI alone ($r^2 = 0.54$, $p = 0.0002$). The ultimate Stress was best explained by CSA alone ($r^2 = 0.68$, $p < 0.0001$) and the elastic modulus by a combination of CSA and vCtBMD ($r^2 = 0.72$, $p < 0.0001$). Overall the authors found that geometrical parameters had a higher correlation with mechanical parameters than vCtBMD. However there was a significant correlation between vCtBMD and the mechanical parameters in all cases.

Muehleman et al. (2000) used cantilever bending of the human second metatarsal in comparison to values taken via DEXA and pQCT. Their data suggested that while BMD from the DEXA scanner was significantly correlated with whole bone strength ($r^2 = 0.4$, $p = 0.001$), the greatest correlation was between vCtBMD and whole bone strength ($r^2 = 0.46$, $p < 0.001$). It was also noted that these two values, BMD and vCtBMD, were very strongly correlated ($r^2 = 0.81$, $p \ll 0.001$) implying that, in the second metatarsal bone, density readings are more important than geometrical parameters in determining cantilever load to failure.

A similar study by Lind et al. (2001) compared torsional testing, pQCT parameters and ashing in rat humeri. Using step-wise linear regression, total CSA correlated best with stiffness ($r = 0.57$, $p < 0.001$), whereas ash weight was superior to the pQCT variables in explaining maximum torque ($r = 0.42$, $p < 0.001$). Finally, Ebbesen et al. (1999) compared the techniques of DEXA, pQCT and ashing with the compressive strength of over one hundred human lumbar vertebrae L3. They concluded that all three were equally capable of predicting vertebral compressive strength *ex vivo* with a degree of determination (r^2) between 75% and 86%.

5.1.3.3 Effect of unloading via Hindlimb Suspension on Bone Mineral Density

A small number of studies have examined the effect of unloading via HLS on the BMD values in a variety of bones, using both DEXA and pQCT. Bloomfield et al. (2002) used pQCT to examine the effect of up to 28 days HLS on both cancellous and cortical sites in adult rat tibiae, femora and humeri. Following suspension there was a 20-21%

reduction in cancellous BMD at the proximal tibia and femoral neck after 28 days HLS vs. 0 day controls. At the mid-diaphyses of the tibiae and humeri greater BMD values were found in both suspended and control groups after 14 days, compared to 0 day controls, and this increase was maintained throughout 28 days HLS. No differences were found in BMD values at the mid-diaphyses between the 28 day suspended and control groups. These results imply that there are compartment specific differences in adult rat bones following HLS and that the changes were greater but not exclusively in cancellous bone. These compartment specific differences following HLS were also identified in a series of studies performed by Wronski and co-workers {Wronski et al. 1983; Wronski et al., 1987).

In another study by Matsumoto et al. (1998), the BMD of young growing rats undergoing HLS for up to 14 days was examined along the length of the femur using DEXA. Following both 7 and 14 days suspension there was a marked reduction in the BMD at the cancellous-rich distal and proximal metaphyses relative to the controls. At the diaphysis the reduction in BMD was apparent although much smaller. A further study by Mosekilde et al. (2000) using DEXA found similar reductions in the BMD of the proximal tibial metaphyses but no differences at the mid-diaphyses of rats undergoing short term mobilisation of the right hindlimb. However, care must be taken in the interpretation of these data, as the changes in cross sectional area along the bone length would automatically result in lower areal BMD readings produced by the DEXA scanner.

5.1.4 Effect of unloading via Hindlimb Suspension on Biomechanical Strength

The effect of hindlimb suspension on the biomechanical properties of bone has been examined in a number of studies. Shaw et al. (1987) hindlimb suspended rats, 120 days old at the onset, for 4 weeks and found that the unloading significantly affected the femoral mechanical characteristics, stiffness, yield stress, load and energy, while in the tibia only bending stiffness was significantly reduced relative to the controls. No differences were noted in the cross-sectional areas in either the tibiae or femora relative to the controls although some regional specific changes in shape were identified. However, this study used adult animals so a reduced effect would be expected in comparison to young growing rats.

Abram et al. (1988) suspended young rats, 42 days old at onset, for periods of up to three weeks, and performed three types of biomechanical testing: non-failure three-point bending, non-failure torsion and failure torsion. Following suspension the product of mass times bone length (values for the individual parameters were not given) was significantly reduced in the femora relative to the controls. This implies that one or both of these parameters has changed as a result of unloading. The torque to failure also decreased by almost 50% for the suspended animals relative to the controls. This was attributed to a reduction of 29% in geometry measured via polar moment of area, J and a 27% reduction in material strength measured via maximum stress, τ .

In a similar study by Martin (1990), rats were hindlimb suspended for 1 or 2 weeks. Bone bending tests however showed no significant differences in strength between suspended animals and controls. However, the suspended group did tend towards a lower strength and it is possible that the experimental period was too short to induce significant differences. This may have implications for this project, as the experimental period in this case was also two weeks.

Van der Meulen et al. (1995) compared biomechanical properties in the femora of basal, age-matched controls and hindlimb suspended growing rats, 39 days old at the onset. After up to 4 weeks of hindlimb suspension significant increases in cross-sectional area (+33%), polar moment of area (+64%), ultimate torque (+67%) and torsional rigidity (+181%) relative to basal controls were recorded. However, the pair fed age-matched controls showed significantly greater growth related increases in cross-sectional area (+71%), polar moment of area (+136%), ultimate torque (+127%) and torsional rigidity (+367%). These differences in mechanical strength were attributed to differences in altered cross-sectional area.

Finally, Bloomfield et al. (2002) tested tibial and humeral diaphyses and femoral necks of 6 month old adult suspended rats in three point bending. They found that unloading induced few differences in cortical mass, geometry and mechanical properties in the mature rodent skeleton. However, the areas most affected by unloading are sites rich in trabecular bone. In this study there were few alterations at the tibial and humeral mid-shafts over 28 days of hindlimb unloading. At the femoral neck, a 10% decrease was noted in ultimate load in 28 day suspended animals versus 28 day controls. These results are less than those reported in young growing rats (Abram et al., 1988, Martin,

1990, Shaw et al., 1987, van der Meulen et al., 1995) and implies that, if these results were applied in the adult skeleton the effect of unloading would be overestimated.

From these previous suspension studies it is clear that bone strength is negatively affected by hindlimb suspension. In general, researchers have found that cross sectional area is reduced (Shaw et al., 1987, Abram et al., 1988, van der Meulen et al., 1995). A number of authors using older animals (Shaw et al., 1987, Bloomfield et al., 2002) found more limited differences in femoral geometric and structural properties between suspended and control animals, and this may be due to the older animals used. The reasons given for the loss of strength found in most studies have been varied with researchers attributing it to either reduced cross sectional area or reductions in both cross sectional area and material properties. Ultimately, the extent of the loss in structural properties depends on the specific site and parameter used, the age of the animals used and the length of time suspended.

5.1.5 Research Questions

The aim of this section of the project was to investigate the effect of altered mechanical loading, via hindlimb suspension, on the structural properties of the left femora of young rats. Changes, due to unloading, in the density of the rats' left femora were assessed by taking pQCT measurements of bone density at three points along the shaft. Changes in the structural behaviour of the left femora of each animal were determined by torsion testing to failure.

The following research questions were asked:

- Is the loss in bone mineral density and total bone mineral content, as measured via pQCT, previously found in adult rats following HLS (Bloomfield et al., 2002), present in the unloaded femora of young growing animals?
 - Is this response similar in both the largely cortical mid shaft and the more trabecular bone nearer to the growth plate?
- To investigate the hypothesis that HLS affects the structural strength of the unloaded femora?
 - Does HLS result in a change in the shear modulus, G , maximum torque to failure and torsional rigidity, GK , of the unloaded femora?

- Does HLS result in a change in the maximum shear stress calculated, τ_{\max} , of the unloaded femora?
- Is this response due to altered structural properties or altered bone shape, or a combination of the two?
- Using pQCT scan data, are the mechanical properties best explained via bone mineral density or geometric properties?

5.2 Materials and Methods

Rat femora vary widely in shape, size and structure along their length. At the mid diaphysis the bones are composed almost entirely of cortical bone while a cross section closer to the distal and proximal ends are composed of a cortical shell surrounding trabecular bone. To investigate the effect of HLS on the composition of the bone a pQCT scanner was used to take 3 transverse cross-sectional scans along the length of the bones.

These 3 scans were also used to take account of the non-prismatic nature and cross-sectional geometry along the length of the bone section. Using the cross-sectional and polar moment of inertia measurements, destructive torsion tests were performed to determine the shear modulus and maximum shear stress for both the whole bones and the bone tissue by following the approach of Levenston et al. (1994).

5.2.1 Experimental Set-up

Following sacrifice and disarticulation of the femora, the bones' weight and length were measured (see section 4.2.1).

The analysis of structural and material properties can be broken up into two main parts (see Figure 5.2 and sections 5.2.2 and 5.2.3):

- Assessing the material properties of the bone via pQCT measurements of density and mineral content.
- Using the same pQCT scans to take account of the non-uniform shape of the bones along their longitudinal length, and combining these data with the data obtained via a destructive torsion test.

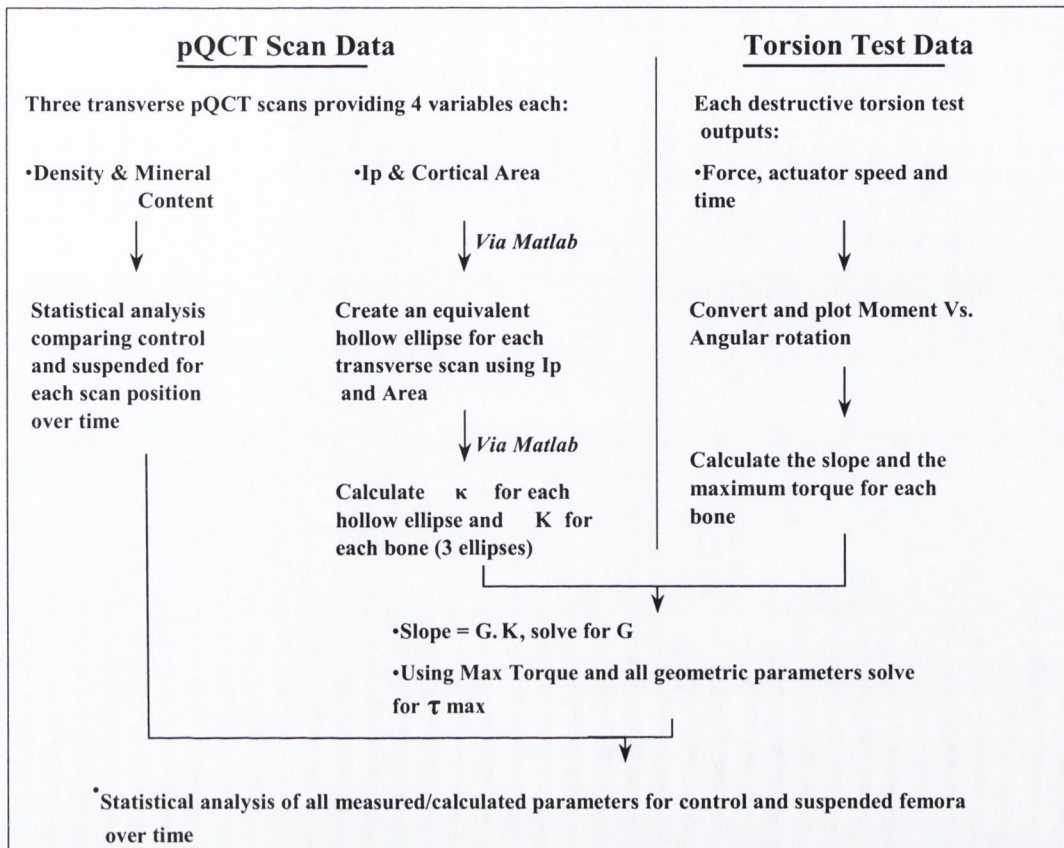


Fig. 5.2 Procedure for evaluating the effect of HLS on the mechanical and structural properties of rat femora

5.2.2 pQCT Scans

Bones have a very irregular geometry both microstructurally and along their length. To determine non-invasively the geometry of a bone at the micrometer level, μ CT and more recently pQCT scanners have been used (Hollister et al., 1994, Muller et al., 1994). These scans have been used to generate three-dimensional finite element models of bone structures (e.g. trabecular bone). In this study, to investigate if HLS resulted in changes in the bones' microstructure, the rats' femora were scanned using a Stratec XCT-960M pQCT scanner (Stratec Medizintechnik GmbH, Germany). The XCT-960M has a single energy source and all tomography scans had a slice thickness of 1.25mm and a voxel size of 0.15mm. Bones were held in place using grips and a longitudinal

'scout scan'² was performed. From this scan the point of the minimum cross section was determined visually. Following this, three transverse pQCT scans were performed, at the minimum cross section and at set distances distal and proximal. In the basal control group this distance was 4mm, in the 3 day groups 4.2mm, in the 7 day groups 4.5mm and in the 14 day groups 5mm. This varying difference was consistent with the changes in length as a result of growth and ensured that the three transverse scans were from equivalent regions in each group. The three scans were designated slice 1 to 3: 1 distal, 2 at the mid-diaphysis and 3 proximal. Each pQCT scan outputs a large number of parameters. In this study the following were examined:

- Mean Volumetric tissue Density: The mean density of the voxel tissue densities within the slice [mg/cm^3]
- Cortical Mineral Content: The mineral content of the total bone within a 1mm slice [mg/mm]
- Total Cortical Area: Cross sectional area of the cortical bone [mm^2]
- Polar Moment of Area, I_p , of the cortical bone [mm^4]

The values for density and mineral content were statistically assessed for any effect of HLS on the femora at each scan site and in total over time. The area and polar moment of inertia of each of the 3 scans were used to create an equivalent hollow ellipse using a specifically designed Matlab Program (Matlab Version 5.3, The MathWorks Ltd. U.K.; see section 5.2.4). The 3 equivalent hollow ellipses were then combined to create a 3-Dimensional equivalent bone section comprised of a series of hollow ellipses of varying size along its length according to the method by Levenston et al. (1994).

5.2.3 Torsion Testing

5.2.3.1 Use of Torsion to determine whole bone strength

The mechanical strength of whole bones can be tested either in bending experiments, three and four point bending and cantilever bending, or via torsion to failure. As an alternative to bending, torsional testing has become more widely used for the evaluation of whole bone strength (Lind et al., 2001, Lepola et al., 1993, Burstein and Frankel, 1971, Taylor et al., 2003). Although the modalities of the two methods are

² A scout scan is a quick low resolution longitudinal 2 dimensional scan used to position the high resolution transverse pQCT scans

complementary to a degree when describing the mechanical characteristics of bone, torsional testing has some advantages. When a bone is subjected to torsion, the torque is constant in every section of the tested bone. In addition, slight variations in the geometry of the bone have an insignificant effect on the torsional strength. During bending of a bone that is not completely straight, even a minor rotation will reduce the precision of the testing. Because long bones are usually slightly curved, the orientation of the bone during bending testing is critical. Finally, since torque is a relatively common fracture mechanism clinically, the torsional testing of long bones in the laboratory is necessary.

5.2.3.2 Positioning Jig and Potting Bones

Pure torsion is impossible in bones as the cross-sectional shape and size varies along their lengths and their central axis curves. As a result, when a bone is torqued, bending moments are introduced in the bone. To investigate the differences in the mechanical properties of bones, these bending moments must be reduced to a minimum. This was achieved by ensuring that the central portion of each bone was positioned in a consistent manner along the correct axis of rotation in a positioning jig, designed and manufactured with the following design parameters in mind:

- To facilitate the application of the end-caps and to fix them and the bone in space while the dental stone, in which the proximal and distal ends of the bone were embedded, hardened
- To ensure that the end-caps in which the bones' ends were embedded were aligned along the central axis of the torsion rig
- To ensure that the central portion of the bone was aligned along the central axis of the torsion rig with a uniform gauge length of 11mm

The above design parameters imply the central section of bones' orientation in the x, y and z axes were controlled.

The bone-ends were embedded in sets of end-caps, made by drilling out 22mm cut-offs of standard 19mm brass and 15mm aluminium rods. The aluminium caps used to embed the distal end had an internal diameter of 11mm while the brass caps used for the proximal ends had an internal diameter of 15mm. Dental stone (Superstone Ultrahard die stone, SDS Kerr GMBH, Germany) was used to hold the bones in place, rather than plaster, as it is stronger, sets more quickly and is not exothermic.

Bones were placed on the first positional slider with the femoral head pointing downward (see fig 5.3a). The second positional slider was then moved down to hold the bone in place. These two positional sliders had a groove cut into them which orientate the bone in x and z-axes. They can also be raised or lowered in the y-axis via a screw at the base of the jig (see fig 5.3b). The height at which each bone was held was determined by measuring the central diameter of the bone and using a standard bar of metal of the same diameter to ensure it was centrally orientated. The two end-caps were then filled with freshly prepared dental stone and immediately slid into place over the two ends of the bone (see fig 5.3c). The whole jig with the bone in-situ was then placed at 4°C for 10 minutes to allow the dental stone to harden while keeping the bones moist. The second slider was then carefully removed, the central bone section cleaned and then removed from the jig and stored at -20°C until testing (see fig 5.3d).

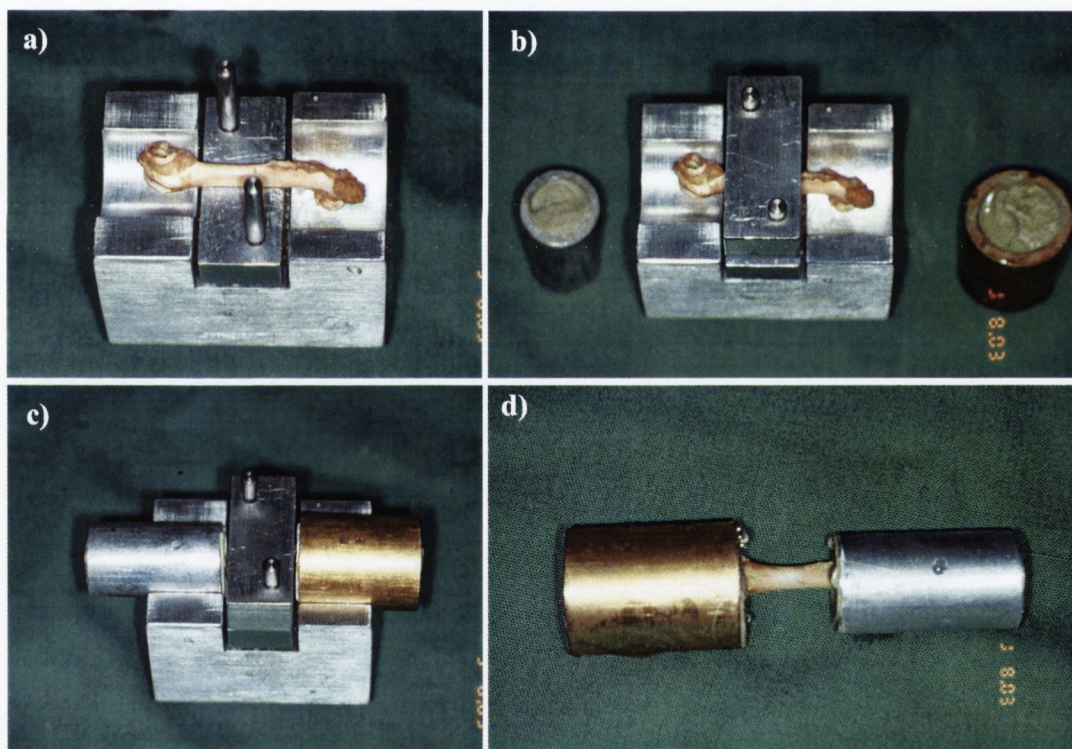


Fig. 5.3 Positioning a femur in the Jig and embedding the ends

5.2.3.3 Torsion Rig and Mechanical Testing

The structural behaviour of the left femur of the control and suspended animals was determined by a destructive torsion test to failure. To differentiate between results at

different time points, the scatter caused by differing set-ups must be minimised. To accomplish this, a micro-torsion rig designed in our research group (Taylor et al., 2003) was used with only minor modifications to allow for smaller bones. This purpose-built rig was attached to a standard Instron servo-hydraulic testing machine, converting the vertical motion of the Instron actuator into a rotary motion. The embedded bones were inserted into the modified chucks. The proximal end of the femora was gripped in a chuck to which load was applied through a lever arm. The distal end of the bone was located in a Perspex plate, which was free to move in an axial direction with minimum friction due to the action of linear bearings on three steel guide rails. To confirm that the machine was capable of applying pure shear, with negligible axial tension or compression, the equipment was calibrated using a copper cylinder to which rosette strain gauges had been attached. Consequently, the central section for each bone was orientated correctly to the central axes of rotation and thus the point of application of load. The actuator was controlled under a constant vertical speed of 10 mm/min giving roughly a 1° per second rotation until failure. The testing direction corresponded to internal rotation of the femur. Values for time, vertical displacement and force were taken 10 times per second until failure using the software package Labview (Labview 5.1, National Instruments, Texas, USA) The vertical displacement was then converted into a rotational displacement and, by knowing the starting position of each test, the length of the lever arm was calculated. Consequently, the torque or moment was calculated for each specimen over time. The torque vs. angular deformation was then plotted until fracture of the bone.

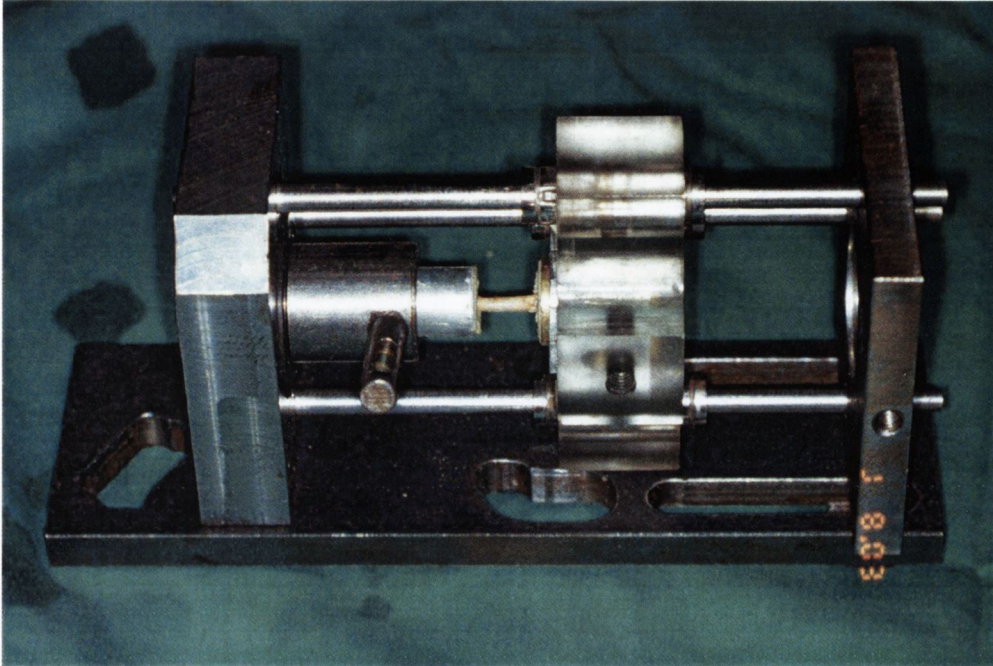


Fig. 5.4 Bone in place in the torsion rig

5.2.4 Data Analysis

The values for density and mineral content were statistically assessed for any effect of HLS on the femora at each scan site over time. Although it does not have a direct physical significance, the three scan sites combined was also examined to get an overall impression of the effect of HLS on the whole bone.

The shear modulus, G , and maximum shear stress, τ_{max} , for both the whole bones and the bone tissue were determined by following the approach of Levenston et al. (1994).

Conventional methods for interpreting torsion test data often involved converting a bone's cross-section into a hollow tube with a constant cross section along its length equal to that of the bone's minimum cross section. Levenston showed that these methods produced errors of up to 42% in the shear modulus and up to 48% in the maximum shear stress. Alternative methods, such as taking numerous scans and converting each bone into a finite element model, were available but were considered too time consuming. Consequently, Levenston proposed taking a number of scans along the bone's length, typically 3-5, and converting these into equivalent ellipses with matching I_p and Area values. These equivalent ellipses were then extended and joined

to form a series of equivalent elliptical bars. Consequently, by following this simple method the errors introduced were reduced to less than 3%

In this study to obtain the values for G and τ_{max} , the geometry of the bone section were determined via pQCT scans at three equidistant points along the bone's length (see section 5.2.2). From each pQCT scans' cross-sectional area and polar moment of Area measurements, an equivalent hollow ellipse was created using a two-step iteration Matlab program (moment.m) (see Figure 5.5 and Appendix A2).

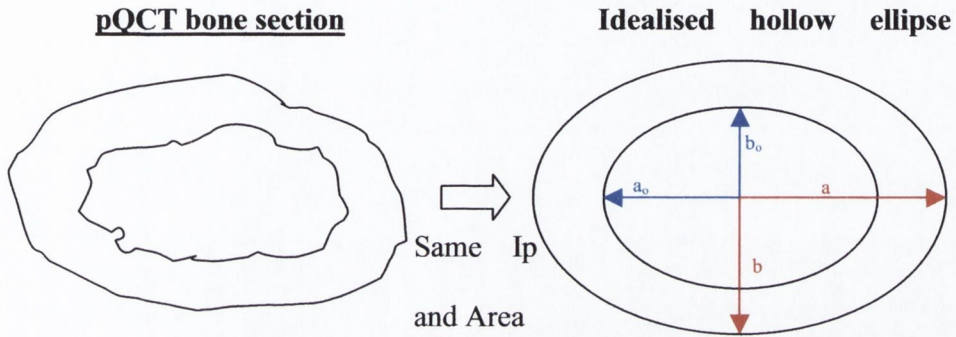


Fig. 5.5 Each pQCT scan was used to create a hollow ellipse with equivalent I_p and area values using Matlab

This program created a matrix of possible values for the maximum and minimum axes between 1mm and 3.1mm, in increments of 0.125mm, for both the inner and outer ellipses. All possible combinations of inner and outer axes dimensions, a , a_o , b , b_o , that obey the following rules were then transferred to a new matrix:

- $a_o/a = b_o/b$
- $a > a_o$
- $b > b_o$
- $a > b$
- $a_o > b_o$
- $a/b = a_o/b_o < 2$

The area and I_p for each combination of inner and outer dimensions was calculated according to the following equations:

$$Area = \pi ab - \pi a_o b_o \quad (2)$$

$$I_p = \frac{\pi ab}{4} [a^2 + b^2] - \frac{\pi a_0 b_0}{4} [a_0^2 + b_0^2] \quad (3)$$

where a , b , a_0 , b_0 are the major and minor axes of the equivalent hollow ellipse (see Figure 5.5)(Levenston et al., 1994).

The percentage errors from the values measured in the pQCT machine were determined and the combination of a , a_0 , b , b_0 with the minimum mean error was taken³. A second Matlab program (refinement.m) was then used to refine the answer for each scan and to calculate the torsional constant, κ , according to the equation 4:

$$\kappa = \frac{\pi a^3 b^3 (1 - q^4)}{(a^2 + b^2)} \quad (4)$$

where $q = a/a_0 = b/b_0$ and κ is a geometrical factor (torsion constant)(Levenston et al., 1994).

The three κ values for each bone were then combined to give an effective torsional constant, K , for the whole simulated bone section from its three individual κ values. The equations for the effective torsional constant, K , for a non-prismatic shape simulated as a series of 3 prismatic sections of equal length is given by equation 5 (Levenston et al., 1994):

$$K = 2 \left[0.5(1/\kappa_1 + 1/\kappa_3) + 1/\kappa_2 \right]^{-1} \quad (5)$$

5.2.4.1 Correlation between Measured and Calculated Variables

To investigate how well the Matlab programs reproduced the geometric parameters I_p and area, when creating an equivalent hollow ellipse, the calculated and measured values were plotted. Figure 5.6 plots the I_p measured via the pQCT scanner against the

³ To check the accuracy of the two Matlab programs, a set of 20 ellipses with a range of axis ratios from 1 to 2.1 were used. Their I_p and Area values were fed into the programs and the resulting a , b , a_0 , b_0 , compared with the original values. In these tests the percentage error was less than 1.5% in all cases.

Ip calculated for the equivalent ellipse created. There was a strong linear correlation between the two variables (Linear Regression Analysis, $P < 0.001$, $r^2 = 0.9999$).

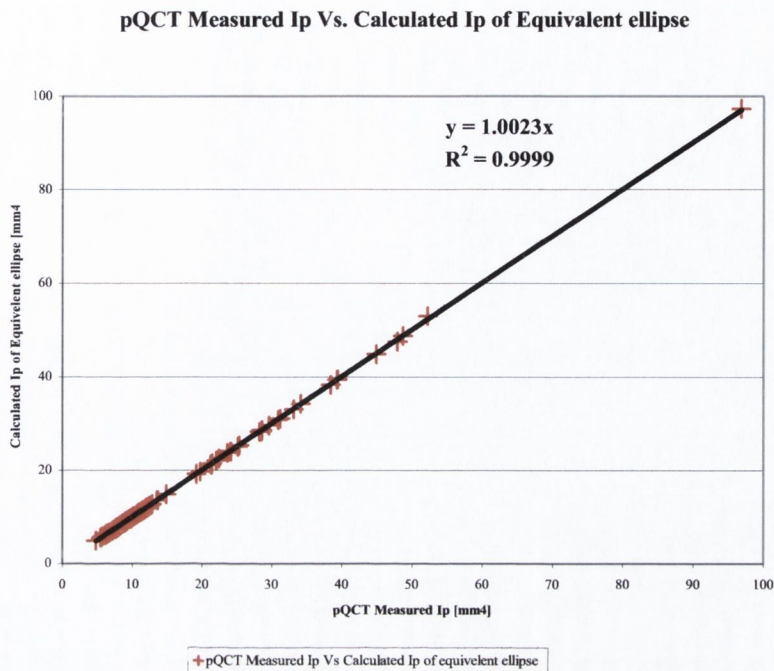


Fig. 5.6 Correlation between Ip values measured via pQCT and those calculated in Matlab

Figure 5.7 plots the cortical area measured via the pQCT scanner against the Area calculated for the equivalent ellipse created. Once again there was a very strong linear correlation between the two variables (Linear Regression Analysis, $P < 0.001$, $r^2 = 0.9979$). In both cases the relationship between the values taken from the pQCT scanner and those generated in the Matlab program is approximately directly proportional with the mean percentage error in both cases less than 1%. In this Matlab program, R^2 will never actually become 1, as there will always be a small error no matter how small the increments used in the initial stages of the program are.

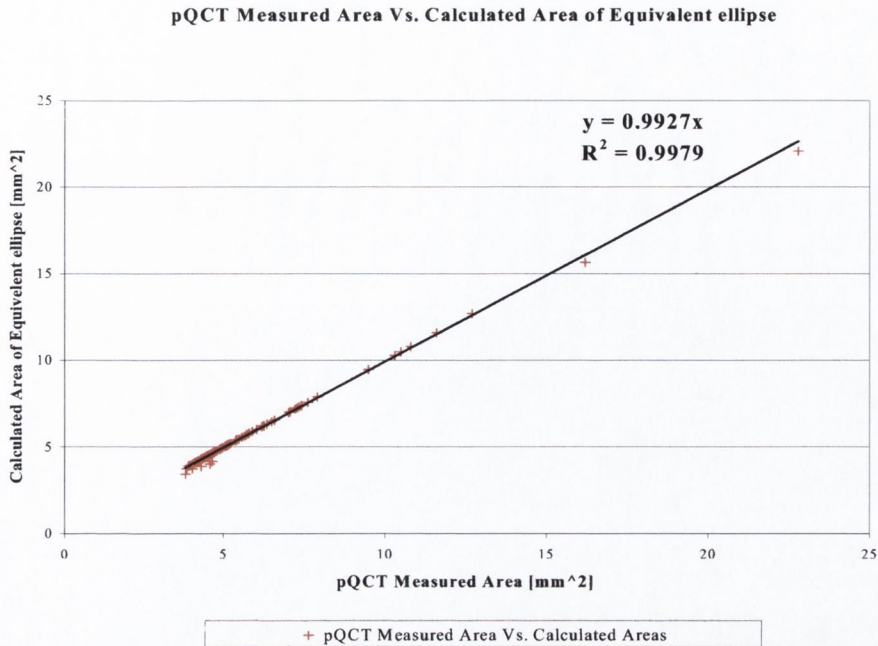


Fig. 5.7 Correlation between Area values measured via pQCT and calculated in Matlab

Following the destructive torsion tests, the Moment vs. Angular rotation was plotted. The slope was calculated and is equal to $G.K$. The previously determined K was then used to determine G . The torsion tests also yielded values for the maximum torsional moment, T . Hence, all of the values necessary for the calculation of the maximum shear stress, τ_{max} and angular deformation, ψ were known, and were calculated using equations 5 and 6:

$$\tau_{max} = \frac{2T}{\pi ab^2 (1 - q^4)} \quad (6)$$

$$\psi = \frac{TL}{KG} \quad (7)$$

Where ψ is the angular deformation, $q = a/a_o = b/b_o$ and L is the gauge length.

5.3.2.4 pQCT scan data as Predictors of Biomechanical Parameters

Finally, the four pQCT properties measured directly, BMD, BMC, Ip and Area were assessed, individually and in combinations, for their ability to predict the mechanical parameters stiffness, angular deformation, maximum torque and maximum stress. Individually, linear regression analysis was used while for the combinations stepwise multivariate linear regression analysis was employed. To negate the effect of differing scales when comparing the results of different regression models, all data sets were standardised using the following formula:

$$\text{Standardised Data} = \frac{(\text{Raw Data values} - \text{Mean of Data set})}{\text{Standard Deviation}} \quad (8)$$

By standardising the data it is possible to directly compare what the effect of a one standard deviation change in the independent variable has on the dependent variable. This relationship between the two variables is given by the regression coefficient, or slope of the regression line. Table 5.3 details the statistical relationships between parameters.

5.2.5 Statistical Analysis

All data measured were statistically analysed using the statistics software Intercooled STATA (StataCorp. 2001. Stata Statistical Software: Release 7.0. College Station, TX: Stata Corporation). Linear regression analysis and ANOVA (Analysis of Variance) were performed on all data sets. The choice of which statistical method to use was governed by the following premise. In cases where it is assumed that there is a linear effect on a particular data set (e.g. for an increase in the independent variable, such as time, there is a linear response in the dependent variable) both ANOVA and linear regression analysis were used. In these cases, ANOVA and linear regression analysis will yield similar results. However, if a pulsatile effect was thought likely (e.g. in cases where for an increase in the independent variable, such as time, there is a transient response in the dependent variable) only ANOVA was used to analyse the data. Also, when ANOVA and Linear regression gave contrasting answers the trend of the graphed data was assessed and the strengths of the two tests (R^2 value) were taken into account in deciding the answer. Finally, although both ANOVA and linear regression are

insensitive to reasonable degrees of variance, in cases where the data appeared skewed a robust linear regression analysis and Kruskal-Wallis ANOVA were performed to check the previously obtained results. For $p < 0.05$, the difference were considered significant, while $p < 0.01$ were noted.

5.3 Results

The results are broken up into a number of sections that parallel those of the materials and methods:

- Analysis of data taken directly from the pQCT scanner
 - Bone Mineral Density, BMD
 - Bone Mineral Content, BMC
 - Cortical Area
 - Polar moment of Inertia, I_p
- Analysis of data obtained directly from the torsion tests
 - Maximum Torque
 - Stiffness (torsional rigidity, GK)
 - Angular deformation
- The relationship between the pQCT cross sectional scans and the equivalent ellipse models created in Matlab
- Data calculated indirectly using the equivalent ellipse models and the torsion test data
 - Maximum stress
- Using pQCT parameters as predictors of biomechanical parameters in torsion

5.3.1 pQCT Results

5.3.1.1 Total Bone Mineral Density

In this section the pQCT scan data that were directly measured are presented for the unloaded femora. To ascertain whether the HLS had resulted in any changes in material properties the total BMD, BMC, cortical area and I_p were examined at three points along the length of the bones.

Figure 5.8 shows the total BMD of the distal slice of the control and suspended femora throughout the experimental period. There was a statistically significant effect of time on the total bone mineral density of the distal slice (ANOVA, $P = 0.0001$). Following HLS, there was also a statistically significant reduction in the femoral densities of the distal slice in the suspended relative to the control groups (Linear Regression Analysis, $P < 0.001$; ANOVA, $P < 0.001$).

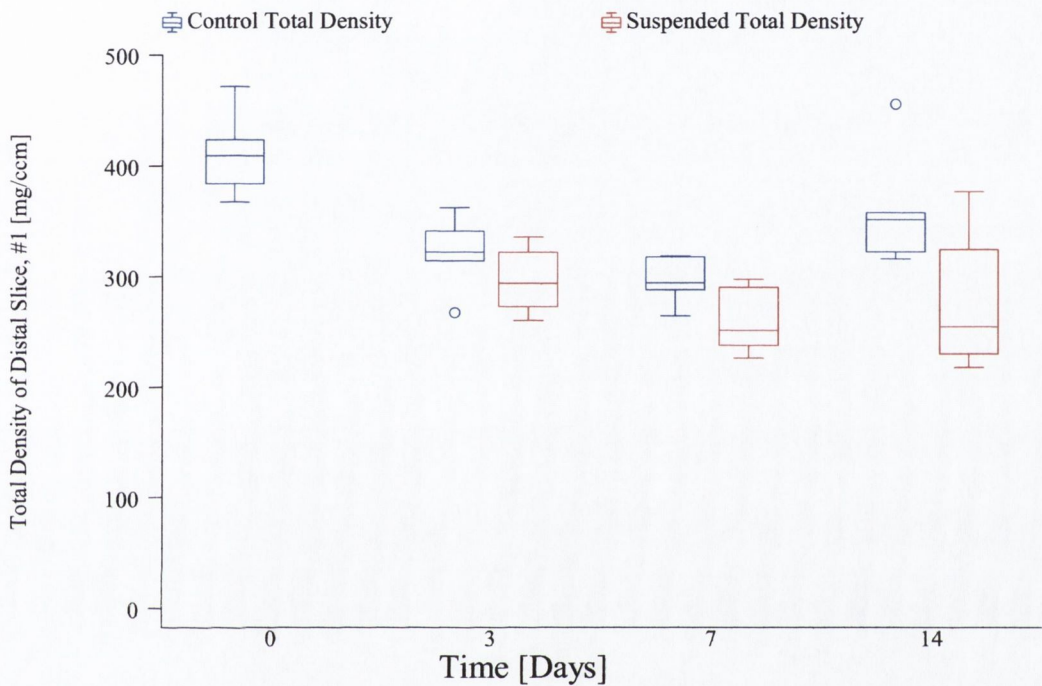


Fig. 5.8 Total Density of Distal slice Vs. Time for Control and Suspended groups
(For boxplot explanation see Fig. 3.14)

Figure 5.9 shows the total BMD of the mid-diaphyseal slice of the control and suspended femora throughout the experimental period. There was a statistically significant effect of time on the density of the distal slice (ANOVA, $P < 0.05$). Following HLS, there was no statistically significant effect in the femoral densities of the mid-diaphyseal slice in the suspended groups relative to the control groups (Linear Regression Analysis, $P = 0.09$; ANOVA, $P = 0.35$).

Figure 5.10 shows the total BMD of the proximal slice of the control and suspended femora throughout the experimental period. There was a statistically significant effect of time on the density of the proximal slice (ANOVA, $P < 0.01$). Following HLS, there

was no statistically significant effect in the femoral densities of the proximal slice in the suspended groups relative to the control groups (Linear Regression Analysis, $P = 0.38$; ANOVA, $P = 0.06$).

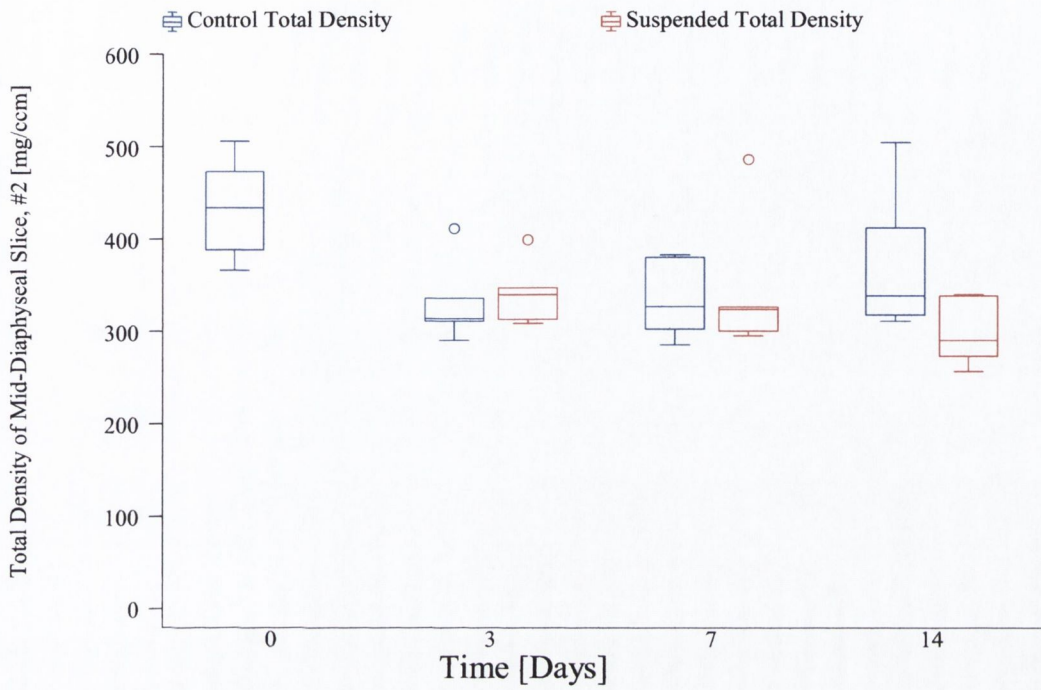


Fig. 5.9 Total Density of Mid-Diaphyseal slice Vs. Time for Control and Suspended groups

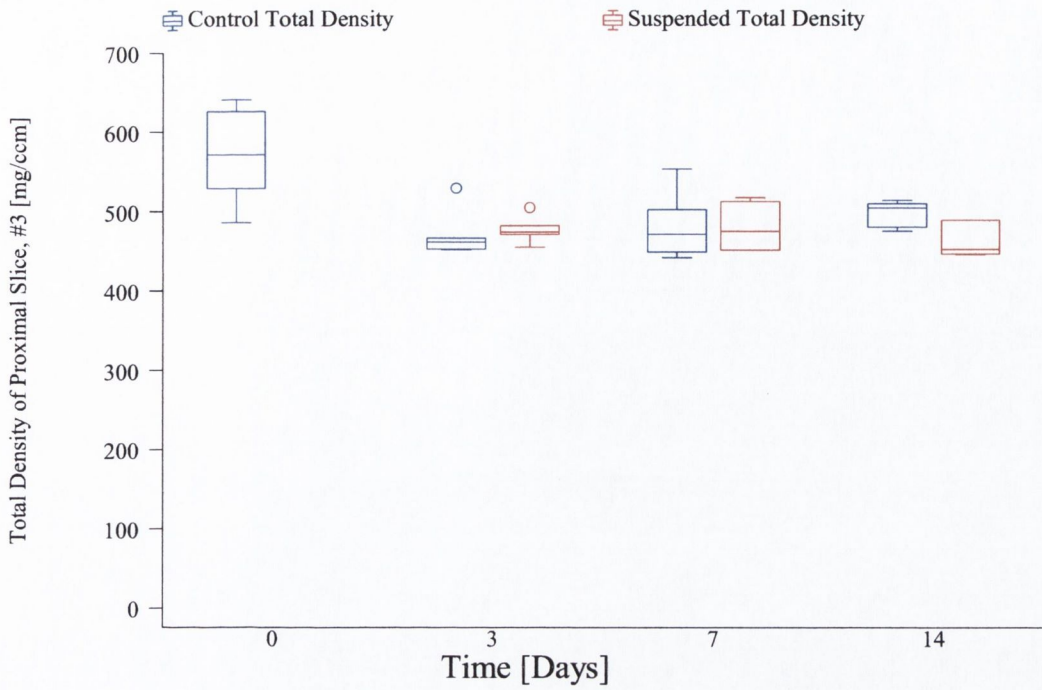


Fig. 5.10 Total Density of Proximal slice Vs. Time for Control and Suspended groups

Figure 5.11 shows the total BMD of the three combined slices of the control and suspended femora throughout the experimental period. There was a statistically significant effect of time on the density of the three combined slices (ANOVA, $P < 0.01$). Following HLS, there was a statistically significant effect in the femoral densities of the three combined slices of the suspended groups relative to the control groups (Linear Regression Analysis, $P < 0.05$).

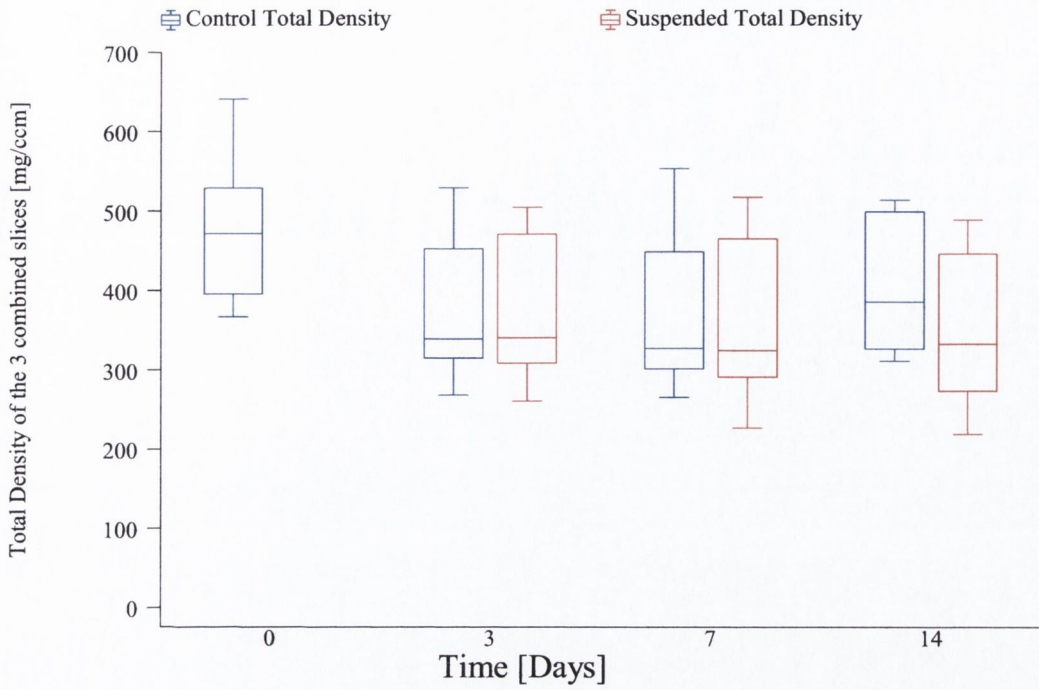


Fig. 5.11 Total Density of the three combined slices Vs. Time for Control and Suspended groups

5.3.1.2 Total Bone Mineral Content

Figure 5.12 shows the total mineral content of the distal slice of the control and suspended femora throughout the experimental period. There was no statistically significant effect of time on the mineral content of the distal slice (Linear Regression Analysis, $P = 0.66$; ANOVA, $P = 0.93$). Following HLS, there was a statistically significant reduction in the mineral content of the distal slice in the suspended groups relative to the control groups (Linear Regression Analysis, $P < 0.05$; ANOVA, $P < 0.05$).

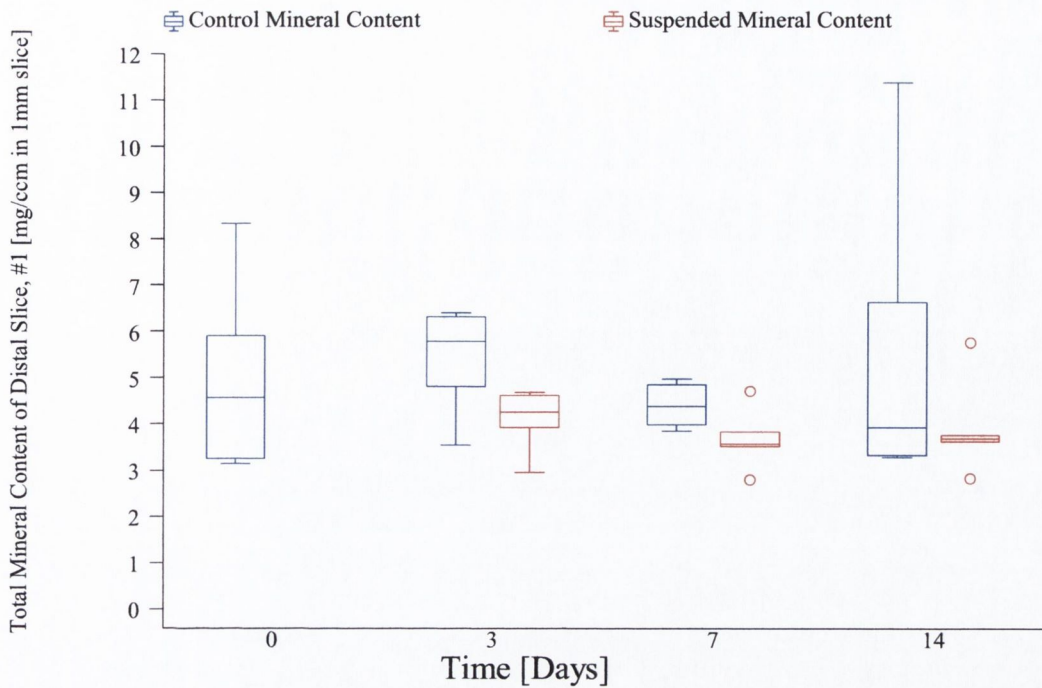


Fig. 5.12 Total Mineral Content of the Distal Slice Vs. Time for Control and Suspended groups

Figure 5.13 shows the total mineral content of the mid-diaphyseal slice of the control and suspended femora throughout the experimental period. There was no statistically significant effect of time on the mineral content of the mid-diaphyseal slice (Linear Regression Analysis, $P = 0.06$; ANOVA, $P = 0.25$). Following HLS, there was a statistically significant reduction in the femoral densities of the mid-diaphyseal slice in the suspended groups relative to the control groups (Linear Regression Analysis, $P < 0.05$; ANOVA, $P = 0.05$).

Figure 5.14 shows the total mineral content of the proximal slice of the control and suspended femora throughout the experimental period. There was a statistically significant effect of time on the mineral content of the distal slice (Linear Regression Analysis, $P < 0.001$; ANOVA, $P < 0.001$). Following HLS, there was no statistically significant effect in the femoral mineral content of the proximal slice in the suspended groups relative to the control groups (Linear Regression Analysis, $P = 0.11$; ANOVA, $P = 0.18$).

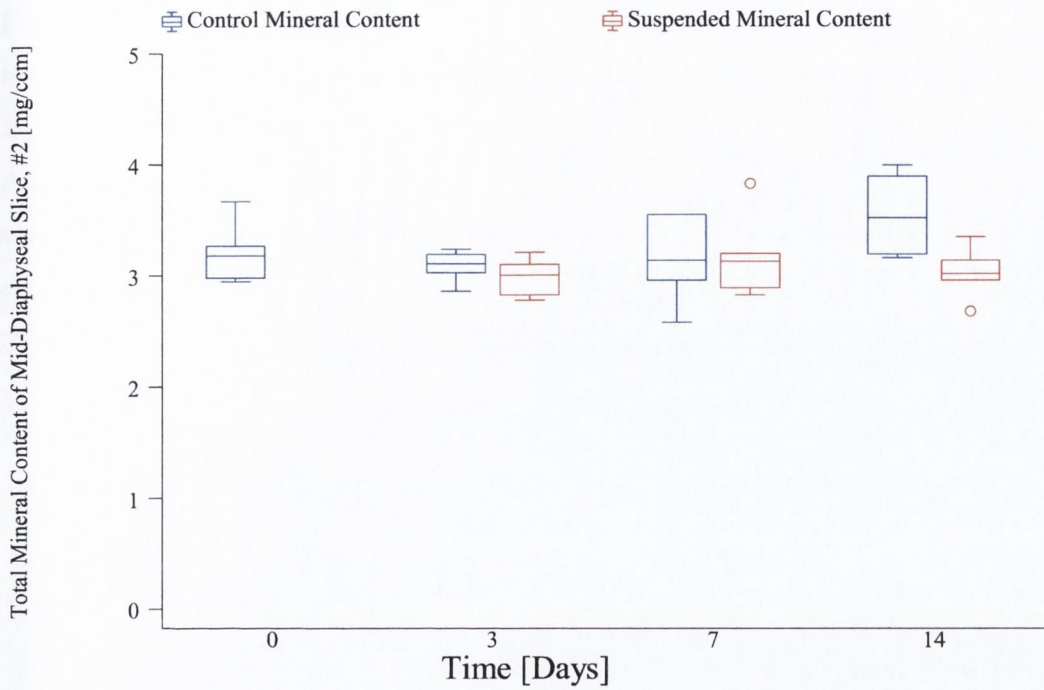


Fig. 5.13 Total Mineral Content of the Mid-Diaphyseal Slice Vs. Time for Control and Suspended groups

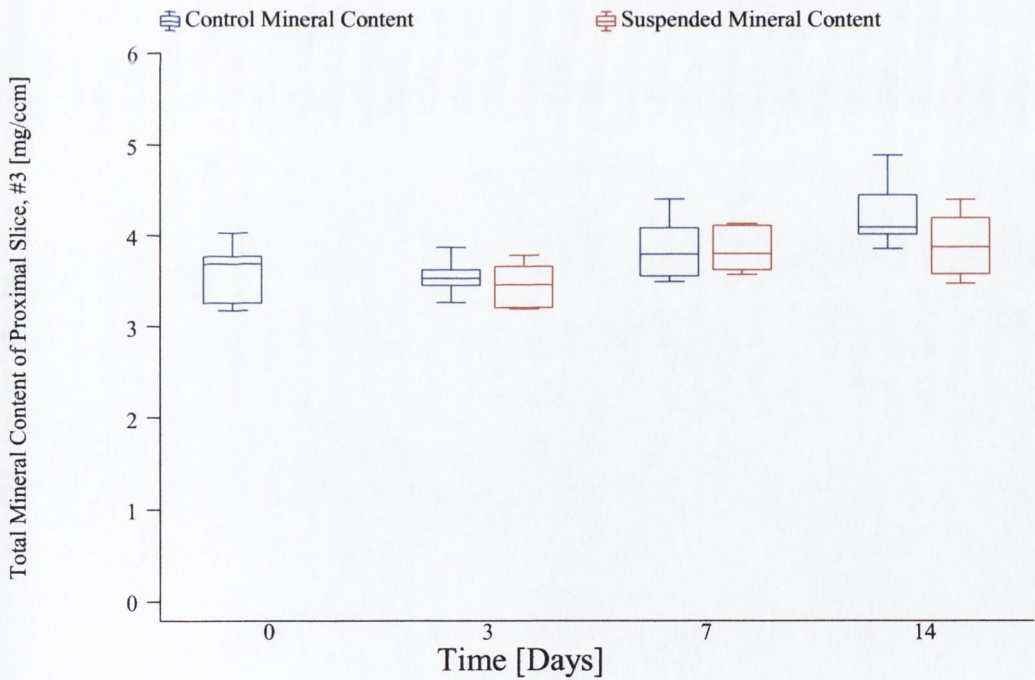


Fig. 5.14 Total Mineral Content of Proximal Slice Vs. Time for Control and Suspended groups

Figure 5.15 shows the total density of the three combined slices of the control and suspended femora throughout the experimental period. There was no statistically significant effect of time on the density of the three combined slices (Linear Regression Analysis, $P = 0.26$; ANOVA, $P = 0.60$). Following HLS, there was statistically significant reduction in the femoral mineral content of the three combined slices in the suspended groups relative to the control groups (Linear Regression Analysis, $P < 0.05$; ANOVA, $P < 0.05$).

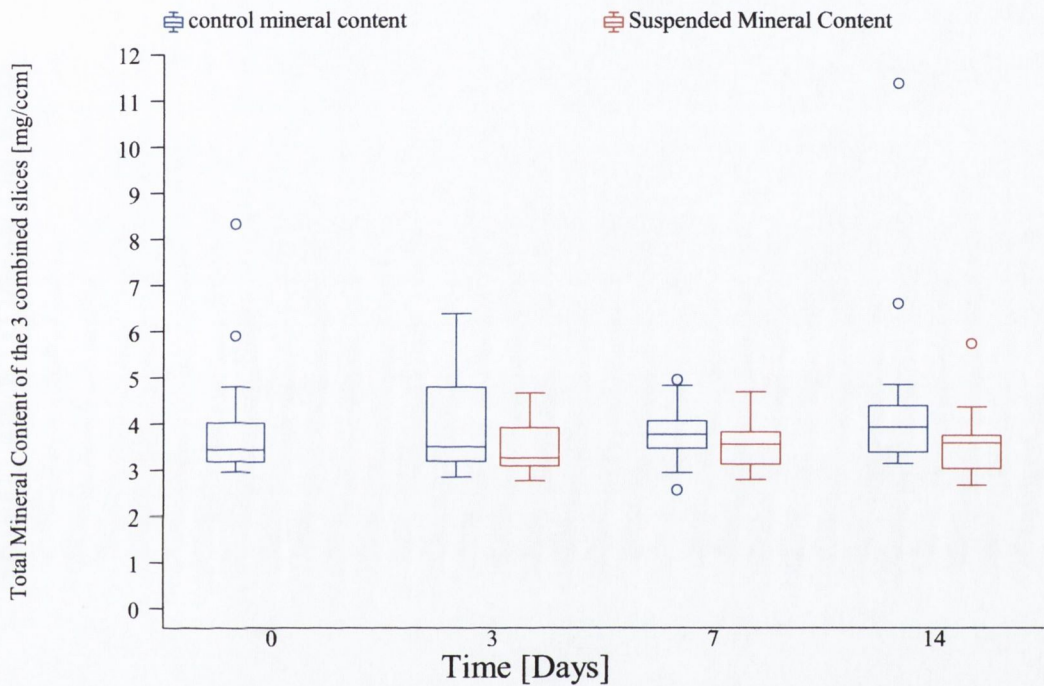


Fig. 5.15 Total Mineral Content of the three combined slices Vs. Time for Control and Suspended groups

Table 5.1 below shows the statistical analysis of BMD and BMC data with respect to time and treatment.

Parameter	Time		Treatment (Control Vs Suspended)	
	ANOVA	Regression	ANOVA	Regression
BMD: <u>Slice 1</u> (Distal)	p < 0.0001	N/A	p < 0.001	p < 0.001
BMD: <u>Slice 2</u> (Mid-Diaphyseal)	p < 0.05	N/A	p = 0.09	p = 0.35
BMD: <u>Slice 3</u> (Proximal)	p < 0.01	N/A	p = 0.38	p = 0.06
BMD: 3 combined slices	p < 0.01	N/A	p = 0.16	p = 0.26
BMC: <u>Slice 1</u> (Distal)	p = 0.93	p = 0.66	p < 0.05	p < 0.05
BMC <u>Slice 2</u> (Mid-Diaphyseal)	p = 0.25	p = 0.57	p = 0.051	p < 0.05
BMC: <u>Slice 3</u> (Proximal)	p < 0.001	p < 0.001	p = 0.18	p = 0.11
BMC: 3 combined slices	p = 0.26	p = 0.60	p < 0.05	p < 0.05

Table 5.1 Statistical analysis of the pQCT scan data for BMD and BMC with respect to Time and Treatment (significant values in bold; N/A: Not applicable)

5.3.1.3 Cortical Area and Polar moment of Inertia, Ip

The values for both the cortical area and Ip were also examined in the three scans over the experimental period. There was a significant effect of time on the mid-diaphyseal and proximal slices in both Ip and Area data. However, HLS had no significant effect on any of the measured Ip and area groups (see table 5.2).

Figures 5.16 and 5.17 are examples of the patterns seen when the area and Ip are plotted for the control and suspended femora over the experimental period. Both figures show the age related increases expected

Parameter	Time		Treatment (Control Vs Suspended)	
	ANOVA	Regression	ANOVA	Regression
Ip: <u>Slice 1</u> (Distal)	p = 0.50	p = 0.59	p = 0.09	p = 0.14
Ip: <u>Slice 2</u> (Mid-Diaphyseal)	p < 0.0001	p < 0.001	p = 0.41	p = 0.97
Ip: <u>Slice 3</u> (Proximal)	p < 0.0001	p < 0.001	p = 0.38	p = 0.82
Ip: 3 combined slices	p = 0.39	p = 0.26	p = 0.16	p = 0.26
Area: <u>Slice 1</u> (Distal)	p = 0.74	p = 0.82	p = 0.06	p = 0.052
Area: <u>Slice 2</u> (Mid-Diaphyseal)	p < 0.05	p < 0.01	p = 0.14	p = 0.29
Area: <u>Slice 3</u> (Proximal)	p < 0.001	p < 0.001	p = 0.20	p = 0.33
Area: 3 combined slices	p = 0.70	p = 0.39	p = 0.07	p = 0.07

Table 5.2 Statistical analysis of the pQCT scan data for Ip and Area with respect to Time and Treatment (significant values in bold)

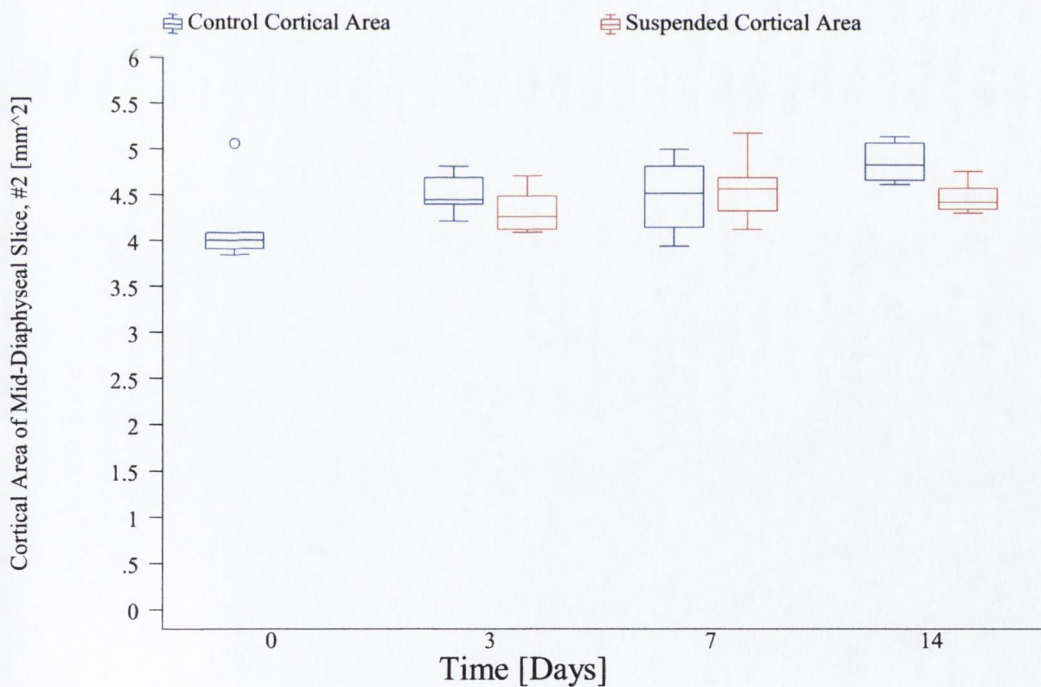


Fig. 5.16 Cortical Area the of the Mid-Diaphyseal Slice Vs. Time for Control and Suspended groups

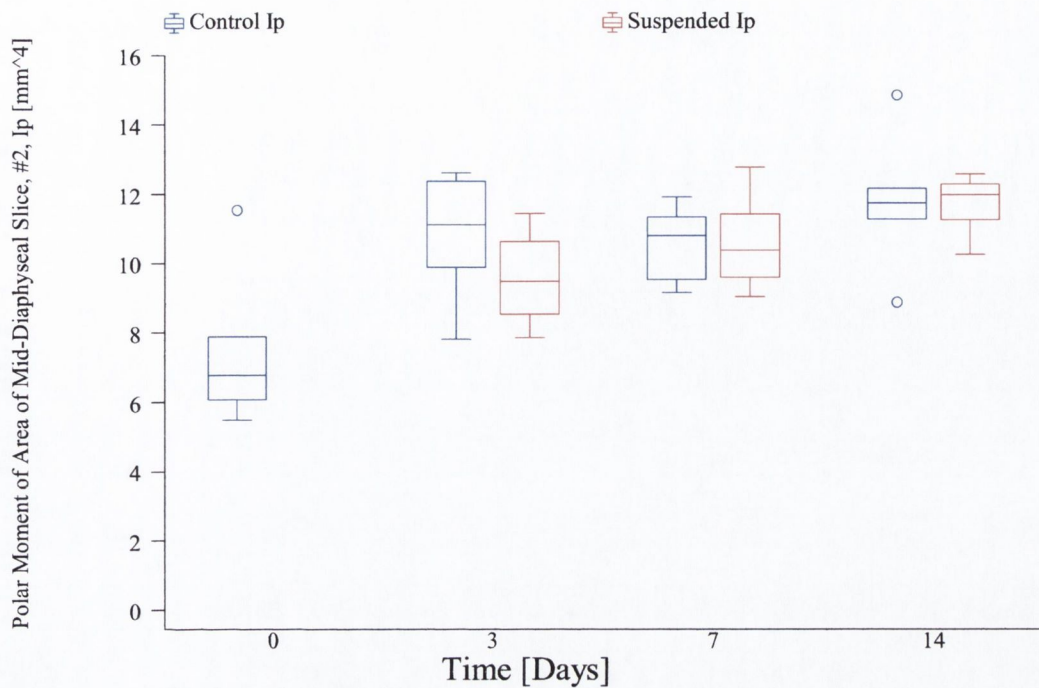


Fig. 5.17 Polar Moment of Inertia of the Mid-Diaphyseal Slice Vs. Time for Control and Suspended groups

5.3.2 Torsion Testing Results

Figure 5.18 shows a typical spiral fracture resulting from a destructive torsion test. Following the destructive torsion tests, the torque was plotted against angular rotation for each bone. The maximum torque was taken and the slope of the initial straight-line elastic deformation region calculated for each bone. Figure 5.19 shows a typical plot of torque vs. angular deformation for the 14 day control and suspended groups.

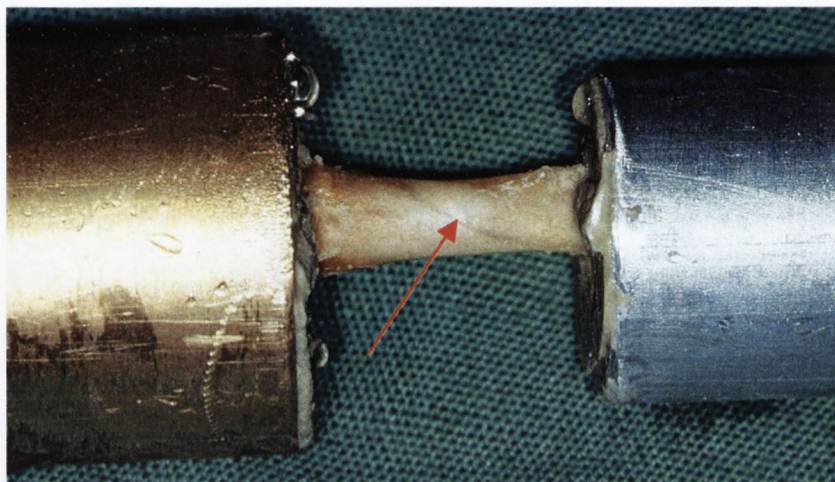


Fig. 5.18 A typical spiral fracture resulting from the destructive torsion test

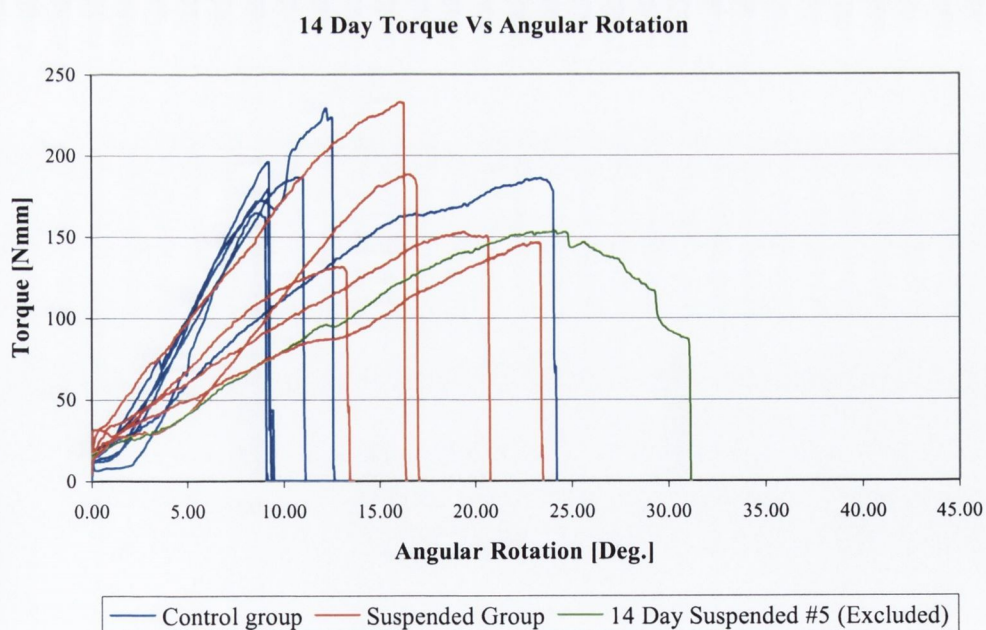


Fig. 5.19 Torque Vs. Angular Rotation for 14 Day Control and Suspended Groups (14 day suspended #5 was excluded as it failed at the growth plate)

5.3.2.1 Biomechanical parameters directly measured

Figure 5.20 shows the maximum torque of the control and suspended femora over the experimental period. There was a statistically significant effect of time on the maximum torque achieved (ANOVA, $P < 0.01$). Following HLS, there was a statistically significant reduction in the maximum torque values in the suspended groups relative to the controls (Linear Regression Analysis, $P < 0.05$, ANOVA, $P < 0.05$).

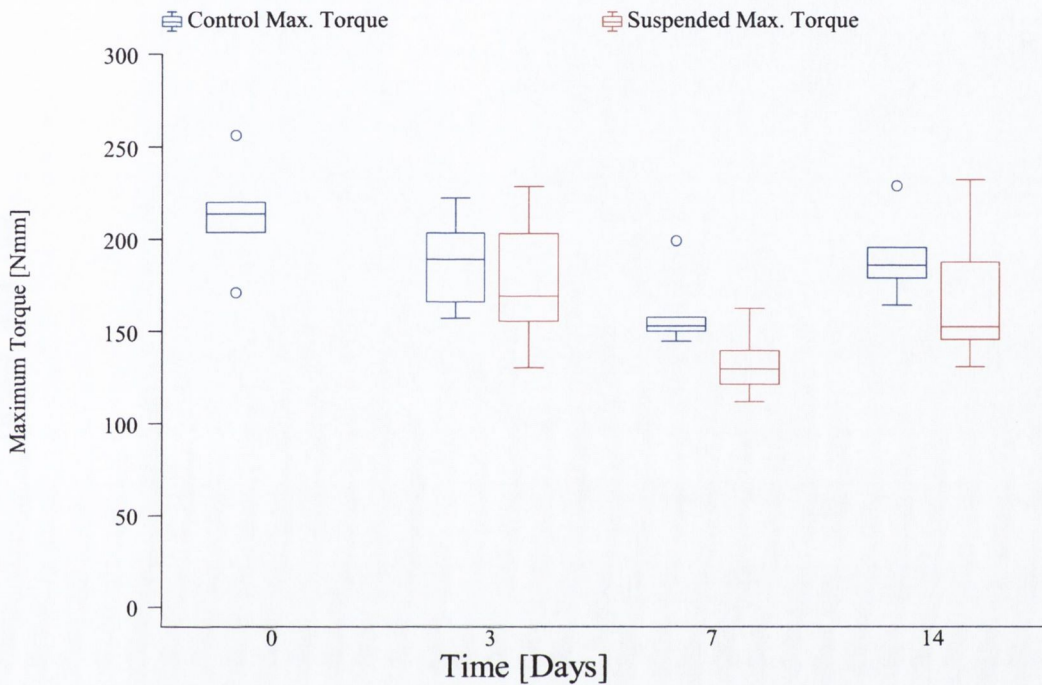


Fig. 5.20 Maximum Torque Vs. Time for Control and Suspended groups

Figure 5.21 shows the stiffness values calculated in the control and suspended femora over the experimental period. There was a statistically significant effect of time on the stiffness values achieved (Linear Regression Analysis, $P < 0.01$, ANOVA, $P < 0.05$). Following HLS, there was a statistically significant reduction in the stiffness values in the suspended groups relative to the controls (Linear Regression Analysis, $P < 0.05$, ANOVA, $P = 0.05$).

Figure 5.22 shows the angular deformation data calculated in the control and suspended femora over the experimental period. There was a statistically significant effect of time on the angular deformation values achieved (Linear Regression Analysis, $P < 0.05$, ANOVA, $P < 0.05$). Following HLS, there was no statistically significant difference in

the angular deformation values in the suspended groups relative to the controls (Linear Regression Analysis, $P = 0.71$, ANOVA, $P = 0.83$).

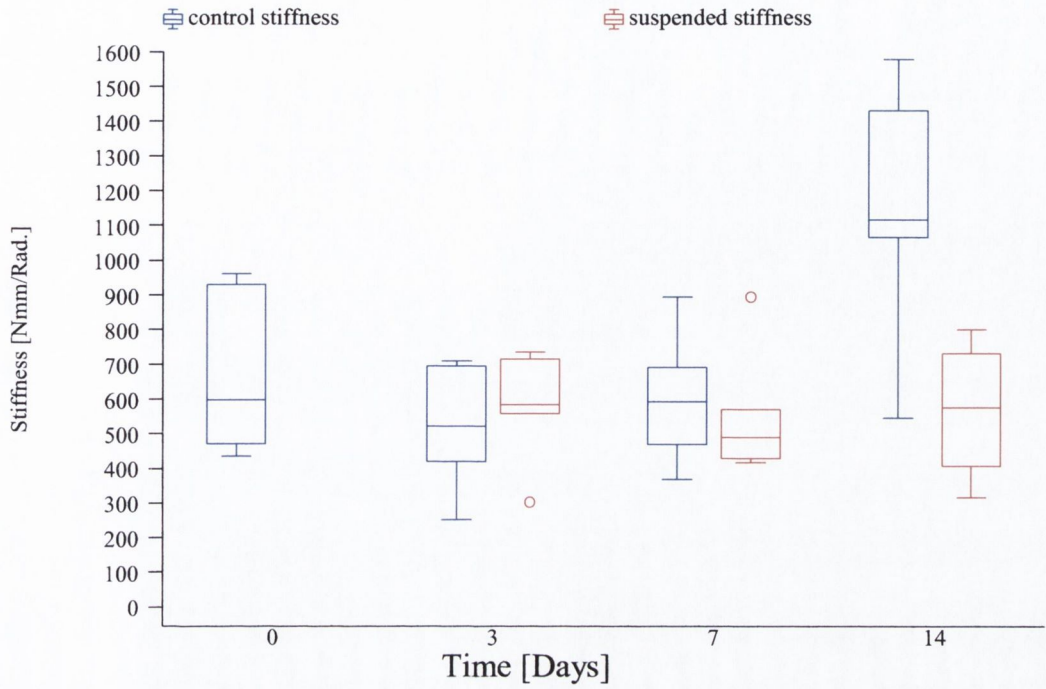


Fig. 5.21 Stiffness Vs. Time for Control and Suspended groups

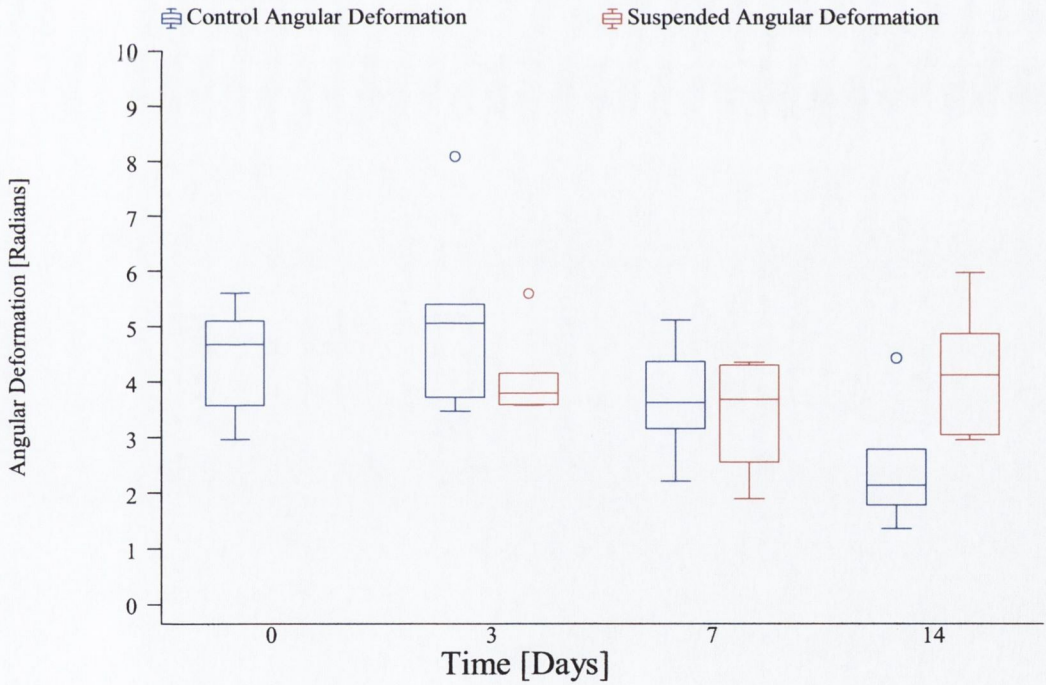


Fig. 5.22 Angular Deformation Vs. Time for Control and Suspended groups

5.3.2.2 Biomechanical parameters indirectly measured

Figure 5.23 shows the maximum stress calculated in the control and suspended femora over the experimental period. The maximum stress was calculated for each of the three slice geometries and the greatest taken. There was no statistically significant effect of time on the maximum stress calculated (Linear Regression Analysis, $P = 0.82$, ANOVA, $P < 0.20$). Following HLS, there was no statistically significant difference in the maximum stress values in the suspended groups relative to the controls (Linear Regression Analysis, $P = 0.38$, ANOVA, $P = 0.71$).

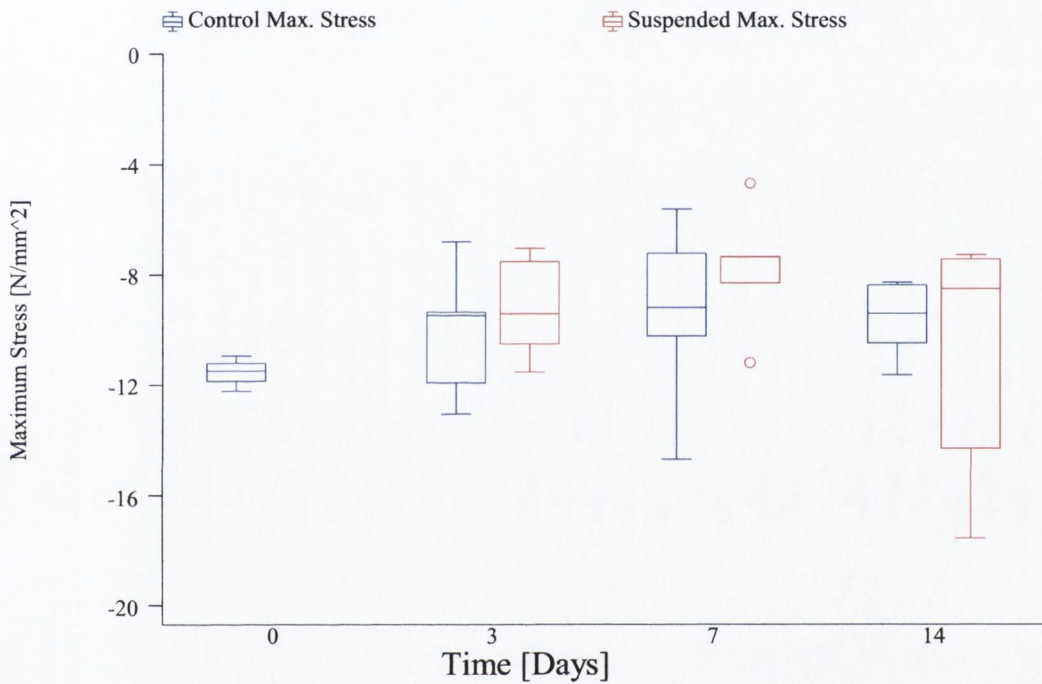


Fig. 5.23 Maximum Stress Vs. Time for Control and Suspended groups

5.3.2.3 pQCT scan data as Predictors of Biomechanical Parameters

In these torsion experiments, bone mineral density predicts the maximum torque values best. This is demonstrated in figure 5.24, where an increase in the measured/raw value for BMD correlates strongly with an increase in the maximum torque. In this regression model an increase of one standard deviation in BMD would result in an increase of 0.4 times the standard deviation in the maximum torque. A similar result is seen when the bone mineral content data is analysed with respect to the stiffness and to a lesser extent the maximum torque (see Figures 5.25 & 5.26).

	Std. Maximum Torque	Std. Maximum Stress	Std. Stiffness (GK)	Std. Angular Deformation
Linear Regression Analysis: Std. BMD	p < 0.01 R² = 0.17 Slope = 0.41	p = 0.75	p = 0.40	0.65
Linear Regression Analysis: Std. BMC	p = 0.06 R² = 0.09 Slope = 0.30	p = 0.96	p < 0.05 R² = 0.13 Slope = 0.36	0.23
Linear Regression Analysis: Std. Ip	p = 0.84	p = 0.36	p = 0.10	p < 0.05 R² = 0.11 Slope = -0.33
Linear Regression Analysis: Std. Area	p = 0.78	p = 0.28	p = 0.05 R² = 0.10 Slope = 0.31	p < 0.05 R² = 0.10 Slope = -0.32

Table 5.3 Statistical analysis of the correlation between mean values of BMD, BMC, Ip and Area and the stiffness, maximum stress and maximum torque (significant values in bold)

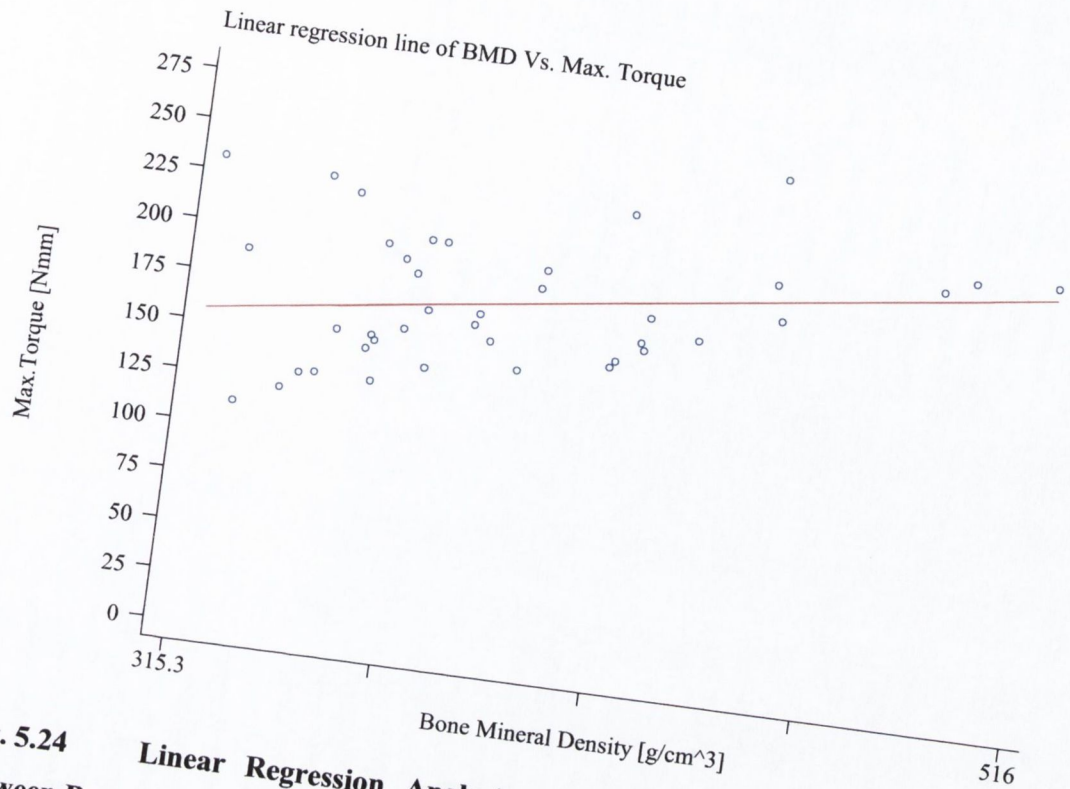


Fig. 5.24 Linear Regression Analysis showing the significant relationship between Bone Mineral Density and Max. Torque ($p < 0.01$, $R^2 = 0.17$)

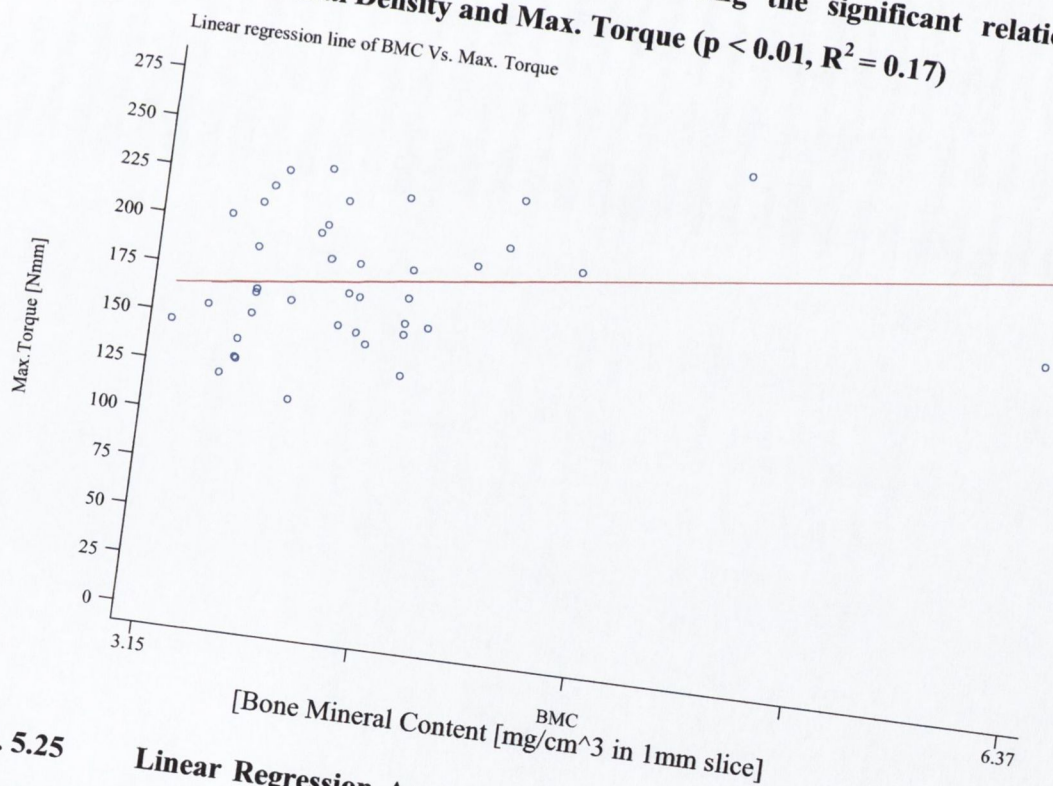


Fig. 5.25 Linear Regression Analysis showing the relationship between Bone Mineral Content and Max. Torque ($p = 0.06$, $R^2 = 0.09$)

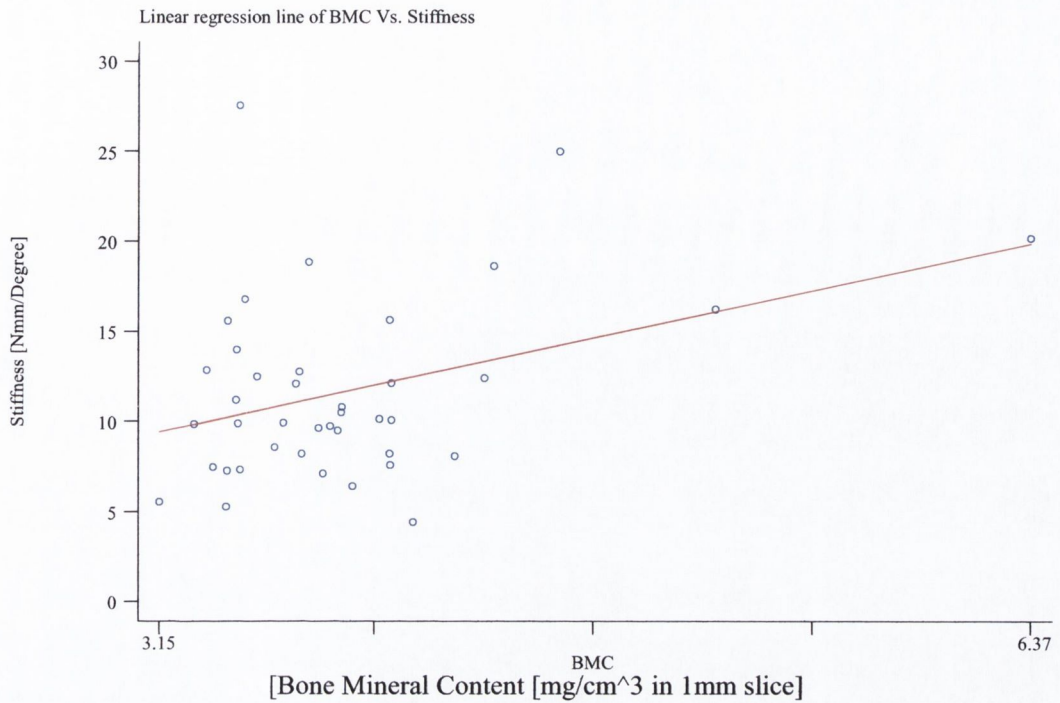


Fig. 5.26 Linear Regression Analysis showing the significant relationship between Bone Mineral Content and Stiffness ($p < 0.05$, $R^2 = 0.13$)

Of the geometric parameters the cortical area was well correlated with the stiffness and angular deformation (see Figure 5.27). The polar moment of inertia was also well correlated with the angular deformation (see Figure 5.28) and also approached significance with respect to stiffness. None of the pQCT scan parameters were well correlated with the maximum stress calculated.

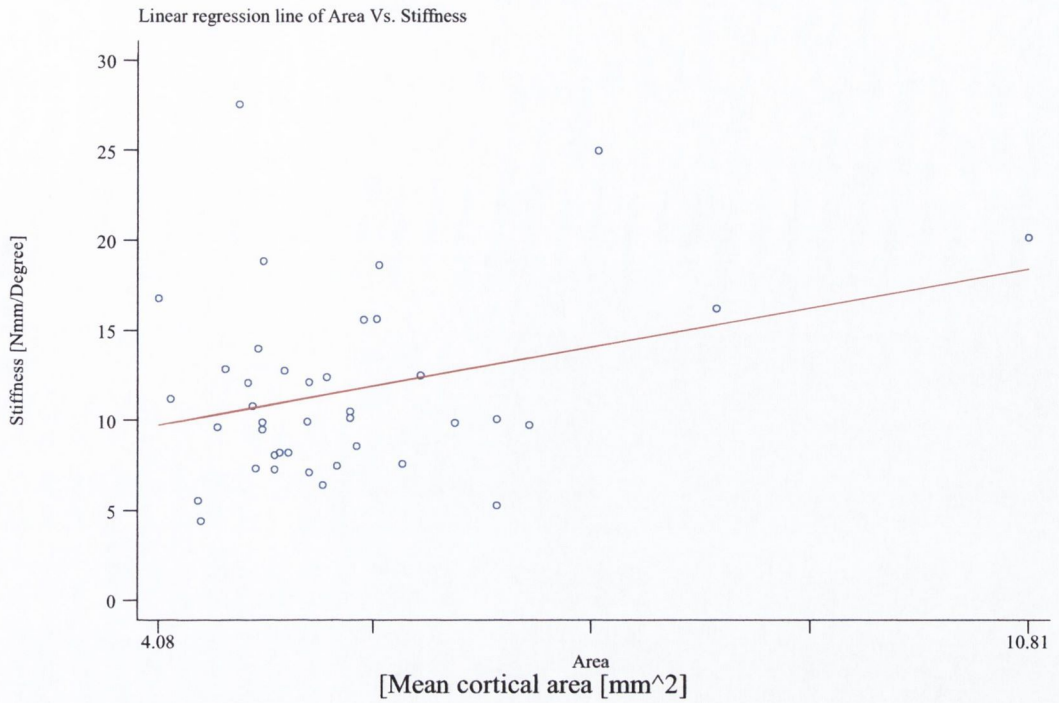


Fig. 5.27 Linear Regression Analysis showing the significant relationship between Mean Cortical Area and Stiffness ($p < 0.05$, $R^2 = 0.10$)

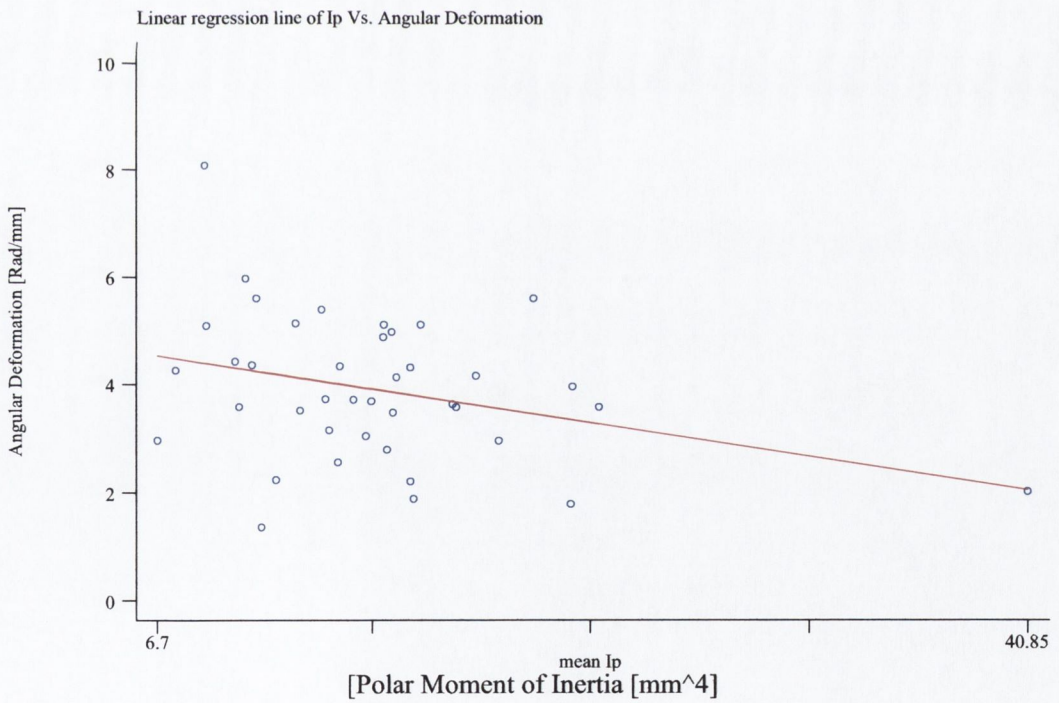


Fig. 5.28 Linear Regression Analysis showing the significant relationship between Mean Ip and Angular Deformation ($p < 0.05$, $R^2 = 0.11$)

5.4 Discussion

In this study, the BMD values were taken at three scan points along the control and suspended groups' bones. Although all animals were obtained from the same supplier and were housed and fed in the same manner it is clear that the basal control groups BMD values were considerably greater than those in any of the other groups. One possible explanation lies in the inherent variability present in all animals resulting in differing BMD values between animals from the same litter. This basal control BMD data may affect the statistical analysis of the groups over time and between the suspended and controls. Possibly, as a result there was a significant effect of time on the BMD values in all three slices individually and combined. In general, there was a drop between the basal control groups followed by the BMD either levelling off or increasing again by 14 days. This drop between 0 and 3 days may be due to the higher than normal basal BMD level, rather than a reduced 3 day level. However, without further study it is not possible to determine whether the BMD of the rats' femora are changing over time in these experiments. Another possibility is that there was a stress response in the animals as a consequence of the experiment. The decrease in BMD and Maximum torque over time in a growing animal indicates that this effect may be present. Attempts were made to negate the stress on the animals (acclimitisation) and the animals were monitored for signs of overt stress. No changes in feeding and grooming levels were observed and coupled with the animals increasing body weight this suggests that the animals were not overtly stressed. However, since stress levels were not directly measured this can not be fully ruled out.

Over the experimental period, as a result of HLS there was a significant reduction in BMD at the distal scan site and in the 3 combined slices relative to controls. At the diaphysis this reduction was also present while not significant, though the high basal control data may again be affecting this result. These findings are consistent with the findings of a number of authors who found compartmental reductions in the BMD of the unloaded limbs in suspended rats (Bloomfield et al., 2002, Matsumoto et al., 1998). BMC values were also assessed throughout the experimental period. In this case, the basal control data seemed in line with the other control groups. Over time only the proximal scan site produced a significant increase in BMC. This increase may be linked to the measured increases in cross sectional cortical area noted at the same scan site. As a result of HLS, there was a significant reduction in BMC values at the distal scan site

and at the three scan sites taken as a whole relative to the controls. This loss in BMC mirrors that of the BMD data and is consistent with the loss in total mineral content noted by Jain et al. (2000).

Following HLS there was no significant effect of unloading on either the I_p or cortical area data at any of the scan sites. However, over time there was a significant increase in both parameters at the mid-diaphysis and proximal scan sites consistent with growth. The pQCT area data seems to be in direct conflict with the bone area data in the morphological study, which found a significant reduction in the amount of bone at the mid-diaphysis. There are a number of points to note however:

- The pQCT area data was approaching significance, which would suggest the same trend is present in both observations.
- The resolution of the pQCT scanner ($150\ \mu\text{m} \times 150\ \mu\text{m} \times 1250\ \mu\text{m}$) is significantly lower than that achievable histologically ($\sim 10\ \mu\text{m}$). Consequently, the variability and reliability of the pQCT area data would not be as good as that from the morphological
- The thresholding method is obviously different in the two observations.

In section 5.3.2.1, the maximum torque data versus time was plotted and statistically analysed for the control and suspended groups femora. Analogous to the BMD results, once more the basal control maximum torque values are greater than both the control and suspended groups. In this case as before, there is a reduction in both groups BMD from day 0 to 7 with the values beginning to rise again by day 14. This effect of time was significant, although the effect of the high basal control levels would somewhat mask the result. As a result of HLS, there was a significant reduction in the maximum torque values of the suspended groups femora. This is comparable with a 50% reduction in torque to failure measured after three weeks suspension by Abram (1988). Although some authors reported larger reductions (van der Meulen et al., 1995) and some less (Martin, 1990) both the length of time suspended and the age of the animals must be taken into account. For example, Van der Meulen suspended the animals for four weeks. Interestingly, although Martin, as in this study, also suspended his animals for two weeks the animals used were mature rats and consequently the effects of underload are diminished. This in turn brings into question whether using young rapidly growing animals is valid in studying the mechanisms involved in osteoporosis, a disease mainly

affecting mature adult bone. It does not however, affect its validity for use in the study of the effects of altered mechanical load and disuse-osteoporosis.

This study followed the method set down by Levenston et al. (1994). Levenston provides a freely available FORTRAN program designed by the author, to determine the geometry of the scans and create an equivalent hollow elliptical model. This program requires the pQCT scanner to output images, which can then be evaluated. Unfortunately, the pQCT scanner used in this experiment could not provide high-resolution graphical images. Therefore, a Matlab program was created. This two-step program used the I_p and cortical area values generated in a pQCT scan to create an equivalent ellipse with the similar I_p and area. The program was tested by inputting known values of I_p and area for a range of over forty ellipses with varying axis ratios. In these tests the accuracy was found to be good with a mean error of less than 1%. In the study, the I_p and area values generated by Matlab were almost directly proportional to those from the pQCT scans with a very strong linear correlation found ($R^2 > 0.997$ in both cases; see Figures 5.6 & 5.7).

Once the non-uniform bone shape had been converted into ellipses of known geometry a number of mechanical parameters, maximum stress and stiffness, were calculated. There was no effect of time on the maximum stress values calculated for the femora. Although there was also no significant effect of HLS on the maximum stress values, the suspended animals values were less than the controls at all time points. One possible explanation is that the stress taken, although the greatest of the three scan sites used, may not actually be the maximum stress in the bone. This differs from work by Abram et al. (1988) and Shaw (1987) who noted significant reductions in maximum stress in the suspended animals. However these studies suspended the animals for longer periods and it is possible that in this experiment the reductions noted would have eventually reached significance.

Over the experiment the stiffness was assessed for changes due to growth and HLS. There was a significant increase in the stiffness values, although this was largely linked to the increase in the control groups stiffness values. Following HLS there was a significant reduction in the suspended groups stiffness values compared to the controls. The results here are comparable with the work by Abram et al. (1988) and van der Meulen et al. (1995) who both found significant reductions in stiffness following HLS.

Clinically, it is of great use to be able to predict the mechanical properties of a bone through a non-invasive test such as DEXA and pQCT scans. However as discussed in section 5.1.3.2, despite a large body of work there is still debate over which scan parameter is the best predictor of mechanical properties. This is largely due to differences in experimental set-up. In this experiment using pQCT scans each scan parameter was checked for its ability to predict the mechanical properties, maximum torque, maximum stress and stiffness. Maximum Torque was best predicted by BMD alone followed by BMC. Stiffness was best explained by BMC alone followed by mean cortical area. Alternatively, the two geometric parameters, I_p and area, best explained angular deformation. None of the scan parameters were significantly correlated to the maximum stress. The reason behind this may be due to the fact that the other three mechanical parameters, stiffness, maximum torque and angular deformation, are whole bone parameters whereas maximum stress was highly dependent on the scan site geometry. These data can be compared to work done by Lind et al. (2001) who found that stiffness of rat humeri in torsion was best correlated with cross-sectional area and with Jamsa et al. (1998) who found the stiffness of mouse femora best explained by cross sectional moment of inertia. Muehleman et al.(2000) found BMD values to be best able to explain whole bone strength in the human metatarsal. Therefore, these data seem to imply that maximum strength as measured by maximum torque is best predicted by material properties like BMD and to a lesser extent BMC. On the other hand, stiffness and angular deformation are best explained by geometric properties such as I_p and area as well as BMC. The fact that BMC values are a composite of material and geometric properties probably explains its ability to predict both maximum torque and stiffness/angular deformation variables. Although there were strong relationships found between the pQCT scan parameters and mechanical properties, as evidenced by the low p values, the r^2 values were generally low. This is indicative of a high level of scatter or variance and means that the predictive or explanatory power is quite low. This problem would be exacerbated by the inclusion of the experimental group in the analysis and by the use of only three scan sites in determining the pQCT data. In particular, the low resolution of the pQCT scanner would be a major cause of variance and hence reliability in this study. Therefore, a further study using more scan points and a high resolution pQCT or μ CT scanner should produce higher r^2 values and hence more predictive ability.

Ultimately these data imply the need for a single all-encompassing comparative study using different types of scanner on a variety of bones and bone types in a number of different animals.

5.5 Conclusions

To conclude, the following research questions have been answered:

- HLS results in a site specific reduction in volumetric BMD in the suspended femora of young growing rats
 - This reduction in BMD was greatest at the distal scan site which contained most trabecular bone but was also present when the three scan sites were assessed together
- A similar site specific reduction in BMC was found in the suspended animals femora
 - This reduction in BMC was greatest at the distal scan site which contained most trabecular bone but was present when the three scan sites were assessed together
- In general, HLS resulted in a reduction in the structural properties of the unloaded femora
 - Following 14 days suspension there was a reduction in the maximum torque of the suspended groups femora relative to the controls
 - A similar reduction in stiffness, measured via the torsional rigidity GK, was also observed in the suspended groups femora relative to the controls
 - HLS had no significant effect on the maximum shear stress calculated, τ_{\max} , calculated for the equivalent ellipse model in the femora
 - This loss of structural strength is largely attributed to changes in the material properties of the bones although the effect of suspension on cross sectional area was approaching significance
- Finally, in combining pQCT scan data with destructive torsion tests of rat femora, the following relationships were found
 - maximum strength as measured by maximum torque is best predicted by material properties like BMD and to a lesser extent BMC.
 - stiffness and angular deformation are best predicted by geometric properties such as I_p and area as well as BMC
 - BMC had strong relationships with both maximum torque and stiffness/angular deformation data

- In general, the pQCT parameters had strong relationships but a low explanatory power with respect to the mechanical properties

Chapter 6 General Discussion

Bone growth is controlled by genetic, hormonal and biomechanical factors. This multifactorial regulation is even present *in utero* with mechanical loading critical in regulating skeletogenesis, with inhibition of muscular contractions resulting in severe skeletal abnormalities. After birth, growth and ossification are strongly influenced by physical activity and externally applied forces. Clinically, reduced loading may occur due to bed-rest or paralysis while overloading may lead to differential growth and skeletal asymmetry. In addition, as the population in the western world ages, degenerative diseases like osteoporosis are of increasingly greater interest clinically.

- The aim of this study was to investigate the effect of altering the mechanical load applied to the long bones of growing rats. An established rat hindlimb-suspension model was used. This HLS model was successfully set up in our laboratory, and following testing, 39 day-old rats were suspended for periods of up to two weeks (1, 3, 7 and 14 days), concurrently with age-matched pair fed controls.

Since the quantity of total RNA isolated from the periosteal tissue samples was low, it was decided to modify an existing commercial product, SMART, to analyse the gene expression patterns via the creation of cDNA arrays. These arrays were then hybridised with gene specific radioactive probes to determine the expression levels of each gene. The system successfully developed here is a quick and easily reproducible method of gene expression analysis. It is proposed that the system would be of particular use as a first step analysis tool when working with a large sample numbers containing limited RNA volumes. For example, the cDNA arrays could be used to narrow down the analysis to a particular time point or to reduce the number of genes of interest.

In this experiment, cDNA arrays were created from the rat femoral periosteal samples collected post-mortem. The initial hypothesis was that HLS would result in a reduction in the expression of genes associated with bone formation. Although this hypothesis could not be verified there was circumstantial evidence that the reduction was present with both *c-fos* and osteocalcin expression reduced (non-significantly) after both one and three days suspension. Consequently, a quantitative method of gene expression

analysis may be required to detect changes, and in particular reductions, in the gene expression levels of lowly expressed genes. In addition, more research with smaller time increments between testing is necessary to validate the hypothesis. Following 7 days suspension a rise in the expression of c-fos and osteocalcin was detected in the suspended animals' periosteum. These elevated levels are consistent with a bone formation response. Previously, and in this study, HLS has been shown to result in a cessation/reduction in bone formation (van der Meulen et al., 1995, Globus et al., 1986b, Bikle et al., 1994b). However, this reduction in the rate of bone formation is transient with growth returning towards normal by fourteen days of continued unloading. This return to normal growth is a result of the reinstatement of the age-related growth potential. It is proposed therefore that the elevated levels of c-fos and osteocalcin found after 7 days in the periosteum are evidence of a return of the cells towards a state of normal growth. The data for the gene expression levels of IGF-I were contradictory with a drop in expression seen after 3 days relative to GAPDH but not when compared against RNRPS9 or when the two housekeeping genes data were combined. Consequently, further study is necessary to elucidate the IGF-I response of periosteal osteoblasts to unloading via HLS.

HLS had no significant effect on the gross morphology, bone length and weight, of either the humeri or femora. HLS resulted in a significant reduction in the total mid-diaphyseal cross sectional area in the femora of the suspended animals compared to controls. This effect of HLS was also evident in the reduced periosteal and total bone formation rates found in the suspended animals even though this did not result in an altered periosteal cross sectional area. Therefore, unloading elicits a coupled response of formation and resorption at periosteal and endosteal surfaces, although in growing animals formation is by far the predominant force.

Microdamage has been shown to be present in a large number of bones from a variety of animals (Lee et al., 2002, Lee et al., 1998, Bentolila et al., 1998, Muir et al., 1999, Burr and Martin, 1993, Lee, 1995, Mori and Burr, 1993, Schaffler et al., 1989) and has been proposed to act as a stimulus for remodelling. This study has shown, for the first time, that *in vivo* microcracks are present under normal conditions in rat bones. These cracks were labelled via intraperitoneal injections of two fluorochromes, oxytetracycline and calcein blue, and were present in both the humeri and femora. There were more *in vivo* microcracks present in the humeri (crack density: $0.17 \pm .35$, surface density: 30 ± 63)

than the femora (crack density: 0.11 ± 0.2 , surface density: 20 ± 40), with both mean crack density and surface density values greater in the humeri. The mean crack lengths were similar in the humeri (62 ± 92) and femora (62 ± 102). Unfortunately, poor absorption of the oxytetracycline label, possibly due to the injections being administered intraluminally rather than intraperitoneally, prevented the sequential labelling of microcracks. Consequently, the effect of HLS on microcrack initiation and propagation could not be assessed.

Previously, a number of authors have examined the effect of HLS on structural strength (Abram et al., 1988, Shaw et al., 1987, van der Meulen et al., 1995, Martin, 1990, Bloomfield et al., 2002). Researchers have generally found a reduction in strength and stiffness in the unloaded limbs. However, this loss in strength has been attributed to changes in purely geometrical or material properties or a combination of the two. This ambiguity has not been helped by the wide variety of testing methods and differences in the age of the animals and duration of suspension. In this study, HLS resulted in a reduction in the maximum torque and stiffness of the suspended animals' femora relative to the controls. To determine the effect of HLS on material properties, pQCT scans were performed at three points along the length of the femora. HLS was found to result in a site-specific reduction in volumetric BMD and BMC in the suspended group's femora relative to controls. This reduction was greatest at the distal scan site, which contained most trabecular bone. In this study, the reduction in structural strength was largely due to changes in material properties, although the effect of HLS on cross sectional area approached significance in the pQCT study and was significantly different in the morphological study. Over a longer suspension period changes in the geometric properties may be increasingly important.

Clinically it would be useful to assess the structural properties non-invasively. Consequently a number of researchers have performed mechanical tests on a variety of bones and attempted to relate the parameters from both DEXA and pQCT scanners to the structural results (Jamsa et al., 1998, Muehleman et al., 2000, Lind et al., 2001, Ebbesen et al., 1999). The results have been mixed, with some finding geometric and others material parameters to be best able to predict mechanical properties. This uncertainty is created by the wide variety in test set-ups and scanners used. Coupled to this, is a misunderstanding of the basic capabilities and differences of the two types of scanners, DEXA and pQCT. In this study using a pQCT scanner, maximum strength

was best predicted by material properties - BMD ($p < 0.01$, $R^2 = 0.17$) - whereas stiffness and angular deformation were best correlated with geometric properties - I_p ($p < 0.05$, $R^2 = 0.11$) and area ($p < 0.05$, $R^2 = 0.10$). Bone mineral content, which takes account of both material and geometric properties, was found to have significant relationships with both maximum strength ($p = 0.06$, $R^2 = 0.09$) and stiffness/angular deformation ($p < 0.05$, $R^2 = 0.13$) variables. However, it must be noted the the explanatory power of the relationships was relatively low (9% - 17%). This low power is largely as a result of the resolution of the pQCT scanner and the variability and inaccuracy produced. Therefore to fully understand the relationships between scan parameters and structural properties further study is required using a standardised series of mechanical tests, high resolution scanners and various bones.

Currently, worldwide trends indicate that the number of people suffering from osteoporosis and osteopenia will continue to increase in the western world. At the end of the day the control systems for the cells involved in bone formation and Resorption remains incompletely understood. Ultimately, this study has shown that following HLS there are widespread changes in the unloaded bones. These changes were tracked from gene expression changes in RNA extracted from periosteal tissue samples, to alterations in the cellular phenotype at the periosteum and to changes in the structural properties of the adapted bones. Therefore, basic research is vital in order to gain greater understanding of the inherent processes involved in osteoporotic bone. In particular, this requires more interdisciplinary research, at a tissue and cell specific level, looking at the genetic pathways involved in bone growth and remodelling. This may require scientists, engineers and clinical doctors to move into new fields of expertise and hence see the problem from a new viewpoint.

6.1 Conclusions

To conclude, the following are the main findings of this study:

- The disuse osteoporosis model, HLS, was successfully set-up in our laboratory
 - The model was used to suspend groups of young growing rats for periods of up to two weeks concurrently with age-matched pair-fed controls.
- Morphological analysis of transverse sections of the mid-diaphysis of the humeri and femora found:
 - HLS resulted in only a limited change in the mid-diaphyseal growth patterns in the humeri, with the suspended animals bones becoming more circular in appearance.
 - In the femora, HLS resulted in a reduction in the total amount of mid-diaphyseal bone present in the suspended group.
 - However in this study, HLS has no significant effect on either the periosteal or endosteal cross sectional area in isolation.
 - HLS resulted in a reduced periosteal and overall bone formation rate in the suspended groups femora.
 - *In vivo* microdamage, labelled using two fluorochromes, was found for the first time in rat bone under normal loading conditions
- pQCT scans were taken at three equidistant points along the length of the femora prior to the bones being mechanically tested in a destructive torsion test.
 - HLS resulted in a reduction in the maximum torque and stiffness values of the suspended groups femora relative to the controls.
 - HLS resulted in a site-specific reduction in the volumetric BMD and BMC values in the suspended femora.
 - This reduction in material properties was greatest in the distal scan site where there was most trabecular bone.
 - The loss of structural strength following HLS was attributed to changes in both the material and geometric properties of the bones.

- Periosteal tissue was harvested from the mid-diaphyseal region of the femora. The RNA was isolated, amplified using a commercial product, SMART, and used to create cDNA arrays.
 - SMART technology can be used with large sample numbers of limited RNA volume to create small-scale cDNA arrays for gene expression analysis.
 - Following HLS there was a consistent drop (not statistically significant) in the levels of c-fos and osteocalcin measured at one and three days.
 - After seven days there was a significant increase in the levels of c-fos and osteocalcin.
 - This increase is consistent with the bone forming response, which was observed between seven and fourteen days in the morphological analysis of the mid-diaphysis of the contra-lateral femora.
 - This bone forming response could be due to systemic or genetic factors reasserting control in these young fast growing rats.

6.2 Future work

The main objectives of this thesis were completed, i.e. to subject bones to altered load and to examine the effects on the growth patterns, structural strength and gene expression patterns. However, a number of opportunities for further analysis and research present themselves. The SMART cDNA array system presents the opportunity to examine in more detail the genetic response of unloaded bone. In particular, smaller increments of time between measurements are necessary especially early on (1, 2, 4, 8, 12 hours and 1 day). The arrays could then be used as a tool to identify time points of interest and to widen the number of genes of interest (*e.g.* other early response transcription factors like COX-2 and the IGF binding proteins). Once points of interest were identified, quantitative analysis could be performed using real-time PCR. In line with this study the need to look at different components of the skeleton separately is imperative to understanding what is happening in the bone's response to under or overload. Hence, the bones from these short-term suspensions could be used in a number of parallel studies. For example, the periosteal tissue of both limbs could be pooled, one leg tangentially sectioned to release RNA from osteocytes (Mason et al., 1996) and the other being used in a parallel protein analysis study.

Another possible project would be to investigate the effect of overload in rat bones. This could be achieved either via reloading previously suspended rats or via immobilisation of a single leg to overload the contra-lateral limb. The relationship between microdamage and remodelling could also be investigated. A continuation of this would be to treat the animals with various doses of bisphosphonates, to examine the effect on the creation of microdamage within the bones. Finally, it would be interesting to use older animals in the study of osteoporosis so as to more easily and clearly separate the biomechanical effects from those of growth.

Ultimately, this work provides a template for further research into the effects of altered load on the skeleton. In addition the multi-factorial nature of bones' response to altered loads necessitates the need for further interdisciplinary work. It is in understanding how each of the different disciplines relate to each other that the true understanding of the processes at work will be found.

Bibliography

- Abram, A. C., Keller, T. S. and Spengler, D. M. (1988) *J Biomech*, **21**, 755-67.
- Alberts, B., Bray, D., Lewis, J., Raff, M., Roberts, K. and Watson, J. D. (1994)
Molecular Biology of the cell, Garland Publishing, New York.
- Amtmann, E. and Oyama, J. (1973) *Z Anat Entwicklungsgesch*, **139**, 307-18.
- Amtmann, E. and Oyama, J. (1976) *Anat Embryol (Berl)*, **149**, 47-70.
- Amtmann, E., Oyama, J. and Fisher, G. L. (1976) *Anat Embryol (Berl)*, **149**, 71-8.
- Andrew, J. G., Hoyland, J., Freemont, A. J. and Marsh, D. (1993) *Calcif Tissue Int*, **53**,
97-102.
- Angel, P. and Karin, M. (1991) *Biochim Biophys Acta*, **1072**, 129-57.
- Arnaud, S. B., Harper, J. S. and Navidi, M. (1995) *J Gravit Physiol*, **2**, P115-6.
- Ashizawa, N., Nonaka, K., Michikami, S., Mizuki, T., Amagai, H., Tokuyama, K. and
Suzuki, M. (1999) *J Appl Physiol*, **86**, 1347-51.
- Astrom, J., Ahnqvist, S., Beertema, J. and Jonsson, B. (1987) *J Bone Joint Surg Br*, **69**,
381-3.
- Bassett, C. A. (1968) *Calcif Tissue Res*, **1**, 252-72.
- Bautista, C. M., Mohan, S. and Baylink, D. J. (1990) *Metabolism*, **39**, 96-100.

Bentolila, V., Boyce, T. M., Fyhrle, D. P., Drumb, R., Skerry, T. M. and Schaffler, M.

B. (1998) *Bone*, **23**, 275-81.

Bhudhikanok, G. S., Wang, M. C., Eckert, K., Matkin, C., Marcus, R. and Bachrach, L.

K. (1996) *J Bone Miner Res*, **11**, 1545-56.

Biewener, A. A. and Bertram, J. E. (1994) *J Appl Physiol*, **76**, 946-55.

Bikle, D. D., Halloran, B. P., Cone, C. M., Globus, R. K. and Morey-Holton, E. (1987)

Endocrinology, **120**, 678-84.

Bikle, D. D., Halloran, B. P. and Morey-Holton, E. (1994a) *Acta Astronaut*, **33**, 119-29.

Bikle, D. D., Halloran, B. P. and Morey-Holton, E. (1994b) *Acta Astronaut*, **33**, 119-29.

Bikle, D. D., Harris, J., Halloran, B. P., Currier, P. A., Tanner, S. and Morey-Holton, E.

(1995) *Endocrinology*, **136**, 2099-109.

Bikle, D. D., Harris, J., Halloran, B. P. and Morey-Holton, E. (1994b) *Am J Physiol*,

267, E822-7.

Bikle, D. D., Harris, J., Halloran, B. P. and Morey-Holton, E. (1994a) *Am J Physiol*,

267, E822-7.

Bikle, D. D., Harris, J., Halloran, B. P. and Morey-Holton, E. R. (1994c) *J Bone Miner*

Res, **9**, 1789-96.

Bikle, D. D., Harris, J., Halloran, B. P., Roberts, C. T., Leroith, D. and Morey-Holton,

E. (1994d) *Am J Physiol*, **267**, E278-86.

- Biryukov, Y. N. and Krasnykh, I. G. (1970) *Kosm. Biol. Med.*, **4**, 42 - 45.
- Bloomfield, S. A., Allen, M. R., Hogan, H. A. and Delp, M. D. (2002) *Bone*, **31**, 149-57.
- Burger, E. H. and Klein-Nulén, J. (1999) *Adv Dent Res*, **13**, 93-8.
- Burr, D. B. and Martin, R. B. (1993) *J Biomech*, **26**, 613-6.
- Burr, D. B., Schaffler, M. B., Yang, K. H., Wu, D. D., Lukoschek, M., Kandzari, D., Sivaneri, N., Blaha, J. D. and Radin, E. L. (1989) *Bone*, **10**, 215-21.
- Burstein, A. H. and Frankel, V. H. (1971) *J Biomech*, **4**, 155-8.
- Cance, W. G., Craven, R. J. and Liu, E. T. (1992) *Surg Oncol*, **1**, 309-14.
- Carter, D. R. (1984) *Calcified Tissue International*, **36**, S19 - S24.
- Carter, D. R., Harris, W. H., Vasu, R. and Caler, W. E. (1981) In *Mechanical properties of bone*(Ed, Cowin, S. D.) American Society of Mechanical Engineers, New York.
- Celeste, A. J., Rosen, V., Buecker, J. L., Kriz, R., Wang, E. A. and Wozney, J. M. (1986) *Embo J*, **5**, 1885-90.
- Chambers, T. J., Fox, S., Jagger, C. J., Lean, J. M. and Chow, J. W. (1999) *Osteoarthritis Cartilage*, **7**, 422-3.
- Chan, Y. L., Paz, V., Olvera, J. and Wool, I. G. (1993) *Biochem Biophys Res Commun*, **193**, 106-12.

- Chenchik, A., Diachenko, L., Moqadam, F., Tarabykin, V., Lukyanov, S. and Siebert, P. D. (1996) *Biotechniques*, **21**, 526-34.
- Chow, J. W., Fox, S., Jagger, C. J. and Chambers, T. J. (1998) *Am J Physiol*, **274**, E146-54.
- Clohisy, J. C., Scott, D. K., Brakenhoff, K. D., Quinn, C. O. and Partridge, N. C. (1992) *Mol Endocrinol*, **6**, 1834-42.
- Cohen, D. R., Ferreira, P. C., Gentz, R., Franza, B. R., Jr. and Curran, T. (1989) *Genes Dev*, **3**, 173-84.
- Collet, P., Uebelhart, D., Vico, L., Moro, L., Hartmann, D., Roth, M. and Alexandre, C. (1997) *Bone*, **20**, 547-51.
- Cowin, S. C., Moss-Salentijn, L. and Moss, M. L. (1991) *J Biomech Eng*, **113**, 191-7.
- Curran, T., Gordon, M. B., Rubino, K. L. and Sambucetti, L. C. (1987) *Oncogene*, **2**, 79-84.
- Currey, J. D. (1984) *Calcif Tissue Int*, **36 Suppl 1**, S118-22.
- Dalen, N., Laftman, P., Ohlsen, H. and Stromberg, L. (1985) *Orthopedics*, **8**, 1139-41.
- Dalen, N. and Olsson, K. E. (1974) *Acta Orthop Scand*, **45**, 170-4.
- Daughaday, W. H. and Rotwein, P. (1989) *Endocr Rev*, **10**, 68-91.
- Diggle, D. T., Liang, K. Y. and Zeger, S. L. (1994) *Analysis of longitudinal data*, Clarendon Press, Oxford.

- Dony, C. and Gruss, P. (1987) *Nature*, **328**, 711-4.
- Ducy, P., Desbois, C., Boyce, B., Pinero, G., Story, B., Dunstan, C., Smith, E., Bonadio, J., Goldstein, S., Gundberg, C., Bradley, A. and Karsenty, G. (1996) *Nature*, **382**, 448-52.
- Dunican, D., ParleMcDermott, A. and Croke, D. T. (1997) *Curr. Diag. Pathol.*, **4**, 170-175.
- Ebbesen, E. N., Thomsen, J. S., Beck-Nielsen, H., Nepper-Rasmussen, H. J. and Mosekilde, L. (1999) *Bone*, **25**, 713-24.
- Erben, R. G. (1997) *J Histochem Cytochem*, **45**, 307-13.
- Esmon, C. T., Sadowski, J. A. and Suttie, J. W. (1975) *J Biol Chem*, **250**, 4744-8.
- Franchimont, N., Gangji, V., Durant, D. and Canalis, E. (1997) *Endocrinology*, **138**, 5248-55.
- Frost, H. M. (1958) *Stain Technol*, **33**, 273-277.
- Frost, H. M. (1986) *Intermediary organisation of the skeleton*, CRC Press, Boca Raton FL.
- Frost, H. M. (1987) *Bone Miner*, **2**, 73-85.
- Frost, H. M. (1992) *Bone Miner*, **19**, 257-71.
- Fyhrie, D. P. and Carter, D. R. (1986) *J Orthop Res*, **4**, 304-17.

- Galileo, G. (1638) In *Two new sciences*. In: "The second day" The University of Wisconsin Press, pp. 109 - 146.
- Gallop, P. M., Lian, J. B. and Hauschka, P. V. (1980) *N Engl J Med*, **302**, 1460-6.
- Gibson, L. J. and Ashby, M. F. (1988) *Cellular Solids - structures and properties*, Pergammon Press, Oxford.
- Globus, R. K., Bikle, D. D., Halloran, B. and Morey-Holton, E. (1986a) *J Bone Miner Res*, **1**, 191-7.
- Globus, R. K., Bikle, D. D. and Morey-Holton, E. (1984) *Endocrinology*, **114**, 2264-70.
- Globus, R. K., Bikle, D. D. and Morey-Holton, E. (1986b) *Endocrinology*, **118**, 733-42.
- Glowacki, J. and Lian, J. B. (1987) *Cell Differ*, **21**, 247-54.
- Glowacki, J., Rey, C., Glimcher, M. J., Cox, K. A. and Lian, J. (1991) *J Cell Biochem*, **45**, 292-302.
- Goodship, A. E., Lanyon, L. E. and McFie, H. (1979) *J Bone Joint Surg Am*, **61**, 539-46.
- Gordon, K. R., Perl, M. and Levy, C. (1989) *Bone*, **10**, 303-12.
- Greendale, G. A., Barrett-Connor, E., Edelstein, S., Ingles, S. and Haile, R. (1995) *Am J Epidemiol*, **141**, 951-9.
- Grigoriadis, A. E., Wang, Z. Q. and Wagner, E. F. (1995) *Trends Genet*, **11**, 436-41.
- Gross, T. and Rubin, C. (1993) In *39th Orthopaedic Research Society*, Vol. 18, pp. 125.

- Halloran, B. P., Bikle, D. D., Wronski, T. J., Globus, R. K., Levens, M. J. and Morey-Holton, E. (1986) *Endocrinology*, **118**, 948-54.
- Hargens, A. R., Tipton, C. M., Gollnick, P. D., Mubarak, S. J., Tucker, B. J. and Akeson, W. H. (1983) *J Appl Physiol*, **54**, 1003-9.
- Hauschka, P. V. and Gallop, P. M. (1977) In *Calcium-binding proteins and calcium function* (Ed, Wasserman, R. H., Corradino, R. A., Carafoli, E., Kretsinger, R. H., MacLennan, D. H. and Siegal, F. L.) Elsevier, Amsterdam, pp. 338-347.
- Hauschka, P. V., Lian, J. B., Cole, D. E. and Gundberg, C. M. (1989) *Physiol Rev*, **69**, 990-1047.
- He, X., Schick, P. K. and Wojenski, C. (1995) *J Lab Clin Med*, **126**, 178-83.
- Heinonen, A., Oja, P., Kannus, P., Sievanen, H., Haapasalo, H., Manttari, A. and Vuori, I. (1995) *Bone*, **17**, 197-203.
- Hill, P. A., Reynolds, J. J. and Meikle, M. C. (1995) *Endocrinology*, **136**, 124-31.
- Hillam, R. A. and Skerry, T. M. (1995) *J Bone Miner Res*, **10**, 683-9.
- Hirai, S. I., Ryseck, R. P., Mechta, F., Bravo, R. and Yaniv, M. (1989) *Embo J*, **8**, 1433-9.
- Hollister, S. J., Brennan, J. M. and Kikuchi, N. (1994) *J Biomech*, **27**, 433-44.
- Jacob, H. A. and Huggler, A. H. (1980) *J Biomech*, **13**, 159-73.
- Jaekel, E., Amtmann, E. and Oyama, J. (1977) *Anat Embryol (Berl)*, **151**, 223-32.

- Jain, P. K., Iyer, E. M., Banerjee, P. K. and Baboo, N. S. (2000) *Indian J Physiol Pharmacol*, **44**, 359-62.
- Jamsa, T., Jalovaara, P., Peng, Z., Vaananen, H. K. and Tuukkanen, J. (1998) *Bone*, **23**, 155-61.
- Jaworski, Z. F., Liskova-Kiar, M. and Uhthoff, H. K. (1980) *J Bone Joint Surg Br*, **62-B**, 104-10.
- Jee, W. S., Wronski, T. J., Morey, E. R. and Kimmel, D. B. (1983) *Am J Physiol*, **244**, R310-4.
- Jehle, P. M., Schulten, K., Schulz, W., Jehle, D. R., Stracke, S., Manfras, B., Boehm, B. O., Baylink, D. J. and Mohan, S. (2003) *Eur J Intern Med*, **14**, 32-38.
- Johansen, J. S., Riis, B. J., Delmas, P. D. and Christiansen, C. (1988) *Eur J Clin Invest*, **18**, 191-5.
- Johnson, R. S., Spiegelman, B. M. and Papaioannou, V. (1992) *Cell*, **71**, 577-86.
- Jones, H. H., Priest, J. D., Hayes, W. C., Tichenor, C. C. and Nagel, D. A. (1977) *J Bone Joint Surg Am*, **59**, 204-8.
- Junqueira, L. C., Carneiro, J. and Kelley, R. O. (1992) *Basic Histology*, Appleton & Lange, Norwalk, CT.
- Kavanagh, B. F., Dewitz, M. A., Ilstrup, D. M., Stauffer, R. N. and Coventry, M. B. (1989) *J Bone Joint Surg Am*, **71**, 1496-503.

- Kawata, A. and Mikuni-Takagaki, Y. (1998) *Biochem Biophys Res Commun*, **246**, 404-8.
- Kimura, T., Amtmann, E., Doden, E. and Oyama, J. (1979) *J Biomech*, **12**, 361-5.
- Kirk, S., Sharp, C. F., Elbaum, N., Endres, D. B., Simons, S. M., Mohler, J. G. and Rude, R. K. (1989) *J Bone Miner Res*, **4**, 515-22.
- Kostenuik, P. J., Halloran, B. P., Morey-Holton, E. R. and Bikle, D. D. (1997) *Am J Physiol*, **273**, E1133-9.
- Kostenuik, P. J., Harris, J., Halloran, B. P., Turner, R. T., Morey-Holton, E. R. and Bikle, D. D. (1999) *J Bone Miner Res*, **14**, 21-31.
- Krolner, B., Toft, B., Pors Nielsen, S. and Tondevold, E. (1983) *Clin Sci (Lond)*, **64**, 541-6.
- Lane, N. E., Bloch, D. A., Jones, H. H., Marshall, W. H., Jr., Wood, P. D. and Fries, J. F. (1986) *Jama*, **255**, 1147-51.
- Lanyon, L. E. (1980) *J Zool Lond*, **192**, 457.
- Lanyon, L. E. (1984) *Calcif Tissue Int*, **36 Suppl 1**, S56-61.
- Lanyon, L. E. (1993) *Calcif Tissue Int*, **53 Suppl 1**, S102-6; discussion S106-7.
- Lanyon, L. E., Goodship, A. E., Pye, C. J. and MacFie, J. H. (1982) *J Biomech*, **15**, 141-54.
- Lanyon, L. E. and Rubin, C. T. (1984) *J Biomech*, **17**, 897-905.

- Lean, J. M., Jagger, C. J., Chambers, T. J. and Chow, J. W. (1995) *Am J Physiol*, **268**, E318-27.
- LeBlanc, A. D., Schneider, V., Shackelford, L. L., West, S., Oganov, V., Bakulin, A. and Voronin, L. (1996) *Journal of Bone and Mineral Research*, **11**, S323.
- LeBlanc, A. D., Schneider, V., Spector, E., Evans, H., Rowe, R., Lane, H., Demers, L. and Lipton, A. (1995) *Bone*, **16**, 301 - 304.
- Lee, K., Deeds, J. D., Chiba, S., Un-No, M., Bond, A. T. and Segre, G. V. (1994) *Endocrinology*, **134**, 441-50.
- Lee, T. C. (1995) University of Dublin, Dublin.
- Lee, T. C., Mohsin, S., Taylor, D., Parkesh, R., Gunnlaugsson, T., O'Brien, F. J., Giehl, M. and Gowin, W. (2003) *Journal of Anatomy*, **203**, 161.
- Lee, T. C., Myers, E. R. and Hayes, W. C. (1998) *J Anat*, **193 (Pt 2)**, 179-84.
- Lee, T. C., Staines, A. and Taylor, D. (2002) *J Anat*, **201**, 437-46.
- Lee, T. C. and Taylor, D. (1999) *Ir J Med Sci*, **168**, 102-5.
- Lepola, V., Vaananen, K. and Jalovaara, P. (1993) *Clin Orthop*, 55-61.
- Levenston, M. E., Beaupre, G. S. and van der Meulen, M. C. (1994) *J Bone Miner Res*, **9**, 1459-65.
- Li, K. C., Zernicke, R. F., Barnard, R. J. and Li, A. F. (1991) *J Appl Physiol*, **70**, 554-60.

- Lian, J. B., Tassinari, M. and Glowacki, J. (1984) *J Clin Invest*, **73**, 1223-6.
- Lind, P. M., Lind, L., Larsson, S. and Orberg, J. (2001) *Bone*, **29**, 265-70.
- Lu, P. W., Cowell, C. T., SA, L. L.-J., Briody, J. N. and Howman-Giles, R. (1996) *J Clin Endocrinol Metab*, **81**, 1586-90.
- Machwate, M., Zerath, E., Holy, X., Hott, M., Modrowski, D., Malouvier, A. and Marie, P. J. (1993) *Am J Physiol*, **264**, E790-9.
- Machwate, M., Zerath, E., Holy, X., Pastoureau, P. and Marie, P. J. (1994) *Endocrinology*, **134**, 1031-8.
- Mack, P. B. (1971) *Aerosp Med*, **42**, 828-33.
- Mack, P. B., LaChance, P. A., Vose, G. P. and Vogt, F. B. (1967) *Am J Roentgenol Radium Ther Nucl Med*, **100**, 503-11.
- Mack, P. B. and LaChance, P. L. (1967) *Am J Clin Nutr*, **20**, 1194-205.
- Marcus, R., Cann, C., Madvig, P., Minkoff, J., Goddard, M., Bayer, M., Martin, M., Gaudiani, L., Haskell, W. and Genant, H. (1985) *Ann Intern Med*, **102**, 158-63.
- Martin, R. B. (1990) *J Biomech*, **23**, 1021-9.
- Martin, R. B. (2000) *Bone*, **26**, 1-6.
- Martin, R. B. and Burr, D. B. (1989) *Structure, function and adaptation of compact bone*, Raven Press, New York.

- Martin, R. B., Burr, D. B. and Sharkey, N. A. (1998) *Skeletal tissue mechanics*, Springer-Verlag, New York.
- Mason, D. J., Hillam, R. A. and Skerry, T. M. (1996) *J Bone Miner Res*, **11**, 350-7.
- Matsui, M., Tokuhara, M., Konuma, Y., Nomura, N. and Ishizaki, R. (1990) *Oncogene*, **5**, 249-55.
- Matsumoto, T., Nakayama, K., Kodama, Y., Fuse, H., Nakamura, T. and Fukumoto, S. (1998) *Bone*, **22**, 89S-93S.
- Matz, M., Shagin, D., Bogdanova, E., Britanova, O., Lukyanov, S., Diatchenko, L. and Chenchik, A. (1999) *Nucleic Acids Res*, **27**, 1558-60.
- McCabe, L. R., Banerjee, C., Kundu, R., Harrison, R. J., Dobner, P. R., Stein, J. L., Lian, J. B. and Stein, G. S. (1996) *Endocrinology*, **137**, 4398-408.
- McCabe, L. R., Kockx, M., Lian, J., Stein, J. and Stein, G. (1995) *Exp Cell Res*, **218**, 255-62.
- McCarthy, T. L., Centrella, M. and Canalis, E. (1989) *Endocrinology*, **124**, 1247-53.
- McCarthy, T. L., Centrella, M., Raisz, L. G. and Canalis, E. (1991) *Endocrinology*, **128**, 2895 - 2900.
- McCauley, L. K., Koh, A. J., Beecher, C. A. and Rosol, T. J. (1997) *Endocrinology*, **138**, 5427-33.

- Meinel, L., Zoidis, E., Zapf, J., Hassa, P., Hottiger, M. O., Auer, J. r. A., Schneider, R., Gander, B., Luginbuehl, V., Bettschart-Wolfisberger, R., Illi, O. E., Merkle, H. P. and Brigitte von Rechenbergd (2003) *Bone*, **IN PRESS**.
- Melton, L. J., 3rd (1996) *Bone*, **18**, 121S-125S.
- Mendenhall, S. (2000) *Orthopedic Network News*, **11**, 7.
- Mikuni-Takagaki, Y., Suzuki, Y., Kawase, T. and Saito, S. (1996) *Endocrinology*, **137**, 2028-35.
- Mohan, S. (1993) *Growth Regul*, **3**, 67-70.
- Morey, E. R. (1979) *Bioscience*, **29**, 168 - 172.
- Morey, E. R. and Baylink, D. J. (1978) *Science*, **201**, 1138-41.
- Morey, E. R., Sabelman, E. E., Turner, R. T. and Baylink, D. J. (1979) *Physiologist*, **22**, S23-4.
- Morey-Holton, E. R. and Globus, R. K. (1998) *Bone*, **22**, 83S-88S.
- Mori, S. and Burr, D. B. (1993) *Bone*, **14**, 103-9.
- Mosekilde, L., Thomsen, J. S., Mackey, M. S. and Phipps, R. J. (2000) *Bone*, **27**, 639-45.
- Mosley, J. R. and Lanyon, L. E. (1998) *Bone*, **23**, 313-8.
- Muehleman, C., Lidtke, R., Berzins, A., Becker, J. H., Shott, S. and Sumner, D. R. (2000) *Bone*, **27**, 709-14.

- Muir, P., Johnson, K. A. and Ruau-Mason, C. P. (1999) *Bone*, **25**, 571-6.
- Muller, R. (1986) *Biochim Biophys Acta*, **823**, 207-25.
- Muller, R., Hildebrand, T. and Ruegsegger, P. (1994) *Phys Med Biol*, **39**, 145-64.
- Nakabeppu, Y., Ryder, K. and Nathans, D. (1988) *Cell*, **55**, 907-15.
- Nakayama, K., Kodama, Y., Fukumoto, S., Fuse, H., Takahashi, H., Kawaguchi, H., Sekiguchi, C., Korokawa, T., Nakamura, T., Matsumoto, T. and Fugita, T. (1996) *Journal of Bone and Mineral Research*, **11**, S150.
- Naruse, K., Mikuni-Takagaki, Y., Azuma, Y., Ito, M., Oota, T., Kameyama, K. and Itoman, M. (2000) *Biochem Biophys Res Commun*, **268**, 216-20.
- Noble, B. S., Peet, N., Stevens, H. Y., Brabbs, A., Mosley, J. R., Reilly, G. C., Reeve, J., Skerry, T. M. and Lanyon, L. E. (2003) *Am J Physiol Cell Physiol*, **284**, C934-43.
- Nudel, U., Zakut, R., Shani, M., Neuman, S., Levy, Z. and Yaffe, D. (1983) *Nucleic Acids Res*, **11**, 1759-71.
- O'Brien, F. J., Taylor, D., Dickson, G. R. and Lee, T. C. (2000) *J Anat*, **197 Pt 3**, 413-20.
- O'Brien, F. J., Taylor, D. and Lee, T. C. (2003) *J Biomech*, **36**, 973-80.
- O'Connor, J. A., Lanyon, L. E. and MacFie, H. (1982) *J Biomech*, **15**, 767-81.
- Olsson, S. and Reiland, S. (1978) *Acta Radiol Suppl.*, **358**, 299-306.

- Parfitt, A. M., Mundy, G. R., Roodman, G. D., Hughes, D. E. and Boyce, B. F. (1996) *J Bone Miner Res*, **11**, 150-9.
- Patterson-Buckendahl, P., Globus, R. K., Bikle, D. D., Cann, C. E. and Morey-Holton, E. (1989) *Am J Physiol*, **257**, R1103-9.
- Peake, M. A., Cooling, L. M., Magnay, J. L., Thomas, P. B. and El Haj, A. J. (2000) *J Appl Physiol*, **89**, 2498-507.
- Peake, M. A. and El Haj, A. J. (2003) *FEBS Lett*, **537**, 117-20.
- Pearman, A. T., Chou, W. Y., Bergman, K. D., Pulumati, M. R. and Partridge, N. C. (1996) *J Biol Chem*, **271**, 25715-21.
- Pedersen, E. A., Akhter, M. P., Cullen, D. M., Kimmel, D. B. and Recker, R. R. (1999) *Calcif Tissue Int*, **65**, 41-6.
- Piechaczyk, M., Blanchard, J. M., Marty, L., Dani, C., Panabieres, F., El Sabouty, S., Fort, P. and Jeanteur, P. (1984) *Nucleic Acids Res*, **12**, 6951-63.
- Pollack, S., Berretta, D., Steinberg, D. and Brighton, C. (1986) In *6th Trans. Biol. Repro. Growth Soc.* Philadelphia, PA.
- Popesko, P., Rajtova, V. and Horak, J. (1992) *A colour atlas of anatomy of small laboratory animals.*, Wolfe Publishing Ltd, Bratislava.
- Popoff, S. N. and Marks, S. C., Jr. (1995) *Bone*, **17**, 437-45.
- Poss, R. (1984) *Calcif Tissue Int*, **36 Suppl 1**, S155-61.

- Prendergast, P. J. and Taylor, D. (1994) *J Biomech*, **27**, 1067-76.
- Rahn, B. A. (1977) *Zeiss Information*, **22**, 36-39.
- Rambaut, P. C. and Johnston, R. S. (1979) *Acta Astronaut*, **6**, 1113-22.
- Rambaut, P. C., Leach, C. S. and Johnson, P. C. (1975) *Nutr Metab*, **18**, 62-9.
- Rambaut, P. C., Leach, C. S. and Whedon, G. D. (1979) *Acta Astronaut*, **6**, 1313-22.
- Reed, B. Y., Zerwekh, J. E., Sakhaee, K., Breslau, N. A., Gottschalk, F. and Pak, C. Y.
(1995) *J Bone Miner Res*, **10**, 1218-24.
- Roberts, C. T., Jr., Lasky, S. R., Lowe, W. L., Jr., Seaman, W. T. and LeRoith, D.
(1987) *Mol Endocrinol*, **1**, 243-8.
- Rodan, G. A. (1992) *Bone*, **13 Suppl 1**, S3-6.
- Roer, R. D. and Dillaman, R. M. (1990) *J Appl Physiol*, **68**, 13-20.
- Rogacheva, I. V., Stupakov, G. P., Volozhin, A. I., Pavlova, M. N. and Poliakov, A. N.
(1984) *Kosm Biol Aviakosm Med*, **18**, 39-44.
- Rosen, C. J., Donahue, L. R. and Hunter, S. J. (1994) *Proc Soc Exp Biol Med*, **206**, 83-102.
- Roux, W. (1895) *Gesammelte Abhandlung über Entwicklungsmechanik der Organismen*, Engelmann W., Leipzig.
- Rubin, C. T. (1984) *Calcif Tissue Int*, **36 Suppl 1**, S11-8.
- Rubin, C. T. and McLeod, K. J. (1994) *Clin Orthop*, 165-74.

- Rubin, C. T., McLeod, K. J. and Bain, S. D. (1990) *J Biomech*, **23 Suppl 1**, 43-54.
- Ruther, U., Komitowski, D., Schubert, F. R. and Wagner, E. F. (1989) *Oncogene*, **4**, 861-5.
- Sakata, T., Sakai, A., Tsurukami, H., Okimoto, N., Okazaki, Y., Ikeda, S., Norimura, T. and Nakamura, T. (1999) *J Bone Miner Res*, **14**, 1596-604.
- Sasaguri, K., Jiang, H. and Chen, J. (1998) *Arch Oral Biol*, **43**, 83-92.
- Saville, P. D. and Whyte, M. P. (1969) *Clin Orthop*, **65**, 81-8.
- Schaffler, M. B., Choi, K. and Milgrom, C. (1995) *Bone*, **17**, 521-25.
- Schaffler, M. B., Radin, E. L. and Burr, D. B. (1989) *Bone*, **10**, 207-14.
- Schiller, A. L. (1994) In *Pathology*(Eds, Rubin, E. and Farber, J. L.) J.B. Lippincott., Philadelphia.
- Schneider, V., Oganov, V., LeBlanc, A., Rakmonov, A., Taggart, L., Bakulin, A., Huntoon, C., Grigoriev, A. and Varonin, L. (1995) *Acta Astronaut*, **36**, 463-6.
- Schonau, E., Wentzlik, U., Michalk, D., Scheidhauer, K. and Klein, K. (1993) *Lancet*, **342**, 689-90.
- Schonau, E., Wentzlik, U., Radermacher, A., Keuth, B., Michalk, D. and Scheidhauer, K. (1994) *Lancet*, **343**, 1635-6.
- Schule, R., Umesono, K., Mangelsdorf, D. J., Bolado, J., Pike, J. W. and Evans, R. M. (1990) *Cell*, **61**, 497-504.

- Seeman, E. (1997) *J Bone Miner Res*, **12**, 509-21.
- Sessions, N. D., Halloran, B. P., Bikle, D. D., Wronski, T. J., Cone, C. M. and Morey-Holton, E. (1989) *Am J Physiol*, **257**, E606-10.
- Shaw, S. R., Vailas, A. C., Grindeland, R. E. and Zernicke, R. F. (1988) *Am J Physiol*, **254**, R78-83.
- Shaw, S. R., Zernicke, R. F., Vailas, A. C., DeLuna, D., Thomason, D. B. and Baldwin, K. M. (1987) *J Biomech*, **20**, 225-34.
- Skerry, T. M., Bitensky, L., Chayen, J. and Lanyon, L. E. (1989) *J Bone Miner Res*, **4**, 783-8.
- Slemenda, C., Hui, S. L., Longcope, C. and Johnston, C. C. (1987) *J Clin Invest*, **80**, 1261-9.
- Slootweg, M. C., Most, W. W., van Beek, E., Schot, L. P., Papapoulos, S. E. and Lowik, C. W. (1992) *J Endocrinol*, **132**, 433-8.
- Smith, M. C., Jr., Rambaut, P. C. and Stadler, C. R. (1977) *Life Sci Space Res*, **15**, 193-7.
- Spengler, D. M., Morey, E. R., Carter, D. R., Turner, R. T. and Baylink, D. J. (1983) *Proc Soc Exp Biol Med*, **174**, 224-8.
- Stein, G. S. and Lian, J. B. (1993) *Endocr Rev*, **14**, 424-42.
- Stover, S. M., Pool, R. R., Martin, R. B. and Morgan, J. P. (1992) *J Anat*, **181 (Pt 3)**, 455-69.

- Stupakov, G. P., Kazeikin, V. S., Kozlovskii, A. P. and Korolev, V. V. (1984) *Kosm Biol Aviakosm Med*, **18**, 33-7.
- Suttie, J. W. (1985) *Annu Rev Biochem*, **54**, 459-77.
- Tanaka, S. M., Li, J., Duncan, R. L., Yokota, H., Burr, D. B. and Turner, C. H. (2003) *J Biomech*, **36**, 73-80.
- Taylor, D., O'Reilly, P., Vallet, L. and Lee, T. C. (2003) *J Biomech*, **36**, 1103-9.
- Uhthoff, H. K. and Finnegan, M. (1983) *J Bone Joint Surg Br*, **65**, 66-71.
- Uhthoff, H. K. and Jaworski, Z. F. (1978) *J Bone Joint Surg Br*, **60-B**, 420-9.
- Vailas, A. C., Deluna, D. M., Lewis, L. L., Curwin, S. L., Roy, R. R. and Alford, E. K. (1988) *J Appl Physiol*, **65**, 373-6.
- van der Meulen, M. C., Morey-Holton, E. R. and Carter, D. R. (1995) *J Orthop Res*, **13**, 700-7.
- Vico, L., Bourrin, S., Very, J. M., Radziszowska, M., Collet, P. and Alexandre, C. (1995) *J Appl Physiol*, **79**, 1426-33.
- Vico, L., Collet, P., Guignandon, A., Lafage-Proust, M. H., Thomas, T., Rehaillia, M. and Alexandre, C. (2000) *Lancet*, **355**, 1607-11.
- Vogel, J. M. and Anderson, J. T. (1972) *J Nucl Med*, **13**, 13-8.
- Vogel, J. M. and Whittle, M. W. (1976) *Aviat Space Environ Med*, **47**, 396-400.
- Wang, L., Banu, J., McMahan, C. A. and Kalu, D. N. (2001) *Bone*, **29**, 141-8.

- Wang, Z. Q., Ovitt, C., Grigoriadis, A. E., Mohle-Steinlein, U., Ruther, U. and Wagner, E. F. (1992) *Nature*, **360**, 741-5.
- Ward, F. O. (1876) *Outlines of human osteology*, Henry Renshaw London.
- Warden, S. J., Favaloro, J. M., Bennell, K. L., McMeeken, J. M., Ng, K. W., Zajac, J. D. and Wark, J. D. (2001) *Biochem Biophys Res Commun*, **286**, 443-50.
- Watson, J. D., Gilman, M., Witkowski, J. and Szoller, M. (1994) *Recombinant DNA*, Scientific American Press, New York.
- Weinbaum, S., Cowin, S. and Zeng, Y. (1992) *Advances in Bioengineering*, **22**, 25 - 28.
- Westerlind, K. C., Morey-Holton, E., Evans, G. L., Tanner, S. J. and Turner, R. T. (1996) *Journal of Bone and Mineral Research*, **11**, S377.
- Westerlind, K. C., Morey-Holton, E. and Turner, R. T. (1994) In *40th annual meeting, Orthopaedic Research Society*, pp. 561.
- Wolff, J. (1892) *Das Gesetz der Transformation der Knochen*, Hirshwald, Berlin.
- Woo, S. L., Kuei, S. C., Amiel, D., Gomez, M. A., Hayes, W. C., White, F. C. and Akeson, W. H. (1981) *J Bone Joint Surg Am*, **63**, 780-7.
- Wronski, T. J. and Morey, E. R. (1983a) *Med Sci Sports Exerc*, **15**, 410-4.
- Wronski, T. J. and Morey, E. R. (1983b) *Am J Physiol*, **244**, R305-9.
- Wronsky, T. J. and Morey-Holton, E. R. (1987) *Aviation, Space and environmental medicine*, **January**, 63 - 68.

Yagodovsky, V. S., Triftanidi, L. A. and Gorokhova, G. P. (1976) *Aviat. Space Environ. Med.*, **47**, 734 - 738.

Yamaguchi, N., Chiba, M. and Mitani, H. (2002) *Arch Oral Biol*, **47**, 465-71.

Yoon, K. G., Rutledge, S. J., Buenaga, R. F. and Rodan, G. A. (1988) *Biochemistry*, **27**, 8521-6.

Zerial, M., Toschi, L., Ryseck, R. P., Schuermann, M., Muller, R. and Bravo, R. (1989) *Embo J*, **8**, 805-13.

Zhu, Y. Y., Machleder, E. M., Chenchik, A., Li, R. and Siebert, P. D. (2001) *Biotechniques*, **30**, 892-7.

Zhumabayeva, B., Diatchenko, L., Chenchik, A. and Siebert, P. D. (2001) *Biotechniques*, **30**, 158-63.

Appendices

Appendix 1 Raw Morphological Data.....	225
Appendix 2 Torsion testing Data.....	235
Appendix 3 Gene expression Data.....	250

Appendix 1 Raw Morphological Data

A1.1 Body weight Data

Group	Day	Suspended	Control
0 days	0		137
	0		145
	0		149
	0		148
	0		144
	0		145
3 days	0	145	155
	0	133	143
	0	140	147
	0	156	170
	0	148	143
	0	146	160
	3	174	180
	3	159	170
	3	165	174
	3	175	195
	3	180	163
	3	160	179
7 days	0	145	132
	0	143	146
	0	146	152
	0	148	136
	0	149	120
	0	128	128
	7	180	180
	7	183	183
	7	193	193
	7	178	191
	7	179	173
	7	165	183
14 days	0	150	127
	0	133	150
	0	132	136
	0	133	146
	0	135	127
	0	130	140
	14	207	210
	14	193	190
	14	200	203
	14	199	219
	14	204	198
	14	196	212

Table A.1 Body weight

A1.2 Bone Length and weight Data

	Femora				Humeri			
	Length		Weight		Length		Weight	
Time	Control length	Suspended Length	Control weight	Suspended weight	Control length	Suspended Length	Control weight	Suspended weight
0	27	27	0.433	0.433	21.3	21.3	0.192	0.192
0	26.7	26.7	0.445	0.445	21	21	0.205	0.205
0	26.8	26.8	0.44	0.44	21	21	0.217	0.217
0	27.2	27.2	0.465	0.465	21.5	21.5	0.23	0.23
0	27.1	27.1	0.45	0.45	21.8	21.8	0.24	0.24
0	27.5	27.5	0.46	0.46	21.6	21.6	0.23	0.23
3	28.1	27.9	0.477	0.48	21.9	21.7	0.224	0.21
3	28	27.5	0.481	0.32	21.9	21.4	0.23	0.205
3	27.5	24.5	0.53	0.4	21.4	21.8	0.2	0.257
3	27.9	28.2	0.495	0.37	22.4	22	0.24	0.25
3	27.9	26.7	0.48	0.44	21.8	21.5	0.23	0.23
3	28.7	29	0.535	0.51	22.4	21.5	0.25	0.24
7	28.4	29.1	0.48	0.53	21.8	22.2	0.23	0.27
7	29.1	29.4	0.54	0.55	22.7	22.3	0.29	0.273
7	29.1	29.8	0.56	0.53	22.9	22.6	0.27	0.294
7	29.4	29	0.55	0.55	22.2	21.6	0.272	0.267
7	27.6	29	0.5	0.45	21.6	21.8	0.253	0.235
7	29	30	0.56	0.55	22.4	22.5	0.283	0.281
14	29.6	29	0.51	0.48	22.7	22.2	0.256	0.27
14	29.3	31	0.46	0.58	23.2	22.7	0.272	0.25
14	29.6	30	0.53	0.5	23.15	22.6	0.29	0.27
14	30.2	31.8	0.46	0.52	23.6	23.1	0.26	0.29
14	30	30	0.49	0.5	23.3	23.7	0.28	0.28
14	29.7	29.6	0.48	0.51	22.9	22.7	0.29	0.288

Table A.2 Humeri and Femora bone length and weight

Eliminated from Analysis

A1.3 Humeral morphological Data

DAYS	Control periosteal area	Suspended periosteal. area	Control endosteal. area	Suspended endosteal. area	Control Total area	Suspended Total area
0	3676560		1400966		2275594	
0	Elim		Elim		Elim	
0	3404841		895952		2508890	
0	3462987		1086771		2376215	
0	3531623		891660		2639963	
0	3461624		880249		2581375	
3	4284171	4873592	1874540	2420293	2409631	2453299
3	3651047	Elim	1383287	Elim	2267760	Elim
3	3610035	4085346	1281474	1818336	2328562	2267010
3	4227831	3793872	1557927	1670913	2669904	2122959
3	3900182	3604381	1595532	1409822	2304650	2194559
3	4185423	3876201	1829986	1570325	2355437	2305876
7	3998214	4322491	1832643	1773237	2165572	2549254
7	4519135	4740679	1798409	1949784	2720726	2790895
7	4192678	4056495	2069685	1656129	2122993	2400366
7	4164679	4688597	1774702	1865854	2389977	2822744
7	4151905	4445049	1859859	1472940	2292046	2972109
7	4090115	4479759	1213416	1536978	2876699	2942781
14	3995251	4995298	1537523	2443626	2457728	2551672
14	4320209	4879314	1778176	2019953	2542033	2859361
14	4783189	4407955	2052654	2006805	2730536	2401149
14	4076660	5337083	1452605	2356050	2624056	2981033
14	5000918	4807715	2376692	2077349	2624226	2730366
14	4506225	4338637	1609804	1851036	2896421	2487601

Table A.3 Humeral sectional area data

DAYS	Control periosteal circularity	Suspended periosteal circularity	Control endosteal circularity	Suspended endosteal circularity	Control periosteal elongation	Suspended periosteal elongation	Control endosteal elongation	Suspended endosteal elongation
0	0.844		0.869		1.251		1.276	
0	Elim		Elim		Elim		Elim	
0	0.854		0.474		1.286		1.499	
0	0.855		0.642		1.14		1.178	
0	0.866		0.427		1.308		1.315	
0	0.929		0.899		1.159		1.25	
3	0.873	0.928	0.444	0.536	1.305	1.094	1.34	1.093
3	0.899	0.923	0.668	0.825	1.13	1.134	1.069	1.088
3	0.846	Elim	0.534	Elim	1.297	Elim	1.266	Elim
3	0.877	0.89	0.683	0.578	1.172	1.123	1.268	1.106
3	0.901	0.945	0.885	0.884	1.257	1.102	1.288	1.132
3	0.902	0.881	0.531	0.827	1.269	1.332	1.234	1.376
7	0.808	0.893	0.818	0.784	1.264	1.184	1.22	1.25
7	0.925	0.906	0.861	0.666	1.203	1.204	1.223	1.152
7	0.907	0.878	0.796	0.485	1.204	1.242	1.105	1.352
7	0.896	0.873	0.286	0.435	1.274	1.261	1.352	1.287
7	0.819	0.88	0.883	0.71	1.276	1.239	1.176	1.12
7	0.893	0.9	0.719	0.522	1.19	1.185	1.141	1.152
14	0.852	0.892	0.483	0.412	1.39	1.211	1.365	1.188
14	0.872	0.904	0.398	0.71	1.265	1.259	1.165	1.21
14	0.843	0.868	0.434	0.759	1.443	1.4	1.45	1.433
14	0.887	0.93	0.301	0.777	1.244	1.118	1.204	1.256
14	0.864	0.914	0.543	0.839	1.352	1.193	1.533	1.172
14	0.862	0.878	0.59	0.841	1.331	1.237	1.381	1.199

Table A.4 Humeral and elongation data

* Following histological analysis Basal2 and 3Day2C were eliminated from the humeral statistical analysis, as they were not mid-diaphyseal sections.

Time [Days]	Control periosteal Bone Formation Index	Control endosteal Bone Formation Index	Control total Bone Formation Index	Suspended periosteal Bone Formation Index	Suspended endosteal Bone Formation Index	Suspended total Bone Formation Index
3	8.3	3.8	12.2	6.0	4.4	10.4
3	6.0	0.7	6.7	4.3	3.1	7.4
3	5.1	3.0	8.2	4.4	1.7	6.1
3	2.3	0.0	2.3	6.7	3.2	9.9
3	6.8	2.3	9.1	8.6	3.5	12.1
7	13.7	3.8	17.5	13.0	4.9	17.9
7	24.8	2.2	27.1	16.0	4.2	20.2
7	6.8	5.3	12.1	16.4	6.5	22.9
7	22.0	1.9	23.9	22.5	5.4	27.9
7	16.0	0.0	16.0	20.6	7.5	28.1
7	21.7	0.0	21.7			
14	21.0	0.0	21.0	12.4	10.5	23.0
14	14.7	10.0	24.7	29.7	6.4	36.1
14	19.4	4.5	23.9			

Table A.5 Humeral Bone formation index data

Animal & slide	Control						Suspended					
	Time	crack length	Section C.S.A.	Crack Density	Surface Density	Location	Animal & slide	crack length	Section C.S.A.	Crack Density	Surface Density	Location
3d 1c 2	3	251.77	2409631	1.660	248.677	E	3d s1 3	177.66	2453299	0.815	118.188	E
3d 1c 2 #2	3	174.39	2267760			E	3d s1 3 #2	112.29				E
3d 1c 2 #3	3	53.09	2328562			E	3d s1 2	91.39		0.408	37.252	E
3d 1c 2 #4	3	119.97	2669904			E	3d s3 2	207.01	2267010	0.441	91.314	E
3d 1c 4	3	169.73	2304650	1.302	196.212	E	3d 3s	155.47		0.441	68.579	E
3d 1c 4 #2	3	162.59	2355437			E	3d 6s	354.69	2305876	0.867	281.854	E
3d 1c 4 #3	3	119.88				E	3d 6s #2	295.23				E
							3d s6 2	139.56		0.867	120.969	E
							3d s6 2 #2	139.38				E
7d 1c 3	7	255.09	2165572	0.462	117.793	E	7d 3s	155.42	2400366	0.417	64.748	E
7d 2c	7	164.36	2720726	0.368	60.410	E	7d 4s 3	188.82	2822744	0.354	66.892	P
7d 2c 2	7	163.41		0.735	120.012	E						
7d 2c 2 #2	7	163.11				E						
7d 3c 3	7	140.62	2122993	0.471	66.237	E						
14d 1c 2	14	139.66	2457728	0.407	56.825	E	14d 2s	128.34	2859361	0.350	44.884	E
14d 1c 4	14	170.05		0.407	69.190	P	14d 3s	158.55	2401149	0.416	66.031	P
14d 2c 3	14	360.55	2542033	0.393	141.835	P	14 3s 1	607.31		0.416	252.925	E
14d 3c 1	14	76.8	2730536	0.732	80.995	E	14 4s 2	288.18	2981033	0.335	96.671	P
14d 3c 1 #2	14	144.36				E	14d 6s	159.11	2487601	0.402	63.961	E
14d 3c 2	14	161.97		0.732	106.375	E	14d 6s 1	404.33		1.608	388.680	E
14d 3c 2 #2	14	128.49				M	14d 6s 1 #2	130.13				E
14d 3c 3	14	173.29		0.732	99.922	E	14d 6s 1 #3	268.92				E
14d 3c 3 #2	14	99.55				E	14d 6s 1 #4	163.5				E
14d 3c 4	14	91.79			33.616	E						
14d 5c	14	61.46	2624226	0.381	23.420	P						
14 6c 2	14	240.04	2896421	0.345	82.875	E						

Table A.6 Humeral microdamage data

Key code:

3d4c2 #1 = 3 day control number 4, slide number 2, crack number 1

E = Endosteal, P = Periosteal, M = middle

A1.4 Femoral morphological Data

Time [Days]	Control Periosteal Area	Suspended Periosteal Area	Control Endosteal Area	Suspended Endosteal Area	Control Total Area	Suspended Total Area	Control Total Area (Corrected)	Suspended Total Area (Corrected)
0	6860810		3768310		3092500		3092500	
0	6355870		3202010		3153860		3153860	
0	6786350		3849760		2936590		2928559	
0	7926620		4409110		3517510		3483210	
0	7717520		4619910		3097610		3097610	
3	Elim	8201520	Elim	4760910	Elim	3440610	Elim	3440610
3	6971280	7576570	3350020	4298540	3621260	3278030	3516927	3178951
3	7362990	6550920	4153850	3479640	3209140	3071280	3209140	2932556
3	7635406.58	7221370	4154389.57	4185680	3481017	3035690	3481017	2997375
3	8834680	6919490	5435150	3683360	3399530	3236130	3399530	3196826
3	9000600	7869270	5253810	4054830	3746790	3814440	3644879	3720445
7	7683060	8128230	4082100	4534600	3600960	3593630	3493215	3500078
7	8621950	9519740	4082160	5974250	4539790	3545490	4205330	3459717
7	8829460	8385960	4392230	4356640	4437230	4029320	4113313	3669102
7	9902850	7769930	6238360	4160870	3664490	3609060	3661624	3509496
7	Elim	7563370	Elim	4185610	Elim	3377760	Elim	3314914
7	8771150	9516020	4635120	5986190	4136030	3529830	3988367	3493426
14	8284320	9236560	4407100	6255420	3877220	2981140	3739690	2981140
14	9288930	10500600	5916250	7187700	3372680	3312900	3372680	3312900
14	9103770	9448360	4601510	5731740	4502260	3716620	4342929	3682229
14	7829150	9787460	3889670	6103900	3939480	3683560	3876430	3610650
14	9248910	9778080	5513690	5536350	3735220	4241730	3735220	4241730
14	8711240	10089900	5080660	6772170	3630580	3317730	3621334	3317730

Table A.7 Femoral cross sectional area data

Time [Days]	Control Periosteal Circularity	Suspended Periosteal Circularity	Control Endosteal Circularity	Suspended Endosteal Circularity	Control Periosteal Elongation	Suspended Periosteal Elongation	Control Endosteal Elongation	Suspended Endosteal Elongation
0	0.94		0.93		1.22		1.29	
0	0.93		0.80		1.24		1.30	
0	0.93		0.90		1.20		1.26	
0	0.95		0.80		1.27		1.34	
0	0.94		0.89		1.24		1.29	
3	Elim	0.88	Elim	0.86	Elim	1.28	Elim	1.40
3	0.85	0.83	0.64	0.73	1.35	1.38	1.38	1.53
3	0.90	0.91	0.90	0.88	1.31	1.28	1.37	1.41
3	0.79	0.92	0.92	0.86	0.86	1.24	1.39	1.32
3	0.92	0.92	0.75	0.73	1.34	1.19	1.47	1.35
3	0.86	0.88	0.75	0.84	1.38	1.33	1.41	1.41
7	0.93	0.93	0.83	0.79	1.25	1.34	1.34	1.51
7	0.89	0.92	0.85	0.66	1.28	1.36	1.43	1.50
7	0.89	0.93	0.87	0.63	1.26	1.32	1.44	1.32
7	0.90	0.92	0.73	0.44	1.27	1.31	1.39	1.47
7	Elim	0.91	Elim	0.82	Elim	1.24	Elim	1.37
7	0.83	0.91	0.73	0.79	1.29	1.27	1.47	1.43
14	0.86	0.92	0.77	0.84	1.30	1.38	1.47	1.45
14	0.93	0.90	0.86	0.59	1.36	1.49	1.48	1.64
14	0.85	0.92	0.80	0.86	1.29	1.28	1.37	1.36
14	0.82	0.94	0.60	0.76	1.28	1.23	1.43	1.33
14	0.92	0.90	0.89	0.67	1.38	1.30	1.43	1.49
14	0.89	0.92	0.85	0.87	1.35	1.46	1.49	1.54

Table A.8 Femoral microdamage data

* Following histological analysis 3Day1C and 7Day5C were eliminated from the analysis, as they were not mid-diaphyseal sections.

Time [Days]	Control periosteal Bone Formation Index	Control endosteal Bone Formation Index	Control total Bone Formation Index	Suspended periosteal Bone Formation Index	Suspended endosteal Bone Formation Index	Suspended total Bone Formation Index
3	16.7	1.4	18.0	9.9	0.0	9.9
3	9.3	3.8	13.0	8.4	0.0	8.4
3	10.5	2.9	13.4	5.2	0.0	5.2
3	11.3	4.3	15.6	8.9	1.7	10.6
3	16.2	0.0	16.2	9.8	0.0	9.8
3				9.5	0.0	9.5
7	17.8	4.9	22.7	16.5	3.4	19.9
7	25.8	5.1	30.9	20.3	6.2	26.5
7	24.9	1.6	26.6	21.2	2.8	24.0
7	13.8	12.3	26.1	10.6	11.6	22.2
7	24.0	3.6	27.6			
14	18	8.4	26	25	1.2	26
14	13	12.0	25	22	18.0	40
14	16	10.6	26			

Table A.9 Femoral Bone formation index data

Control							Suspended					
Animal & slide	Time	Crack length	Section C.S.A	Crack Density	Surface Density	Location	Animal & slide	Crack length	Section C.S.A	Crack Density	Surface Density	Location
bc1 2	0	505.8	3092500	0.323	163.557	E						
bc2 2	0	253.6	3153860	0.317	80.406	E						
bc2 3	0	131.6	2928559	0.341	44.920	E						
bc5 1	0	251	3483210	0.574	113.631	E						
bc5 1 #2	0	144.8	3097610			E						
bc5 3	0	209.7		0.574	119.350	E						
bc5 3 #2	0	160				E						
3d 2c 3	3	126.9	3209140	0.312	39.543	E	3d 1s 2	113.9	3440610	0.291	33.105	E
3d 3c 2	3	287.8	3481017	0.287	82.677	E	3d 2s 2	317	3178951	0.629	198.179	E
3d 6c 1	3	196.9	3644879	0.549	86.313	E	3d 2s 2 #2	313				E
3d 6c 1 #2	3	117.7				E	3d 4s 2	143.5	2997375	0.667	91.080	E
3d 6c 2	3	96.2		0.274	26.393	E	3d 4s 2 #2	129.5				E
3d 6c 3	3	103.5		0.274	28.396	E	3d 5s 1	185.2	3196826	0.626	81.049	P
							3d 5s 1 #2	73.9				P
							3d 6s 1	267.8	3720445	0.269	71.981	P
7d 1c 1	7	323.3	3493215	0.286	92.537	E	7d 2s 3	194.7	3459717	0.578	146.385	E
7d 2c 1	7	158.4	4205330	0.238	37.666	M	7d 2s 3 #2	311.8				E
7d 3c 1	7	133.7	4113313	0.486	73.469	E	7d 3s 2	92.9	3669102	0.545	43.735	E
7d 3c 1 #2	7	168.5				E	7d 3s 2 #2	67.6				E
7d 3c 3	7	192.5	4113313	0.243	46.799	M	7d 4s 1	124.5	3509496	0.285	35.475	E
7d 6c	7	125.6	3988367	0.251	31.492	E	7d 5s 2	78.5	3314914	0.603	53.148	E
							7d 5s 2	97.7				E
							7d 6s 2	147.2	3493426	0.286	42.136	E
14d 1c	14	138.9	3739690	0.267	37.142	E	14d 1s 2	352.6	2981140	0.335	118.277	E
14d 2c	14	271	3372680	0.297	80.352	E	14d 2s 2	346.3	3312900	0.302	104.531	E
14d 5c	14	288.9	3735220	0.268	77.331	E	14d 3s 1	104.3	3682229	0.815	117.157	E
14d 6c 2	14	92	3621334	0.276	25.405	E	14d 3s 1 #2	137.2				M
							14d 3s 1 #3	189.9				M
							14d 5s 1	100.6	4241730	0.235	23.705	E

Table A.10 Femoral microdamage data

Key code:

3d4c2 #1 = 3 day control number 4, slide number 2, crack number 1

E = Endosteal, P = Periosteal, M = middle

Appendix 2 Torsional Data

A2.1 Matlab Program

Creating the matrix of possible ellipse major and minor axes

```
n=1;
res=[];
%remember to make n the right value for the input matrix
%also consider using a smaller value for the increment
while n<127;
a=1;
b=1;
ao=1;
bo=1;
outer=[];
inner=[];

% loop for outer variable matrix
while a<3.1
    while (b<3.1)
        outer=[outer;a b];
        b=b+0.125;
    end
    b=1;
    a=a+0.125;
end
%redo loop for inner variable matrix
while ao<3.1
    while (bo<3.1)
        inner=[inner;ao bo];
        bo=bo+0.125;
    end
    bo=1;
    ao=ao+0.125;
end
%now make sure a>b
z=1;
outer2=[];
while z<length(outer);
    a=outer(z,1);
```

```

    b=outer(z,2);
    if (a>b)& (a/b<2.5);
        outer2=[outer2; a b];
        z=z+1;
    else
        z=z+1;
    end
end
%clear outer
clear outer;

%now make sure ao>bo
y=1;
inner2=[];
while y<length(inner);
    ao=inner(y,1);
    bo=inner(y,2);
    if (ao>bo)& (ao/bo<2.5);
        inner2=[inner2; ao bo];
        y=y+1;
    else
        y=y+1;
    end
end
%clear inner
clear inner;
%now make sure that a/b=ao/bo
combined=[];
q=0;
while q<(length(outer2));
    r=1;
    q=q+1;
    while r<(length(inner2)+1);
        a=outer2(q,1);
        b=outer2(q,2);
        ao=inner2(r,1);
        bo=inner2(r,2);
        x=(abs((a/b)-(ao/bo)));
        if (x<0.1);
            combined=[combined; a b ao bo];

```



```

    r=r+1;
else
    r=r+1;
end
end;
end;
combined;
%now make sure that a>ao and b>bo
combined2=[];
f=1;
while f<(length(combined));
a=combined(f,1);
b=combined(f,2);
ao=combined(f,3);
bo=combined(f,4);
if (a>ao) & (b>bo);
    combined2=[combined2; a b ao bo];
    f=f+1;
else
    f=f+1;
end;
end;
combined2;
% clear all the unnecessary matrices
clear inner outer inner2 outer2 combined;
% check accuracy
load matlabctdata.txt;
M=matlabctdata;
ipct=M(n,1);
area=M(n,2);
% now calculate a value for Ip
l=length(combined2);
ipcalc=[100,100,100,100,100,100,100,100,100,100,1000];
x=1;
while (x<l);
    a=combined2(x,1);
    b=combined2(x,2);
    ao=combined2(x,3);
    bo=combined2(x,4);
    ip=(0.25*pi*(a*b)*(a^2+b^2))-(0.25*pi*(ao*bo)*(ao^2+bo^2));

```

```

areacalc=(pi*a*b)-(pi*ao*bo);
k=((pi*a^3*b^3)*(1-(ao/a)^4))/(a^2+b^2);
iperror=((abs(ipct-ip))/ipct)*100;
Aerror=((abs(area-areacalc))/area)*100;
error=(iperror + Aerror)/2;
t=ipcalc(1,11);
    if (error<t);
        ipcalc=[a b ao bo ip ipct iperror areacalc area Aerror error k];
        x=x+1;
    else
        x=x+1;
    end;
end;
res=[res; ipcalc];
% clear combined2
clear combined2

n=n+1;
end;
save('method2results','res','-ascii');

```


Refinement iterative Program

```
n=1;
res=[];
%check the n value.
while n<127;

%load up the first run data
load method2results.txt;
M=method2results;
ipct=M(n,6);
area=M(n,9);
a=method2results(n,1)-0.12;
b=method2results(n,2)-0.12;
ao=method2results(n,3)-0.12;
bo=method2results(n,4)-0.12;
outer=[];
inner=[];

% loop for outer variable matrix
j=1;
s=1;
while j<9;
    while (s<9);
        outer=[outer;a b];
        b=b+0.03;
        s=s+1;
    end
    b=method2results(n,2)-0.12;
    a=a+0.03;
    j=j+1;
    s=1;
end
%redo loop for inner variable matrix
q=1;
p=1;
while q<9;
    while (p<9);
        inner=[inner;ao bo];
        bo=bo+0.03;
```

```

    p=p+1;
end
bo=method2results(n,4)-0.12;
ao=ao+0.03;
q=q+1;
p=1;
end
%now make sure a>b
z=1;
outer2=[];
while z<length(outer);
    a=outer(z,1);
    b=outer(z,2);
    if (a>b)& (a/b<2.5);
        outer2=[outer2; a b];
        z=z+1;
    else
        z=z+1;
    end
end
%clear outer
clear outer;

%now make sure ao>bo
y=1;
inner2=[];
while y<length(inner);
    ao=inner(y,1);
    bo=inner(y,2);
    if (ao>bo)& (ao/bo<2.5);
        inner2=[inner2; ao bo];
        y=y+1;
    else
        y=y+1;
    end
end
%clear inner
clear inner;
%now make sure that a/b=ao/bo
combined=[];

```



```

q=0;
while q<(length(outer2));
r=1;
q=q+1;
while r<(length(inner2)+1);
a=outer2(q,1);
b=outer2(q,2);
ao=inner2(r,1);
bo=inner2(r,2);
x=(abs((a/b)-(ao/bo)));
if (x<0.1);
    combined=[combined; a b ao bo];
    r=r+1;
else
    r=r+1;
end
end;
end;
combined;
%now make sure that a>ao and b>bo
combined2=[];
f=1;
while f<(length(combined));
a=combined(f,1);
b=combined(f,2);
ao=combined(f,3);
bo=combined(f,4);
if (a>ao) & (b>bo);
    combined2=[combined2; a b ao bo];
    f=f+1;
else
    f=f+1;
end;
end;
combined2;
% clear all the unnecessary matrices
clear inner outer inner2 outer2 combined;
% check accuracy

% now calculate a value for Ip

```

```

l=length(combined2);
ipcalc=[100,100,100,100,100,100,100,100,100,100,1000];
x=1;
while (x<1);
    a=combined2(x,1);
    b=combined2(x,2);
    ao=combined2(x,3);
    bo=combined2(x,4);
    ip=(0.25*pi*(a*b)*(a^2+b^2))-(0.25*pi*(ao*bo)*(ao^2+bo^2));
    areacalc=(pi*a*b)-(pi*ao*bo);
    k=((pi*a^3*b^3)*(1-(ao/a)^4))/(a^2+b^2);
    iperror=((abs(ipct-ip))/ipct)*100;
    Aerror=((abs(area-areacalc))/area)*100;
    error=(iperror + Aerror)/2;
    t=ipcalc(1,11);
    if (error<t);
        ipcalc=[a b ao bo ip ipct iperror areacalc area Aerror error k];
        x=x+1;
    else
        x=x+1;
    end;
end;
res=[res; ipcalc];
% clear combined2
clear combined2;

n=n+1;
end;
res;
% save the result file as an ascii file of the form
%[a b ao bo ip ipct iperror areacalc area Aerror error k];
00
save('refinedresults','res','-ascii');

```


A2.2 Raw pQCT Data

Time [days]	Control area Scan 1	Suspended area scan 1	Control area scan 2	Suspended area scan 2	Control area scan 3	Suspended area scan 3
0	10.53		4.03		3.82	
0	7.4		3.91		4.03	
0	5.65		3.98		4.59	
0	4.5		4.09		4.32	
0	16.18		5.06		4.5	
0	4.3		3.85		4.66	
3	11.63	7.02	4.81	4.48	4.52	4.72
3	5.11	6.23	4.21	4.09	4.52	4.18
3	10.33	4.36	4.39	4.12	4.5	4.75
3	9.49	7.22	4.45	4.36	4.45	4.21
3	10.84	6.57	4.43	4.16	4.9	4.27
3	7.06	7.27	4.68	4.7	4.99	4.75
7	7.9	5.58	3.94	4.12	4.57	4.63
7	5.89	6.48	4.81	4.68	5.08	4.95
7	7.9	5.42	4.36	4.5	4.79	4.54
7	7.33	4.43	4.66	5.17	4.9	5.71
7	6.34	5.71	4.14	4.32	4.5	4.63
7	6.03	7.6	4.99	4.63	5.4	5.15
14	4.63	10.78	5.06	4.43	4.97	4.93
14	4.57	5.8	4.66	4.75	4.88	5.22
14	6.25	5.78	4.99	4.3	6.19	4.5
14	12.67	5.47	4.66	4.34	5.11	5.38
14	22.77	5.06	5.13	4.57	5.2	5.08
14	4.63	4.34	4.61	4.41	5.4	4.41

Table A.11 Femoral pQCT area data

Scan 1 Distal, scan 2: mid-diaphyseal, scan 3: proximal

Time [days]	Control Ip Scan 1	Suspended Ip scan 1	Control Ip scan 2	Suspended Ip scan 2	Control Ip scan 3	Suspended Ip scan 3
0	34.09		7.91		4.8	
0	19.18		7.09		5.54	
0	13.6		6.08		6.24	
0	9.9		6.48		5.68	
0	52.22		11.54		7.75	
0	8.06		5.49		6.36	
3	48.66	25.35	12.37	9.83	7.93	8.33
3	14.91	21.54	7.81	8.55	7.18	6.45
3	38.38	9.69	9.9	7.87	7.34	8.32
3	39.25	30.86	11.04	10.63	7.6	6.78
3	44.9	23.66	11.19	9.16	8.56	6.7
3	33.05	28.32	12.63	11.45	9.56	8.18
7	28.43	22.12	9.17	9.93	8.06	8.19
7	21.41	28.57	10.84	12.77	9.58	9.98
7	31.15	21.39	10.76	10.82	8.79	8.48
7	28.6	11.07	11.91	9.05	9.8	11.17
7	24.09	19.77	9.53	9.6	8.3	7.66
7	21.33	29.62	11.35	11.42	9.78	9.06
14	11.46	39.41	8.88	12	9.05	9.18
14	10.96	24.08	12.16	11.97	9.28	10.87
14	22.49	25.2	11.34	11.26	13.52	8.7
14	47.85	24.16	12.15	12.29	9.31	12.17
14	96.79	11.68	14.85	12.58	10.21	10.11
14	12.18	11.95	11.28	10.27	10.91	8.21

Table A.12 Femoral pQCT Ip data

Scan 1 Distal, scan 2: mid-diaphyseal, scan 3: proximal

Time [days]	Control BMD Scan 1	Suspended BMD scan 1	Control BMD scan 2	Suspended BMD scan 2	Control BMD scan 3	Suspended BMD scan 3
0	384.3		366.8		547.2	
0	424.1		395.9		529.4	
0	419.1		473.2		596.8	
0	368.1		472.1		627.1	
0	471.9		388.9		486.3	
0	400.3		506.2		641.6	
3	329.4	322.8	315.4	347.3	456.7	471.3
3	316.5	295.4	411.7	344.6	529.7	472.5
3	362.8	336.6	335.9	399.3	452.3	505.4
3	314.8	261.3	312.5	308.7	466.7	454.7
3	341.8	273.8	290.6	313.6	452.5	482.5
3	268.1	293.9	311.6	335.1	466.2	476
7	318.8	239.1	285.9	301.1	466	465.3
7	289.8	227.3	380.6	295.6	502.3	450.9
7	289.2	239.8	302.8	326.8	476.9	451.2
7	319.6	291.3	328.3	485.9	441.5	483.8
7	265.3	264.5	326.9	325.3	448.8	517.3
7	301.3	298.7	382.8	323	553.7	512.4
14	351.7	325.7	504.3	257.1	499.3	446.1
14	352.7	239	311.4	338.6	474.5	488.8
14	316.9	230.9	412.3	295.2	513.8	445.2
14	358.9	219.1	317.6	273.6	508.9	453.3
14	456.1	377.8	326.8	286.1	479.8	489
14	323.2	273.1	350	340	509.4	450.5

Table A.13 Femoral pQCT BMD data

Scan 1 Distal, scan 2: mid-diaphyseal, scan 3: proximal

Time [days]	Control BMC Scan 1	Suspended BMC scan 1	Control BMC scan 2	Suspended BMC scan 2	Control BMC scan 3	Suspended BMC scan 3
0	5.91		2.95		3.18	
0	4.81		2.98		3.26	
0	4.34		3.14		3.76	
0	3.26		3.27		3.77	
0	8.34		3.67		3.62	
0	3.15		3.22		4.03	
3	6.41	4.69	3.19	3.09	3.48	3.59
3	3.55	3.93	3.18	2.83	3.62	3.21
3	6	2.95	3.03	3.1	3.26	3.78
3	5.57	4.43	3.03	2.92	3.45	3.19
3	6.32	4.08	2.86	2.78	3.57	3.33
3	4.81	4.62	3.24	3.21	3.87	3.66
7	4.85	3.59	2.58	2.83	3.55	3.62
7	3.99	3.84	3.55	3.15	4.08	3.85
7	4.7	3.53	2.96	3.11	3.84	3.57
7	4.98	2.8	3.31	3.83	3.74	4.11
7	3.86	3.57	2.97	2.89	3.49	3.74
7	4.08	4.71	3.55	3.2	4.4	4.13
14	3.45	5.76	3.99	2.68	4.01	3.61
14	3.33	3.75	3.16	3.35	3.85	4.19
14	4.41	3.77	3.89	2.96	4.88	3.58
14	6.63	3.63	3.19	3	4.09	4.39
14	11.39	3.62	3.64	3.04	4.09	4.14
14	3.29	2.83	3.4	3.14	4.44	3.47

Table A.13 Femoral pQCT BMC data

Scan 1 Distal, scan 2: mid-diaphyseal, scan 3: proximal

A2.2 Torsion testing Data

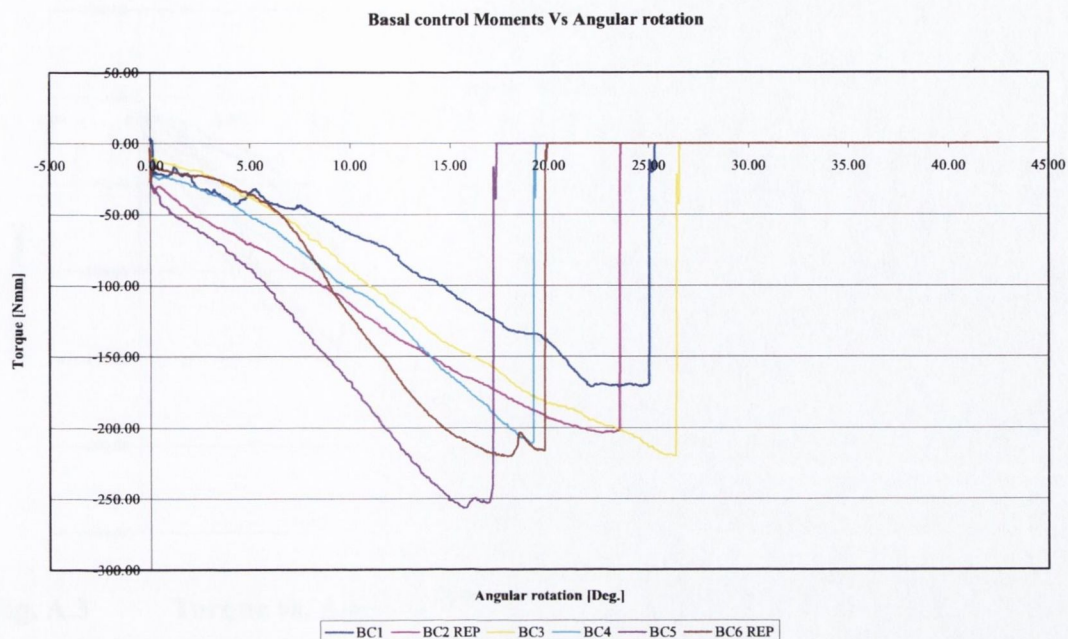


Fig. A.1 Torque vs. Angular rotation for Basal controls

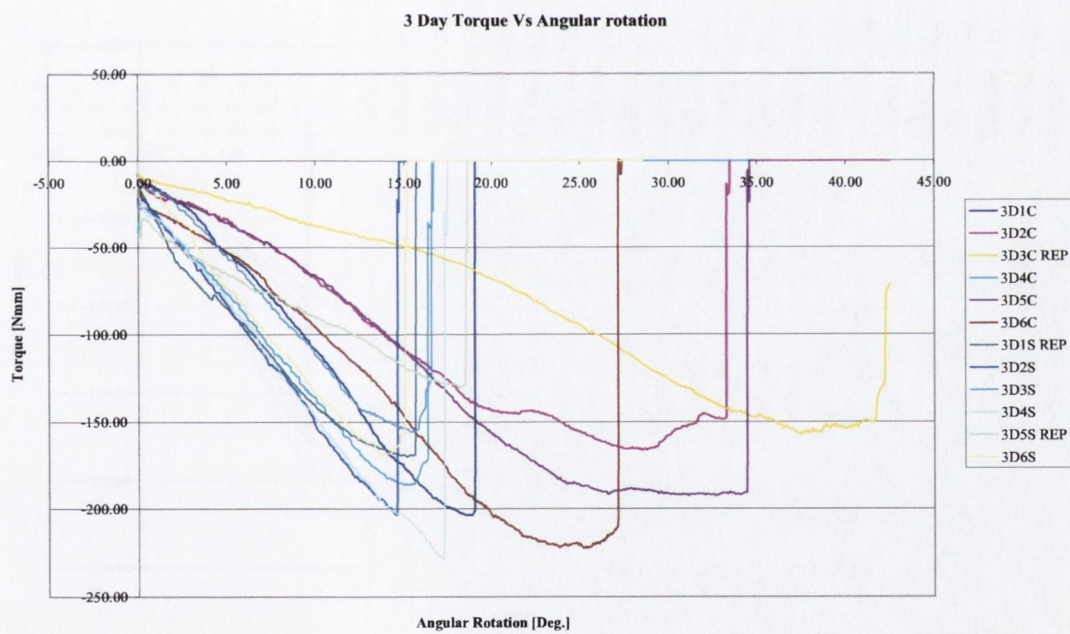


Fig. A.2 Torque vs. Angular rotation for 3 day control and suspended groups

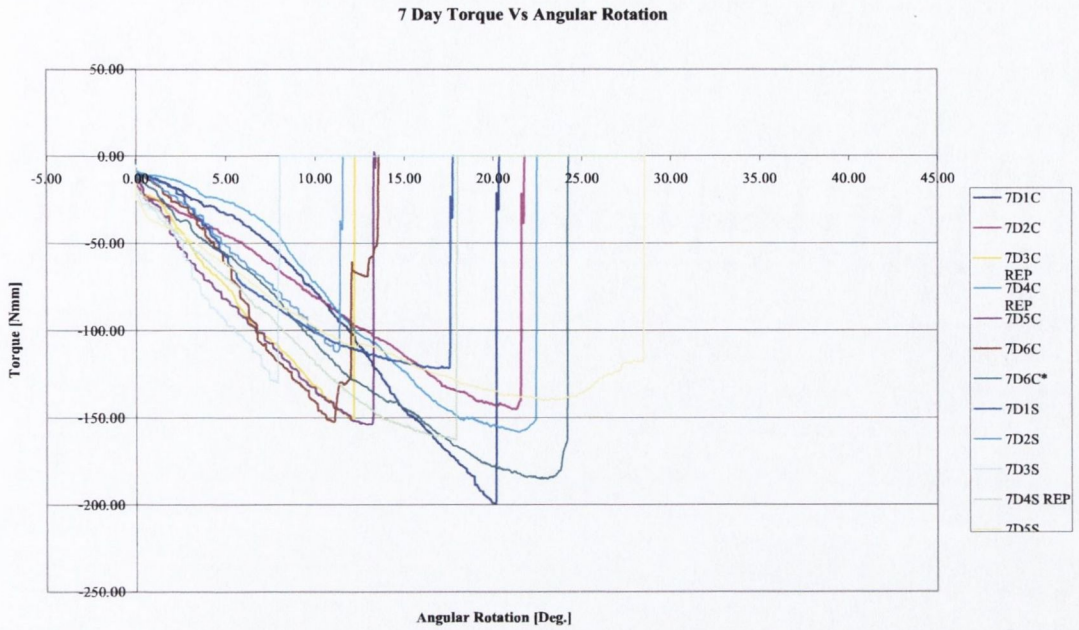


Fig. A.3 Torque vs. Angular rotation for 7 day control and suspended groups

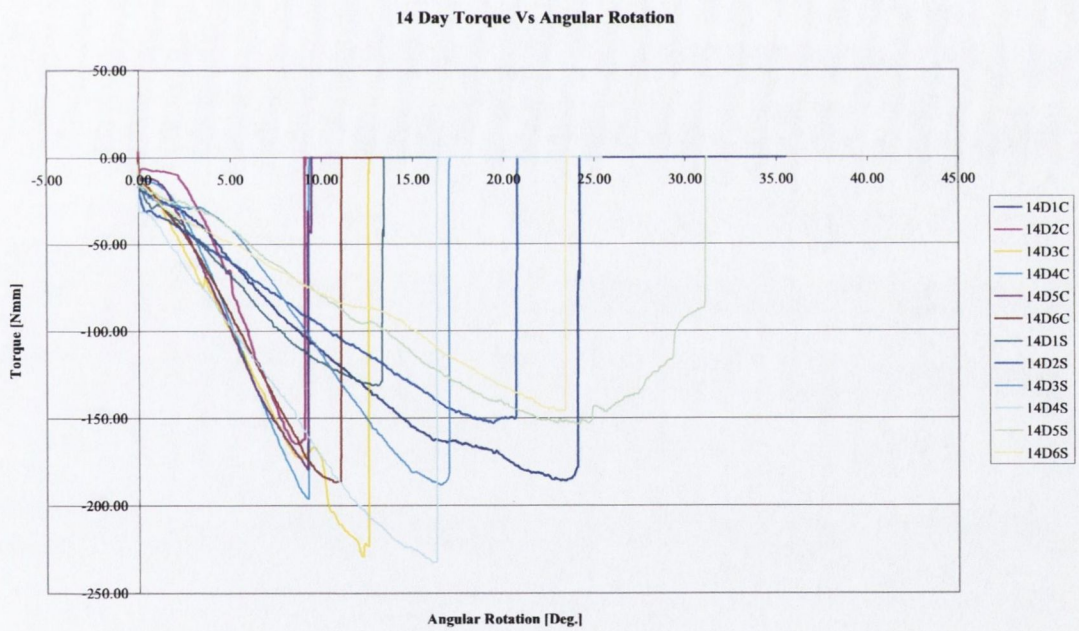


Fig. A.4 Torque vs. Angular rotation for 14 day control and suspended groups

	slope	Mean Slope	Median Slope	S.D. Slope	Intercept	cracks present	Max Torque
BC1	7.6	11.6	10.4	4.0	-12.4	1	171.2
BC2 REP	8.2				28.6	2	203.7
BC3	9.7				-10.5	0	217.1
BC4	11.2				-5.0	0	210.9
BC5	16.2				7.1	4	256.4
BC6 REP	16.8				-48.3	0	220.1
3D1C	12.4	9.1	9.1	3.1	-9.8	0	203.6
3D2C	7.3				-3.5	1	166.3
3D3C REP	4.4				-6.4	1	157.4
3D4C	12.1				15.6	0	186.1
3D5C	8.1				-5.0	0	192.4
3D6C	10.1				1.6	4	222.4
3D1S REP	9.8	10.1	10.2	2.7	35.9	1	170.1
3D2S	12.9				18.2	2	203.3
3D3S	9.9				5.1	0	155.7
3D4S	12.5				17.3	2	228.9
3D5S REP	5.3				38.7	2	130.4
3D6S	10.5				20.7	1	168.8
7D1C	12.1	10.5	10.4	3.2	-43.0	1	199.2
7D2C	6.4				13.6	1	145.0
7D3C REP	10.8				20.0	3	150.5
7D4C REP	8.2				-10.0	0	158.1
7D5C	9.9				32.1	0	153.9
7D6C	15.6				-15.6	0	152.3
7D1S	7.5	9.8	8.6	3.4	20.3	0	121.6
7D2S	10.0				-1.0	2	112.2
7D3S	15.6				11.1	2	130.0
7D4S REP	8.6				26.7	1	162.7
7D5S	7.3				37.2	2	140.1
7D6S						1	
14D1C	9.5	19.9	19.5	6.2	12.1	1	185.9
14D2C	27.6				-63.9	1	164.6
14D3C	18.6				5.6	0	229.1
14D4C	25.0				-31.6	0	195.9
14D5C	20.1				-5.2	1	179.2
14D6C	18.9				-5.4	1	186.5
14D1S	10.1	9.9	10.1	3.6	17.0	1	131.3
14D2S	7.1				24.1	1	152.9
14D3S	14.0				-29.0	3	188.1
14D4S	12.8				33.5	0	232.5
14D5S						1	153.5
14D6S	5.5				21.2	0	146.1

Table A.14 Femoral max torque and slope (=GK) data

Appendix 3 Gene expression Data

PIN 1	c-fos	oc	igf	rnrps9	gapdh
Name	Volume	Volume	Volume	Volume	Volume
ELPS-1D1C	30077	576184	390915	605266	55877
ELPS-1D2C	78116	824893	654378	609980	92740
ELPS-1D3C	103549	540834	617519	470589	23939
ELPS-1D4C	479118	176999	527758	93261	37930
ELPS-1D5C	40194	639146	1314653	969728	57168
ELPS-1D6C	216144	1159218	2690864	2151025	545447
ELPS-1D1S	666534	1512541	1559975	2193133	433620
ELPS-1D2S	81434	909924	805543	1475687	219345
ELPS-1D3S	132413	933852	976961	1507269	232540
ELPS-1D4S	1008983	2057527	5379049	10146422	547900
ELPS-1D5S	182269	1235752	1793243	2040812	381129
ELPS-1D6S	141016	1171553	1719435	3604755	395538
ELPS-3D1C	422652	828364	704322	536973	396911
ELPS-3D2C	234842	829437	682984	425029	232085
ELPS-3D3C	90528	799617	586139	484343	284387
ELPS-3D4C	105030	780567	780185	424577	664616
ELPS-3D5C	40806	533632	519827	261603	581475
ELPS-3D6C	47619	637539	3330978	371432	256826
ELPS-3D1S	87620	766686	817036	637574	463628
ELPS-3D2S	180223	1436283	2733383	1558358	15458597
ELPS-3D3S	78648	661827	360990	421794	1273366
ELPS-3D4S	298107	1386421	3024526	1752380	1245912
ELPS-3D5S	58258	528549	836991	424174	675916
ELPS-3D6S	354926	1055959	1483729	658857	1771963
ELPS-7D1C	288557	883386	2094488	2686449	481959
ELPS-7D2C	296055	806076	2678630	5838499	1600296
ELPS-7D3C	142022	531137	977918	972643	180639
ELPS-7D4C	616255	1737771	4142643	5570118	2729490
ELPS-7D5C	-707	198671	19550	-11327	87113
ELPS-7D6C	254888	435378	650004	488595	770719
ELPS-7D1S	237289	935512	1294169	1300616	411149
ELPS-7D2S	260259	769788	1022747	1684495	526713
ELPS-7D3S	77028	492340	222447	252211	256791
ELPS-7D4S	98831	178905	76753	-85788	42093
ELPS-7D5S	101773	400616	454333	225234	150256
ELPS-7D6S	87568	380611	108094	277615	79627
ELPS-14D1C	27959	609968	249026	276858	103647
ELPS-14D2C	71470	321128	-27922	215377	-7640
ELPS-14D3C	237452	785391	185821	853438	108471
ELPS-14D4C	316630	1066866	1591593	2034119	514904
ELPS-14D5C	452356	1288605	2814546	2129952	820306
ELPS-14D6C	171697	473124	54423	561400	145306
ELPS-14D1S	81201	695310	246965	296883	117673
ELPS-14D2S	86253	662680	287998	516979	74343
ELPS-14D3S	175902	876781	720209	659172	190047
ELPS-14D4S	-1314	98445	87960	4851	12383
ELPS-14D5S	298937	1064249	2258845	1989985	487098
ELPS-14D6S	123845	515316	734136	905702	113278
ELPS-36 ng	dirty 10%	4816915	314953	290490	4550385
ELPS-72 ng	461955	5493205	472406	590251	5255984
ELPS-144 ng	639272	6797201	776078	1114422	6787281
ELPS-288 ng	2660642	9104741	1316897	1911613	6196300
ELPS-576 ng	2192709	10442312	2374322	4218473	13209288
ELPS-1152 ng	3437867	12898335	3058949	8247590	42095896
ELPS-2304 ng	48194304				14961328

Table A.15 Pinloaded Array 1: raw volume data

Red boxes ruled out on basis of < 5% above background, Green boxes ruled out as too many of that dots ruled out

PIN 2	c-fos/RNRPS9	c-fos/GAPDH	oc/RNRPS9	oc/GAPDH	IGF1/RNRPS9	IGF1/GAPDH
Name						
ELPS-1D1C	0.05	0.54	0.95	10.31	0.65	7.00
ELPS-1D2C	0.13	0.84	1.35	8.89	1.07	7.06
ELPS-1D3C	0.22	4.33	1.15	22.59	1.31	25.80
ELPS-1D4C	5.14	12.63	1.90	4.67	5.66	13.91
ELPS-1D5C	0.04	0.70	0.66	11.18	1.36	23.00
ELPS-1D6C	0.10	0.40	0.54	2.13	1.25	4.93
ELPS-1D1S	0.30	1.54	0.69	3.49	0.71	3.60
ELPS-1D2S	0.06	0.37	0.62	4.15	0.55	3.67
ELPS-1D3S	0.09	0.57	0.62	4.02	0.65	4.20
ELPS-1D4S	0.10	1.84	0.20	3.76	0.53	9.82
ELPS-1D5S	0.09	0.48	0.61	3.24	0.88	4.71
ELPS-1D6S	0.04	0.36	0.33	2.96	0.48	4.35
ELPS-3D1C	0.79	1.06	1.54	2.09	1.31	1.77
ELPS-3D2C	0.55	1.01	1.95	3.57	1.61	2.94
ELPS-3D3C	0.19	0.32	1.65	2.81	1.21	2.06
ELPS-3D4C	0.25	0.16	1.84	1.17	1.84	1.17
ELPS-3D5C	0.16	0.07	2.04	0.92	1.99	0.89
ELPS-3D6C	0.13	0.19	1.72	2.48	8.97	12.97
ELPS-3D1S	0.14	0.19	1.20	1.65	1.28	1.76
ELPS-3D2S	0.12	0.01	0.92	0.09	1.75	0.18
ELPS-3D3S	0.19	0.06	1.57	0.52	0.86	0.28
ELPS-3D4S	0.17	0.24	0.79	1.11	1.73	2.43
ELPS-3D5S	0.14	0.09	1.25	0.78	1.97	1.24
ELPS-3D6S	0.54	0.20	1.60	0.60	2.25	0.84
ELPS-7D1C	0.11	0.60	0.33	1.83	0.78	4.35
ELPS-7D2C	0.05	0.18	0.14	0.50	0.46	1.67
ELPS-7D3C	0.15	0.79	0.55	2.94	1.01	5.41
ELPS-7D4C	0.11	0.23	0.31	0.64	0.74	1.52
ELPS-7D5C	0.06	-0.01	-17.54	2.28	-1.73	0.22
ELPS-7D6C	0.52	0.33	0.89	0.56	1.33	0.84
ELPS-7D1S	0.18	0.58	0.72	2.28	1.00	3.15
ELPS-7D2S	0.15	0.49	0.46	1.46	0.61	1.94
ELPS-7D3S	0.31	0.30	1.95	1.92	0.88	0.87
ELPS-7D4S	-1.15	2.35	-2.09	4.25	-0.89	1.82
ELPS-7D5S	0.45	0.68	1.78	2.67	2.02	3.02
ELPS-7D6S	0.32	1.10	1.37	4.78	0.39	1.36
ELPS-14D1C	0.10	0.27	2.20	5.89	0.90	2.40
ELPS-14D2C	0.33	-9.35	1.49	-42.03	-0.13	3.65
ELPS-14D3C	0.28	2.19	0.92	7.24	0.22	1.71
ELPS-14D4C	0.16	0.61	0.52	2.07	0.78	3.09
ELPS-14D5C	0.21	0.55	0.60	1.57	1.32	3.43
ELPS-14D6C	0.31	1.18	0.84	3.26	0.10	0.37
ELPS-14D1S	0.27	0.69	2.34	5.91	0.83	2.10
ELPS-14D2S	0.17	1.16	1.28	8.91	0.56	3.87
ELPS-14D3S	0.27	0.93	1.33	4.61	1.09	3.79
ELPS-14D4S	-0.27	-0.11	20.29	7.95	18.13	7.10
ELPS-14D5S	0.15	0.61	0.53	2.18	1.14	4.64
ELPS-14D6S	0.14	1.09	0.57	4.55	0.81	6.48

Table A.16 Pinloaded Array 1: volume ratio data

PIN 2	c-fos	oc	igf	rnrps9	gapdh
Name	Volume	Volume	Volume	Volume	Volume
ELPS-1D1C	933928	80207	35062	37867	233859
ELPS-1D2C	92976	210658	52510	19452	248267
ELPS-1D3C	160708	28190	54142	17318	153440
ELPS-1D4C	872816	43753	616588	17179	72522
ELPS-1D5C	189912	38929	79801	23732	235148
ELPS-1D6C	226632	102617	149935	37785	418343
ELPS-1D1S	960961	135726	704020	41606	414878
ELPS-1D2S	147504	230176	65541	53204	357445
ELPS-1D3S	83337	89793	57791	22949	304376
ELPS-1D4S	1614403	232207	1195882	472690	785379
ELPS-1D5S	251448	270892	148992	40600	539143
ELPS-1D6S	171199	169268	107180	126681	394855
ELPS-3D1C	487022	218524	475987	17871	329733
ELPS-3D2C	209071	343718	136186	16800	256099
ELPS-3D3C	132651	103927	84377	19226	199744
ELPS-3D4C	140112	252170	91896	20346	296046
ELPS-3D5C	112414	190934	39012	20561	281555
ELPS-3D6C	69029	146542	70021	13032	259296
ELPS-3D1S	81125	201706	43042	12935	169604
ELPS-3D2S	229993	324530	121236	71790	3736236
ELPS-3D3S	126444	237442	68459	19992	267084
ELPS-3D4S	345545	304720	219610	91454	994961
ELPS-3D5S	100161	258988	63348	35958	443171
ELPS-3D6S	299688	385857	270694	30212	677855
ELPS-7D1C	90199	154754	97796	145316	423300
ELPS-7D2C	143630	138219	92114	403913	802785
ELPS-7D3C	132693	159165	104064	55916	260620
ELPS-7D4C	308944	310340	227620	340178	1330992
ELPS-7D5C	27598	133585	30176	15720	132672
ELPS-7D6C	182597	195971	227609	37366	394959
ELPS-7D1S	80483	268567	108690	58533	402093
ELPS-7D2S	118730	254401	52328	88726	383112
ELPS-7D3S	49714	184856	58471	8741	175434
ELPS-7D4S	68424	128153	40794	21926	94020
ELPS-7D5S	95442	217332	67861	26812	179056
ELPS-7D6S	-27163	217881	61129	13769	167917
ELPS-14D1C	26400	193008	33629	922	71282
ELPS-14D2C	112254	107896	33883	5876	108933
ELPS-14D3C	160916	230472	95646	39639	233549
ELPS-14D4C	194108	315822	104947	82992	440767
ELPS-14D5C	327502	306535	151436	87180	719321
ELPS-14D6C	165989	190636	206596	22306	400362
ELPS-14D1S	9159	151045	19257	4096	88655
ELPS-14D2S	50517	160715	30327	9859	232960
ELPS-14D3S	22225	174111	42169	14352	166627
ELPS-14D4S	36354	86	5889	9468	11239
ELPS-14D5S	143248	255100	88940	100020	488076
ELPS-14D6S	61639	125056	76632	47820	190870
ELPS-36 ng	78620	47359	313375	966762	211798
ELPS-72 ng	83433	91617	468699	1934832	567202
ELPS-144 ng	149950	165065	784279	2951529	588442
ELPS-288 ng	180439	188094	1327637	6547605	901005
ELPS-576 ng	278378	276664	2374322	11454660	1452978
ELPS-1152 ng	566880	399332	3092842	20536070	1845057

Table A.17 Pinloaded Array 2: Raw volume data

PIN 2	c-fos/RNRPS9	c-fos/GAPDH	oc/RNRPS9	oc/GAPDH	IGF1/RNRPS9	IGF1/GAPDH
Name						
ELPS-1D1C	24.66	3.99	2.12	0.34	0.93	0.15
ELPS-1D2C	4.78	0.37	10.83	0.85	2.70	0.21
ELPS-1D3C	9.28	1.05	1.63	0.18	3.13	0.35
ELPS-1D4C	50.81	12.04	2.55	0.60	35.89	8.50
ELPS-1D5C	8.00	0.81	1.64	0.17	3.36	0.34
ELPS-1D6C	6.00	0.54	2.72	0.25	3.97	0.36
ELPS-1D1S	23.10	2.32	3.26	0.33	16.92	1.70
ELPS-1D2S	2.77	0.41	4.33	0.64	1.23	0.18
ELPS-1D3S	3.63	0.27	3.91	0.30	2.52	0.19
ELPS-1D4S	3.42	2.06	0.49	0.30	2.53	1.52
ELPS-1D5S	6.19	0.47	6.67	0.50	3.67	0.28
ELPS-1D6S	1.35	0.43	1.34	0.43	0.85	0.27
ELPS-3D1C	27.25	1.48	12.23	0.66	26.64	1.44
ELPS-3D2C	12.44	0.82	20.46	1.34	8.11	0.53
ELPS-3D3C	6.90	0.66	5.41	0.52	4.39	0.42
ELPS-3D4C	6.89	0.47	12.39	0.85	4.52	0.31
ELPS-3D5C	5.47	0.40	9.29	0.68	1.90	0.14
ELPS-3D6C	5.30	0.27	11.24	0.57	5.37	0.27
ELPS-3D1S	6.27	0.48	15.59	1.19	3.33	0.25
ELPS-3D2S	3.20	0.06	4.52	0.09	1.69	0.03
ELPS-3D3S	6.32	0.47	11.88	0.89	3.42	0.26
ELPS-3D4S	3.78	0.35	3.33	0.31	2.40	0.22
ELPS-3D5S	2.79	0.23	7.20	0.58	1.76	0.14
ELPS-3D6S	9.92	0.44	12.77	0.57	8.96	0.40
ELPS-7D1C	0.62	0.21	1.06	0.37	0.67	0.23
ELPS-7D2C	0.36	0.18	0.34	0.17	0.23	0.11
ELPS-7D3C	2.37	0.51	2.85	0.61	1.86	0.40
ELPS-7D4C	0.91	0.23	0.91	0.23	0.67	0.17
ELPS-7D5C	1.76	0.21	8.50	1.01	1.92	0.23
ELPS-7D6C	4.89	0.46	5.24	0.50	6.09	0.58
ELPS-7D1S	1.38	0.20	4.59	0.67	1.86	0.27
ELPS-7D2S	1.34	0.31	2.87	0.66	0.59	0.14
ELPS-7D3S	5.69	0.28	21.15	1.05	6.69	0.33
ELPS-7D4S	3.12	0.73	5.84	1.36	1.86	0.43
ELPS-7D5S	3.56	0.53	8.11	1.21	2.53	0.38
ELPS-7D6S	-1.97	-0.16	15.82	1.30	4.44	0.36
ELPS-14D1C	28.64	0.37	209.37	2.71	36.48	0.47
ELPS-14D2C	19.10	1.03	18.36	0.99	5.77	0.31
ELPS-14D3C	4.06	0.69	5.81	0.99	2.41	0.41
ELPS-14D4C	2.34	0.44	3.81	0.72	1.26	0.24
ELPS-14D5C	3.76	0.46	3.52	0.43	1.74	0.21
ELPS-14D6C	7.44	0.41	8.55	0.48	9.26	0.52
ELPS-14D1S	2.24	0.10	36.88	1.70	4.70	0.22
ELPS-14D2S	5.12	0.22	16.30	0.69	3.08	0.13
ELPS-14D3S	1.55	0.13	12.13	1.04	2.94	0.25
ELPS-14D4S	3.84	3.23	0.01	0.01	0.62	0.52
ELPS-14D5S	1.43	0.29	2.55	0.52	0.89	0.18
ELPS-14D6S	1.29	0.32	2.62	0.66	1.60	0.40

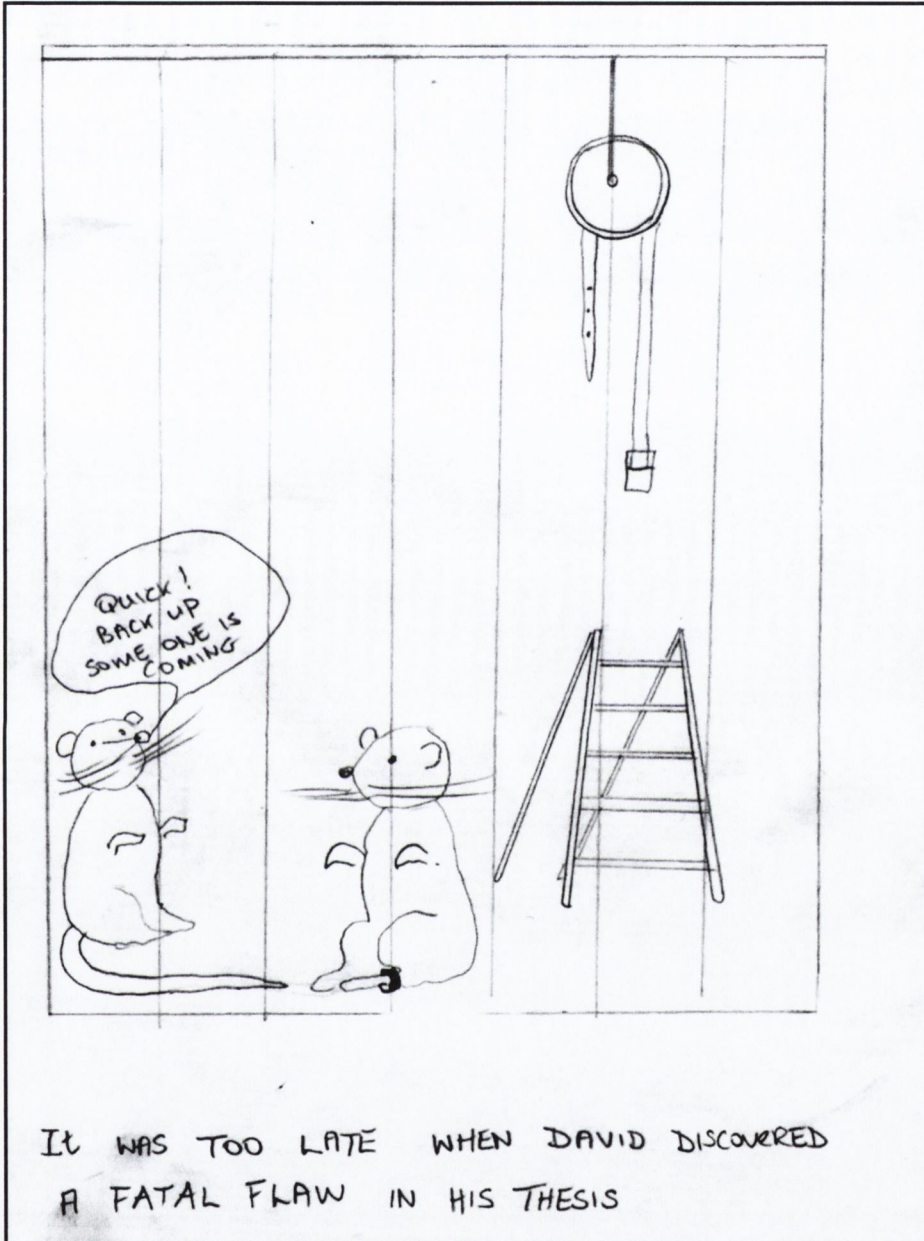
Table A.18 Pinloaded Array 2: Volume ratio data

HAND	c-fos	osteocalcin	igf	rnrps9	gapdh
Name	Volume	Volume	Volume	Volume	Volume
ELPS-1D1C	1822808	1623924	428137	1151042	350428
ELPS-1D2C	3797019	2463161	1668358	1453300	1066254
ELPS-1D3C	2411286	2320387	683681	1144594	290161
ELPS-1D4C	214787	311349	155504	281228	84517
ELPS-1D5C	3064427	2821549	1235972	2171560	690104
ELPS-1D6C	6817118	4484417	2724615	3301807	1551720
ELPS-1D1S	15953631	5824410	10043813	4652096	2984466
ELPS-1D2S	3942115	3702083	1902216	4714526	1478141
ELPS-1D3S	4754561	3903159	2242352	2079675	1783083
ELPS-1D4S	21978834	8203967	25798219	20431352	8432862
ELPS-1D5S	7842937	5985344	6157701	3719034	3400323
ELPS-1D6S	6152475	5809649	2812701	11196098	1158839
ELPS-3D1C	2133779	2078857	1601646	1040838	826011
ELPS-3D2C	1502287	2577412	671456	784128	149152
ELPS-3D3C	1184027	3321213	514104	624983	134009
ELPS-3D4C	1371778	3199732	1014062	1203721	1206562
ELPS-3D5C	2294767	5103998	1946293	2064094	4144896
ELPS-3D6C	1370704	3612832	5340209	822143	172291
ELPS-3D1S	2330392	1629757	3792697	765279	1560532
ELPS-3D2S	2727045	6044731	6640551	3243386	44642228
ELPS-3D3S	993103	1970067	615402	527803	178010
ELPS-3D4S	4847379	4205667	8459940	3349337	5734731
ELPS-3D5S	824468	2687470	912254	811716	1139913
ELPS-3D6S	2209046	7529102	2799162	2927543	6407274
ELPS-7D1C	3516565	3179170	7859544	12164596	3496921
ELPS-7D2C	10882933	7503701	24445476	58397024	23929531
ELPS-7D3C	2420280	3442880	7191195	8588591	1978559
ELPS-7D4C	8869048	5049452	24215090	20162571	18514468
ELPS-7D5C	279961	2247730	729638	420456	209572
ELPS-7D6C	1800678	3950741	2882349	4215271	5234297
ELPS-7D1S	2156586	2162130	3826404	6060920	1800745
ELPS-7D2S	1427826	1524073	2112979	7346891	1456285
ELPS-7D3S	15493	307088	854221	829447	558269
ELPS-7D4S	331073	591822	728774	1960858	145332
ELPS-7D5S	880510	1033024	917712	1934723	669794
ELPS-7D6S	460944	660923	253388	1720934	259258
ELPS-14D1C	-85812	727184	334855	801863	326529
ELPS-14D2C	1565877	1475656	1999243	1290528	2321576
ELPS-14D3C	4706284	2817687	5796426	6177273	1619445
ELPS-14D4C	4435199	2805818	5944341	7912755	1846621
ELPS-14D5C	8971516	3399363	11756568	8922381	5427861
ELPS-14D6C	4786853	3047521	6072414	9203098	2970951
ELPS-14D1S	701638	1231239	523875	1871916	589531
ELPS-14D2S	1771287	1675016	1479243	2237386	2230017
ELPS-14D3S	2616876	1470100	2346527	2317885	2520025
VOID 14D4S	-26421	24967	-17499	-65702	128949
ELPS-14D5S	5580010	2609581	6780586	6396447	3752906
ELPS-14D6S	1267090	1665876	528698	4302557	382594
Ladder 42ng	2234499	1767678	1327560	2175651	286559
Ladder 84ng	4681590	2858585	2413188	3248940	503684
Ladder 168ng	2214468	3868579	3413452	4118085	1090794
Ladder 336ng	3411609	5986373	4939380	5118752	1551553
Ladder 672ng	4432565	7096030	7964675	9739837	4035417
Ladder 1344ng	8081941	10326350	23022493	36930306	9085868
Ladder 2688ng	10537613	12378148	23790655	43470253	11597412

Table A.19 Hand-loaded Array: Raw Volume data

HAND	c-fos/RNRPS9	c-fos/GAPDH	oc/RNRPS9	oc/GAPDH	IGF1/RNRPS9	IGF1/GAPDH
Name						
ELPS-1D1C	1.58	5.20	1.41	4.63	0.37	1.22
ELPS-1D2C	2.61	3.56	1.69	2.31	1.15	1.56
ELPS-1D3C	2.11	8.31	2.03	8.00	0.60	2.36
ELPS-1D4C	0.76	2.54	1.11	3.68	0.55	1.84
ELPS-1D5C	1.41	4.44	1.30	4.09	0.57	1.79
ELPS-1D6C	2.06	4.39	1.36	2.89	0.83	1.76
ELPS-1D1S	3.43	5.35	1.25	1.95	2.16	3.37
ELPS-1D2S	0.84	2.67	0.79	2.50	0.40	1.29
ELPS-1D3S	2.29	2.67	1.88	2.19	1.08	1.26
ELPS-1D4S	1.08	2.61	0.40	0.97	1.26	3.06
ELPS-1D5S	2.11	2.31	1.61	1.76	1.66	1.81
ELPS-1D6S	0.55	5.31	0.52	5.01	0.25	2.43
ELPS-3D1C	2.05	2.58	2.00	2.52	1.54	1.94
ELPS-3D2C	1.92	10.07	3.29	17.28	0.86	4.50
ELPS-3D3C	1.89	8.84	5.31	24.78	0.82	3.84
ELPS-3D4C	1.14	1.14	2.66	2.65	0.84	0.84
ELPS-3D5C	1.11	0.55	2.47	1.23	0.94	0.47
ELPS-3D6C	1.67	7.96	4.39	20.97	6.50	31.00
ELPS-3D1S	3.05	1.49	2.13	1.04	4.96	2.43
ELPS-3D2S	0.84	0.06	1.86	0.14	2.05	0.15
ELPS-3D3S	1.88	5.58	3.73	11.07	1.17	3.46
ELPS-3D4S	1.45	0.85	1.26	0.73	2.53	1.48
ELPS-3D5S	1.02	0.72	3.31	2.36	1.12	0.80
ELPS-3D6S	0.75	0.34	2.57	1.18	0.96	0.44
ELPS-7D1C	0.29	1.01	0.26	0.91	0.65	2.25
ELPS-7D2C	0.19	0.45	0.13	0.31	0.42	1.02
ELPS-7D3C	0.28	1.22	0.40	1.74	0.84	3.63
ELPS-7D4C	0.44	0.48	0.25	0.27	1.20	1.31
ELPS-7D5C	0.67	1.34	5.35	10.73	1.74	3.48
ELPS-7D6C	0.43	0.34	0.94	0.75	0.68	0.55
ELPS-7D1S	0.36	1.20	0.36	1.20	0.63	2.12
ELPS-7D2S	0.19	0.98	0.21	1.05	0.29	1.45
ELPS-7D3S	0.02	0.03	0.37	0.55	1.03	1.53
ELPS-7D4S	0.17	2.28	0.30	4.07	0.37	5.01
ELPS-7D5S	0.46	1.31	0.53	1.54	0.47	1.37
ELPS-7D6S	0.27	1.78	0.38	2.55	0.15	0.98
ELPS-14D1C	-0.11	-0.26	0.91	2.23	0.42	1.03
ELPS-14D2C	1.21	0.67	1.14	0.64	1.55	0.86
ELPS-14D3C	0.76	2.91	0.46	1.74	0.94	3.58
ELPS-14D4C	0.56	2.40	0.35	1.52	0.75	3.22
ELPS-14D5C	1.01	1.65	0.38	0.63	1.32	2.17
ELPS-14D6C	0.52	1.61	0.33	1.03	0.66	2.04
ELPS-14D1S	0.37	1.19	0.66	2.09	0.28	0.89
ELPS-14D2S	0.79	0.79	0.75	0.75	0.66	0.66
ELPS-14D3S	1.13	1.04	0.63	0.58	1.01	0.93
ELPS-14D4S	0.40	-0.20	-0.38	0.19	0.27	-0.14
ELPS-14D5S	0.87	1.49	0.41	0.70	1.06	1.81
ELPS-14D6S	0.29	3.31	0.39	4.35	0.12	1.38

Table A.20 Hand-loaded Array: Volume ratio data



Commemorative plaque by the soon to be Dr. Orna Tighe.